

The role of lymph node-derived
lymphatic endothelial cells
in immune modulation
in the tumour microenvironment

Jennifer Nicole Harris

Darwin College

Student Name (CRSid): Jennifer Nicole Harris (jnh42)

Dissertation Title: The role of lymph node-derived lymphatic endothelial cells in immune modulation in the tumour microenvironment

Abstract: The lymphatic vasculature is a key player in progression of many cancers, with lymphangiogenesis at the primary tumour and tumour-draining lymph nodes (TDLNs) associated with poor patient prognosis. As well as providing a highway for metastatic tumour cells, recent reports propose lymphatics as modulators of immunity, highlighting a need for greater understanding of immune regulation by lymphatics. The specific role of lymphatic endothelial cells (LECs) in this context, particularly in TDLNs, is unknown. As TDLNs are immune hubs, yet anti-tumour immune responses are often ineffective, this thesis aimed to investigate functional changes to lymphatics in TDLNs and the role of TDLN-derived LECs in anti-tumour immunity. I hypothesised that factors from the tumour microenvironment alter functionality of TDLN-LECs from early stages of tumour development. I further hypothesised that these changes would promote immune tolerance, with this thesis exploring specific impact on dendritic cell (DC) mediated immunity. Using the B16-F10 melanoma model, this work confirmed expansion of TDLN-LECs prior to metastasis and demonstrated transcriptional reprogramming of immune-associated pathways in LECs isolated from early TDLNs. This was accompanied by differentially localized migratory DCs, clustered at lymphatic subcapsular sinuses. *In vitro* using co-culture assays revealed mature DCs undergo prolonged interactions with LECs conditioned with B16-F10 tumour-conditioned media, suggesting a change in the physical interactions occurring *in vivo* in early TDLNs. Additionally, we investigated possible mechanistic contributors, demonstrating using *in vitro* and *in vivo* blockade and knockout models, a role for lymphatic expressed Podoplanin in DC interactions and migration. Prolonged physical interactions were further found to facilitate antigen transfer from ovalbumin-loaded LECs to DCs yet inhibit DC priming of T-cells, with DCs found capable of acquiring TDLN-LEC archived antigen *in vivo*. These results show that in lymph nodes conditioned by factors derived from the tumour microenvironment, prolonged physical interactions between LECs and DCs impact DC migration and T-cell priming. As immune tolerance is a key feature of the tumour microenvironment, this work has highlighted lymphatics as key modulators of the anti-tumour immune response. Furthermore, this work provides new insight into lymphatic involvement during tumour development, identifying lymphatics as a potential target for early intervention therapies.

i. Declaration

This dissertation is the result of my own work and includes nothing, which is the outcome of work done in collaboration except as declared in the Preface and specific in the text.

It is not substantially the same as any that I have submitted, or, is being concurrently submitted for a degree or diploma of other qualification at the University of Cambridge or any other University or similar institution except as declared in the Preface and specified text.

I further state that no substantial part of my dissertation has already been submitted, or, is being concurrently submitted for any such degree, diploma, or other qualification at the University of Cambridge or any other University or similar institution except as declared in the Preface and specified in the text.

It does not exceed the prescribed work limit of 60,000 words for the Clinical Medicine and Clinical Veterinary Medicine Degree Committee.

A handwritten signature in black ink, appearing to read 'J. Harris'.

Miss. Jennifer Nicole Harris

ii. Acknowledgements

First and foremost, I would like to thank my PhD supervisor Dr Jacqui Shields, who not only has given me the opportunity to work in her lab for the past few years but has also been incredibly supportive and helpful. From experimental design to conversations about cycling and running – you have genuinely been a friend as well as a mentor.

Secondly, I would like to thank every single Agent of S.H.I.E.L.D who have been best friends as well as colleagues, thank you so much for always being there – Luisa Pedro, Matthew Lakins, Angela Riedel, Hafsa Munir, Ehsan Ghorani, James Jones, Sarah (Dave) Davidson, Jake Cridge, Carlo Zimarino, Rebecca White, Bastian Schmied, Lisa Haas, Jonathan Swietlik, Garrett Beeghly and Will Moody. I would also like to thank Emma Kerr, Frances Turrell, Eleanor Heaton, Annalise Katz-Summercorn and Jason Crawte for always being there as a friend to have a laugh with and to turn to in tough times. Finally, Nadeera de Silva – I wish you had been here to share this PhD rollercoaster with us; you are forever missed.

Thirdly, I would like to thank Thilo Richter who has been my best friend and partner throughout, supporting me and helping me through all the late nights, long weekends and celebratory wins along the way - I love you so very much. Alongside all those at Darwin College and beyond, especially BarComm, Alki, Gaby and Joana, you have been my Cambridge bedrock through the happiest and toughest moments of this PhD, and without you all, I'm not sure how I would have coped – many many thanks.

Last but not least, I would like to thank my beautiful family. Coming to the University of Cambridge was always an ambition of mine and you have all sacrificed a lot to allow me to fulfil that goal. From that life-changing moment in 2004, right up to current day, you have all been nothing other than a gift. My support network and my constant – I thank you from the bottom of my heart for being the best family a woman could ask for. So, Josephine Harris-Cook, Rachel Harris, Bex-Harris Cook, Arwyn Harris-Cook, Maisie Double-Cook and Leo Double-Cook – I love you all and I am forever grateful and indebted.

iii. List of presentations and prizes awarded at scientific meetings

Poster presentations

- **Cambridge Immunology Network PhD & Post-Doc Day**, Cambridge, June 2016
- **Hutchison / MRC Research Centre Annual Retreat**, Cambridge, November 2015 and November 2017
- **BMS-UKCAS Conference**, Birmingham, April 2017
- **1st Crick International Cancer Conference**, London, September 2017

Oral presentations

- **Hutchison / MRC Research Centre Lunchtime Seminar**, Cambridge, May 2016
- **Hutchison / MRC Research Centre Annual Retreat**, Cambridge, December 2016

Prizes

- **Best Oral Presentation** at the Hutchison / MRC Research Centre Annual Retreat, Cambridge, December 2016
- **Poster Prize** at the joint British Microcirculation Society (BMS) and UK Cell Adhesion Society (UKCAS) conference, Birmingham, April 2017

Other Attended Conferences

- **Cambridge Cancer Centre Annual Symposia**, Cambridge, June 2014, 2015, 2016, 2017
- **Cancer Research UK Cambridge Institute Annual International Symposium**, Cambridge, March 2015
- **2nd AstraZeneca-MedImmune Cambridge Cancer Science Symposium**, Cambridge, September 2015

Table of Contents

Abstract	2
i. Declaration	3
ii. Acknowledgements	4
iii. List of presentations and prizes awarded at scientific meetings	5
Table of Contents	6
List of Figures	8
List of Tables	11
Abbreviations	13
CHAPTER 1	15
INTRODUCTION	15
1. General Introduction	16
1.1. Overview of lymphatics in cancer	16
1.2. Structure and function of the lymphatic system	17
1.3. The role of lymphatics in inflammation	31
1.4. The role of lymphatics in cancer	36
1.5. Summary	43
1.6. Hypothesis and Aims	44
CHAPTER 2	46
METHODS	46
2. Methods	47
2.1. Cell Culture	47
2.2. Isolation of primary murine cell populations	48
2.3. <i>In vivo</i> mouse studies	50
2.4. RNA Isolation, Amplification and Quantification	58
2.5. Microarray Hybridisation and Data Normalisation	61
2.6. Quantitative real-time polymerase chain reaction (qRT-PCR)	62
2.7. Dendritic Cell and Antigen Presenting Cell PCR Array	63
2.8. Flow Cytometry analysis of primary and cell line populations	67
2.9. Immunofluorescent Imaging (IF)	68
2.10. Functional Assays	72
2.11. Statistical Analysis	78
CHAPTER 3	82
RESULTS	82
3. Functional characterisation of lymphatics from melanoma TDLNs	83
3.1. Introduction	83
3.2. Methods	84
3.3. Results	89
3.4. Discussion	114

CHAPTER 4	118
RESULTS	118
4. Determining the interactions between DCs and LECs in TDLNs	119
4.1. Introduction	119
4.2. Methods	121
4.3. Results	126
4.4. Discussion	164
CHAPTER 5	171
RESULTS	171
5. Determining the role of lymphatic-DC cross-talk in T-cell priming in TDLNs	172
5.1. Introduction	172
5.2. Methods	174
5.3. Results	179
5.4. Discussion	216
CHAPTER 6	220
DISCUSSION	220
6. General Discussion	221
6.1. Project rationale and overview	221
6.2. Lymphangiogenesis in the tumour microenvironment	222
6.3. Modulation of DC migration in TDLNs mediated by Podoplanin positive lymphatics	225
6.4. Lymphatics as modulators of antigen-mediated immune priming	230
6.5. Driving factors involved in altered lymphatic and DC behaviour in the tumour microenvironment	232
6.6. Summary and Future Perspectives	234
Bibliography	238
APPENDICES	262
Appendix 1 – Altered gene targets in TDLN-derived LECs	263
Appendix 2 – Gene targets altered in Day 4 and Day 11 TDLN-derived LECs	264
Appendix 3 – Gene ontology pathways for altered genes	265
Appendix 4 – Altered canonical pathways and associated gene targets	267
Appendix 5 – Manual categorisation of canonical pathways	269
Appendix 6 – Altered <i>Immunity</i> associated gene targets	272
Appendix 7 – Flow cytometry gating for profiling dendritic cells	273
Appendix 8 – Flow cytometry gating for profiling LECs <i>in vitro</i>	274
Appendix 9 – Flow cytometry gating for <i>in vitro</i> OVA assays	275
Appendix 10 – Optimisation of the <i>in vitro</i> antigen transfer assay	276
Appendix 11 – FACS gating for isolating TRITC immune cells	277
Appendix 12 – Flow cytometry gating strategy for profiling lymph node cells	278

List of Figures

CHAPTER 1 - INTRODUCTION

- Figure 1.1 Hierarchal organisation of lymphatics in the periphery
- Figure 1.2 Lymphatic endothelial cells junctions
- Figure 1.3 Journey of lymph through the lymphatic and blood system
- Figure 1.4 Structure and organisation of the lymph node
- Figure 1.5 Mechanisms of lymphangiogenesis and metastasis in the tumour microenvironment

CHAPTER 2 - METHODS

- Figure 2.1 Agarose gels for genotyping of mouse lines
- Figure 2.2 Schematic of *in vivo* B16-F10 mouse model
- Figure 2.3 Amelanotic tumours and pigmentation in *Braf*^{V600E}/*Pten* mice.
In vivo model of tracking tumour-derived dendritic cells
- Figure 2.4 Schematic of experimental murine set-up for microarray samples
- Figure 2.5
- Figure 2.6 96-well format for PCR Profiler Arrays
- Figure 2.7 Dermal sheet preparation from whole ears derived from C57BL/6 mice

CHAPTER 3 – RESULTS

- Figure 3.1 Method of quantifying lymphatic coverage in lymph nodes
- Figure 3.2 Lymph node and lymphatic expansion in TDLNs of B16-F10 tumours
- Figure 3.3 Lymphatic networks expand in TDLNs over time
- Figure 3.4 Lymphatic expansion occurs at the subcapsular sinus and in medullary regions of TDLNs
- Figure 3.5 Whole lymph node coverage of LYVE-1 is significantly increased in late TDLNs
- Figure 3.6 Lymphatic expansion occurs in peritumoural regions of melanoma tumours
- Figure 3.7 TDLN-derived LECs undergo time-specific transcriptional changes
- Figure 3.8 Immune signatures and key endothelial pathways are deregulated in TDLN-derived LECs

- Figure 3.9 *Immunity* pathways are highly represented in early and late TDLNs, relative to other canonical pathways
- Figure 3.10 Specific *Immunity* pathways with altered gene expression profiles in TDLNs
- Figure 3.11 Genes associated with *Immunity*, with altered gene expression profiles in TDLNs
- Figure 3.12 Verification of LN-LEC RNA expression trends of junctional molecules
- Figure 3.13 CCL21 protein expression is unaltered in early TDLNs
- Figure 3.14 Podoplanin protein expression is upregulated on early TDLN-derived LECs
- Figure 3.15 Microarray identified gene targets of interest correlate with dendritic cell marker, *Ilgax*, in human melanoma

CHAPTER 4 – RESULTS

- Figure 4.1 Schematic outlining methods of quantifying TRITC+ cells
- Figure 4.2 Schematic outlining methods of quantifying morphological features of DCs
- Figure 4.3 Migratory TRITC+ DCs cluster in outer regions of early TDLNs in association with subcapsular lymphatics
- Figure 4.4 Increased clustering of migratory TRITC+ DCs in outer regions of early TDLNs
- Figure 4.5 Gating strategy for dendritic cell profiling in TDLNs from TRITC painted tumours
- Figure 4.6 Lymph node cellularity and dendritic cell counts is increased in early TDLNs
- Figure 4.7 Altered profiles of TRITC+ dendritic cell subpopulations in early TDLNs
- Figure 4.8 *In vitro* LECs express canonical lymphatic markers and lymphatic transcription factor, PROX-1
- Figure 4.9 Schematic of *in vitro* dendritic cell assays used to assess lymphatic interactions
- Figure 4.10 Enhanced adhesion of dendritic cells to TCM-conditioned LECs *in vitro*
- Figure 4.11 Altered dendritic cell morphology upon co-culture with TCM-conditioned LECs *in vitro*
- Figure 4.12 Perturbed transmigration of dendritic cells across TCM-conditioned LECs *in vitro*

Figure 4.13	Perturbed motility of dendritic cells across TCM-conditioned LECs <i>in vitro</i>
Figure 4.14	Microarray data of gene targets involved in immune cell interactions
Figure 4.15	Immunofluorescent imaging of TRITC+ DCs in the subcapsular sinus of LNs
Figure 4.16	Enhanced Podoplanin expression in LECs treated with TCM for 48hrs <i>in vitro</i>
Figure 4.17	Podoplanin blockade inhibits DC adhesion to LECs <i>in vitro</i> , in resting conditions
Figure 4.18	CLEC-2 expression is expressed in DCs derived from spleen and lymph node.
Figure 4.19	<i>In vivo</i> Podoplanin blockade does not alter migratory DC localisation in LNs
Figure 4.20	Podoplanin blockade does not significantly alter DC counts in early TDLNs
Figure 4.21	Podoplanin blockade does not significantly alter total counts of migratory TRITC DC infiltrate in early TDLNs
Figure 4.22	Podoplanin blockade does not significantly alter the percentage of migratory TRITC DC infiltrate in early TDLNs
Figure 4.23	Characterisation of lymphatic networks and Podoplanin expression in ear dermis from PDPN-FL mice
Figure 4.24	Dendritic cell composite and lymph node cellularity is altered in PDPN-FL homozygous mice
Figure 4.25	Migratory dendritic cell infiltrate is altered in PDPN-FL homozygous mice
Figure 4.26	Podoplanin expression is perturbed in lymph nodes and ear dermis from heterozygous and homozygous PDPN-FL mice

CHAPTER 5 – RESULTS

Figure 5.1	Method of TRITC quantification within T-cell zones
Figure 5.2	Migratory DCs are delocalised in T-cell zones of early TDLNs
Figure 5.3	Migratory DCs are clustered at the edge of B-cell follicles in Day 4 TDLNs
Figure 5.4	Migratory DCs are clustered at the Tcell-Bcell margin in Day4 TDLNs

- Figure 5.5 OVA uptake and processing by LECs *in vitro*
- Figure 5.6 Schematic showing *in vitro* model of antigen transfer
- Figure 5.7 Gating strategy for flow cytometry analysis of OVA transfer
- Figure 5.8 LEC-derived antigen is transferred to physically interacting DCs
- Figure 5.9 No change in antigen transfer between TCM-conditioned LECs and DCs
- Figure 5.10 Gating strategy for quantification of OT-1 CD8+ T-cell proliferation and viability
- Figure 5.11 OT-1 T-cells do not proliferate in the presence of LEC-primed DCs
- Figure 5.12 Flow cytometry gating strategy used to identify FITC-OVA localisation in TDLNs
- Figure 5.13 Antigen is taken-up primarily by LECs in NDNLNs and TDLNs
- Figure 5.14 Antigen localises to LYVE-1 positive regions in Day 4 TDLNs
- Figure 5.15 Flow cytometry gating strategy used to identify DQ-OVA processing in TDLNs
- Figure 5.16 LECs efficiently process antigen in NDNLNs and early TDLNs
- Figure 5.17 No difference in antigen processing by CD11c+ DCs between control NDNLNs and early TDLNs
- Figure 5.18 Migratory DCs process drained antigen in LNs
- Figure 5.19 Migratory DCs are activated and mature in early TDLNs
- Figure 5.20 No change in PD-L1 and PD1 expression in immune compartments between NDNLNs and early TDLNs
- Figure 5.21 Altered T-cell profiles in TDLNs across time

CHAPTER 6 – DISCUSSION

- Figure 6.1 LN expansion and transformation during tumour development

List of Tables

CHAPTER 2 - METHODS

Table 2.1	PCR mastermix components used for genotyping
Table 2.2	PCR program used for genotyping
Table 2.3	Primers used for genotyping of mouse lines
Table 2.4	PCR programs for amplification
Table 2.5	qRT-PCR program for ABI StepOnePlus™ Cyclers
Table 2.6	Reverse transcription mix for first strand cDNA synthesis for PCR Profiler Arrays
Table 2.7	Amplification PCR programs for PCR Profiler Arrays
Table 2.8	qRT-PCR program for ABI StepOnePlus™ Cyclers for PCR Profiler Arrays
Table 2.9	Buffer and reagent recipes
Table 2.10	Antibodies for flow cytometry
Table 2.11	Antibodies for immunofluorescent imaging
Table 2.12	Fluorescently conjugated secondary antibodies

Abbreviations

ANOVA	Analysis of variance
APC	Antigen presenting cell
BEC	Blood endothelial cell
BSA	Bovine serum albumin
CAF	Cancer associated fibroblasts
CAM	Cell adhesion molecule
CCM	Control conditioned media
CCL	CC-type chemokine ligand
CXCR	CXC-type chemokine receptor
CXCL	CXC-type chemokine ligand
CCR	CC-type chemokine receptor
DAPI	4",6-diamidino-2-phenylindole
DAMP	Danger associated molecular pattern
DC	Dendritic cell
ECM	Extracellular matrix
FACS	Flow assisted cell sorting
FBS	Foetal bovine serum
FRC	Fibroblast reticular cell
FSC SSC	Forward side scatter Side scatter
ICAM	Intracellular adhesion molecule
IDO	Indoleamine-2,3-dioxygenase
IL	Interleukin
GSEA	Gene set enrichment analysis
HEV	High endothelial venule
KEGG	Kyoto Encyclopedia of Genes and Genomes
LEC	Lymphatic endothelial cell
LN	Lymph node
LN-LECs	Lymph nodes lymphatic endothelial cells
LYVE-1	Lymphatic endothelial hyaluronan receptor-1
MHC	Major histocompatibility complex
NDLN	Non-draining lymph node
OVA	Ovalbumin
PAMP	Pathogen associated molecular pattern
PD-L1	Programmed death ligand-1
PDPN	Podoplanin
PFA	Paraformaldehyde
PLVAP	Plasmalemma vesicle-associated protein
PROX-1	Prospero-related homeobox-1
ROI	Region of interest
RNA	Ribonucleic acid
qRT-PCR	Quantitative real-time polymerase chain reaction
SCS	Subcapsular sinus
SEM	Standard error of the mean
SEMs	Semaphorins
SMCs	Smooth muscle cells
TCGA	The Cancer Genome Atlas

TCM	Tumour-conditioned media
TDLN	Tumour-draining lymph node
TLR	Toll-like receptor
VCAM	Vascular cell adhesion molecule
VEGF	Vascular endothelial growth factor
VEGF-R3	Vascular endothelial growth factor receptor-3
Hr(s)	Hour(s)
Min(s)	Minute(s)
Mg(s)	Milligram(s)
ml(s)	Millilitre(s)
ng	Nanogram
µg	Microgram
µl	Microlitre
µM	Micromolar
%	Percentage

CHAPTER 1

INTRODUCTION

1. General Introduction

1.1. Overview of lymphatics in cancer

Lymphatic vasculature plays a critical role in tumour progression in many cancers. Until recently, lymphatics were considered to be passive bystanders serving as avenues for tumour metastasis. The lack of reliable markers of lymphatic endothelial cells (LECs) hindered accurate discrimination of lymphatic vasculature from blood vasculature, and this was compounded by the scarcity of suitable experimental models. Over the past decade however, significant progress has been made in the field of lymphatic biology in the context of physiology, pathology and immunology. Within the tumour microenvironment, we now know lymphatics to be active participants, contributing not only to tumour development at the primary site and tumour metastasis, but also to the anti-tumour immune response. The adaptive functions and changes occurring in lymphatics at the primary site and distal tumour-draining lymph nodes remain undefined and hence there is a renewed focus on lymphatics in cancer research. With much to be discovered and defined in terms of specific mechanistic contributions to tumour progression and avenues for targeting, outstanding questions include: how do LECs respond and adapt to factors derived from the tumour microenvironment? What are the driving stimuli? And what are the functional consequences? Recent studies have begun to answer some of these questions by transcriptionally profiling lymphatics from the primary tumour site to understand better how factors derived from the tumour microenvironment alter lymphatic phenotype and function. Studies have identified significant changes pertaining to immune-associated receptors and tight junction molecules, in lymphatics isolated from murine fibrosarcomas¹ and identified a distinct gene signature, in collecting lymphatic vessels from metastatic VEGF-D-expressing tumours, with changes to cell surface markers, secreted factors and ECM proteins described². These two studies demonstrated that factors derived from the tumour microenvironment likely have multiple effects on lymphatics depending on their site, be it capillaries at the primary tumour or larger collecting vessels. Thus, it would be entirely feasible to propose that factors derived from the tumour microenvironment are also likely to alter lymphatics in a manner specific to tumour-draining lymph nodes

(TDLNs). Collectively, this highlights a need for better understanding of how lymphatics adapt within the tumour microenvironment and what their role is within TDLNs. The following literature review will outline our current understanding of lymphatic biology in health and disease and introduce emerging roles of lymphatics and mechanisms of lymphatic involvement within the tumour microenvironment.

1.2. Structure and function of the lymphatic system

The lymphatic system comprises of a network of capillaries, collectors, nodes and ducts, which primarily function to maintain tissue fluid homeostasis. Lymphatic vessels operate closely with the blood vasculature, collecting protein-rich exudates from blood vessels. Once in the connective tissue compartment these exudates are referred to as interstitial fluid or pre-lymph, and the subtle movement of this fluid, through the interstitium towards lymphatics, interstitial flow. Disruption to this finely tuned balance of vessel leakage and drainage can result in fluid accumulation and pathologies such as lymphedema. Throughout the lymphatic system distinct molecular patterns and morphologies exist to support location-specific functions. The following will outline the structure and function of lymphatic vasculature focusing on lymph composition, the role of lymphatic endothelial cells and lymph node morphology.

1.2.1. Structure and organisation of lymphatic vasculature

The lymphatic system comprises a hierarchal structure of initial, pre-collecting, collecting lymphatic vessels and lymph nodes (Figure 1.1a). Initial lymphatics are small blind-ended (30-80µm diameter) vessels with thin walls generated by loosely connected, overlapping LECs, commonly referred to as 'primary valves'³. LECs are attached to surrounding elastic fibers in the ECM via anchoring filaments⁴. Upon elevated interstitial pressure, initial lymphatics respond to the need for drainage via the anchoring filaments, which "pull" due to the expanding interstitium. This in turn opens adjacent LECs permitting interstitial fluid to enter^{6,7} (Figure 1.1b).

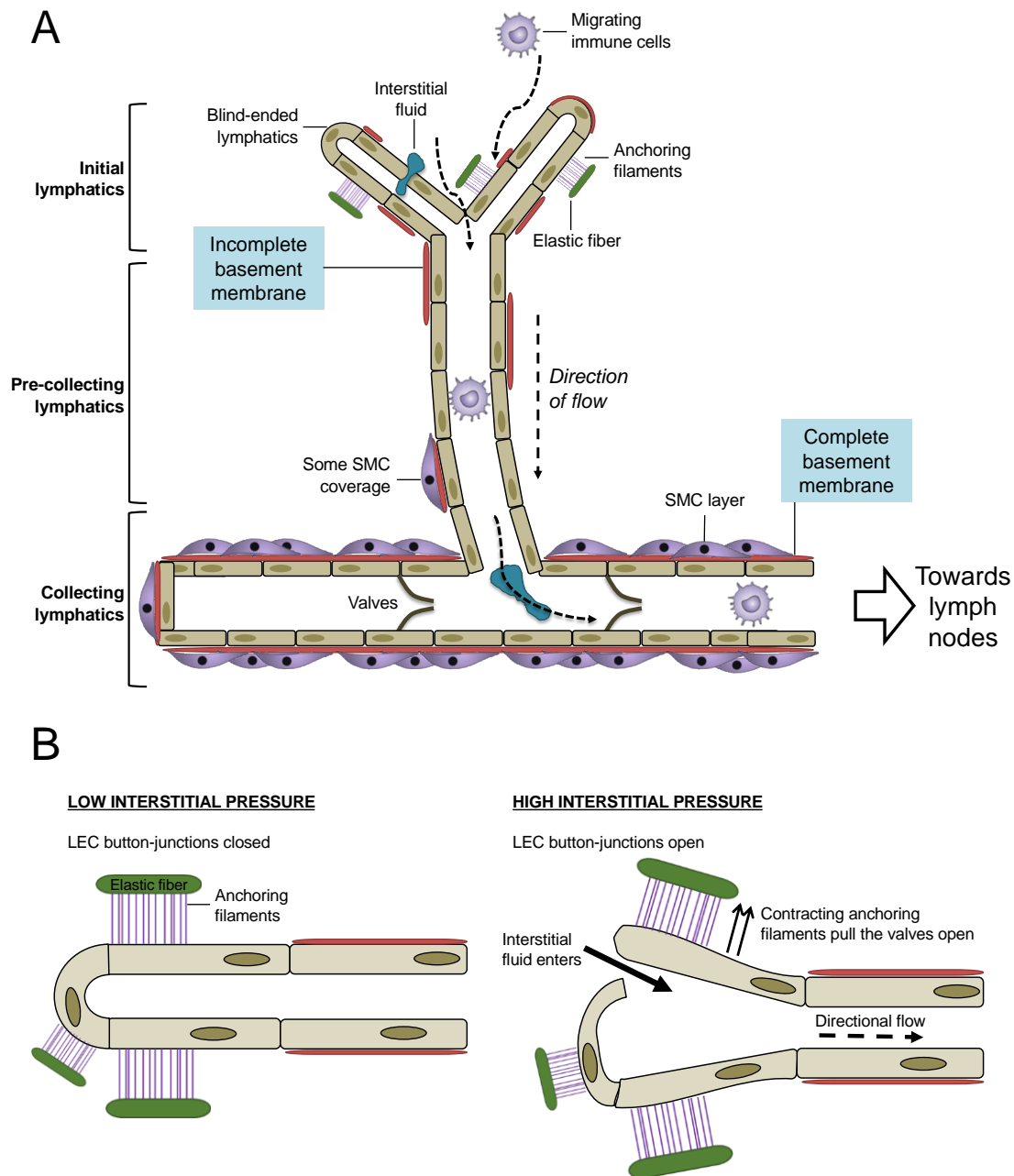


Figure 1.1. Hierarchical organisation of lymphatics in the periphery. The lymphatic network in the periphery comprises of a hierarchal structure of initial, pre-collecting and collecting lymphatic vessels, with lymph lying downstream. Initial lymphatics are blind-ended vessels with incomplete basement membrane, which permit easy access to interstitial fluid and migrating immune cells. Pre-collecting lymphatics exhibit similar characteristics and drain lymph towards larger collecting lymphatics, which are similar to blood vessels, with a complete basement membrane that provides vessel support and play a role in formation and maintenance. Assisting in movement of lymph in pre-collecting and collecting lymphatics are smooth muscle cells (SMCs), which act as the motor unit for lymphatic drainage. Their contractile properties provide rhythmic contractions, which represent the principal mechanism for lymphatic flow. Valves throughout the collecting lymphatics then assist in directional flow. Throughout the system, anchoring filaments, which LECs use to attach to the surrounding elastic fibers in the ECM, provide structural support (A). They further assist by opening adjacent LECs to permit fluid entry when the tissue is under high interstitial pressure by contracting (B). Adapted from Stacker et al., *Nat Rev Cancer* (2014)⁵.

In contrast to blood vessels, initial and pre-collecting lymphatic vessels have a discontinuous basement membrane and no supporting smooth muscle cells (SMCs), with occasional valves found in pre-collecting vessels (Figure 1.1a). Collecting lymphatics, however, adhere to more conventional vasculature characteristics with continuous basement membrane, intraluminal valves dispersed between functional units, called lymphangions, and associated SMCs to assist in the peristaltic, unidirectional flow of lymph^{8,9,10}.

1.2.2. Characterisation of lymphatic endothelial cells

Despite lymphatic vasculature being observed as early as the 17th century and documented in 1902^{11,12}, the lack of specific lymphatic markers hampered accurate characterisation of LECs. Since then, lymphatic markers such as podoplanin (PDPN), lymphatic endothelial hyaluronan receptor-1 (LYVE-1)^{13,14} prospero-related homeobox-1 (PROX-1)¹⁵ and vascular growth factor receptor-3 (VEGFR-3)¹⁶ have been identified enabling the isolation and characterisation of LECs, and exploration of lymphatic function in health and disease^{17,18}. Further characterisation via microarray identified over 400 differentially expressed genes in cultured lymphatic and blood endothelial cells. Amongst these genes, distinct sets of cytokines, chemokines, receptors, adhesion molecules and cytoskeletal proteins were identified, with PROX-1 found to be a cell fate determinant – driving transcription of LEC-specific targets such as vascular endothelial growth factor-C (VEGF-C) and VEGFR-3^{19,20}, prior to budding of the earliest lymphatic vessels during embryonic development. PROX-1 knockout models highlighted defects in lymphangiogenesis²¹ and reprogramming of LECs into blood endothelial cells (BECs)^{15,22}. Original microarray datasets have also been revisited and new differential markers identified, such as melanoma cell adhesion molecule expressed on BECs, and collectin placenta-12 expressed on LECs²³.

More in depth characterization of LECs using murine ear wholemounts revealed distinct junctional characteristics that discriminate between initial and collecting lymphatics. Whilst all lymphatic vessels examined expressed typical lymphatic markers LYVE-1, PROX-1, CD31 and VE-Cadherin, the distribution of VE-Cadherin

differed³. In initial lymphatics, VE-Cadherin was observed in discontinuous hotspots interspersed between CD31, whereas in collecting LECs, expression of VE-Cadherin was continuous, and the terms “button” and “zipper” junctions respectively were coined (Figure 1.2). Unlike “zipper” junctions which are a general characteristic of vascular endothelium, “button” junctions are unique to initial lymphatic capillaries. VE-Cadherin in both initial and collecting vessels also localised with typical junctional molecules Occludin, Claudin-5, Zonulin-1, ESAM, and Jam-A³. Confirming these observations, Murfee et al., (2007) showed CD31 and VE-Cadherin expression was discontinuous in initial lymphatics, with terminal lymphatics exhibiting lower CD31 expression and smaller junctional gaps between neighbouring cells²⁴. Little is known of the precise functional differences in lymphatics across the broader network, but it is likely that variance in expression of certain markers contributes to functional distinction.

As well as variance in expression based on LEC locality, transmural flow (across the endothelial barrier), as occurs when fluid enters initial lymphatics has been shown to stimulate delocalisation of CD31 and VE-Cadherin, and decrease their expression at both RNA and protein levels²⁵. Identified as endothelial-specific flow sensors in blood endothelial cells, CD31 and VE-Cadherin are already known to modulate endothelial cell remodelling and junctional integrity in response to shear stress^{26,27}; hence these results suggest similar mechanisms occur in lymphatic vessels.

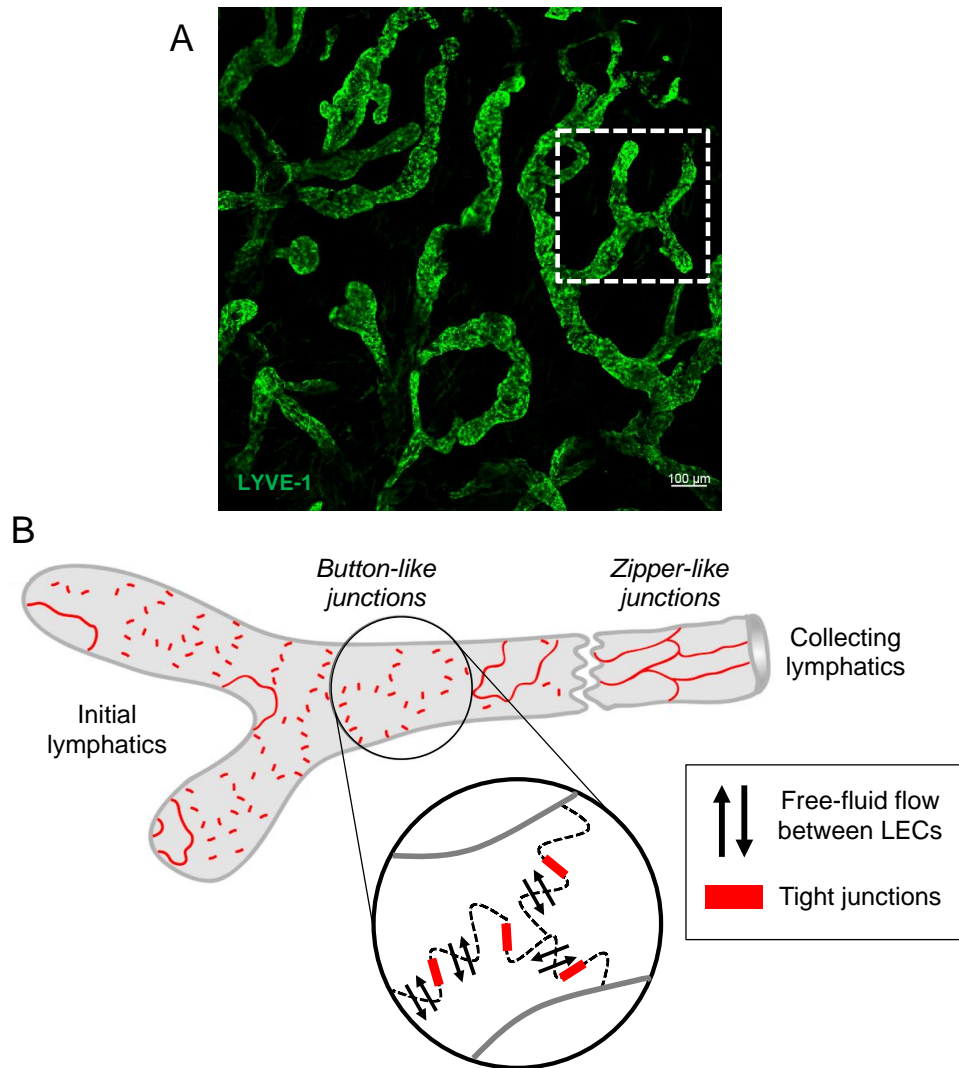


Figure 1.2. Lymphatic endothelial cells junctions. Representative image of lymphatic vessels in murine ear dermal sheets, stained for lymphatic marker, LYVE-1 (1:300), and imaged using confocal microscopy at 20x magnification. Scale bar represents 100μm (A). Blind-ended initial lymphatics and pre-collecting lymphatic vessels have similar junctional organisation, with “button” junctions between flap-like lymphatic endothelial cells. These contain proteins of adheren and tight junctions and enable free-fluid flow between neighbouring cells. In contrast, collecting lymphatics have continuous “zipper” junctions, which are less permeable to prevent fluid loss of lymph in collecting lymphatics (B). Adapted from Baluk et al., *J Exp Med* (2007)³.

Variability in junctional molecule expression across the lymphatic network may also be induced by other factors. VEGF has been shown to disrupt endothelial barrier function through the activation of VEGF-R2, which in turn mediates phosphorylation of a serine motif in the intracellular tail of VE-Cadherin in a Rac/Src-dependent manner^{28,29}. This resulted in β-arrestin2 dependent internalization of phosphorylated

VE-Cadherin via clathrin-coated vesicles and consequent junctional disassembly. To demonstrate its requirement in VE-Cadherin internalization, shRNA against β -arrestin2 protected against VEGF-induced permeability²⁹. Furthermore, blocking VE-Cadherin with neutralizing antibodies increased pulmonary metastasis of CT29 carcinoma cells in mice, and significantly fewer metastatic lesions were observed in Src-deficient mice²⁸. This supports previous findings showing pharmacological inhibition of Src attenuates VEGF-dependent endothelial permeability but does not affect VEGF-mediated angiogenesis³⁰. In addition to VEGF family members, a number of other regulators have been identified, including TGF- β and MMP-9^{31,32} RhoA and Rac^{33,34,35,36}, β -catenin and p120-catenin^{37,38,34}.

Collectively, these studies have contributed to the progressive understand of lymphatic biology, identifying network arrangements, key lymphatic markers and important functional characteristics. Lymphatics are still however relatively overlooked compared to blood vessels and more research is needed to explore further the role of lymphatic identifying markers and how these functional molecules respond in health and disease.

1.2.3. Lymph Composition

The predominant role of lymphatics is to maintain tissue fluid homeostasis. Protein rich interstitial fluid crosses the endothelial barrier, governed by junctional molecules such as CD31 and VE-Cadherin, and enters the lymphatics. Once within lymphatic vessels interstitial fluid, now referred to as lymph, flows into progressively larger collecting vessels onto lymph nodes throughout the body. Lymph enters lymph nodes through afferent lymphatics and exits through efferent vessels, draining through sequential lymph nodes (Figure 1.3). This is a critical process due to the contents of the lymph carried by lymphatics to the lymph node. Proteomic analyses have identified lymph to be enriched with extracellular matrix components, metabolic and catabolic substrates, cell debris, products of tissue growth and remodelling, and a pool of self-antigens^{39,40,41,42,43}. Lymph also carries peripheral tissue-derived immune cells, with the first observations of immune cells in lymph described in 1970⁴⁴. Transporting

immune cells from the periphery to lymph node is an important feature of lymphatic vasculature, explored further in Section 1.2.5.

Once the lymph has drained through sequential lymph nodes, it returns to the blood via the thoracic duct into the left and right subclavian veins, which deliver the lymph into the vena cava and ultimately back to the blood circulation (Figure 1.3). Overall, this process serves as the means by which our immune system continuously samples the periphery, and since lymph nodes are key centres for priming of immune responses, lymphatics hence directly assist in immune surveillance through the supply of antigen and immune cell-rich lymph. The structure and role of the lymph node is explored further in the next section (Section 1.2.4).

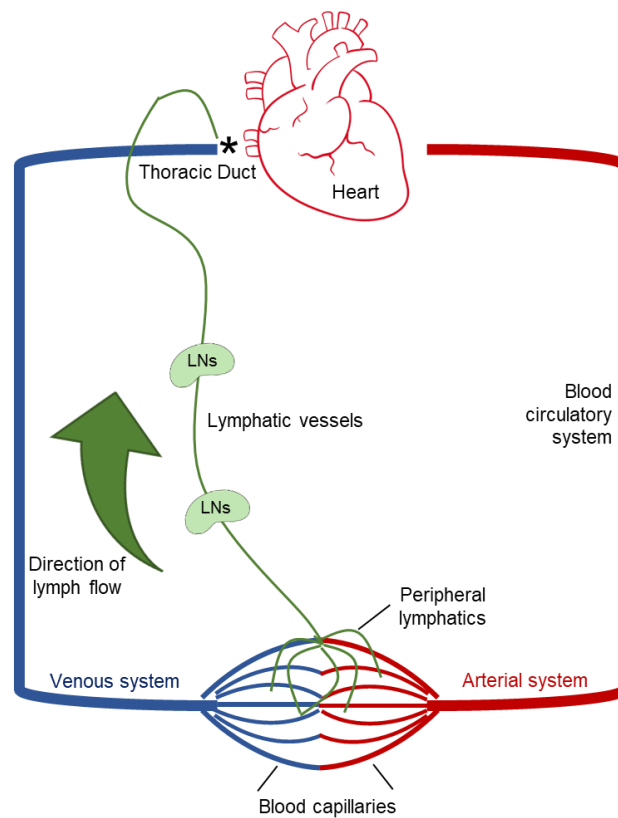


Figure 1.3. Journey of lymph through the lymphatic and blood system. Interstitial fluid entering peripheral lymphatics, referred to as lymph, flows through lymphatic vessels via a daisy-chain of lymph nodes. Arrow indicative of direction of flow. This is a critical step in mounting an immune response, as it facilitates lymph node sampling of the lymph's content, such as antigen. Lymph returns to the blood circulatory system via the largest lymphatic vessel in the body, the thoracic duct (*).

1.2.4. Lymph Node Morphology and Function

With over 500 lymph nodes dispersed throughout the human body, lymph nodes are secondary lymphoid organs essential for draining lymph carried from the periphery by lymphatic vessels. The primary role of lymph nodes is to provide a centre for leukocyte activation and mobilization, assisting in effective immune surveillance and optimal immune responses through the drainage of peripheral material and antigen-loaded APCs.

To enable these functions, the lymph node relies on a high degree of structural organization and compartmentalisation (Figure 1.4a). This structure is critical for disseminating lymph across the node and ensuring immune cell organisation optimal for mounting an immune response. The lymphatics form a key component of the lymph node with lymphatic tissue present in afferent and efferent lymphatic vessels, the subcapsular sinus (SCS), the cortex, and the medulla (Figure 1.4b). This network of lymphatic sinuses allows lymph to infiltrate the lymph node and access the zones containing diverse immune populations. Lymph entering via afferent lymphatic vessels, first traverses the subcapsular sinus (SCS), whereby LECs line both the ceiling and floor of the capsule. From there lymph permeates the lymph node via cortical sinuses into medullary sinuses and leaves via the efferent lymphatic vessels. Size-exclusive properties of LECs at the subcapsular sinus, ensures that large molecules within the lymph do not have direct access to the lymph node. Instead small molecules (<70kDa), such as chemokines and antigens are permitted to rapidly cross the endothelium and reach the T-cell and B-cell follicles through the conduit system^{67,56}. This characteristic is shared by all lymphatic tissue in the lymph node and is crucial in supporting antigen sampling in a controlled manner. The manner to which this size-exclusion barrier is altered in health and disease and in particular in the context of the tumour microenvironment and metastasis, is yet to be elucidated. Components of the lymph can also be sampled actively by LECs and particularly by interspersed CD169⁺ macrophages, shown to uptake lymph-derived exosomes⁶⁸, dead tumour cells⁶⁹, viral particles⁷⁰ and antigen immune complexes⁷¹. The medullary sinuses, also lined by lymphatic endothelium and medullary macrophages complete the network by which lymph bathes the lymph node. From here, lymph egresses via efferent lymphatic vessels.

In addition to the lymphatic infrastructure, the lymph node cortex and paracortex regions are comprised of specific T-cell zones and B-cell follicles interspersed with high endothelial venules (HEVs). These HEV portals provide further access points for migratory immune cells, with ingress and egress both occurring at these sites^{72,73,74}. Access to these regions is permitted by collagen conduits lined with fibroblast reticular cells (FRCs), which provide physical highways for migratory immune cells to crawl along, and further directional cues, in the form of chemokine gradients^{75,76,77}.

In particular, chemokines CCL19, CCL21 and CXCL13 have been identified as the main stromal cell-derived factors that guide migration and localisation of lymphocytes within the node. CCL21 in particular is of key importance to the migration of DCs from the edge of the lymph node to the inner regions of the lymph node. LECs secrete CCL21, which acts as a directional cue for DCs expressing the CCL21-receptor, CCR7. This is assisted by expression of chemokine scavenger, CCRL1, which promotes the establishment of a gradient in favour of lymph node⁶⁶ (Figure 1.4c). In addition to guiding DCs, CCL19 and CCL21^{78,79} control motility and migration of naïve T-cells, and retention of cells in T-cell zones. CXCL13 is however essential for homing of naïve B-cells to B-cell follicles⁸⁰, although the chemical cues for B-cell retention are yet to be defined. The mechanistic role of lymphatics in immune trafficking from periphery to lymph node is explored further in Section 1.2.5.

This tier of structural organisation, held together by guiding chemokines, is the foundation of mounting an effective immune response. To mount an adaptive immune response, interactions between naïve T-cells and APCs such as DCs must occur. CCR7 is a critical to this interaction, with expression of CCR7 on mature DCs guiding them, not only across the subcapsular sinus, but then onto FRC conduits into T-cell zones, where they come across awaiting naïve T-cells⁸¹. Expressed by T-cells, CCR7 guides CD62L+ naïve and central memory T-cells into the T-cell cortex of lymph nodes via HEVs where they come across antigen-bearing dendritic cells. In order to become activated by an APC, T-cells constantly recirculate from the blood to a lymph node and survey the lymph node until it encounters an APC expressing antigen peptide displayed on MHC molecules, that it can bind to⁸². This physical engagement, known as the formation of an immunological synapse, can last for over an hour and initiates an activation and proliferation programme that drives expansion of antigen-specific T-

cells⁸³. Conversely, effective initiation of this programme has also been reported to require multiple transient interactions⁸⁴. Once activated, T-cells proliferate in the lymph node for 3-7 days and acquire egress receptors that allow them to exit the lymph node and traffic to the inflamed peripheral tissue in question⁸⁵. Loss of CCR7 expression and S1P signalling are both well understood to govern the process of egress from the lymph node back into the circulation⁸⁶.

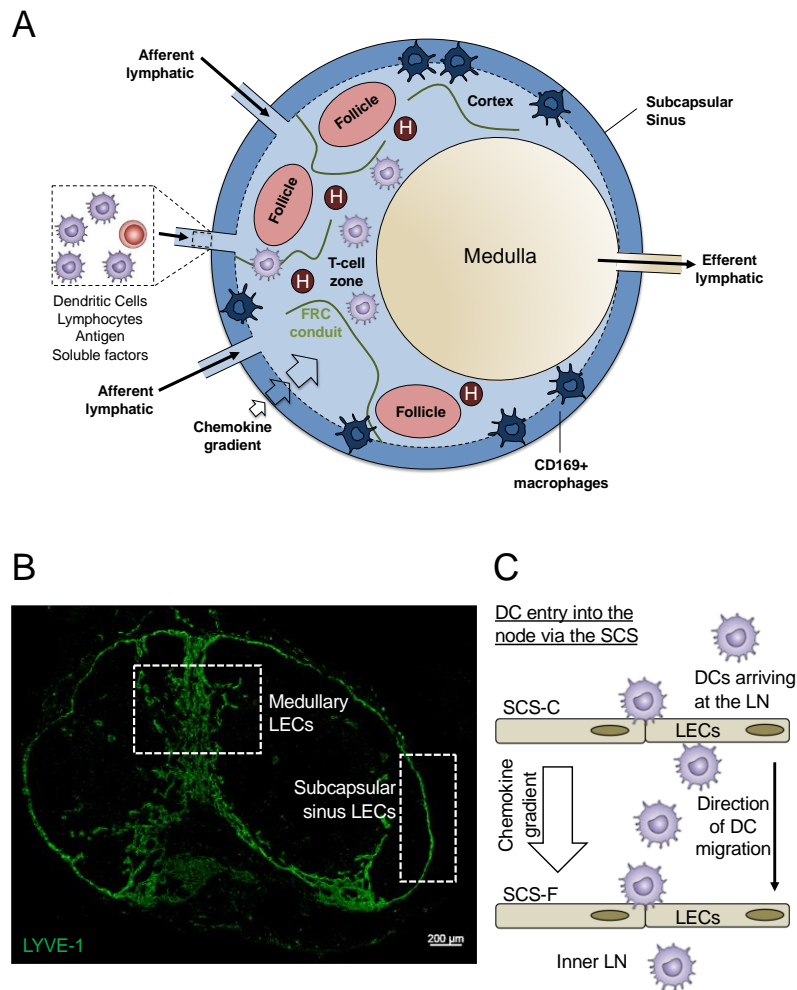


Figure 1.4. Structure and organisation of the lymph node. Lymph nodes are highly organised lymphoid organs, with three main regions – the subcapsular sinus, the medulla and the cortex. The subcapsular sinus encapsulates the node and is predominantly comprised of lymphatic endothelial cells and CD169+ macrophages. In addition to filtering cellular entry the subcapsular sinus (SCS) also controls entry of antigen and other soluble factors through permeable features of the lymphatic lining (dashed line). Incoming migratory immune cells and peripheral material enters the node via afferent lymphatics and other immune cells, such as naïve T-cells, enter through high endothelial venules (H). This is assisted by chemokine cues, which guide immune cells into the node from afferent lymphatics (grey arrows). Incoming immune cells traffic to their relative locations within the node via fibroblast reticular cell (FRC) collagen-rich conduits. A critical region for T-cell accumulation is the paracortex, which is the primary location for T-cell priming by antigen-loaded DCs. This interaction results in an immune response being mounted. The outer cortex is the site of B-cell antigen searching, comprised of B-cells and follicular DCs clustered into follicles. Upon exit, egressing immune cells leave the lymph node through the medulla and efferent lymphatic vessels, as well as high endothelial venules (A). Lymphatics are a key compositional element of the lymph node, with LYVE-1 expressing LECs found in the medulla and subcapsular sinus, acting to disseminate arriving lymph throughout the node, as visualised using confocal microscopy (B). Lymphatics at the subcapsular sinus, specifically function to ensure arriving immune cells from the periphery, e.g. DCs, can enter the lymph node. This is achieved from establishing a chemokine gradient which promotes migration from the subcapsular sinus ceiling (SCS-C) to the subcapsular sinus floor (SCS-F). With the appropriate chemotactic cues, DCs are able to transigrate across LEC monolayers, which form the lining of the SCS-C and SCS-F, entering the inner lymph node (LN) space (C). Adapted from Girard et al., *Nat Rev Immunol* (2012)⁷².

1.2.5. LECs as mediators of immune cell trafficking

Recent findings from investigations into DC trafficking, demonstrate that migration into and within lymphatics occurs in stages^{55,63}. Firstly, haptotactic migration of chemokine receptor-expressing DCs, guided by lymphatic-derived chemokines, attracts DCs towards initial lymphatic vessels. Secondly, DCs physically dock to LECs through adhesion to CAMs; a process also supported by chemokines⁶². Thirdly, DCs enter initial lymphatic vessels by squeezing through flaps between neighbouring LECs^{3,58} with the characteristic discontinuous basement of initial lymphatics leaving physical gaps for entering cells²⁷⁰. Recent research has further found that once within initial lymphatic vessels, DCs proceed to actively crawl along the vessels, with bidirectional patrolling behaviour described^{62,63}. The role of chemokines and CAMs in these initial stages of migration has been well documented and is described below. The final stage of migration is a passive process, whereby immune cells that reach the downstream collecting lymphatic vessels are subject to rapid lymph flow which transports peripheral-derived immune cells to lymph nodes within 6hrs to 24hrs^{62,220,271}. Within these collecting lymphatic vessels, valves prevent backwards flow of lymph, similarly to the role of valves in blood vessels, further assisting in the movement of immune cells along the lymphatic vessels.

As stated above, chemokines are essential for directional migration of immune cells. Two lymphatic-derived chemokines, CCL19 and CCL21, are well-documented in lymph node homing through interactions with their receptor CCR7, expressed on migratory immune cell populations. Evidence for CCL21 in DC migration in particular, was first determined by tracking DC migration from footpads to draining lymph nodes in the presence of administered CCL21-neutralising antibody²⁷⁹. Administration of CCL21-neutralising antibody blocked migration of skin-derived DCs by 50%, demonstrating a critical role for CCL21 in DC lymph node homing²⁷⁹. It was later revealed that murine CCL21 exists in two isoforms, CCL21-A (CCL21-serine) and CCL21-B (CCL21-leucine), whereby CCL21-A was found in both peripheral lymphatics and lymphoid tissue lymphatics, whereas CCL21-B was found exclusively in peripheral lymphatics^{280,281}. Recent work has been focused on identifying mechanisms of how CCL21 expression is regulated and how lymphatic-derived CCL21 guides DC migration.

In initial lymphatics, CCL21 is produced and secreted by LECs, which binds the basement membrane^{62,63} and heparan sulfates in the interstitium²⁷². This creates an immobilised gradient which guides CCR7-expressing cells, such as DCs, through the interstitium towards lymphatic vessels. A positive feedback loop has also been described, with the physical interaction of DCs with LECs shown to induce calcium-dependent secretion of CCL21 to extracellular sites⁵⁷. Secreted CCL21 was found to localise to endothelial cell-to-cell junctions, demonstrating a role in transmigration of DCs across lymphatic endothelium⁵⁷. The secretion of CCL21 has also been shown to be an inflammation inducible mechanism, with intracellular CCL21 rapidly secreted in a calcium-dependent manner, by LECs upon exposure to the inflammatory cytokine, TNF- α ^{57,231}. CCL21 deficient mice not only demonstrated perturbed migration, but also dendritic cell maturation and T-cell priming functionality was seen to be perturbed proposing additional roles in dendritic cell immunity²³⁰. The role of CCL21 in migration of DCs at the lymph node is described later in this section.

Other soluble factors have been reported to govern immune cell migration, with Semaphorin-3A and Semaphorin-7A found to be critical for chemokine-driven dendritic cell lymph node homing, transmigration and associated cytoskeletal rearrangements²²³. Semaphorins however also regulate T-cell and neutrophil immunity, with Class-3, 4 and 7 Semaphorins described to modulate neutrophil migration^{224,225,226} and Semaphorin-6D and -3A shown to regulate T-cell activation and proliferation²²⁷. Interestingly, Semaphorins can also act on endothelial cells, with Semaphorin-6A and -6D driving VEGF-mediated angiogenesis²²⁸ and Semaphorin-3F regulating lymphatic endothelial cell migration²²⁹.

In addition to establishing chemotactic cues for immune cell migration, LECs express many molecules to facilitate tethering of migrating immune cells. During inflammation, DC entry into the lymphatics and downstream LNs is dependent on up-regulation and engagement of adhesion molecules ICAM-1 and VCAM-1 on LECs^{25,45}. Specifically, inflammatory cytokines TNF- α , and myeloid derived IFN- γ , have been described as key regulators of CAM expression^{45,46,47,48}. TNF α -mediated, integrin-dependent trafficking has also been described for neutrophil and T-cell migration into and along lymphatic vessels^{49,50,51}. More recent research has also demonstrated a role for

lymphatic marker, LYVE-1, in DC docking to lymphatic endothelium. Here, *in vitro* and *ex vivo* studies demonstrated that DCs dock to the basolateral surface of lymphatic vessels through interactions between DC-expressed hyaluronan and LYVE-1 to form 'transmigratory cups' around the migrating cell⁵². CD31 has also been cited as a critical adhesion molecule in the transmigration of human dendritic cells across lymphatic endothelium⁵⁹. Conversely, Jam-C is a negative regulator of immune cell migration, with blockade resulting in increased DC migration to draining lymph nodes and reduced monocyte infiltration into inflamed tissues^{60,61}. Other membrane bound molecules involved in immune cell trafficking include, the OX-2 membrane glycoprotein, CD200, and Chemerin receptor, CMKLR1. Endothelium-expressed CD200 binds immune cell receptor CD200-R, is regulated by LPS during tissue inflammation and facilitates immune cell adhesion²³². The role of Chemerin is variable and not well understood; studies have reported actions on both endothelial cells and immune cells to promote angiogenesis and transmigration via enhanced affinity association with VCAM-1²³³, with chemerin receptor found to be expressed on both endothelial cells and trafficking immune cells²³⁴.

Having arrived at the lymph node, recent evidence demonstrates that immune cell migration across the subcapsular sinus can occur via conventional paracellular modes, or transcellular migration via the formation of transcellular pores comprised of Plasmalemma vesicle-associated protein (PLVAP) and F-actin⁵⁶. *In vivo* work conducted using PLVAP-deficient mice observed hyperpermeability at the lymphatic subcapsular sinus, with loss of antigen filtration and augmentation of lymphocyte entry to the lymph node. As wild-type immune cells traverse the sinus with similar efficacy as CCR7 knockout cells⁵³, this is the first to document a mechanism for immune cell migration across the lymph node sinus. However, whether this protein is also important for immune cell entry to lymphatic vessels at the periphery is unknown. CCL21 is also critical for lymph node entry, with LECs and FRCs within the lymph node secreting the chemokine, assisting in directional migration across the lymph node. LECs lining the ceiling of the subcapsular sinus also express chemokine scavenger, ACKR4, also known as CCRL1, which mops-up CCL21 and establishes a chemokine gradient across the subcapsular sinus, in favour of lymph node entry⁶⁶. CCRL1 knockout mice exhibit a significant reduction in the number of migratory CD103+ DCs in draining lymph nodes, showing its specific importance for migration of skin-derived DCs⁶⁵. This

has been further reported to occur in the dermis, with dermal LECs expressing CCRL1, enabling the scavenging of CCL19⁶⁵ and thus facilitating egress of dermal migratory dendritic cells from the skin, in a CCL19-dependent manner⁶⁵; this further supports entry and transmigration into initial lymphatics. Recent work has also identified stromal marker, Podoplanin, as critical for dendritic cell mobility within lymph nodes, describing CLEC-2 ligand interaction to induce cytoskeletal rearrangements and promote crawling along reticular networks⁷⁷.

Lymphatics therefore, provide not only a means of maintaining interstitial homeostasis through tissue fluid drainage, but also act as a critical component of the immune system as conduits for antigen sampling and immune cell trafficking, via secretion of guidance cues and essential tethering molecule expression to facilitate transmigration.

1.3. The role of lymphatics in inflammation

1.3.1. Lymphangiogenesis in inflamed tissues

Further to their role in immune cell trafficking, the role of lymphatics during inflammation has been an area of investigation. Lymphangiogenesis is considered to be a critical part of the initiation and resolution of inflammation, with the expansion of lymphatic networks at sites of inflammation and in draining lymph nodes^{87,88,89}. The VEGF family has been identified as dominant drivers, with VEGF-A/C/D all capable of inducing lymphangiogenesis through ligation of their cognate receptors, VEGFR-2/3, expressed on the surface of LECs⁹⁰.

Macrophages are a significant source of VEGF-C/D^{91,92} with reports of high expression by CD11b+ macrophages⁹³ and M2 subtypes⁹⁴. Macrophages have further been shown to act as direct lymphatic vessel precursors, with CD11b+ macrophages forming tube-like structures and expressing LYVE-1 and Podoplanin⁹³. Macrophages also migrate to draining lymph nodes, whereby production of VEGF-A induces localised lymphangiogenesis⁹⁵. Beyond the macrophage, neutrophils are implicated in lymphatic expansion, driving inflammatory lymphangiogenesis through production of active VEGF-A and VEGF-D in experimental models of inflammation⁹⁶. In addition,

resident B-cell and FRC populations drive VEGF-A/C mediated lymphangiogenesis in lymph nodes^{97,98}. Intrinsic NF-kappaB signalling has also been shown to up-regulate expression of VEGFR-3 on the surface of LECs, promoting lymphatic responsiveness to lymphangiogenic factors⁹⁹.

As well as growth factors, a number of cytokines have been reported as regulators of lymphangiogenesis during inflammation with TNF- α found to drive vessel remodelling and lymphangiogenesis *in vivo* in *M.pulmonis*-infected mice²⁶⁹ and pro-inflammatory cytokine IL-33 found to promote proliferation, migration and tube formation in LECs *in vitro*²⁶⁸. Cytokines IL-4 and IL-13 has also been found to inhibit lymphatic vessel formation and down-regulate LEC-specific markers PROX-1 and LYVE-1 in *ex-vivo* and *in-vitro* experiments¹⁰¹.

The precise function of lymphangiogenesis at the site of inflammation is considered primarily to be a homeostatic response that ensures drainage of excessive tissue fluid, which accumulates by enhanced blood vessel permeability. Indeed, in the case of lymphatic dysfunction, aberrant lymphatic vasculature is associated with tissue swelling and fluid accumulation, also known as lymphedema^{102,103}. Its other defined role in inflammation is in immune modulation, as enhanced lymphatic drainage also increases the delivery rate of antigen and antigen-bearing DCs to draining lymph nodes. As previously described, exposure to antigen and antigen-bearing DCs is absolutely critical for the initiation of an immune response, hence expanded lymphatic networks facilitate this during inflammation.

1.3.2. Lymphatics as innate responders to inflammatory stimuli

As well as responding to inflammatory stimuli through lymphangiogenesis, LECs express a wide range of immune receptors that opens them up to further modulation by inflammatory cues. LECs express IFN-receptors, IFN α -R1/2 and IFN γ -R1/2, allowing IFN to induce proliferation and up-regulation of a number of surface markers, namely E-selectin, ICAM-1 and MHC-II^{48,100}. IFN- γ has been further shown to drive NOS2-dependent NO production andIDO expression in lymphatics^{104,100}; further implications of this for the immune response are described later in this chapter. LECs

also express functional TLRs. In both murine and human LECs, TLR-1, 2, 3, 4, 5, 6 and 9 allow LECs to respond to pathogen associated molecular patterns (PAMPs) and danger associated molecular patterns (DAMPs)¹⁰⁵. TLR stimulation led to IL-1 β , TNF- α and IL-6 expression in primary dermal LECs *in vitro*, which was further accompanied by increased mRNA expression of VEGF-C and VCAM-1/ICAM-1. This suggests a TLR-mediated role in lymphangiogenesis and immune cell migration, through enhanced expression of cell adhesion molecules. Collectively this data indicates LECs as active responders during the inflammatory process, suggesting an important role in inflammatory regulation beyond cellular and fluid trafficking.

1.3.3. Lymphatics as regulators of inflammation

As described above, lymphatics expand during inflammation and express a repertoire of immune receptors that propose a more active role in the inflammatory process than originally thought. As well as responding to inflammatory cues, lymphatics also play an active role in orchestrating localised immunity. LECs have been shown to express a plethora of cytokines and other immune modulatory soluble factors, as reviewed in¹⁰⁵. As well as a wealth of chemokines, expression of pro-inflammatory cytokines IL-1 β and IL-6 have been reported in murine and human LECs cultured *in vitro*, with toll-like receptor (TLR) ligation inducing expression¹⁰⁶. IL-8 is also produced by lymphatics¹⁰⁶, a cytokine known to promote neutrophil recruitment and activation. These findings support LECs as responders to pathogen-induced inflammation and promoters of immune cell recruitment capable of sustaining a pro-inflammatory cytokine milieu. However, lymphatics also produce the potent anti-inflammatory cytokine TGF- β ^{106,108,16}, which may further act in an autocrine fashion to drive lymphangiogenesis¹⁰⁹ and adhesion to the extracellular matrix in low oxygen conditions¹¹⁰. Lymphatics also assist in maintenance of T-cells in lymph nodes through IL-7 production, which is required for survival of naïve and memory T-cells¹¹¹ and is an important factor for lymphangiogenesis, as both LN and peripheral LECs respond to IL-7 in an autocrine fashion¹¹².

Moreover, LECs produce a number of other factors; with LEC/T-cell co-culture studies confirming IFN- γ inducible, NOS-dependent NO production and IDO expression^{104,100}.

Both NO and IDO have immune regulatory properties with NO considered an anti-inflammatory under steady state conditions and a mediator of inflammation in disease states¹¹³.

Overall, these findings suggest a complex interaction between immune populations and LECs, emphasising lymphatics as active immune modulators in both healthy and inflamed tissues. As we know the immune status of the tumour microenvironment is instrumental in defining tumour fate, investigation into the immune contributions of lymphatics both at the primary site and draining nodes may identify novel mechanisms for LEC-mediated immune modulation and tumour progression.

1.3.4. LECs as amateur antigen presenting cells

Further to their roles in mobilising and transporting immune cells in the lymph node to initiate immune responses, it is becoming clear that LECs have a much more complex role within the immune system. It is emerging that LECs have tolerogenic properties, replicating the function of professional APCs such as dendritic cells, by directly presenting antigen to T-cells to drive T-cell deletion.

The first to describe stromal cells as having the capacity to present peripheral antigen, found that within lymph nodes, professional DCs were not essential for inducing effector T-cell tolerance. Instead, lymph node stromal cells expressing peripheral tissue antigens (PTAs) could present to naïve CD8+ T-cells, leading to the elimination of antigen-specific self-reactive T-cells *in vivo*¹¹⁴. This occurred via MHC Class I, with some evidence indicating expression via MHC Class II also¹¹⁴. Of interest was the T-cell specific nature of this mechanism, as stroma-mediated T-cell activation and deletion did not affect CD4 T-cells¹¹⁵. Of particular relevance to anti-tumour immunity, constitutively expressed melanocyte/melanoma tyrosinase antigen in peripheral and mesenteric lymph nodes, led to apoptosis of tyrosinase-specific T-cells. Similarly to other publications, DCs were not involved in tyrosinase-induced tolerance, suggesting another cell type with APC capacity¹¹⁶. Lymph node resident melanoblasts, which act as precursor cells for melanocytes, also drove antigen-specific CD8+ T-cell deletion, proposing a global phenomenon of induced tolerance to peripheral antigens governed

lymph nodes resident stromal cells¹¹⁷. Upon closer examination of the specific stromal cell responsible for T-cell deletion, antigen-specific *in vivo* models identified LECs as capable of direct antigen presentation. Self-antigens presented on MHC Class-I by LN-LECs led to subsequent deletion of self-reactive CD8+ T-cells^{118,119} identifying LECs as modulators of self-antigen driven tolerance.

As lymph nodes are bathed in peripheral-derived exogenous antigen, more recent studies have explored the interaction between lymphatics and antigen that drains to the lymph node. In the context of viral challenge, one group demonstrated that injected fluorescently conjugated ovalbumin (OVA) drained to lymph nodes and co-localised with LYVE-1 positive regions¹²⁰. Antigen persisted in the lymphatic compartment, thus the group proposed the phenomenon of antigen uptake, but also antigen “archiving” by LN-resident LECs. This process appeared dependent on T-cell expansion, however did not depend on an antigen-specific response, suggesting an intrinsic mechanism for lymphatic expansion during inflammatory responses¹²⁰. In contrast, another study implied that LECs are unable to present antigen, instead archiving material to be passed on to dendritic cells that induce T-cell deletion¹²¹.

These findings initiated a growing number of investigations into lymphatic antigen presentation capacity, where murine LECs were shown *in vitro* and *in vivo* to actively scavenge and present peripheral antigens in steady state conditions. Extending upon this foundational knowledge, the authors investigated mechanisms of antigen uptake and presentation in LN-LECs. Using a panel of inhibitors, *in vitro* uptake and presentation was shown to rely on clathrin- and caveolin-dependent pathways, with inhibition of late endosomal / lysosomal transition further affecting antigen presentation¹²². Following this through to T-cell priming, cross-presentation of antigen by MHC Class-I led to impaired activation of naïve CD8+ T-cells, through PD-L1 engagement and concurrent increases in PD-1 expression, resulting in decreased IFN- γ and IL-2 production and early-apoptosis, suggesting an important role for PD-L1 mediated lymphatic deletion of CD8+ T-cells^{119,122}. In support, LN-LECs were found to induce CD8+ T-cell tolerance through complementary Lag-3 and PD-1 engagement, proposing lymphatics as capable of inducing both T-cell death and anergy¹²¹. Interestingly, PD-L1 expression was only detected on LN-LECs with no PD-L1

observed in peripheral LECs¹²³, implying a site-specific function of LN-LECs in T-cell immunity.

1.3.5. Antigen transfer between LECs and DCs

Adding further complexity to the journey of draining antigen through the lymph node, an emerging feature of lymphatic biology is the capacity to transfer antigen to DCs. Two very recent studies demonstrate that LN-LECs in fact rely on antigen transfer to hematopoietic APCs for effective T-cell priming¹²⁰, with migratory DCs specifically identified as the subset capable of doing this¹²⁴. These studies propose an intriguing mechanism by which LN-LECs can indirectly induce T-cell deletion through antigen transfer to professional APCs, in the form of incoming, migratory DCs.

1.4. The role of lymphatics in cancer

1.4.1. Lymphangiogenesis in the tumour microenvironment

Within the tumour microenvironment, a number of soluble and biophysical factors exist to drive lymphangiogenesis (Figure 1.5). In terms of biophysical factors, elevated intratumoural pressure and resultant increased interstitial flow is created by the ever-expanding tumour bulk and is an observational hallmark of tumour progression. This increased flow, changes the tumour-associated stroma, and is sufficient to stimulate the lymphangiogenesis observed. However, as intratumoural pressure leads to the compression of weak-walled lymphatics and loss of function, most lymphangiogenesis in solid tumours is observed in the peritumoural regions^{125,126}. Therefore, fluid is pushed towards the surrounding tumour-associated tissues, rich in lymphatics, where it can be drained^{126,127}. Vessels associated with tumours are either newly formed (lymphangiogenic) or re-modelled from pre-existing vessels. These vessels are frequently hyperplastic or functionally abnormal^{128,129} but can still drain interstitial fluid that leaves the tumour to draining lymph nodes¹²⁵.

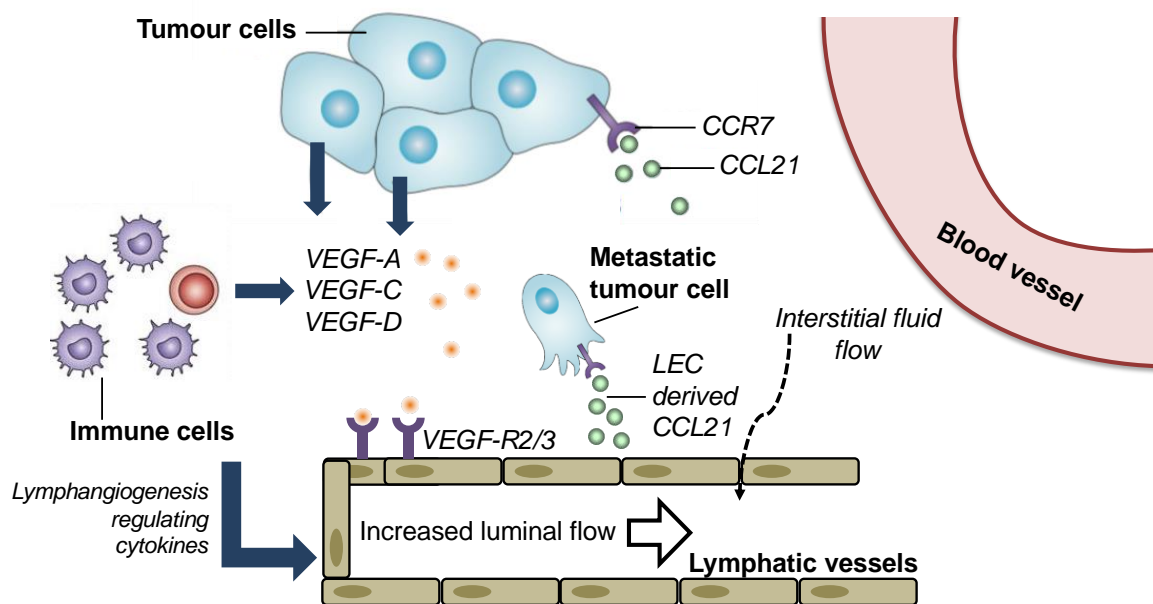


Figure 1.5. Mechanisms of lymphangiogenesis and metastasis in the tumour microenvironment. A number of mechanisms are involved in the process of lymphatic expansion and tumour metastasis in the tumour microenvironment. Vascular endothelial growth factor (VEGF) A, C and D have all been reported to drive lymphangiogenesis through ligation of receptors (VEGF-R2/3) on lymphatic endothelial cells comprising the lymphatic vessels. In addition to pro-angiogenic growth factors, a few immune-cell derived cytokines have been reported to modulate lymphangiogenesis. In addition to cytokines and growth factors, chemokines in the tumour microenvironment guide both immune trafficking and tumour metastasis, with both dendritic cells and metastatic tumour cells using lymphatic-derived CCL21 as a guidance cue. Expression of CCR7 on the surface of dendritic cells and tumour cells facilitates this, with directional cues from interstitial flow further assisting in metastasis. As well as biochemical cues, biophysical cues modulate lymphatic function in the tumour microenvironment, with increased luminal flow regulating both production of CCL21 and intravasation of migrating immune and metastatic cells. VEGF-C can also promote tumour cell metastasis by inducing CCL21 production.

As well as a tissue fluid homeostatic response, lymphangiogenesis has been positively correlated with and causally associated with metastasis. Many tumours, including melanoma^{130,126,137}, squamous cell carcinoma^{138,139}, breast¹²⁷, colorectal¹³¹ and non-small lung cancer¹³², exploit the lymphatics to metastasize to lymph nodes. In fact, the density of lymphatic vessels is predictive of metastasis and was accurate in predicting metastasis in 90% of patients^{126,133}.

To support the process of metastasis, tumour cells use biophysical and biochemical cues to enter lymphatic vessels. Tumour cells have been described to use an

autocrine chemokine-dependent mechanism to drive directional migration. Tumour cells bind self-secreted CCL21 ligand through CCR7 receptor, which paired with interstitial fluid movement, creates autocrine chemokine gradients directed specifically towards functional lymphatics, thus promoting lymphatic homing and dissemination (Figure 1.5). Self-secreted CCL21 and subsequent CCR7-dependent metastasis has been described in melanoma¹³⁴ and breast cancer models^{135,136}. In addition to the role of interstitial movement in creating chemokine gradients, the increased interstitial flow out of tumours can physically separate and 'push' loose tumour cells into associated lymphatics¹²⁹.

In addition to CCL21, other soluble cues contribute to tumour-associated lymphangiogenesis. Secretion of VEGF-C and VEGF-D by the tumour and subsequent ligation of VEGFR-3 on lymphatic vessels has been shown to drive lymphangiogenesis^{127,140} (Figure 1.5). As well as tumour-derived secretion, tumour-associated macrophages (TAMs) also produce pro-lymphangiogenic VEGF-C and VEGF-D¹⁴¹, highlighting both tumoural and immune derived lymphangiogenic cues in the tumour microenvironment. Manipulating the VEGF signalling axis has been the focus of many developing targeted therapies, with VEGF-R targeting shown to block lymphangiogenesis^{145,146,90}. However, little is still known of the role VEGF-C and VEGF-D play in lymph node lymphangiogenesis and how blockade affects lymphatic changes in tumour-draining lymph nodes.

In addition to growth factors, hypoxia associated HIF-1 α , has been proposed to drive lymphangiogenesis, suggesting that the development of hypoxic regions in developing tumours, as well as canonical inflammatory factors control lymphangiogenesis¹⁴². Interestingly, as hypoxia and lymphangiogenesis are both associated with metastasis^{143,144}, this association further implies that hypoxia may indirectly promote metastasis through expansion of the lymphatic network.

There is now a significant body of evidence regarding the association between lymphangiogenesis and tumour progression at the primary tumour site, with the mechanistic work mentioned above mostly focusing on the interaction between tumour cells and the present lymphatic network. However how lymph node LECs respond to

factors derived from the tumour microenvironment beyond lymphatic growth, or indeed how such expansion in the tumour-draining lymph node aids metastasis and tumour progression remain to be elucidated.

1.4.2 T-cell dysfunction in the tumour microenvironment

Despite identifying novel roles for lymphatics in modulating the immune response in healthy and inflammatory states, the context in which lymphatics engage in immune responses within the tumour microenvironment is still relatively unclear. The following section aims to highlight key immune compartments that are dysfunctional in the tumour microenvironment and outline new avenues of research into the role of lymphatics in immune modulation in the tumour microenvironment.

Immune dysfunction in the tumour microenvironment has predominantly focused on alterations at the primary tumour site itself, identifying dysfunction of T-cells and dendritic cells as two of the main features that promote tumour survival and progression. Analysis of solid tumours, both in *in vivo* models and clinically, demonstrate recruitment of both naïve T cells that expand *in situ*¹⁴⁷ and activated effector CD8+ T-cells to the tumour and peritumoural stroma-rich regions^{148,149,150,151,152}. Considering a number of tumour cell types express a plethora of antigens on their surface¹⁵³, the assumption would be that infiltrating CD8+ T-cells could be intrinsically primed towards these antigens and hence should drive antigen-specific tumour clearance. Indeed, there is some evidence that CD8+ T-cell infiltrate is associated with stunted tumour progression and disease-free intervals¹⁵⁴. However, more often, infiltrating CD8+ T-cells exhibit poor proliferative capacity and aberrant cytokine production^{155,156}. In cancers such as melanoma, the underpinning reason for T-cell dysfunction predominantly lies in a number of suppressive processes in the tumour microenvironment. Despite infiltration of melanoma-antigen specific CD8+ T-cells identified in the tumour^{157,158}, high expression of programmed death-ligand 1 (PD-L1), and other inhibitory molecules such as indoleamine-2,3-dioxygenase (IDO), have been shown to switch-off effector T-cell responses and induce T-cell anergy^{159,160,158}. In addition, a feedback loop exists around CD8+ T-cell infiltrates and suppression, whereby CD8+ T-cells secrete IFN- γ which drives expression of PD-L1

and IDO on both surrounding stromal cells and tumour cells^{161,162-164}, leading to further CD8+ T-cell suppression. Further to PD-L1 and IDO, molecules such as Lag-3^{165,166} and CTLA-4^{167,168,169}, a number of cytokines^{170,171,172} and the non-immune tumour stroma¹⁷³, are directly involved in suppressing effector T-cell immunity in the tumour microenvironment.

As well as suppression of infiltrating effector CD8a+ T-cells, the presence of regulatory T-cells (Tregs) has been well documented, with Tregs found in head & neck, colorectal, pancreatic, gastric and ovarian, as well as hepatocellular carcinoma. In particular, increased representation of FoxP3+ regulatory T-cells in the tumour microenvironment is a predictor for poor patient survival¹⁷⁴, with this being predominantly due to their role in modulating effector T-cell function¹⁵⁰. FoxP3+ Tregs exhibit a suppressive expression profile, secreting TGF- β , IL-10, cyclooxygenase-2 (COX-2) and prostaglandin E-2 (PGE-2) which dampen effector CD4+ and CD8+ T-cell responses^{175, 176,177,178}. Their suppressive role in the tumour microenvironment goes beyond secretion of inhibitory cytokines, with a number of other roles identified, such as T-cell cytotoxicity, induction of tolerogenic DCs and expression of a range of inhibitory receptors, as reviewed in¹⁷⁹. Collectively, a complex system of T-cell suppression exists in the developing tumour microenvironment to maintain poor T-cell function, ultimately resulting in tumour cell survival and disease progression. The mechanism underpinning T-cell suppression remains the focus of much research, but little is known of the steps involved in establishing such a suppressive microenvironment in the early stages of tumour development. This thesis focuses at immune changes early in disease to better understand how the tumour microenvironment adapts to support the developing tumour.

1.4.3 Dendritic cell dysfunction in the tumour microenvironment

To better understand how T-cell immunity is altered in the tumour microenvironment, events preceding T-cell mediated immunity must be considered. T-cell priming and “education” occurs via antigen presenting DCs, with critical interactions between the two occurring downstream in draining lymph nodes, as previously described. In order to mount an appropriate immune response, DCs must be mature, activated, have the

capacity to process and present antigen, and express the appropriate co-stimulatory repertoire. They must also be able to traffic from the tumour where they acquired the antigen, to the lymph node, where they initiate an antigen-specific immune response through direct antigen presentation to naïve T-cells. Thus, DCs encounter a number of potential barriers before mounting an anti-tumoural response; perturbations to DC phenotype or trafficking behaviour can influence the priming and ultimate outcome of the immune response.

Indeed, much research carried out in the past two decades has characterised the phenotype of DCs in the tumour microenvironment, with much of our understanding derived from complementary *in vitro* and *in vivo* mouse models. When assessing DC function, the most informative functional read-out reported is assessment of T-cell proliferation. DCs within the tumour microenvironment are widely described as poor inducers of T-cell proliferation, with two bodies of evidence describing impaired maturation and activation, and the development of a regulatory phenotype as the presiding causes.

Evidence for impaired maturation demonstrates DCs in the tumour microenvironment express reduced levels of MHC-II and CD40, with low CD40 expression associated with tumour growth and high CD40 expression associated with T-cell induced tumour regression^{180,181,182}. Reciprocal *in vitro* observations using human derived cells with low levels of maturation markers CD1a and CD83 confirmed that immature DCs resulted in poor stimulation of T-cell proliferation¹⁸³.

Reduced expression of essential co-stimulatory molecules CD80 and CD86, has also been reported in tumour associated DCs, showing that where levels of MHC-II are unchanged, the total percentage of CD80 and CD86 expressing tumour infiltrating DCs *in vivo* can be very low (<1%)¹⁸⁴. Similar observations were made *in vitro* to derive the source of inhibition, with tumour-conditioned media from colorectal tumour cells shown to inhibit up-regulation of CD86 in the presence of LPS¹⁸⁵. This demonstrates that even in the presence of pro-inflammatory stimuli DC maturation can be inhibited by tumour-derived factors. As CD80 and CD86 are critical for facilitating APC/T-cell interactions^{186,187}, this data gives insight to the mechanisms underpinning DC suppression in the tumour microenvironment.

1.4.4 A novel role for lymphatics in immune modulation in the tumour microenvironment

Peripheral and LN-resident LECs have been shown to modulate immunity in steady and inflamed states, as described previously. However, very little is known of their role in modulating immunity in the tumour microenvironment. The role of lymphatics in melanoma in particular has been explored, with *in vivo* data demonstrating a capacity to antigen prime CD8⁺ T-cells in TDLNs and a critical role in regulating immune infiltrate at the primary tumour site. These studies were all conducted in VEGF-C over-expressing B16-F10 tumours, which are highly lymphangiogenic. LN-LECs were found to present tumour-associated OVA on MHC Class-I to OVA-specific CD8⁺ T-cells, resulting in dysfunctional activation and apoptosis, as measured by IFN- γ production, proliferation and Annexin-V staining¹⁸⁸. This was shortly followed by two studies exploring the role of peripheral lymphatics in tumour immune infiltrate. Using an *in vivo* model that lacks dermal lymphatic vessels, impaired dendritic cell migration, reduced immune infiltrate and altered tumour cytokine profiles were reported¹⁸⁸. Upon assessment of human The Cancer Genome Atlas (TCGA) data, lymphangiogenesis correlated with T-cell markers, CD3e, CD4, CD8a and FoxP3 and myeloid markers, CD11b and F4/80, demonstrating the transferability of *in vivo* findings to clinical melanoma, and supporting the notion that lymphatics have an important role in tumour immunity¹⁸⁸. Further investigation into the mechanisms underpinning this association, confirmed that lymphangiogenesis promoted immune cell infiltrate, determining VEGFR-3 and CCR7 to be critical mechanistic drivers¹⁸⁹.

Overall, these are some of the first studies to demonstrate the active role played by lymphatics modulating immunity in the tumour microenvironment. As the aforementioned studies have identified antigen uptake and presentation by TDLN-resident LECs, it poses the question as to whether this is altered relative to resting lymph nodes and whether some of the complex mechanisms of antigen transfer also occur in TDLNs. It further alludes to the process of mounting an anti-tumour immune response as being multifaceted and incredibly complex. Hence more mechanistic insight is needed to precisely determine the role of lymphatics in immunity, especially at TDLNs where immune responses are initiated. As most of the evidence highlighted

above has explored lymphatics in the context of melanoma, this thesis will continue to look at the role of lymphatics in melanoma.

1.5. Summary

Most lymphatic research in the context of the tumour microenvironment remains at the correlative level – linking lymphatic presence with poor prognosis. More detailed mechanistic investigation into emerging roles of lymphatics in systemic biology has so far focused on the steady state or inflammation. There is hence a lack of knowledge of the role of lymphatics in the tumour microenvironment, with some understanding of how they promote tumour cell metastasis, but little in the way of other mechanistic contributions to tumour development and progression. Furthermore, with recent papers identifying roles in governing the immune infiltrate in primary tumours, T-cell priming in TDLNs and tumour responsiveness to immunotherapy, there is growing evidence to suggest lymphatics as key players in the anti-tumour immune response. This project centres on identifying lymphatic changes in early stages of tumour development with particular focus on alterations in TDLNs. We will also focus on whether tumour conditioning alters immune functionality of lymphatics in TDLNs and how these changes affect early anti-tumour immune responses.

1.6. Hypothesis and Aims

Microarrays of lymphatics from normal tissue and primary tumours have identified tumour-specific transcriptional profiles pointing to functional changes in tumour-associated LECs, but to date have not examined lymphatics in TDLNs, especially during early stages of tumour development.

We hypothesise that lymphatics are differentially altered in early TDLNs due to conditioning from the early developing tumour. As lymph nodes are immune hubs, we hypothesise that tumour-conditioned lymphatics in TDLNs will exhibit altered functionality in favour of tolerance, ultimately laying down the foundations for a continued anti-tumoural immune response. Furthermore, as one of the main roles of lymphatic vessels is to assist in dendritic cell trafficking, we hypothesise the pro-tolerogenic features of tumour-associated lymphatics, will influence dendritic cell-mediated immunity.

The goal of this PhD project is hence to define how lymphatics at the TDLN are altered by factors derived from the tumour microenvironment and how conditioned lymphatics contribute to immune dysfunction in the early stages of tumour development.

We will address the following specific aims:

1. Identify and characterise changes within the lymphatic compartment of TDLNs

- a. Determine the extent of lymphatic expansion within tumour draining lymph nodes, using *in vivo* tumour models.
- b. Determine lymphatic-specific transcriptional reprogramming using microarray of lymphatic compartments derived from TDLNs
- c. Verify any transcriptional changes *ex vivo*

2. Explore the functional impact of these changes on lymph node architecture and immune organisation

- a. Determine whether lymphatic adaptation influences immune compartments

- b. Determine whether lymphatic adaptation influences behaviour of incoming tumour-derived dendritic cells

3. Determine the functional consequences of these changes on immune priming and T-cell function

- a. Define changes in immune cell dynamics within TDLNs throughout tumour development
- b. Determine whether lymphatic adaptation effects T-cell priming
- c. Explore links between lymphatic adaptations and immune cell dynamics within TDLNs throughout tumour development

CHAPTER 2

METHODS

2. Methods

2.1. Cell Culture

2.1.1. Cells

C57BL/6 murine primary dermal lymphatic endothelial cells (LECs) were purchased from CellBiologics® (Cat No: C57-6064L) and cultured in endothelial cell medium purchased from CellBiologics® (Cat No. M1168) supplemented with 10% Foetal Calf Serum (FCS), 1% L-Glutamine, 0.1% Hydrocortisone, 0.1% Heparin, 0.1% Endothelial Growth Factor (EGF), 0.1% Vascular Endothelial Growth Factor (VEGF), 0.1% Endothelial Cell Growth Supplement (ECGS) and 1% Antibiotic-Antimycotic Solution, purchased as a kit from CellBiologics® (Cat No. M1168-Kit). C57BL/6 murine melanoma cell line B16-F10 were purchased from ATCC® (Cat No. CRI-6475) and cultured in Dulbecco's Modified Eagle Medium (DMEM) with glucose (4.5g/L), L-glutamine (4mM) (Gibco, Cat No. 41966-029) supplemented with 10% FCS and 1% Penicillin Streptomycin (PS). *Ex vivo* splenocytes were cultured in Roswell Park Memorial Institute formulation 1640 (RPMI-1640) medium (Gibco, Cat No. 21875-034), supplemented with 10% FCS, 1% PS and β -mercaptoethanol (15 μ M) (Sigma Aldrich). For all media, FCS and PS were supplied by in-house media facilities.

2.1.2. Cell Passage

B16-F10s were cultured in 75cm³ tissue culture flasks (Thermo Scientific) and LECs were cultured in collagen-coated 25cm³ tissue culture flasks (Thermo Scientific). Collagen coating solution was prepared using sterile nuclease-free water (Ambion), 50 μ g/ml Rat-Tail Collagen Type 1 (Corning, Cat No. 354236) and 0.1% acetic acid (VWR International). Cells were cultured at 37°C with 5% CO₂ and allowed to reach 70-90% confluency before being passaged. Culture medium was removed by aspiration and discarded. Cells were washed with tissue culture phosphate buffered saline (TC-PBS) without Ca²⁺/Mg²⁺, followed by the addition of 0.25% trypsin for 5 minutes. Once all cells were detached, full tissue culture media was added to flasks to neutralise the trypsin, and cell suspensions were retrieved. For B16F10s, cells were

counted and re-suspended at a 1:10 dilution, with approximately 1×10^6 resuspended in full tissue culture media and transferred to 75cm^3 culture flasks. For LECs, cells were counted and re-suspended at a density of 500,000/flask in full endothelial cell media. Cells were then transferred to 25cm^3 culture flasks, coated as described above. All cell counts were carried out using trypan blue exclusion, with LECs and primary immune cells counted manually with a haemocytometer and B16-F10s counted with the automated Countess® cell counter (Thermo Fisher Scientific Invitrogen). Trypsin and TC-PBS were supplied by in-house media facilities.

2.1.3. Cryopreservation

Cells were cryopreserved in freezing medium (90% FBS, 10% DMSO), aliquoted into 2ml cryovials (Thermo Scientific), and transferred to a Nalgene® Mr. Frosty freezing container containing 100% isopropyl alcohol for optimal rate freezing. Cells were stored in liquid nitrogen at -80°C . Recovery of frozen cells was carried out by rapid thawing of frozen vials, followed by re-suspension in warm medium. Cells were transferred to respective culture flasks and incubated overnight at 37°C with 5% CO_2 . Following overnight incubation, media was exchanged.

2.2. Isolation of primary murine cell populations

2.2.1. Digestion of primary tissue

To digest primary lymph nodes and spleens, samples were excised from mice, broken up using a 25 gauge (0.5mm x 25mm) needle and transferred to eppendorfs (lymph nodes) or 15ml falcon flasks (spleens). Samples were then incubated with Collagenase-A and Collagenase-D (Roche), prepared in basic RPMI at a concentration of 10mg/ml and used at a 1:10 dilution and DNase (Roche) prepared in deionised water at a concentration of 10mg/ml and used at a dilution of 1:25. Firstly, samples were incubated for 30 minutes at 37°C , with Collagenase-A (1mg/ml) and DNase (0.4mg/ml) in a shaking heat block at 550rpm. Collagenase-D (1mg/ml) and DNase (0.4mg/ml) was then added to the pre-existing digestion mix of each sample and incubated for a further 30 minutes at 37°C in a shaking heat block at 550rpm.

Digestion was deactivated using 50µl of 0.5M EDTA. Digested tissue was added to a 70µm cell strainer (FisherBrand), remnant tissue manually crushed through with a 1ml syringe plunger (Soft-Ject) and the filter flushed with 2ml of PBS. Single cell suspensions were collected in a 50ml falcon flask, followed by centrifugation at 1800rpm for 5 minutes. EDTA and PBS were supplied by in-house media facilities at MRC Cancer Unit, UK.

2.2.2. MACS enrichment of CD11c dendritic cells

For CD11c dendritic cell enrichment, spleens were digested as described above in Section 2.2.1. Single cell suspensions were then lysed with Red Blood Cell (RBC) lysis buffer at room temperature for 5 minutes. Lysis was deactivated by addition of 15ml of full RPMI and samples centrifuged at 1800rpm for 5 minutes. Splenocytes were then counted with a haemocytometer, using trypan blue exclusion and re-suspended in 400µl of MACS buffer and 100µl of CD11c Ultra-Pure MicroBeads (Miltenyi Biotec Cat No: 130-108-338), per 10^8 splenocytes and incubated on ice for 15 minutes. Following incubation, 30ml of MACS buffer was added and samples centrifuged at 300g for 5 minutes. The cells were re-suspended in 1ml of MACS buffer and loaded onto a LS column (Miltenyi Biotec, Cat No: 130-042-041) that had been attached to a MidiMACS™ Separator on a MACS MultiStand (both from Miltenyi Biotec) and primed with 3ml MACS buffer. The column was then washed with 3ml of MACS buffer twice to remove unlabelled CD11c negative cells. Once all liquid had drained from the column, the column was removed from the separator, and labelled CD11c positive cells flushed out into a 15ml falcon flask using the provided plunger and 5ml of MACS buffer. Viable cells were counted with a haemocytometer using trypan blue exclusion, centrifuged at 300g for 5 minutes and re-suspended at the desired concentration for functional assays. Recipes for all buffers used here are listed in Table 2.9. Purity was confirmed using flow cytometry, with a yield of >70% purity.

2.2.3. MACS Enrichment of OT-1 CD8a T-cells

For CD8a T-cell enrichment, spleens from OT-1 mice spleens were digested as described above in Section 2.2.1. Single cell suspensions were then RBC lysed and

enriched using the CD8a+ T-cell isolation kit (Miltenyi Biotec, Cat No: 130-104-075). Splenocytes were re-suspended in 400µl of MACS buffer and 100µl of Biotin-Antibody Cocktail per 10⁸ splenocytes and incubated on ice for 5 minutes. Following incubation, 300µl of MACS buffer was added with 200µl of Anti-Biotin MicroBeads per 10⁸ splenocytes and incubated on ice for 10 minutes. The splenocytes were then loaded directly onto a LS column, prepared as previously described. The flow-through, containing unlabelled cells, representing CD8a+ T-cells was collected into a 15ml falcon flask and the column washed once with 3ml of MACS buffer to collect remnant unlabelled CD8a+ T-cells. Viable cells were counted with a haemocytometer using trypan blue exclusion and, centrifuged at 300g for 5 minutes and re-suspended at the desired concentration for functional assays.

2.3. *In vivo* mouse studies

2.3.1. In vivo mouse lines

To determine the role of lymphatics in the tumour microenvironment, a number of *in vivo* mouse models were used, conducted under Home Office approved Personal Licence I1b141bfa, and Project Licences 80/2574 (2014-2017) and P88378375 (2017-2018). For syngeneic tumours, immune competent male and female C57BL/6 mice aged 8-12 weeks were primarily used. C57BL/6JOlaHsd were sourced either from breeding stocks at the animal facility (MRC ARES, Cambridge, UK) or externally from Envigo, USA (www.envigo.com). To assess changes in the tumour microenvironment in the context of aberrant Podoplanin expression, PDPN-FL mice, generated by Dr. Dayong Guo²⁵⁸ and generously donated by Professor Bonewald from the University of Missouri-Kansas City (USA), were used. In addition, the transgenic mouse model, C57BL/6-Tg(CAG-EGFP)131Osb/LeySopJ, was purchased from The Jackson Laboratory (Stock No: 006567) and maintained for acquisition of EGFP fluorescent samples for *in vitro* studies. Genotyping of PDPN-FL and CAG.EGFP litters and subsequent breeding management was carried out personally and is described below.

2.3.2. Genotyping of mouse lines

In-house genotyping was carried out for CAG.EGFP and PDPN-FL mice using ear punch biopsies from mice. Biopsies were provided by the animal facility in 1.5ml eppendorfs, with each eppendorf containing a single mouse sample. To lyse cells and extract DNA, 40µl of 25mM NaOH was added to each eppendorf, and samples incubated at 95°C for 15 minutes on a heat-block. Samples were then removed and allowed to cool before adding 40µl of 40mM Tris-HCl (pH 7.5) to neutralise and stop lysis. At this stage, samples could be stored for a short time at 4°C until needed for PCR.

For PCR, 2µl of solution from each sample was added to a mastermix, prepared as stated below (Table 2.1) using reagents purchased from (Thermo Scientific). PCR was conducted using the program stated below (Table 2.2) on a PTC-225 Thermal Cycler (MJ Research) and samples subsequently run on 1% (w/v) agarose gels prepared by diluting agarose (APExBio) in 1x TBE buffer supplemented with 1:10 ethidium bromide (Sigma Aldrich). Details of primers used can be found below in Table 2.3. All buffer recipes used here are listed in Table 2.9.

Components of PCR Mastermix	Volume (μ l)
HF-Buffer (Green)	4.0
10mM dNTPs	0.4
10 μ M Transgene primers	2.0
10 μ M Internal control primers	2.0
Phusion Polymerase	0.2
RNase-Free Water	9.4
Genomic DNA from ear biopsies	2.0
Total	20.0

Table 2.1. PCR mastermix components used for genotyping.

Temperature ($^{\circ}$ C)	Time	No. Cycles
98	30secs	
98	10secs	30
60	30secs	
72	60secs	
72	10mins	
10	Forever	

Table 2.2. PCR program used for genotyping.

Primer	Primer Sequence 5' \rightarrow 3'
Podoplanin (gp38 mouse)	Forward: TGCTCAGCGCCTTCCAACCT
Podoplanin (gp38 mouse)	Reverse: GCTCCCCAAAACCCAGAACA
CAG.EGFP oIMR0872	Forward: AAGTTCATCTGCACCACCG
CAG.EGFP oIMR1416	Reverse: TCCTTGAAGAAGATGGTGCG
CAG.EGFP oIMR7338	Forward: CTAGGCCACAGAATTGAAAGATCT
CAG.EGFP oIMR7339	Reverse: GTAGGTGGAAATTCTAGCATCATCC

Table 2.3. Primers used for genotyping of mouse lines.

For CAG.EGFP mice, transgene insertion could be detected by a band at 173 base pairs (bps), indicating expression of Green Fluorescent Protein (GFP). Internal controls were included in the PCR mastermix, with bands detected at 324bps (Figure 2.1a). For PDPN-FL mice, the wild-type allele could be detected at 196bp and floxed allele at 296bps (Figure 2.1b). Hence, in homozygous mice, only a band at 296bps could be seen, whereas in heterozygous mice a double band could be detected at 196bps and 296bps.

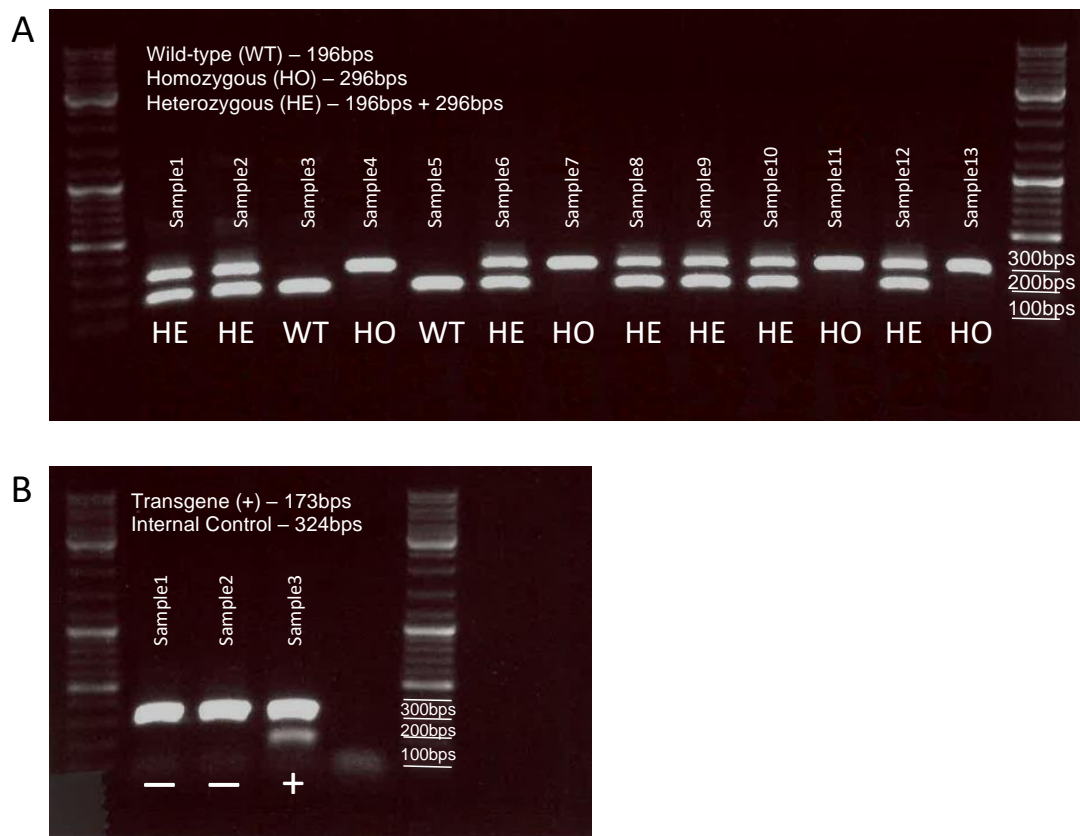


Figure 2.1. Agarose gels for genotyping of mouse lines. Phenotype of PDPN-FL mice determined by bands at 196bps and 296bps (A). Phenotype of CAG.EGFP mice determined by presence (+) or absence (-) of the transgene band at 173bps. Internal control bands expected on all samples at 324bps (B). BPs, Basepairs.

2.3.3. Transplanted tumour generation *in vivo*

B16-F10 melanoma cells were prepared following standard cell passage protocol (Section 2.1) and counted using trypan blue exclusion. For shoulder tumours, cells were prepared at a density of 2.5×10^5 cells in 50 μ l of sterile PBS and for ear tumours, prepared at a density of 1×10^5 in 50 μ l of sterile PBS.

Prior to inoculation with tumour cells, mice were anaesthetised using either Isoflurane or injectable anaesthesia. Isoflurane was administered using an induction chamber in 100% oxygen at a flow rate of 2litres/min. Injectable anaesthesia was administered intraperitoneally using 150 μ l anaesthetic stock solution, comprising of ketamine (100mg/kg) and xylazine (10mg/kg), made up using 0.5ml (50mg) ketamine + 0.25ml (5mg) xylazine + 4.25ml 1x PBS. For shoulder tumours, mice were anaesthetised using isoflurane or injectable anaesthesia, shoulders shaved and tumour cells injected subcutaneously into each shoulder. For ear tumours, mice were anaesthetised via injectable anaesthesia and tumour cells injected subcutaneously on the dorsal side of each ear. After being inoculated with tumour cells, mice injected with anaesthesia were transferred to a Vetbed chamber for recovery.

Mice bearing shoulder tumours were sacrificed at Day 4 and Day 11 post-inoculation and mice bearing ear tumours sacrificed 3-weeks post-inoculation. Throughout experiments, tumour growth was monitored by staff at the animal facility using calipers and sacrificed when a maximal tumour size of 12mm diameter was reached. Humane killing of mice was conducted using Schedule 1 methods, with exposure to carbon dioxide as the primary method and dislocation of the neck as the secondary method for confirmation of death. For mice bearing shoulder tumours, brachial tumour-draining lymph nodes (TDLNs) were harvested, with brachial non-draining lymph nodes (NDLNs) taken from non-tumour bearing control mice injected with PBS (Figure 2.2). For mice bearing ear tumours, cervical TDLNs were harvested, with cervical NDLNs taken from control mice injected with PBS. For all *in vivo* experiments, mice were age matched and assigned to control or tumour groups randomly, with animals only excluded in the event of poor health.

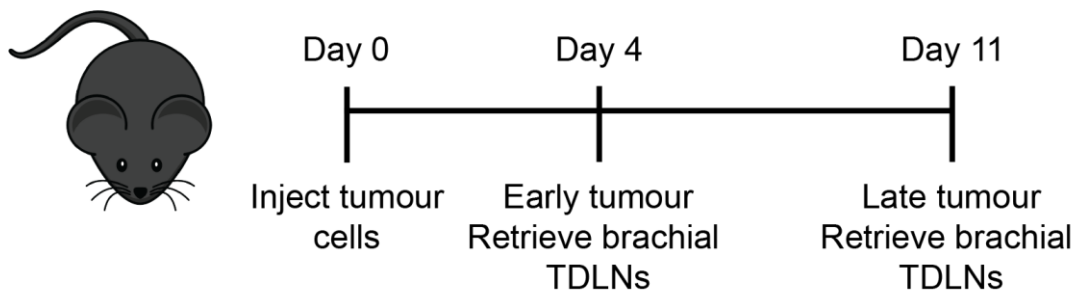


Figure 2.2. Schematic of *in vivo* B16-F10 mouse model. B16-F10 tumour cells injected subcutaneously on the shoulders. At early (Day 4) and late (Day 11) time-points, brachial TDLNs and respective control NDLNs were retrieved.

2.3.4. Autochthonous tumour generation *in vivo*

The most common point mutation in human melanoma is in the *BRAF* proto-oncogene, occurring in approximately 65% of individuals, resulting in constitutive expression of $\text{Braf}^{\text{V600E}}$, a protein serine kinase that drives activation of the Braf-MEK-ERK pathway. Full malignancy in human melanoma is however only acquired through silencing of tumour suppressor genes, for which silencing of *PTEN* occurs in roughly 20% of Braf mutant melanomas. Dankort et al., (2009)²⁶⁸ hence developed the $\text{Tyr}^{\text{CreER}}\text{Braf}^{\text{CA}}\text{Pten}^{\text{lox}}$ model of melanoma in order to establish a preclinical model that recapitulated human melanoma better than currently used murine models of melanoma. Authors developed this mouse model using $\text{Tyr}^{\text{CreER}}\text{Braf}^{\text{CA}}$ mice expressing conditional *PTEN* alleles flanked by *loxP* sites. This allowed for tamoxifen-inducible Cre-mediated conversion of Braf^{CA} to $\text{Braf}^{\text{V600E}}$ alongside deletion of exons 4 and 5 of *Pten*, specifically in melanocytes with conditionally active Cre recombinase.

Authors reported topical or systemic administration of tamoxifen (4-HT) led to the appearance of a range of lesions and tumours, accompanied with reliable lymph node metastasis. In our hands, we find topical administration directly to the skin, induces pigmentation as early as 14 days with tumours developing from 21 days post-induction. Mostly these tumours are amelanotic, with black pigmentation on the external facing surface of the tumour in small regions; which authors did not report (Figure 2.3a). Mice induced with 4-HT also exhibited pigmentation on the tail and in non-induced mice

report the development of spontaneous tumours (Figure 2.3a,b). In line with Dankort and colleagues²⁶⁷, we observe reliable lymph node drainage and metastasis.

The $Tyr^{CreER}Braf^{CA}Pten^{lox}$ mouse model was used to observe lymphangiogenesis in ear tumours, whereby mice were anaesthetised by i.p using injectable anaesthesia, as described in 2.3.3, and 4-HT applied to the ear skin (2 μ l, 5mM) using a pipette. This step was then repeated daily for 4-days. After Cre activation, mice were checked regularly and pigmented lesion development observed (Figure 2.3c). Malignant melanomas develop between 4-7 weeks and once reached a diameter of 5mm on the ear, mice culled using Schedule 1 methods.

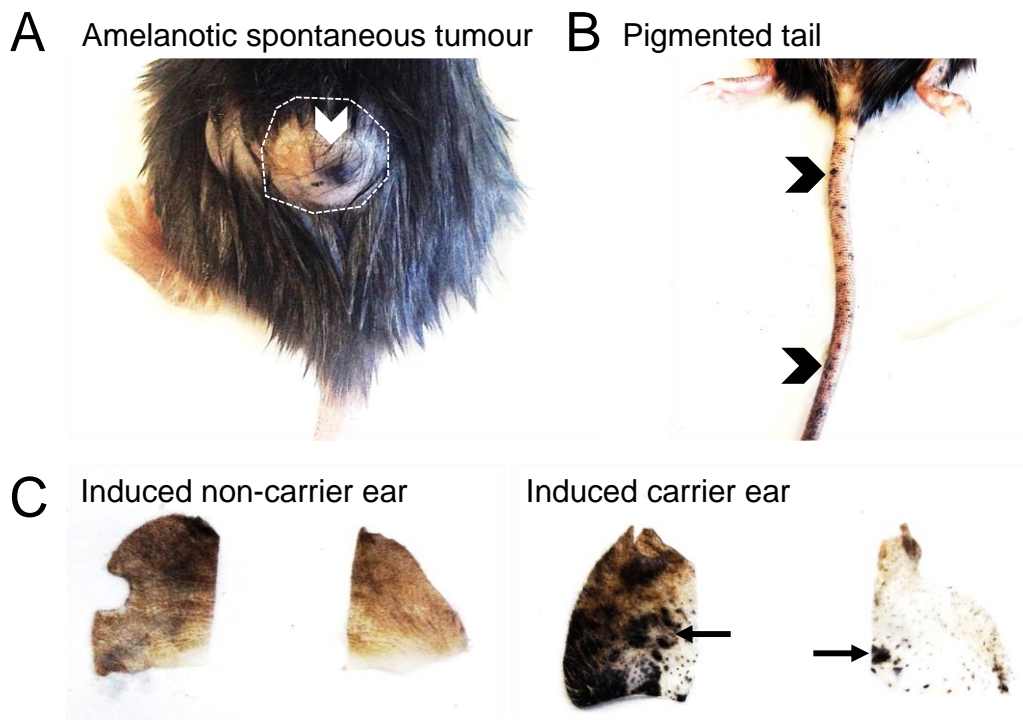


Figure 2.3. Amelanotic tumours and pigmentation in $Braf^{V600E}/Pten$ mice. The $Tyr^{CreER}Braf^{CA}Pten^{lox}$ mouse model was used to observe lymphangiogenesis in ear tumours. In some instances, $Tyr^{CreER}Braf^{CA}Pten^{lox}$ mouse developed spontaneous amelanotic tumours (outlined region) with small black pigmentations (A, white arrow head). Mice with both spontaneous and tamoxifen (4-HT) induced tumours had black pigmentation visible on the tail (B, black arrow heads). For experimental purposes, mice without spontaneous tumours were anaesthetised by i.p using injectable anaesthesia and 4-HT applied to the ear skin (2 μ l, 5mM). In mice lacking the Cre (non-carriers), ears treated with 4-HT (induced) were free of pigmentation and melanoma lesions (C, left panel). In mice carrying the Cre (carriers, malignant melanomas developed over 4-7 weeks, with extensive coverage found on the dorsal side of the ear (C, right panel, arrows). Shown are ears split into the dorsal (left) and ventral (right) sides (C).

2.3.5. Tracking dendritic cell migration in vivo

To assess localization within lymph nodes of tumour-derived migratory DCs, C57BL/6 wild type and PDPN-FL mice were inoculated with B16F10 tumours and painted with fluorescent tetramethylrhodamine isothiocyanate (TRITC) (Sigma Aldrich, Cat No: 87918). TRITC was prepared in a 1ml solution of acetone (Fisher Chemical) and skin-sensitising agent, dibutyl phthalate (Sigma Aldrich) at a ratio of 1:1 to enable transit of TRITC across the epithelial barrier. For application of TRITC, mice were anaesthetised under isoflurane and 10µl of TRITC pipetted on to the tumour injection site. Control non-tumour bearing mice were shaved and then painted with TRITC. Mice were culled 18 hours after application to skin to ensure the skin absorbed TRITC, and to allow TRITC+ cells from the periphery to migrate to draining brachial lymph nodes (Figure 2.4). Mice were culled in accordance with Schedule 1 methods described previously in Section 2.3 and brachial lymph nodes taken for histology or flow cytometry.



Figure 2.4. *In vivo* model of tracking tumour-derived dendritic cells. Day4 tumours are painted with TRITC to allow for non-invasive labelling of migratory dendritic cells. TDLNs and control NDNLs are retrieved 18 hours after painting.

2.3.6. Blocking Podoplanin in vivo

To assess migration of tumour-derived DCs in the context of perturbed interactions with Podoplanin, C57BL/6 wild type mice were inoculated with B16F10 tumours as previously described. To block Podoplanin, azide-free purified monoclonal Syrian Hamster 8.1.1 antibody against Podoplanin (BioXCell, Cat No. BE0236) was used. After a 24-hour period to allow injected tumour cells to settle, blocking antibody or control LEAF™ Syrian Hamster IgG Isotype control antibody (Biolegend, Cat No. 402014) were injected daily at a concentration of 1mg/ml in 50µl of sterile PBS.

Injections were made subcutaneously into the fore legs to ensure maximal drainage to brachial lymph nodes. In conjunction, we used the TRITC model (Section 2.3) to track tumour-derived migratory DCs in draining lymph nodes in the context of Podoplanin blockade. The antibodies and concentrations used in these experiments are identical to those used in a study conducted by Astarita et al., (2015), which assessed *in vivo* the role of the Podoplanin-CLEC2 axis in DC migration along FRC conduits in lymph nodes²³⁶.

2.4. RNA Isolation, Amplification and Quantification

2.4.1. RNA isolation of primary lymph node cells

For isolation of primary lymph node-derived LECs and migratory dendritic cells, lymph nodes were digested in accordance to Section 2.2 and single cell suspensions processed for FACS as described in Section 2.8. Specific antibody protocols are stated in relevant chapters and details listed in Table 2.11. Populations of interest were then sorted from total stained single cell suspensions, using an Influx™ Cell Sorter (BD Biosciences). Populations of interest were sorted directly into 350µl of RLT, RNA lysis buffer, vortexed and snap frozen on dry ice, before transfer to -80°C until needed for RNA isolation.

For RNA extraction the RNeasy Micro Kit (Qiagen, Cat No. 74004) was used. Samples stored at -80°C in RLT buffer were thawed and vortexed before proceeding with the RNA isolation protocol. Firstly, ethanol (VWR International) was diluted in nuclease-free water (Ambion) to working solutions of 70% and 80%. Equal volumes of 70% ethanol were added to homogenised cells in RLT buffer (350µl RLT to 350µl Ethanol). Samples were then transferred to RNeasy MiniElute spin columns (Qiagen) in 2ml collection tubes. Samples were centrifuged at 15 seconds at 10,000rpm and the flow-through discarded. To eliminate contaminating DNA, a solution of 10µl DNase-I in 70µl of RDD buffer (Qiagen) was added to each column membrane and incubated at room temperature for 20 minutes. If multiple samples were being processed for RNA extraction, a stock solution of DNase-I in RDD buffer was prepared. Columns were then washed with 350µl RW1 buffer and centrifuged for 15 seconds at 10,000rpm. The

flow-through was discarded and followed by two washes with 500µl RPE buffer. Columns were centrifuged for 15 seconds at 10,000rpm, the flow-through discarded and 500µl 80% ethanol added to each column. Columns were centrifuged for 2 minutes at 10,000rpm and the flow-through and collection tube discarded. Columns were placed in new collection tubes and centrifuged with open lids for 5 minutes at 10,000rpm to dry the membrane. The flow-through and collection tube was discarded and columns placed in 1.5ml nuclease-free eppendorfs. To elute RNA from the columns, 14µl of nuclease-free water was added directly to each column and left on the bench for 5 minutes to allow full absorption of water. Columns were finally centrifuged for 2 minutes at 10,000rpm and elute the RNA. Eppendorfs were then stored at -80°C until needed for quantification. RNA quantification was conducted using the Eukaryote Agilent RNA 6000 Pico Kit (Agilent Technologies Cat No. 5067-1513) and 2100 Bioanalyser Instrument (Agilent Technologies).

2.4.2. Amplification and quantification of cDNA for primary LECs

For amplification of lymph node-derived LECs, RNA samples were processed for whole transcriptome amplification using the Ovation® PicoSL WTA System V2 kit (NuGEN, Cat No. 3302). Based on their eukaryotic total RNA integrity number (RIN), which is based on a scale of 1 to 10, with 1 being highly degraded RNA and 10 being most intact; samples were chosen with a RIN value above 8 and a total concentration of 100pg/µl. This amplification process then involves a multi-step process of cDNA synthesis, purification and amplification. cDNA synthesis was conducted using thermal cycling programmes.

Firstly, cDNA synthesis was carried out using 2µl of First Strand Primer Mix and 500pg of RNA sample. Samples were then incubated at 65°C for 2 minutes in 0.5ml tubes in a thermal cycler. Samples were then removed and placed on ice and 3µl of mastermix added to each sample. This mastermix was prepared using 2.5µl of First Strand Buffer mix and 0.5µl of First Strand Enzyme Mix, with a stock mastermix made-up for multiple samples. Samples were then incubated in accordance to the First Strand cDNA Synthesis program outlined in Table 2.4.

For Second Strand cDNA Synthesis, a mastermix of Second Strand Buffer Mix (9.7µl) and Second Strand Enzyme Mix (0.3µl) was prepared per sample, with a stock mastermix made-up for multiple samples. For each sample, 10µl was added and tubes were incubated in a pre-cooled thermal cycler using the Second Strand cDNA Synthesis program outlined in Table 2.4. At this stage, samples were directly processed for cDNA purification.

Purification was conducted using Agencourt RNAClean XP beads (provided with the kit), which bind cDNA and use magnetism and ethanol washes to purify the cDNA. Firstly, beads were allowed to reach room temperature and mixed to ensure beads were fully resuspended. Secondly, to each sample, 32µl of beads were added, the PCR tubes transferred to the magnet stand and the samples left to stand on the magnet for 5 minutes until the solution appeared clear. Whilst keeping the tubes on the magnet, 45µl of sample solution was removed and 200µl of freshly prepared RNase-free 70% ethanol added. Finally, samples were again left to stand on the magnet for a further 30 seconds, the ethanol removed, and an additional two washes with ethanol performed. On the last wash, as much ethanol as possible was removed and the samples allowed to air dry for 20 minutes.

Samples were then processed immediately for amplification, with a mastermix added to each sample. The amplification mastermix is composed of 20µl SPIA™ Buffer Mix, 10µl SPIA™ Primer Mix and 10µl SPIA™ Enzyme Mix, with a stock mastermix made-up for multiple samples. Samples were then placed in a pre-cooled thermal cycler and incubated in accordance to the SPIA Amplification program outlined in Table 2.4. Once the cycling program is complete, carefully remove all of the cleared supernatant, transfer to a new PCR tube and store at -20°C; this is the amplified cDNA. The remaining beads can then be discarded. When removing samples from storage for quantification, amplified cDNA samples were thawed and 1.0µl used for quantification with the Nanodrop 1000 (Thermo Scientific).

Program	Temperature	Time
First Strand cDNA Synthesis	4°C 25°C 42°C 70°C 4°C	2 mins 30 mins 15 mins 15 mins HOLD
Second Strand cDNA Synthesis	4°C 25°C 50°C 80°C 4°C	1 min 10 mins 30 mins 20 mins HOLD
SPIA Amplification	4°C 47°C 95°C 4°C	1 min 75 mins 5 mins HOLD

Table 2.4. PCR programs for amplification

2.5. Microarray Hybridisation and Data Normalisation

To determine transcriptional changes in LECs derived from NDNLs and TDLNs, RNA was extracted from FACS sorted LN-derived LECs (Section 2.8). NDNLs and TDLNs were retrieved from tumour bearing and non-tumour bearing mice and RNA isolated as outlined previously (Section 2.4). Samples with a RIN value above 7 were then processed for microarray analysis. Microarray experiments were performed externally at Cambridge Genomic Services, University of Cambridge using the Mouse WG-6 v2.0 Expression BeadChip Kit (Illumina, Cat No. BD-201). Across conditions, LECs isolated from four brachial lymph nodes, derived from two mice were pooled to create a single sample, as shown in Figure 2.5. This was then repeated to provide triplicate samples, with a total of n=6 mice used per time-point.

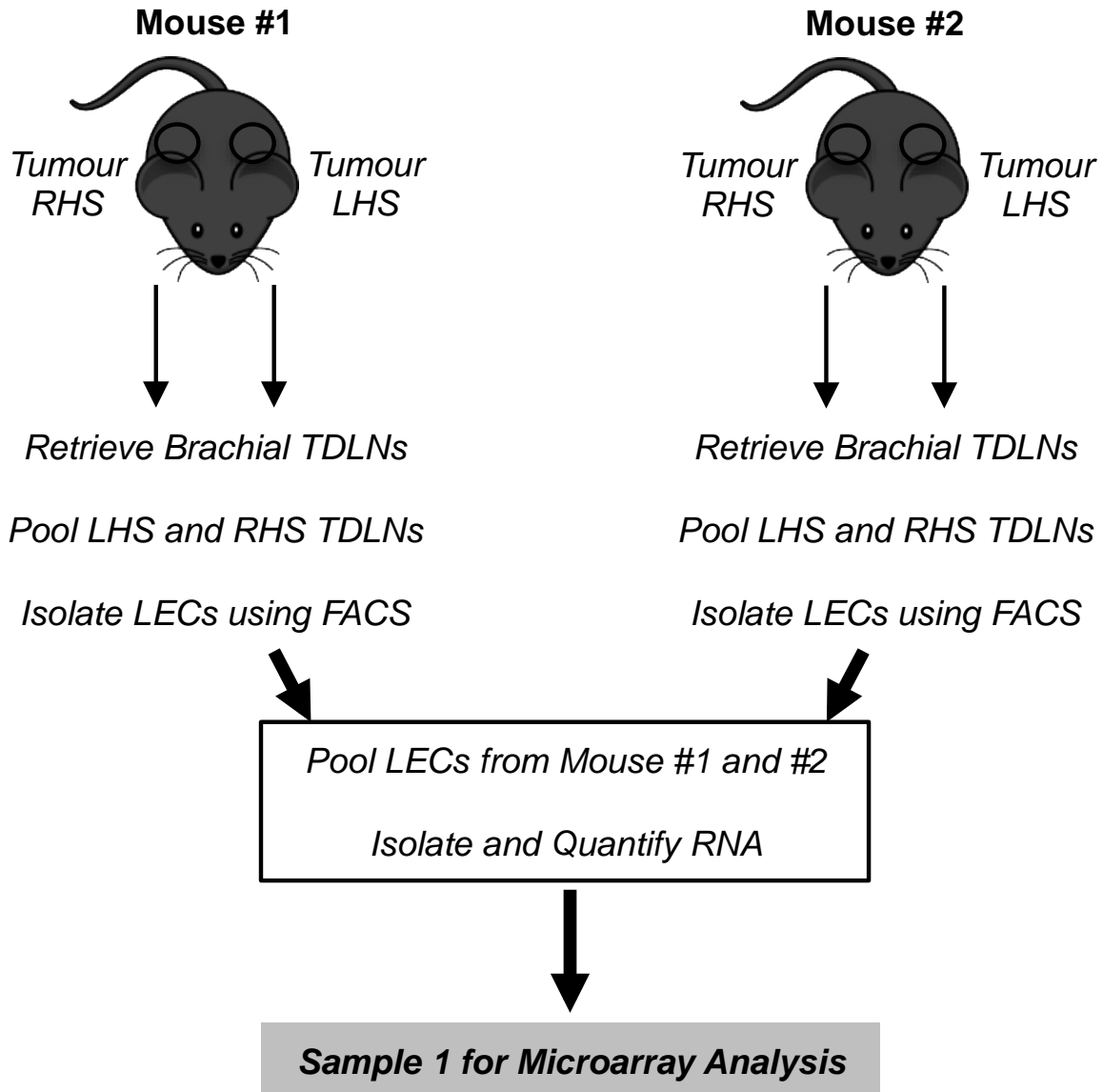


Figure 2.5. Schematic of experimental murine set-up for microarray samples. Isolated RNA from NDLN and TDLN LECs was derived from n=6 mice per condition, across triplicates. This was conducted across one independent experiment. LHS, Left-hand side; RHS, Right-hand side.

2.6. Quantitative real-time polymerase chain reaction (qRT-PCR)

Quantitative Real-Time PCR (qRT-PCR) was conducted using TaqMan™ Gene Expression FAM-dye assays for targets of interest, CDH5 (Probe ID: Mm00486938_m1), JAM3 (Probe ID: Mm00499214_m1), and CLDN11 (Probe ID: Mm00500915_m1) (Life Technologies, UK). Each PCR mix was prepared with 5.5µl mastermix per sample, prepared using 0.5µl TaqMan™ Assay and 5µl diluted cDNA

(2µg/µl), with a stock mastermix made-up for multiple samples. Samples were incubated on a thermal cycler (ABI) for a standard 2hrs comparative program, as outlined in Table 2.5. The software q-base (<https://www.qbaseplus.com>) was used to calculate change in Ct values (ΔCT), using the housekeeping gene GAPDH (Probe ID: Mm99999915_g1) and Control NDNLs as endogenous controls. Relative fold changes were then calculated using the formula, $2^{-\Delta\Delta\text{Ct}}$.

Cycles	Temperature Time
1	2 mins 50°C
1	15 mins 95°C
40	15 secs, 95°C 1 min, 60°C

Table 2.5. qRT-PCR program for ABI StepOnePlus™ Cycler

2.7. Dendritic Cell and Antigen Presenting Cell PCR Array

2.7.1. Dendritic cell isolation and RNA purification

In order to assess functional changes in migratory dendritic cells from early TDLNs, lymph nodes were taken from TRITC painted control mice and tumour-bearing mice at Day 4 and Day 11 post-inoculation. RNA from TRITC+ migratory dendritic cells was extracted as described in Section 2.4.

2.7.2. cDNA Amplification

Due to low levels of RNA per sample, the amplification RT² PreAMP cDNA Synthesis Kit (Qiagen, Cat. No. 330451) was used. Samples with a RIN value above 8.0 were selected, with 1ng of RNA used per sample. This kit utilises PCR to pre-amplify gene-specific cDNA, using specific primer mixes. As these samples were needed for the Mouse Dendritic and Antigen Presenting Cell RT² Profiler PCR Array (Qiagen, Cat.

No. PAMM-406Z), the specific primer mix for this array was used - Mouse Dendritic and Antigen Presenting Cell (Qiagen, Cat No. RT²-PBM-406Z).

The protocol first involves first genomic DNA elimination, conducted by mixing RNA samples (1ng) with Buffer GE (2µl) in RNase-free water to a total volume of 10µl and incubating at 42°C for 5 minutes in a thermal cycler. This is followed by first strand cDNA synthesis using a reverse transcription mix in accordance with volumes stated in Table 2.6. The reverse transcription mix (10µl) is added to the genomic DNA elimination mix (10µl) from the previous step, followed by initial incubation at 42°C for 30 minutes then 95°C for 5 minutes in a thermal cycler. Samples were then stored overnight at -20°C.

Reagent	Volume per Sample
5x Buffer BC3	4µl
Control P2	1µl
cDNA Synthesis Enzyme Mix	1µl
RNase Inhibitor	3µl
Total	10µl

Table 2.6. Reverse transcription mix for First Strand cDNA Synthesis for PCR Profiler Arrays

After first strand cDNA synthesis, primer specific amplification was conducted by incubating 5µl of first strand cDNA samples with 20µl of mastermix composed of PCR mastermix (12.5µl) and primer mix (7.5µl). Samples were then amplified in a thermal cycler, in accordance with the program stated in Table 2.7. Post-amplification, samples were placed on ice and residual primers eliminated by the addition of 2µl (per sample) of Side Reaction Reducer. Finally, samples were incubated at 37°C for 15 minutes, followed by heat inactivation at 95°C for 5 minutes in a thermal cycler. Nuclease-free water (84µl) was then added to each sample immediately after. Samples were then stored overnight at -20°C until needed for qRT-PCR. All incubation and cycler programs were conducted in a Tetrad PTC-225 Thermal Cycler (MJ Research).

Cycles	Temperature Time
1	10 mins 95°C
12	15 secs, 95°C 2 mins, 65°C

Table 2.7. Amplification PCR program for PCR Profiler Arrays

2.7.3. qRT-PCR for RT² Profiler PCR Array

As previously stated, the Mouse Dendritic and Antigen Presenting Cell RT² Profiler PCR Array was used to assess changes in functionality in early and late TDLN-derived migratory dendritic cells, relative to control NDNLs. Amplified cDNA (102µl) was added to RT² SYBR Green Rox qPCR Mastermix (1350µl) (Qiagen, Cat. No. 330520), prepared in RNase free water (1248µl) and aliquoted into RT² Profiler PCR Array 96-well plates (Figure 2.6), with 25µl pipetted into each well.

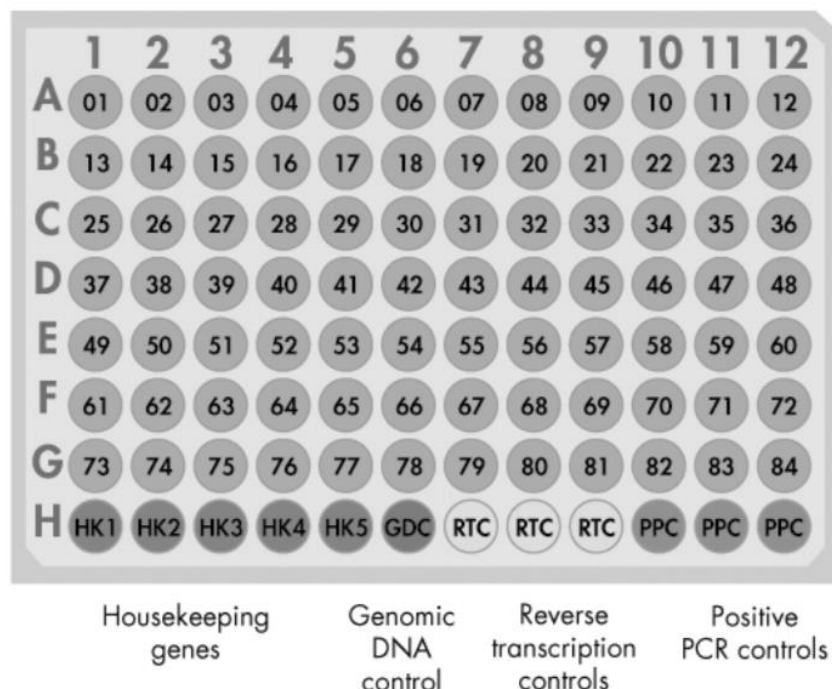


Figure 2.6. 96-well plate format for PCR Profiler Arrays.

As per schematic in Figure 2.5, each well contains specific primers, with A1 – G12 containing Dendritic and APC target genes. Housekeeping genes *Actnb*, *B2m*, *Gapdh*, *Gusb* and *Hsp90ab1*, are contained in wells H1 – H5, with H6 – 12 containing controls to assess Genomic DNA contamination, Reverse Transcription efficiency and PCR reproducibility. Plates were cycled in a real-time StepOnePlus™ cyclor (Applied Biosystems) according to the PCR program outlined in Table 2.8.

Cycles	Temperature Time
1	10 mins 95°C
40	15 secs, 95°C 1 min, 60°C

Table 2.8. qRT-PCR program for ABI StepOnePlus™ Cyclor for PCR Profiler Arrays

2.7.4. Data Analysis and Quality Control

Prior to data export, the C_T threshold was set across samples in accordance with SHAM control NDNLNs. For these samples, a C_T threshold of 0.107 was used across samples. Data was exported in Excel and formatted as suggested by the manufacturer's guidelines. For data analysis and quality control, the resource from Qiagen – *Sample Insight*, was used. Sample management, data quality control and calculation of fold change values were all conducted online by automated analysis. Any samples that failed to meet criteria for PCR reproducibility, Reverse Transcription efficiency and Genomic DNA contamination were excluded from the analysis. If Average PPC C_T was 19 ± 3 and if no two arrays had an Average PPC $C_T > 2$ away from each other within groups, the PCR was considered reproducible and passed criteria. If Delta C_T (Average RTC – Average PPC) was ≤ 7 then the reverse transcription efficiency passed criteria. If C_T (GDC) ≥ 30 , then samples were considered to have no genomic DNA contamination. For normalisation, reference genes from the whole plate were selected, as inconsistencies in classic housekeeping genes were found. The following genes were hence used as normalisation genes *Tgfb1*, *Fas*, *Ccl5*, *Itgam* and *Thbs*. Data analysis was then carried out automatically online; with fold change data

exported and plotted using heatmap visualisation. As there were n=2 samples per group, p-values could not be calculated by automated analyses. Heatmap visualisation hence represents fold changes in gene targets, independent of statistical significance.

2.8. Flow Cytometry analysis of primary and cell line populations

2.8.1 Preparation of ex vivo samples for flow cytometry

Prepared single cell suspensions were first transferred into 96-round bottom plates (Corning) and centrifuged for 1 minute at 2000rpm. Cells were then stained with conjugated antibodies against targets of interest, in FACS buffer for 30 minutes at 4°C. Where biotin primary antibodies were used, samples were incubated with appropriate conjugated streptavidin antibodies in FACS buffer for an additional 20 minutes at 4°C following removal of primary antibodies. To ensure non-specific binding of antibodies, BSA was added as a component of FACS buffer, prepared according to Table 2.9. Non-specific binding was not conducted using incubation steps with Fc receptor blocking antibodies. Specific antibody protocols are stated in relevant chapters and details listed in Table 2.10. Finally, samples were washed with PBS and transferred into round-bottom polystyrene tubes (Corning) for flow cytometry. Recipes for all buffers used here are listed in Table 2.10.

2.8.2 Preparation of cultured cells for flow cytometry

Following culture or functional assays with adherent cells, media was removed and cells were washed with PBS. Staining with fluorophore-conjugated antibodies in FACS buffer was conducted in-plate for 20 minutes at 4°C. For non-adherent cells, suspensions were transferred from culture plates directly into 96-well round bottom plates, centrifuged for 1 minute at 2000rpm and incubated with fluorophore-conjugated antibodies in FACS buffer for 20 minutes at 4°C. Where biotin primary antibodies were used, samples were incubated with appropriate fluorophore-conjugated streptavidin antibodies, in FACS buffer for an additional 20 minutes at 4°C. Specific antibody protocols are stated in relevant chapters and details listed in Table 2.10. For adherent

cells, wells were washed with PBS and detachment using Accutase® Cell Detachment Solution (Biolegend). Once stained, samples were transferred into polystyrene tubes for flow cytometry. Where stated, samples were stained with LIVE/DEAD™ Fixable Dead Cell Stain (Thermo Fisher Scientific, Cat No. L34955). This cell stain was prepared in 50µl of DMSO for a 1000x stock solution and was used to stain cells for 10mins at 4°C, prior to primary and secondary staining steps. Recipes for all buffers used here are listed in Table 2.10.

2.8.3. Flow cytometry data acquisition and analysis

Following cell staining, in accordance to the above protocols described, samples were run on a LSR BD Fortessa™ (BD Biosciences), supported by BD FACSDIVA™ software package (BD Biosciences). As multi-parameter staining was performed, single stained anti-rat/hamster compensation beads (BD Biosciences, Cat No. 51-90-9000949) and unstained controls were run to determine signal overlap between fluorophores. Laser settings were altered to ensure fluorescent signal was below $<10^2$ in unstained controls for each fluorophore, and that fluorescent signal between any two fluorophores had a minimum of 10^1 difference. Once parameters were finalised, compensation was calculated automatically by BD FACSDIVA™ software, with $<10\%$ spectral overlap across fluorophores. Subsequent data analysis was carried out offline using the software application FlowJo® (<https://www.flowjo.com>).

2.9. Immunofluorescent Imaging (IF)

2.9.1. Immunofluorescent staining of sectioned tissue

Freshly isolated ears, lymph nodes and tumours were retrieved from culled mice and placed in cryo-moulds with Optimal Cutting Temperature Compound (OCT) (VWR International), ensuring correct tissue orientation using tweezers. OCT was then added to the cryomold to fully cover the tissue sample and snap frozen on dry ice. Samples were stored at -80°C until needed for sectioning. For sectioning, samples were transferred to -20°C for 24 hours prior to sectioning using a cryostat and

sectioned to a width of 10µm. Slides were stored in slide boxes at -80°C, until required for staining.

Prior to immunofluorescent staining, sections were left to dry at room temperature for approximately 3 hours. Sections were then fixed in an ice-cold solution of acetone (Fisher Chemicals) and methanol (Fisher Chemicals) at a 1:1 ratio, for 2mins and washed (x1) with PBS. As there were multiple sections per slide, individual samples were isolated using a hydrophobic pen before non-immune blocking steps were performed in PBS supplemented with 2% BSA (Fisher Scientific) and 10% chicken serum (Alpha Diagnostics International, Cat No. NCHS-500) at room temperature for 1 hour. Sections were then incubated with primary antibodies using 75µl per section overnight at 4°C. Primary antibodies were removed by washing (x3, 15 minutes per wash) in PBS supplemented with 0.1% Tween (PBS-Tween) (NBS Biologics), followed by staining with appropriate conjugated secondary antibodies at room temperature for 1 hour. After slides had been washed (x3, 15 minutes per wash) in PBS-Tween, and where stated, nuclei counterstained with DAPI (1:10,000) (Biotium), slides were mounted with 22x50mm glass coverslips and SlowFade® Gold Antifade Mountant (Life Technologies, Cat No. S36936). Specific antibody protocols are stated in relevant chapters and details listed in Table 2.11.

2.9.2 Dermal sheet preparation of murine ears

The use of lymphatic-rich whole mouse ears for either immunofluorescent imaging or *in vitro* assays is well documented^{273,274}. To prepare dermal sheets for these techniques whole mouse ears were removed by excision at the base of the ear, using scissors. If needed for immunofluorescent wholemount imaging, ears were placed whole in bijoux with 4% paraformaldehyde (PFA) prepared in distilled water. After fixation, ear sheets were separated using tweezers, into dorsal and ventral sides, and placed directly into 48-well plates (Figure 2.7). The ventral sheet is the most optimal for immunofluorescent imaging as it is cartilage-free, yielding clearer images with better imaging depth. If needed for *in vitro* assays, ears were immediately split without fixation and processed in accordance to Section 2.10.

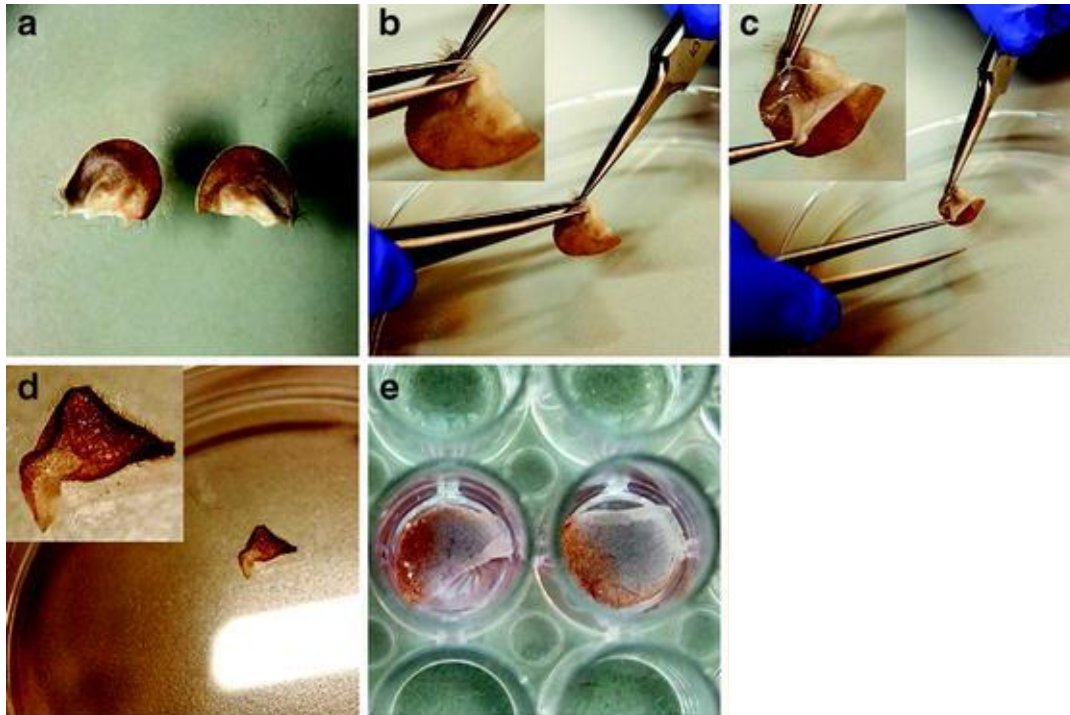


Figure 2.7. Dermal sheet preparation from whole ears derived from C57BL/6 mice. Visualisation of the steps involved in ear sheet preparation for *in vitro* assays. Whole ears are excised using scissors from culled mice (A). Using fine dissecting tweezers the dorsal and ventral sides of the ear are removed, by anchoring one side of the ear to a petri dish with a set of tweezers, and gently pulling the other side with the other set of tweezers (B,C). The thinnest layer of two ear sheets is the most optimal, due to cartilage-free properties, which allow for better visualisation during microscopy (D). Ear sheets are placed dermis side up in 48-well plates with full RPMI (E). Adapted from Weber et al., *Methods Mol Biol* (2013)²⁷³.

2.9.3 Immunofluorescent staining of ear wholemounts

Fixed ears in 48-plates were placed in 250µl of PBS supplemented with 0.2% Triton-X (Sigma Aldrich), for 5 hours to permeabilise the tissue. Ears were then washed with PBS and incubated with primary antibodies for 48 hours at 4°C. Ears were then washed with PBS-Tween for 1 hour and incubated with conjugated secondary antibodies for 24 hours at 4°C, followed by further washing with PBS-Tween. Ears were mounted on a glass bottom petri dish (Mat Tek Corporation) with SlowFade® Gold Anti-fade Mountant and sealed with 12mm circular glass coverslips. Specific antibody protocols are stated in relevant chapters and details listed in Table 2.11.

For enhanced visualisation of ears, RapiClear®, from the SunJin Lab, was used (Cat No. RC152001). RapiClear® is a water-soluble clearing reagent, used to improve optics of biological sample characteristics (1-5mm penetrance). In this instance,

clearing of the ear is helpful to better visualize lymphatic vasculature and immune cell localisation relative to such vasculature. RapiClear®1.52, which has a refractive index similar to immersion oil and coverslips, of 1.52nD, is advised for use with tissues >0.5mm in thickness. Post-immunofluorescent staining, each ear half were placed in 350µl of RapiClear®1.52 solution in 48-well plates for >6 hours at room temperature or overnight at 4°C. This is akin to a mounting step, so anti-fade was not used in conjunction with this protocol.

2.9.4. Immunofluorescent staining of cultured cells

To assess characterise LECs cultured *in vitro*, cells were cultured on collagen-coated 12mm circular glass coverslips in 24-well plates and cultured until a monolayer was formed. Cells were washed with PBS, fixed in 4% PFA for 5 minutes at room temperature and permeabilised using PBS + 0.2% Triton-X for 5 minutes at room temperature. Non-immune blocking steps were performed in PBS supplemented with 2% BSA and 10% chicken serum for 1 hour at room temperature. Cells were then stained with primary antibodies against targets of interest with 200µl added to each well, followed by incubation overnight at 4°C. Following incubation, primary antibody was removed by PBS-Tween. Appropriate conjugated secondary antibodies were prepared, added to samples and incubated for 1 hour at room temperature. Nuclei were counterstained using DAPI (1:10,000) for 10 minutes at room temperature. Coverslips were then delicately removed from wells using fine tweezers and mounted on glass slides using EverBrite™ hard-set mounting medium (Biotium, Cat No. 23003). Specific antibody protocols are stated in relevant chapters and details listed in Table 2.11.

2.9.5. Microscopy and Image Analysis

Prepared sections, wholemount ears and cells were imaged on a Zeiss LSM 880 confocal microscope. Plan-Apochromat objectives were used, with the following numerical apertures; 0.45 (10x), 0.75 (20x), 0.95 (40x), 1.4 (63x oil), 1.4 (100x oil).

Whole lymph node and tumour images were acquired using the Convex Hull Tile Scan setting, using 20x magnification and 1024x1024 resolution, with 5% overlap between each tile, a line average of 2 and scanning speed of 7.45 seconds/frame. On average over 40 tiles were needed to scan whole tissue sections. Whole images were then stitched online, using the medium stitching setting, before being exported as a CZI file for further analysis.

For region of interest images of lymph nodes, 20x magnification was used with 1024x1024 resolution, a line average of 8 and a scanning speed of 81 seconds/frame. For z-stacks of DCs in co-cultures, 100x magnification was used, with 2048x2048 resolution and a line averaging of 1. ZEN Blue software from Zeiss was used to conduct offline image analysis.

For quantitative image analysis of lymph node tile-scans and ROIs, HALO™ image analysis software from PerkinElmer was used. Volocity 6.3 software from PerkinElmer, was used specifically for 3D z-stacked images of *in vitro* cultures, high magnification lymph node ROIs and ear wholemounds. Quantitative analysis of images acquired from *in vitro* and *ex-vivo* co-cultures, *FIJI* image analysis software was used²⁷⁵. Specific methods are detailed in relevant chapter sections.

2.10. Functional Assays

2.10.1. In vitro conditioning of cell lines and primary cells

Tumour conditioning of LECs and splenic DCs was performed by culturing cells *in vitro* with 50% tumour-conditioned media (TCM) for varying periods of time. TCM was derived from B16F10s seeded at 3.0×10^6 in a 75cm³ flask overnight, then treated overnight with basal endothelial cell media supplemented with 2% FCS for LEC conditioning, or basal RPMI supplemented with 2% FCS for DC conditioning. Control conditioned media (CCM) was composed of 50% full endothelial cell media and 50% used media from LEC single cultures of 70% confluency.

2.10.2. *In vitro* LEC antigen uptake and processing assays

For assessment of antigen uptake and processing by lymphatic endothelial cells *in vitro*, fluorescently-labelled ovalbumin (OVA) was used to track uptake of antigen, and DQ-ovalbumin (DQ-OVA) to track processing of antigen. Fluorescent OVA is a protein labelled with a bright, photostable and pH-insensitive dye which can be detected using flow cytometry and immunofluorescent imaging. DQ-OVA is a protein heavily labelled with BODIPY dyes, designed to yield single, bright fluorescent-labelled peptides upon proteolysis. DQ-OVA is hence used for immunoassays assessing antigen degradation of processing as the amount of fluorescent-signal detected increases as the OVA is degraded.

For antigen uptake assays, LECs were seeded at a density of 100,000 cells per well, in collagen-coated 6-well plates, and were stated treated with TCM, as per methods outlined above in Section 2.10. LECs were then washed gently with TC-PBS and pulsed with fluorescent 647-ovalbumin conjugate (647-OVA) (Thermo Fisher Scientific Invitrogen, Cat No. 034784), diluted in PBS for a final concentration of 100µg/ml. LECs were cultured at 37°C in 5% CO₂ for 15 minutes and washed three times with ice-cold PBS, supplemented with 2% FCS, to remove any unbound antigen. LECs were then retrieved using 350µl of Accutase® solution per well and processed for flow cytometry.

For antigen processing assays, LECs were seeded and treated as stated above and pulsed with DQ ovalbumin (DQ-OVA) (Thermo Fisher Scientific Invitrogen, Cat No. D12053), diluted in PBS for a final concentration of 100µg/ml. LECs were cultured at 37°C in 5% CO₂ for up to 75 minutes, with cells retrieved at a number of time-points to assess extent of antigen processing. Cells were washed three times with ice-cold PBS, supplemented with 2% FCS, to remove any unbound antigen. LECs were then retrieved using 350µl of Accutase® solution per well and processed for flow cytometry.

For detection of fluorescent antigen in both 647-OVA and DQ-OVA assays, OVA uptake and processing was detected using flow cytometry, whereby the 488nm laser detected processed DQ-OVA and the 647nm laser detected uptake of 647-OVA.

Specific antibody protocols and detailed methods for flow cytometry are stated in relevant chapters.

2.10.3. LEC-DC co-culture assays – Cell culture and conditioning

For LEC-DC co-cultures, LECs were seeded on collagen-coated 6-well plates (Eppendorf) at a density of 100,000 cells per well for adhesion assays or 8µm pore 12mm transwell inserts (Merck Millipore) at a density of 10,000 cells per insert for transmigration assays. LECs were allowed to settle overnight and then treated with CCM or TCM for 48 hours, as described in Section 2.10. Every 24 hours media was supplemented with fresh CCM or TCM. Where stated, LECs were also treated with Syrian Hamster 8.1.1 anti-podoplanin blocking antibody (Biolegend, Cat No. 127401) at a concentration of 0.5µg/ml for 3 hours prior to co-culture with DCs. For isolation of DCs, splenic CD11c dendritic cells were isolated from either wild-type C57BL/6 mice or CAG.EGFP mice for GFP-DCs, as described in Section 2.2.

2.10.4. LEC-DC co-culture assays – adhesion, transmigration and motility

To define interactions between DCs and LECs, simple adhesion assays were used to assess whether DCs exhibited altered adherent properties when interacting with TCM-conditioned LECs. Firstly, GFP-DCs were isolated re-suspended in full RPMI to a density of 1×10^5 per ml and 2×10^5 added to a monolayer of LECs cultured as stated above in Section 2.10.1. Co-cultures were incubated at 37°C in 5% CO₂ for 1 hour, after which the suspension was removed, hence removing the unattached DCs. Co-cultures were then gently washed with PBS and subsequently the number of adherent GFP-DCs counted.

For transmigration assays, GFP-DCs were co-cultured with LECs seeded as stated above and incubated at 37°C for 1 hour to allow adhesion. After the initial incubation period, the suspension was removed, hence removing the unattached DCs, and co-cultures gently washed. Co-cultures were then incubated at 37°C and the number of transmigration GFP-DCs in the bottom chamber after 18 hours was then counted.

For both adhesion and transmigration assays, GFP-DCs were visualised and imaged using the EVOS® FL Cell Imaging System (Thermo Fisher Scientific). Multiple fields of views (FOVs) were imaged with 3-5 taken per well. The number of GFP-DCs per FOV was manually counted using *FIJI* image analysis software, with the counting overlay tool.

For motility GFP-DCs were visualised and imaged using the Zeiss Live Cell microscope. Multiple fields of views (FOVs) per well across conditions were imaged over durations of an hour. Mobile GFP-DCs were then identified and tracked offline using automated modules from image analysis software Volocity 6.3 (Perkin Elmer). Quantitative outputs included velocity, displacement rate, meandering index and distance.

For morphology imaging of adherent DCs, co-cultures were incubated at 37°C for 1 hour, after which the non-adherent compartment was removed by extracting the media. Co-cultures were then gently washed with PBS, fixed with 4% PFA (350µl per well) at room temperature for 2 minutes and permeabilised with PBS supplemented with 0.1% Triton-X (350µl per well). Co-cultures were then stained with VE-Cadherin at 4°C overnight, to outline intercellular junctions and cell borders. Following primary antibody incubation, co-cultures were incubated with 594-conjugated donkey-anti-rabbit secondary antibody at room temperature for 1 hour. Cells were counterstained with DAPI (1:10,000) in PBS at room temperature for 10 minutes. Slides were mounted using Anti-Fade mountant and imaged using a Zeiss 880. Details of antibody clones, concentrations and suppliers are provided in Table 2.11.

2.10.5. LEC-DC co-culture assays – antigen transfer

LECs and DCs were prepared for co-culture in 6-well plates as described in Section 2.10.2. Immediately before co-culture, LECs were pulsed with 100µg/ml of 647-conjugated full-length ovalbumin (647-OVA), at 37°C in 5% CO₂ for 15 minutes. OVA was washed three times using ice-cold PBS supplemented with 2% FCS. DCs were re-suspended in full RPMI to a density of 1x10⁵ per ml and 2x10⁵ added to each well. Co-cultures were incubated at 37°C in 5% CO₂ for 1 hour, after which the non-

adherent compartment was removed by extracting the media. Co-cultures were then gently washed with PBS and the adherent compartment removed by adding 350 μ l of Accutase® Cell Detachment Solution to each well, yielding both LECs and DCs. For co-culture assays intended for T-cell proliferation assays, the adherent compartment removed by adding 350 μ l 0.5mM EDTA to each well and incubating until adherent DCs detached. A sample of the adherent and non-adherent DCs were then immediately processed for flow cytometry analysis to quantify OVA uptake. Specific antibody protocols and detailed methods for flow cytometry are stated in relevant chapters.

2.10.6. T-cell proliferation assays

For preparation of antigen-specific T-cells, OT-1 CD8⁺ T-cells were isolated as per methods outlined in Section 2.2. Cells were then counted and re-suspended at a density of $1-10 \times 10^6$ in 1ml of PBS and transferred into 15ml falcon flasks. CFSE (Invitrogen, Molecular Probes®) was prepared in 110 μ l of PBS (1:100, 1.1 μ l of stock 5mM CFSE), added to T-cell suspensions and incubated at room temperature for 10minutes. Cells were then washed (x3) with ice-cold PBS supplemented with 2% FCS and re-suspended in full RPMI media. Cells were counted using trypan blue exclusion and a haemocytometer.

For assessing whether lymphatic conditioned DCs differentially prime T-cells, splenic DCs were cultured with antigen-primed LECs as per Section 2.10.4. LEC-conditioned DCs were then retrieved from both adherent and non-adherent compartments for T-cell assays. DCs were counted and re-suspended in full RPMI at a density of 1×10^5 per ml. OT-1 CD8⁺ T-cells were cultured at 37°C in 5% CO₂ in round-bottom 96-well plates with DCs at a ratio of 1:10, with 10,000 DCs and 100,000 T-cells. After 72 hours, all cells were retrieved and processed for flow cytometry as per Section 2.8. Throughout these co-cultures, both with LECs and T-cells, the DCs were not pre-activated with any cytokine or bacterial-derived product. Specific antibody protocols and detailed methods for flow cytometry are stated in relevant chapters.

Bulk splenic dendritic cells pulsed directly with 647-OVA, at a range of concentrations, were also cultured with T-cells using the same seeding densities outlined above. These conditions acted as positive controls for APC-mediated T-cell priming. Appropriate negative controls were also used, 1) co-culture with CFSE-negative T-cells 2) co-culture with antigen non-specific wild-type T-cells and 3) co-culture with dendritic cells primed with LECs in the absence of OVA.

2.10.7. *In vivo* antigen assays

For assessment of antigen uptake and processing by stromal cells and dendritic cells in lymph nodes *in vivo*, fluorescent ovalbumin (OVA) was used to track uptake of ovalbumin antigen, and DQ-OVA to track processing of antigen. How OVA and DQ-OVA works is described in Section 2.10.2. To assess antigen uptake and processing *in vivo*, 50µl of FITC-OVA (Thermo Fisher Scientific Invitrogen, Cat No. 023030) or DQ-OVA diluted in sterile PBS to a concentration of 50µg/ml were injected subcutaneously into the front legs of C57BL/6 mice. This injection site is immediately upstream of brachial lymph nodes, and hence allows rapid delivery of antigen to said lymph nodes for detection of uptake and processing by resident stromal populations. After 15 minutes post-injection, mice were culled and brachial lymph nodes retrieved. Where stated, lymph nodes were also taken from TRITC painted mice to determine migratory dendritic cell uptake of antigen drained to the lymph node. This was conducted as outlined in Section 2.3.

For immunofluorescent imaging, control NDNLNs and Day 4 TDLNs were isolated from control and tumour-bearing mice. Lymph node sections were prepared as per methods in Section 2.9 and stained with rabbit anti-LYVE1. Specific antibody protocols are stated in relevant chapters and details listed in Table 2.11. Whole lymph node tile-scans were taken using confocal microscopy, whereby OVA positive cells were detected using the 488nm laser. Automated Halo™ image analysis software was used to quantify OVA positive staining as a percentage of total lymph node area. Details on methods of quantification are stated in relevant chapters.

For flow cytometry, control NDNLs and Day 4 TDLNs were isolated from control and tumour-bearing mice. Lymph nodes were digested as per methods described in Section 2.2 and processed for flow cytometry as described in Section 2.8. Lymph nodes were stained with markers for dendritic cell and non-immune stromal markers to determine relative OVA uptake and processing across lymph node compartments. As stated above, OVA positive cells were detected using the 488nm laser. Flow cytometry data was acquired and analysed as stated in Section 2.8, with specific methods stated in relevant chapters.

2.11. Statistical Analysis

Statistical analysis was performed using GraphPad Prism Version 7.00 for Mac, (GraphPad Software, La Jolla California USA, www.graphpad.com). Statistical tests were conducted as appropriate to the dataset and detailed in figure legends. Student t-tests were used for parametric data, when comparing two groups with sample sizes above $n=15$. Mann-Whitney tests were used for non-parametric data, when comparing two groups with sample sizes below $n=15$. One-way analysis of variance (ANOVA) was used to conduct parametric analyses of datasets with three or more groups, with Tukey's multiple comparisons conducted between groups. The Kruskal-Wallis test with Dunn's multiple comparisons, was conducted for non-parametric datasets with three or more groups and sample sizes below $n=15$. For all data, bar charts are presented with error bars representing the standard error of the mean (SEM); as stated in figure legends Statistics are hence reported in the written text as the value \pm SEM. Box and whisker plots are presented as 25th to 75th percentile box plots with, 5-95% percentile whiskers and median line shown; as stated in figure legends. Where data was found to be significant, p-values are denoted by asterisks, with (*) denoting $P \leq 0.05$, (**) denoting $P \leq 0.01$, (***) denoting $P \leq 0.001$ and (****) denoting $P \leq 0.0001$. Where data was found not to be significant, this is not stated, or referred to as not significant (ns).

Table 2.9. Buffers and Reagents

Buffer / Reagent	Contents
RBC Lysis Buffer	0.1mM EDTA, 150mM NH ₄ Cl, 1mM KHCO ₃ prepared in deionised water
MACS Buffer	0.5% (w/v) BSA and 2mM EDTA prepared in 1x PBS and filtered with a 0.2µm filter
FACS Buffer	0.5% (w/v) BSA and 2mM EDTA prepared in 1x PBS
Immunofluorescence Blocking Buffer	10% chicken serum and 2% BSA prepared in 1x PBS

Table 2.10. Antibodies for flow cytometry

Target	Clone	Isotype	Supplier	Stock Conc ^N Dilution Used
Live/Dead Viability Dye	Ref: L34955		Invitrogen	1:1000
Biotin LYVE-1	ALY7	Rat IgG1	LS Bio	0.5mg/ml 1:300
Biotin PD-1	TY25	Rat IgG2a, κ	eBioscience	0.5mg/ml 1:300
Biotin PD-L1	10F.9G2	Rat IgG2b, κ	Biolegend	0.5mg/ml 1:300
488 CD3e	145-2C11	Armenian Hamster IgG	Biolegend	0.5mg/ml 1:300
421 CD8a	53-6.7	Rat IgG2a, κ	Biolegend	0.05mg/ml 1:300
450 CD11c	N418	Armenian Hamster IgG	eBioscience	0.2mg/ml 1:300
BV-780 CD8a	53-6.7	Rat IgG2a, κ	eBioscience	0.2mg/ml 1:300
488 CD103	2E7	Armenian Hamster IgG	Biolegend	0.5mg/ml 1:300
488 CD4	GK1.5	Rat IgG2b, κ	Biolegend	0.5mg/ml 1:300
488 ICAM1	YN1/1.7.4	Rat IgG2b, κ	Biolegend	0.5mg/ml 1:300
488 VCAM1	429	Rat IgG2a, κ	Biolegend	0.5mg/ml 1:300
FITC CD31	390	Rat IgG2a, κ	eBioscience	0.5mg/ml 1:300
PE CLEC-2	17D9	Rat IgG2b, κ	Biolegend	0.2mg/ml 1:300
PE ESAM	1G8	Rat IgG2a, κ	Biolegend	0.2mg/ml 1:300
PeCy7 CD11c	N418	Armenian Hamster IgG	Biolegend	0.2mg/ml 1:300
PeCy7 CD31	MEC13.3	Rat IgG2a, κ	Biolegend	0.2mg/ml 1:300
PeCy7 CD45	30-F11	Rat IgG2b, κ	Biolegend	0.2mg/ml 1:300
PeCy7 PD-1	RMP1-30	Rat IgG2b, κ	Biolegend	0.2mg/ml 1:300
PeCy7 PD-L1	10F.9G2	Rat IgG2b, κ	Biolegend	0.2mg/ml 1:300
APC FoxP3	FJK-16s	Rat IgG2a, κ	eBioscience	0.2mg/ml 1:300
APC PDPN	8.1.1	Syrian Hamster IgG	Biolegend	0.2mg/ml 1:300
APC MHC-II	KH74	Rat IgG2a, κ	Biolegend	0.5mg/ml 1:300
APC-Cy7 CD11b	M1/70	Rat IgG2b, κ	Biolegend	0.2mg/ml 1:300
APC-Cy7 CD25	PC61	Rat IgG1, λ	BD Pharmingen	0.2mg/ml 1:300
APC-Cy7 CD45	30-F11	Rat IgG2b, κ	Biolegend	0.2mg/ml 1:300

Table 2.11. Antibodies for immunofluorescence

Target	Clone	Species	Supplier	Concentration Used
DAPI	Ref: 40011		Biotium	1:10,000
B220	RA3-6B2	Rat	BD Pharmingen	0.5mg/ml 1:100
CCL21/6Ckine	AF457	Goat	R&D Systems	0.2mg/ml
CD3e	500A2	Syrian Hamster	BD Pharmingen	0.5mg/ml 1:100
CD31	MEC13.3	Rat	Biolegend	0.5mg/ml 1:100
CDH5	Polyclonal	Rabbit	Abcam	1mg/ml
LYVE-1	Polyclonal	Rabbit	Abcam	0.5mg/ml 1:300
PDPN	8.1.1	Syrian Hamster	Biolegend	0.5mg/ml 1:100
PROX-1	Polyclonal	Rabbit	Abcam	1mg/ml

Table 2.12. Fluorescently conjugated secondary antibodies

Antibody	Conjugate	Supplier	Concentration Used
Donkey anti-rat	405	Abcam	2mg/ml 1:300
Donkey anti-goat	405	Abcam	2mg/ml 1:300
Chicken anti-rabbit	488	Invitrogen	2mg/ml 1:300
Goat anti-hamster	488	Invitrogen	2mg/ml 1:300
Donkey anti-rabbit	594	Invitrogen	2mg/ml 1:300
Goat anti-hamster	647	Invitrogen	2mg/ml 1:300
Conjugated streptavidin	Pe-Cy7	Biolegend	0.2mg/ml 1:300
Conjugated streptavidin	APC-Cy7	Biolegend	0.2mg/ml 1:300

CHAPTER 3

RESULTS

3. Functional characterisation of lymphatics from melanoma TDLNs

3.1. Introduction

Until recently, lymphatics were mostly considered as passive participants in tumour progression, serving largely as routes for metastasis. As lymphangiogenesis was frequently observed in primary tumours of many human cancers including melanoma^{130, 126}, breast¹²⁷, colorectal¹³¹ and non-small lung cancer¹³², much focus has been placed on exploring the role of lymphatics at the tumour site to define their role in LN metastasis and patient survival. Specifically, lymphangiogenesis has been strongly linked with metastasis of melanoma^{130,126}, with much research showing lymphatic expansion at primary and draining lymph nodes positively correlated with poor patient survival and prognosis^{127,130,126}. While studies have also demonstrated the presence of lymphangiogenesis at tumour draining lymph nodes, which correlated with metastasis incidence in murine models^{126,133}, the adaptations and functional changes occurring in lymphatics both at the primary site and TDLNs, and how these changes support tumours, however, remain poorly defined. In steady states and inflammation, lymphatics are accepted to regulate trafficking of immune cells^{44,45,46,47,48,49,50,51}. An emerging role for lymphatics and lymphangiogenesis in the tumour suggests a role in regulation of immune microenvironments, with lymphatic expansion associated with immune suppression^{188,190}. This was further found to be associated with susceptibility to immunotherapy¹⁸⁹. Hence, there exists an understanding that lymphangiogenesis is a characteristic of tumour progression, and some evidence to suggest an active role in immune modulation in the primary tumour. However, there is a lack of knowledge in lymphatic function beyond the primary tumour, and in the specific mechanisms of lymphatic-mediated immune modulation. Hence, we aimed to better characterise functional changes and determine the relative immune contribution of these changes, in lymphatics from TDLNs.

3.2. Methods

3.2.1. Flow cytometry analysis of lymphatic expansion in TDLNs

To assess the extent of lymph node and specific lymphatic expansion in TDLNs, LNs were retrieved from tumour bearing and non-tumour bearing mice as described in Section 2.3. Samples were digested and processed for flow cytometry as described in Section 2.9. LN single-cell suspensions were stained with 405-conjugated live/dead viability dye and fluorescently conjugated antibodies against CD45, Podoplanin and CD31, then run and analysed as described in Section 2.9. Stromal subpopulations were gated based on Podoplanin and CD31 expression, within CD45 negative populations, with LECs defined as CD45- Podoplanin+ CD31+, FRCs defined as CD45- Podoplanin+ CD31- and BECs defined as CD45- Podoplanin- CD31+. This gating strategy has been used by other publications investigating lymph node stroma¹⁰⁸ and details of all antibodies used are listed in Table 2.10 in Methods. Two independent experiments were used, with n=25 NDNLs and n=33 TDLNs across various time-points. Data was statistically tested using Two-way ANOVA with Sidak's multiple comparison tests. This was conducted and published by colleagues¹⁹¹.

3.2.2. Immunofluorescent imaging of lymph node and tumour lymphatics

To assess the extent of lymphangiogenesis in lymph nodes and tumours, tissues were retrieved from tumour bearing and non-tumour bearing mice as described in Section 2.3. Lymph nodes were sectioned and stained for the lymphatic marker, LYVE-1 (1:300) and 488-conjugated chicken-anti-rabbit secondary (1:300), using methods outlined in Section 2.9. Details of all antibodies used are listed in Table 2.11 and 2.12 in Methods. Lymph nodes were imaged in accordance to methods outlined in Section 2.9.

For quantitative image analysis of whole lymph nodes, HALO™ software (PerkinElmer, USA) was used. Using DAPI counterstain, the edge of the lymph node was defined, and a mask created to detect LYVE-1 positive regions (Figure 3.1) within that defined area. Lymph nodes from three independent experiments were quantified,

with n=12 control NDNLs, n=13 Day 4 TDLNs and n=5 Day 11 TDLNs. Data was presented as box and whisker plots and statistically tested using One-way ANOVA with Tukey's multiple comparison test.

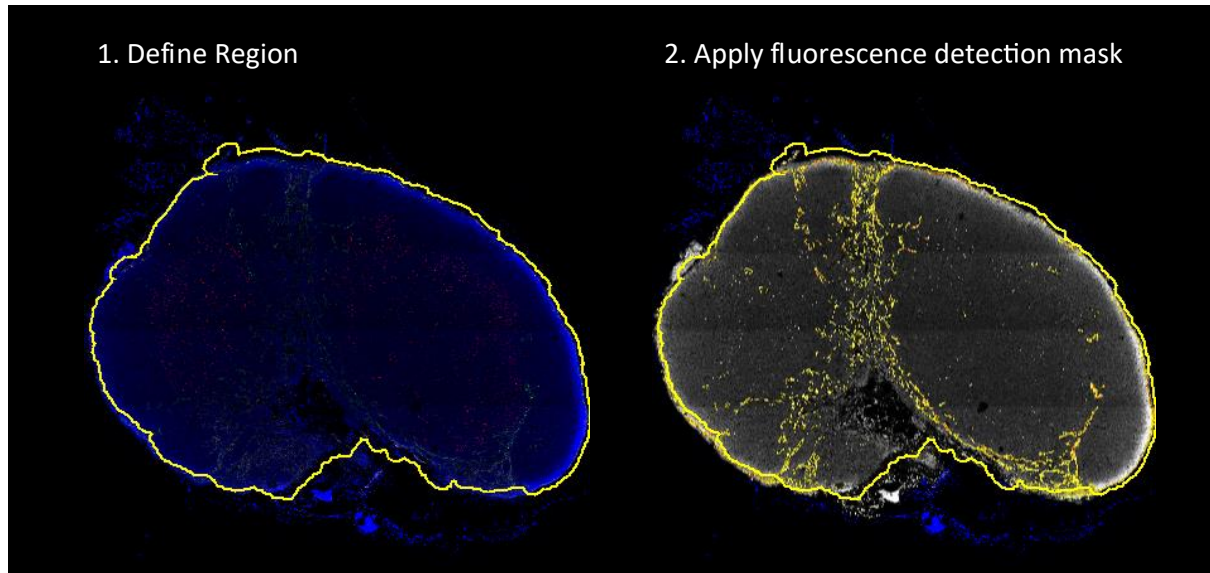


Figure 3.1. Method of quantifying lymphatic coverage in lymph nodes. Quantification of percentage lymphatic coverage relative to lymph node area using Halo™ image analysis software. A threshold mask was set to determine negative and positive LYVE1 staining. The area of quantification was then defined (1), followed by application of the fluorescent staining mask to detect positive LYVE1 staining (2). The defined area was then analysed for positive staining, and results generated and exported in Excel.

3.2.2. Bioinformatic Microarray Analysis

To define transcriptional changes across tumour development in LECs derived from early and late TDLNs, microarray analysis was conducted as described in Section 2.5. To visualise broad changes in gene expression between NDNLs and TDLNs volcano plots were generated in R-studio using package, ggplot2. Log₂ transformed fold change data was plotted against log₁₀ transformed p-values, with targets of significant fold changes visually identified and quantified on plots. Individual plots were created for Day 4 and Day 11 TDLNs respectively, comparing their gene target changes with control NDNLs. To identify changes in expression of specific gene targets, heatmaps were generated using the TIGR Multi-Experiment Viewer (MeV_4_8 Version 10.2) software (<http://en.bio-soft.net/chip/MeV.html>). Analysis was restricted to expression fold changes of ± 1.25 and p-value ≤ 0.05 . Fluorescent intensity values relative to the mean chip value for the top altered gene targets in Day 4 and Day 11 TDLNs were uploaded and subsequently normalized using row-centred mean. To elucidate

whether any of the altered gene targets in Day 4 and Day 11 TDLNs overlapped, online software Venny 2.0, was used (<http://bioinfogp.cnb.csic.es/tools/venny/>). Gene targets with significantly altered expression levels in Day 4 and Day 11 TDLN-LECs, were input and the number of genes overlapped, quantified and listed. Overlapping gene targets are listed in Appendix 1.

3.2.3. Gene Ontology Microarray Analysis

In order to investigate the specific functional implications of these transcriptional changes, pathway analysis was conducted using the Broad Institute's Gene Set Enrichment Analysis (GSEA) Molecular Signatures Database online (<http://software.broadinstitute.org/gsea>). This tool allows overlaps to be computed between a given gene set and gene sets in the database. Specific overlap analysis was carried out between 1,329 gene sets within Canonical Pathways, and significantly altered gene sets from our Day 4 and Day 11 TDLNs. Gene sets within Canonical Pathways are curated from a number of sources, including online databases and published literature, and includes gene sets derived from the BioCarta, Kyoto Encyclopedia of Genes and Genomes (KEGG) and Reactome pathway databases. The extent of overlap is quantified using FDR q-values, which represent probability that the normalized enrichment score represents a false positive finding. An FDR q-value of 0.05 implies that 5% of significant tests will be false positives. Only pathways with FDR q-values of <0.05 were hence selected.

The resulting ontology data was used to devise heatmaps, as described in Section 3.2, highlighting gross ontology changes across our dataset. Altered ontology pathways were also visualised using bar charts, plotting inverse log₁₀ transformed false discovery rate (FDR) q-values against GO Canonical Pathways, displaying significantly enriched pathways sorted in order of increasing transformed (inverse log₁₀) q-values. Ontology analysis was repeated with separate Day 4 and Day 11 data, and altered ontology pathways manually sorted into categories. Percentage representation of each pathway was then calculated relative to the total number of pathways and presented as pie charts. This gave us an indication of the most represented pathway at both early (Day 4) and late (Day 11) time-points. Pathways

were categorised as such; *Cell Signalling, Cell Cycle, Immunity, Endothelial, DNA Replication, Metabolism, Hypoxia, Apoptosis, Transcription* and *Other*. The categorisation of these pathways is listed in full in Appendix 2. As *Immunity* associated pathways were of particular interest, these were visualised using bar charts, with transformed FDR q-values plotted, as described above. Gene targets listed within *Immunity* associated pathways were then collated and visualised using heatmaps, as described in Section 3.2.

3.2.5. Verification of Microarray Data

In order to verify targets of interest from the microarray data, LECs were isolated from lymph nodes retrieved from tumour-bearing and non-tumour bearing mice, as described in Section 2.3. Samples were then processed for flow cytometry and immunofluorescent analysis.

For flow cytometry, lymph nodes were retrieved, digested and stained as previously described in Section 2.8. Podoplanin expression, within LECs (CD45- Podoplanin+ CD31+), was quantified using the geometric mean of fluorescent intensity (gMFI). Fold changes were calculated, within independent experiments, with individual NDLN and TDLN expression calculated relative to average expression of NDLNs. Fold changes were calculated relative to control NDLNs within independent experiments and statistically tested using One-way ANOVA with Tukey's multiple comparison tests.

For immunofluorescence, NDLNs and TDLNs were sectioned and stained for CCL21 (1:100) and Podoplanin (1:100), with the following secondary antibodies; 488-conjugated chicken-anti-rabbit (1:300), 405-conjugated donkey-anti-goat (1:300) and 647-conjugated goat-anti-Syrian hamster (1:300), using methods outlined in Section 2.9. Details of all antibodies used are listed in Table 2.11 and 2.12. Prepared sections were imaged as described in Section 2.9. For CCL21, murine experiments and imaging was conducted by colleagues.

3.2.6 Analysis of Cutaneous Melanoma TCGA Data

Using the Cancer Genome Atlas (TCGA) Cutaneous Melanoma dataset, published in 2015, of which included 333 primary and/or metastatic melanomas from 331 patients with 160 lymph node samples. From these lymph node samples, mRNA expression data for targets of interest were downloaded from the online portal cBioPortal Version 1.10.2. Targets of interest were restricted to lymphatic markers – *Prox1*, *Lyve1* and *Pdpr*; top up-regulated and down-regulated hits from Day 4 and Day 11 TDLNs – *Col5a1*, *Zbp1*, *Lpar1* and *Reln* and other altered immune-associated genes, namely *Ccl20*, *Ccl21*, *Sema6d*, *Ptx3*, *Vegfa* and *Jam3*.

To determine the correlation between these markers and dendritic cell infiltrate, mRNA expression for dendritic cell marker, *Itgax*, was grouped into low, medium and high expression, based on quartile ranges, with low expression defined as data \leq lower quartile; high expression defined as data \geq upper quartile; and medium expression defined as data ranging from the lower quartile to upper quartile. This data was then plotted against reciprocal expression data for the aforementioned gene targets. This determines whether any key lymphatic markers, or altered gene targets in our microarray, correlate with dendritic cell immunity, in the context of human melanoma. Overall this provides further insight into the role of lymphatic gene targets in anti-tumour immunity in a clinical context, with further work needed to elucidate the translational application of our observations in the human tumour microenvironment.

3.3. Results

3.3.1 Lymphatic expansion in TDLNs

In order to study the role of LECs in tumour progression, we chose a pre-metastatic model of melanoma, utilising the well-described syngeneic injectable B16.F10 melanoma model^{192,191,189,134}. The importance of using a pre-metastatic melanoma model lies in the lack of understanding in early tumour immune response kinetics. We wished to determine the relative contributions of lymphatics in immune modulation, at early stages of tumour development, in order to ascertain when and how immune suppression evolves in the tumour microenvironment. With published work demonstrating stromal responses in distal sites, such as lymph nodes, there is a strong indication that early tumour development can condition sites beyond the primary tumour. As stated in this project's hypotheses and aims (Section 1.6), we hypothesise that tumours in early stages of development, already begin to condition in particular TDLNs, which due to being essential sites for mounting immune responses, subsequently leads to altered immunity. Finally, we hypothesise that stromal changes in TDLNs, suggests that stromal cells, including lymphatic endothelial cells, have an active role in tumour progression and may play a critical role in immune modulation. Therefore, we first wished to assess lymphatic involvement in brachial lymph nodes draining of B16.F10 tumours.

Across tumour development, total TDLN cellularity was seen to increase progressively across time-points, with significant LN expansion seen as early as Day 4 post-injection, with LN cellularity fold changes of 2.32 and 2.98 at Day 4 and Day 11, respectively. The lymphatic compartment specifically was seen to expand in late TDLNs, with a significant increase in the number of LECs per LN seen at Day 14 (NDLNs Mean, 306.6 ± 182.15 ; TDLNs Mean, 1219.8 ± 265.41 ; $\Delta 913.13$) (Figure 3.2). These experiments were carried-out by and published by colleagues in the lab¹⁹¹. Interestingly, colleagues also showed that this was applicable to other stromal compartments with the number of BECs and FRCs per node also increasing, at Day 10 and Day 14¹⁹¹. This was also recapitulated in the $\text{Tyr}^{\text{CreER}}\text{Braf}^{\text{CA}}\text{Pten}^{\text{lox}}$ model, demonstrating these observations to be applicable to multiple murine melanoma systems¹⁹¹. The pre-metastatic state of these TDLNs was confirmed by colleagues in

the lab, with quantitative real-time PCR used to detect mRNA levels of melanoma markers, Tyrosinase-related protein-1 (Tyrp1) and Tyrosinase-related protein-2 (Dct), which were not detectable in TDLNs¹⁹¹. This hence demonstrates that the stromal changes occurring in TDLNs across these time-points is occurring in a pre-metastatic state.

To verify published data, and build upon these observations, we sought to determine the spatial lymphangiogenic patterns in TDLNs. We assessed the extent of lymphangiogenesis in TDLNs using whole node confocal imaging of LYVE-1-positive lymphatics. TDLNs were clearly enlarged at both Day 4 and Day 11, with apparent expanded lymphatics in Day 11 (Figure 3.3). Upon closer assessment of lymphangiogenesis, expansion was observed in Day 4 TDLNs, but this was limited to the subcapsular sinus, with little expansion seen in medullary regions. Whereas, in Day 11 TDLNs, extensive expansion could be seen both at the subcapsular sinus and in medullary regions (Figure 3.4).

Lymphatic coverage was subsequently quantified using image analysis software, confirming a significant increase in LYVE-1 structures per lymph node in Day 11 TDLNs (NDLNs Mean 6.08% \pm 0.58%; Day 11 TDLNs Mean, 11.73% \pm 1.91%). An increasing trend in lymphatic coverage, although more variable, was measured in Day 4 TDLNs (NDLNs Mean 6.08% \pm 0.58%; Day 4 TDLNs Mean, 9.11% \pm 1.47%) (Figure 3.5).

In contrast to the lymph nodes, matched tumours showed no intra-tumoural lymphangiogenesis, with limited expansion confined to peri-tumoural regions. Individual LYVE-1 positive cells could also be seen, indicating perhaps poor vessel formation in B16-F10 tumours (Figure 3.6a). This was also seen in *Braf*^{V600E}/*Pten* tumours, whereby tamoxifen induction on ear dermis, induced lymphatic expansion, with lymphatic rich regions also confined to the peri-tumoural areas in more developed tumours (Figure 3.6b, c). This suggests a communicative link between tumours and TDLNs, whereby microenvironment cues inducing lymphatic expansion at the primary tumour site, may indeed induce similar changes downstream in TDLNs.

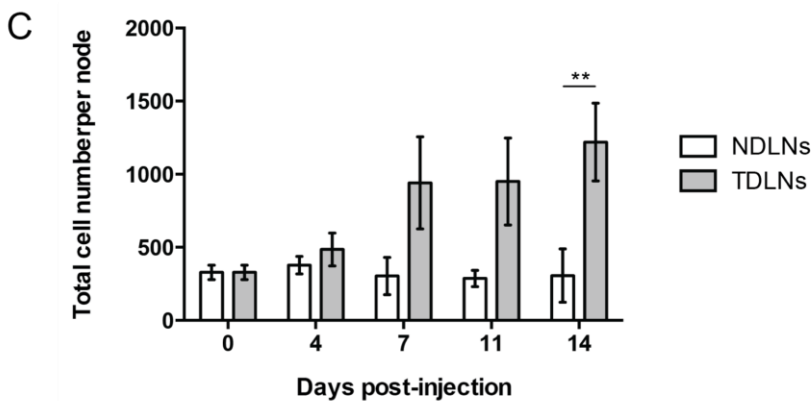
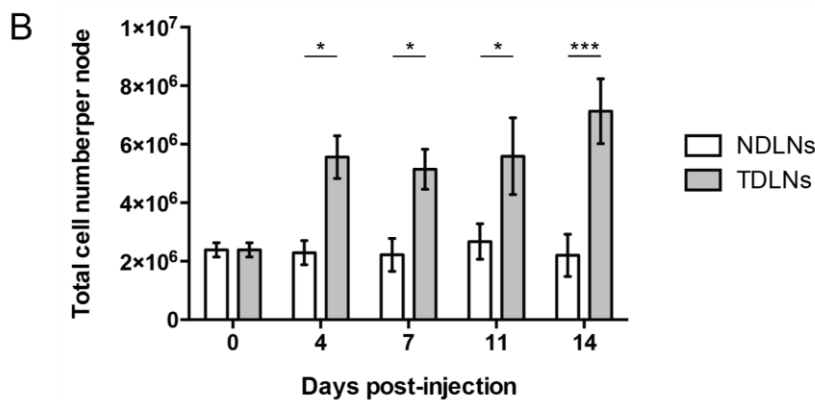
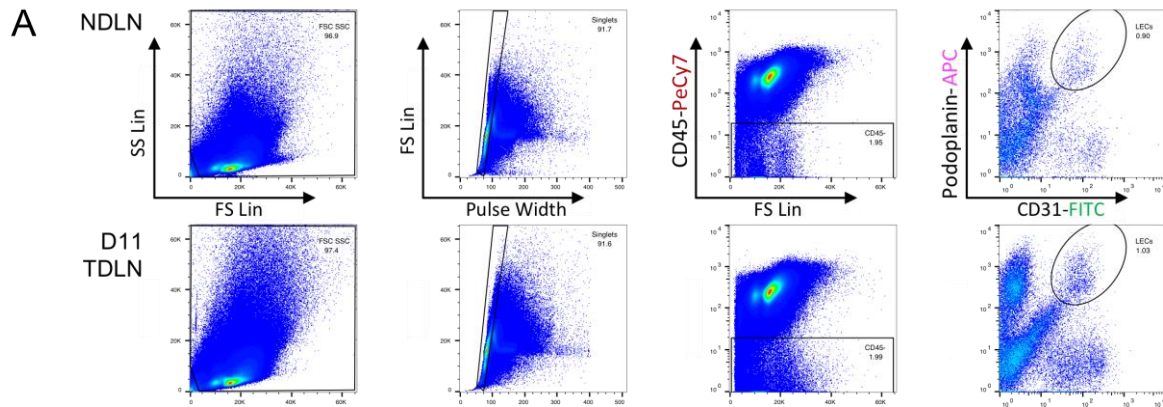


Figure 3.2. Lymph node and lymphatic expansion in TDLNs of B16-F10 tumours. Representative gating strategy to identify stromal populations in dLNs, shown here NDNLs (top panel) and Day 11 TDLNs (bottom panel). Gated within singlets CD45- Podoplanin+ CD31- denote FRC populations, CD45- Podoplanin- CD31 denote BEC populations and CD45- Podoplanin+ CD31+ denote LEC populations of interest, highlighted within the oval gate (A). NDNLs and TDLNs retrieved after 4-14 days post-inoculation with B16 F10 tumour cells, were analysed for total lymph node cellularity (B) and total count of CD45- Podoplanin+ CD31+ LECs (C). Shown is data from two independent experiments, with n=25 NDNLs and n=33 TDLNs total across time-points. Data presented as mean \pm SEM. Statistical significance was calculated using One-way ANOVA ($P \leq 0.05$). This data was acquired by Dr. Angela Riedel¹⁹¹.

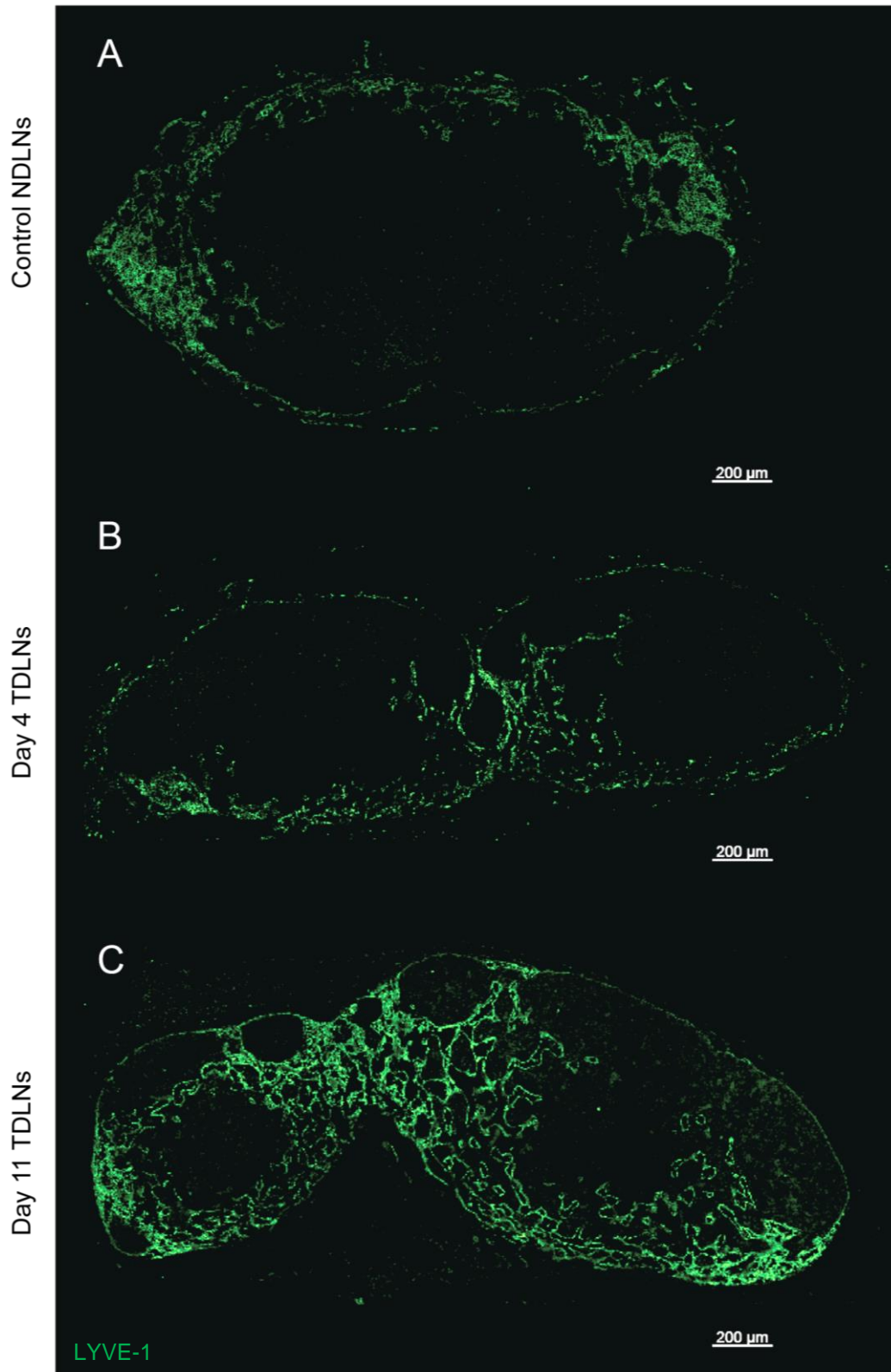


Figure 3.3. Lymphatic networks expand in tumour draining LNs over time. Control NDLNs (A), Day 4 early TDLNs (B) and Day 11 late TDLNs (C) from B16-F10 tumour bearing mice, were immunofluorescently stained for lymphatic marker, LYVE-1 (green). Whole lymph node tile scans taken at 20x magnification and imaged using a confocal microscope. Shown are representative whole node images from three independent experiments, with n=12 control NDLNs, n=13 Day 4 TDLNs and n=5 Day 11 TDLNs. Scales represent 200μm.

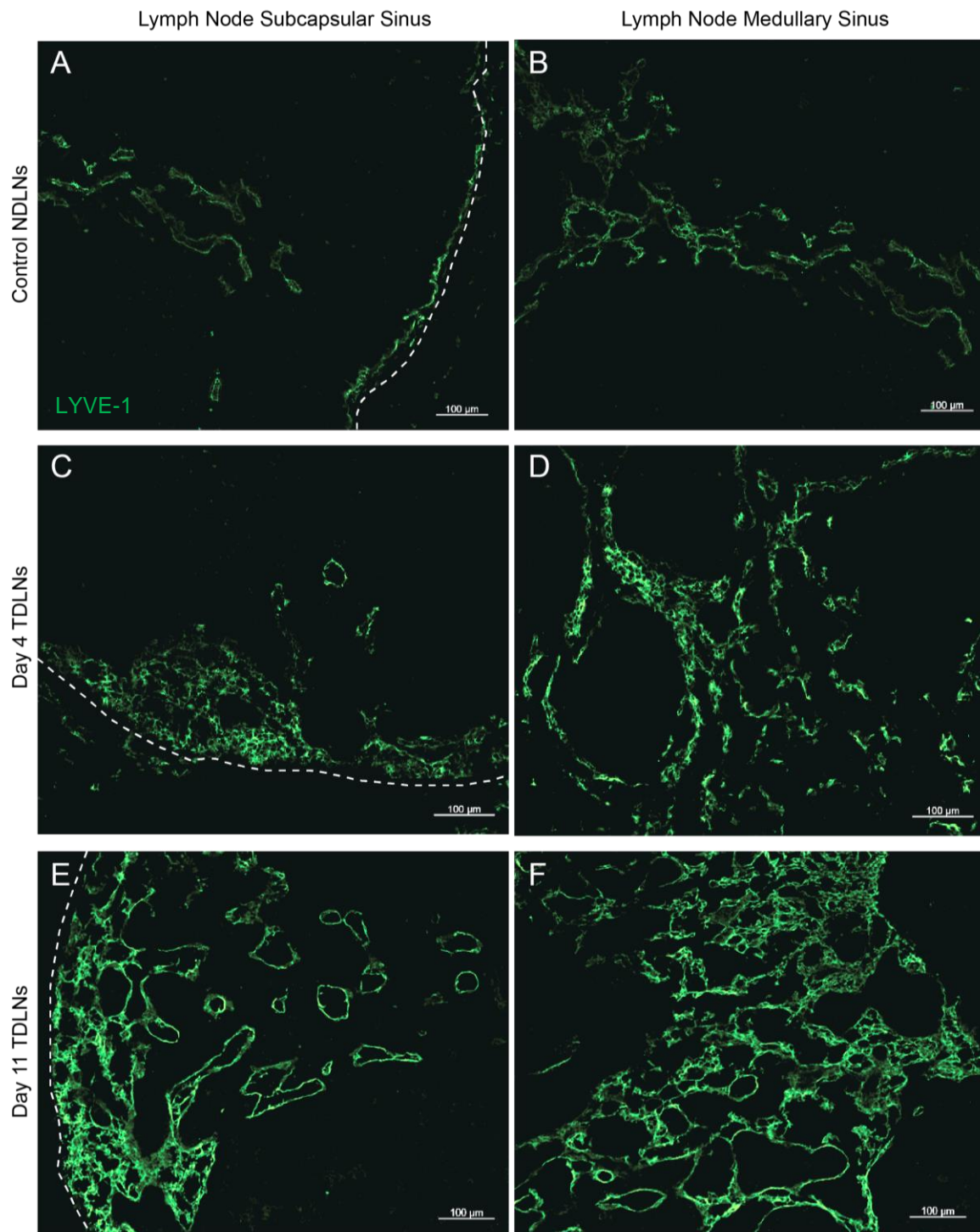


Figure 3.4. Lymphatic expansion occurs at the subcapsular sinus and in medullary regions on TDLNs. Control NDNLs (A), Day 4 early TDLNs (B) and Day 11 late TDLNs (C) from B16-F10 tumour bearing mice, were immunofluorescently stained for lymphatic marker, LYVE-1 (green). Whole lymph node tile scans taken at 20x magnification and imaged using a confocal microscope. Shown are representative regions of interest at the subcapsular sinuses (A, C, E) and medullary sinuses (B, D, F), with the dotted white line representing the lymph node edge. Shown are images from three independent experiments, with n=12 control NDNLs, n=13 Day 4 TDLNs and n=5 Day 11 TDLNs. Scales represent 100μm.

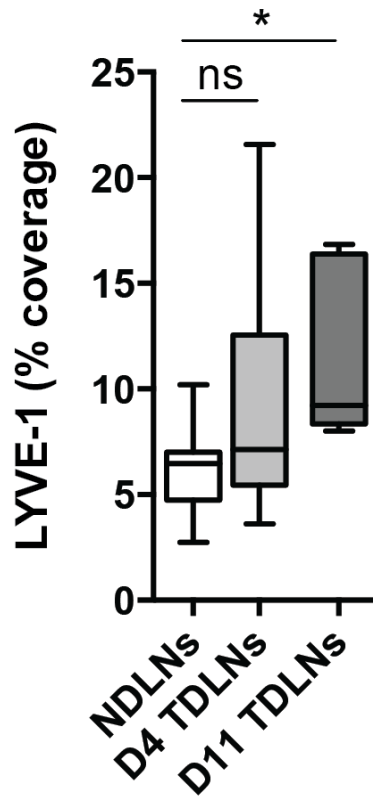


Figure 3.5. Whole node lymphatic coverage is significantly increased in late TDLNs. Control NDLNs (A), Day 4 early TDLNs (B) and Day 11 late TDLNs (C) from B16-F10 tumour bearing mice, were immunofluorescently stained for lymphatic marker, LYVE-1. Whole lymph node tile scans taken at 20x magnification were imaged using a confocal microscope and analysed for LYVE-1 coverage using Halo™ software. Using manually created detection masks, lymphatic coverage was quantified as the percentage of LYVE-1 positive staining (%) relative to the whole node area. Shown is data from three independent experiments, with n=12 NDLNs, n=13 Day 4 TDLNs and n=5 Day 11 TDLNs. Data presented as 25th to 75th percentiles box plots, with 5-95% percentile whiskers and median line shown. Statistical significance was calculated using One-way ANOVA ($P \leq 0.05$).

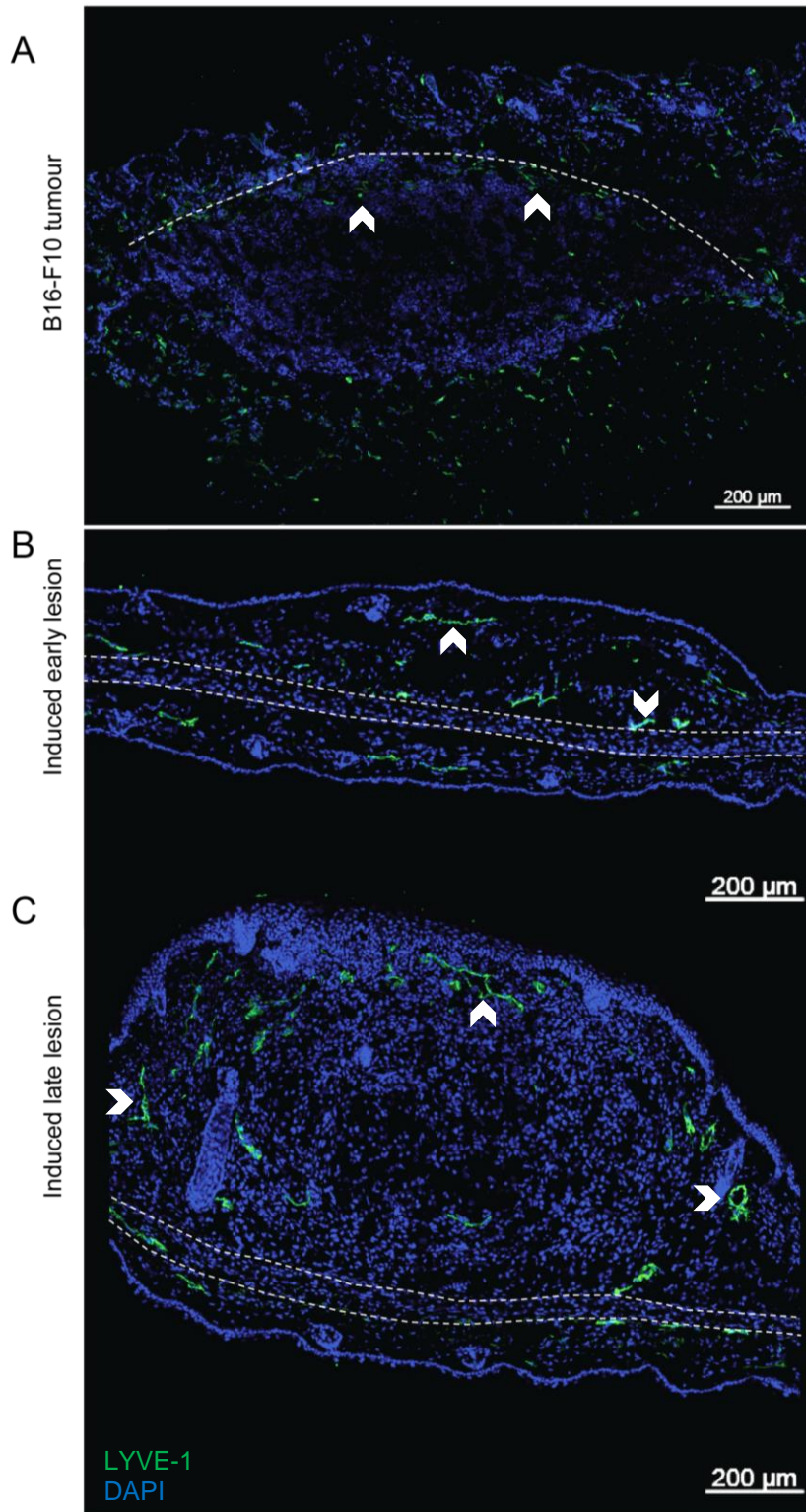


Figure 3.6. Lymphatic expansion occurs in peritumoural regions of melanoma tumours. Representative images of B16-F10 tumours retrieved from tumour-bearing mice at Day 11 post-inoculation (A) and $Braf^{V600E}Pten$ tamoxifen-induced tumours Day 14 (early) and Day 21 (late) post-induction (B, C). Tumours were immunofluorescently stained for lymphatic marker, LYVE-1 (green) and nuclei counterstained using DAPI (blue). Whole tumour tile scans were taken at 20x magnification and imaged using a confocal microscope. Arrow heads define lymphatic regions and dotted lines define the epithelial-tumour barrier (A) and auricular cartilage (B, C). Scale bars represent 200µm.

3.3.2 *Transcriptional alterations in LECs derived from TDLNs*

As described in the literature, lymphatic expansion serves to provide greater access to TDLNs once metastatic cells leave the primary tumour. However, TDLNs drain lymph rich in factors derived from the tumour microenvironment that have potential to act on cells of the lymph node. Indeed, the observation of expanded stromal compartments does suggest a TDLN response to factors and stresses derived from the tumour microenvironment. Thus, to elucidate whether expansion of the lymphatic compartment was accompanied by more extensive functional adaptations, we conducted whole-genome transcriptional profiling on freshly isolated LECs of NDNLs and TDLNs. LECs were isolated using flow cytometry, based on expression of both Podoplanin and CD31, within CD45 negative populations. As the number of LECs per lymph node is very low, with NDNLs ~500; TDLNs ~1000 (Figure 3.2c), we were unable to spare a sufficient number of cells for purity checking, cells were sorted directly into lysis buffer for RNA processing pre-transcriptional profiling. Using R-Studio package ggplot2 and software package MeV 4.8, microarray data was visualized using volcano plots and heatmaps (Figure 3.7). By plotting log-transformed fold changes against log-transformed p-values, trends in statistically significant targets could be visualised. A fold change cut off of 1.25 and p-value cut-off of 0.05 identified 149 genes to be down-regulated and 364 genes up-regulated in early Day 4 TDLNs (Figure 3.7a), with 303 genes down-regulated and 456 up-regulated genes in late Day 11 TDLNs (Figure 3.7b). Using the same statistical cut-offs, heatmap visualisation provided a list of altered genes at both Day 4 and Day 11 (Figure 3.7c), as listed in Appendix 1. As ranked by expression, the top up-regulated and down-regulated gene targets in early and late TDLNs were determined. This revealed distinct changes between LECs from NDNLs and TDLNs, as well as distinct changes between LECs from early and late TDLNs indicative of time-dependent reprogramming events specific to LECs of 'early' and 'late' TDLNs. The top up-regulated and down-regulated genes for Day 4 and Day 11, as shown in the heatmap (Figure 3.7c), are listed in Appendix 1. Despite distinct signatures, overlap analysis of Day 4 and Day 11 gene lists, visualised using Venn diagrams (Figure 3.7d), demonstrated that the expression of a number of gene targets were altered at both early and late time-points, with 43 genes commonly down-regulated and 53 genes commonly up-regulated in Day 4 and Day 11 TDLNs, as listed in Appendix 2.

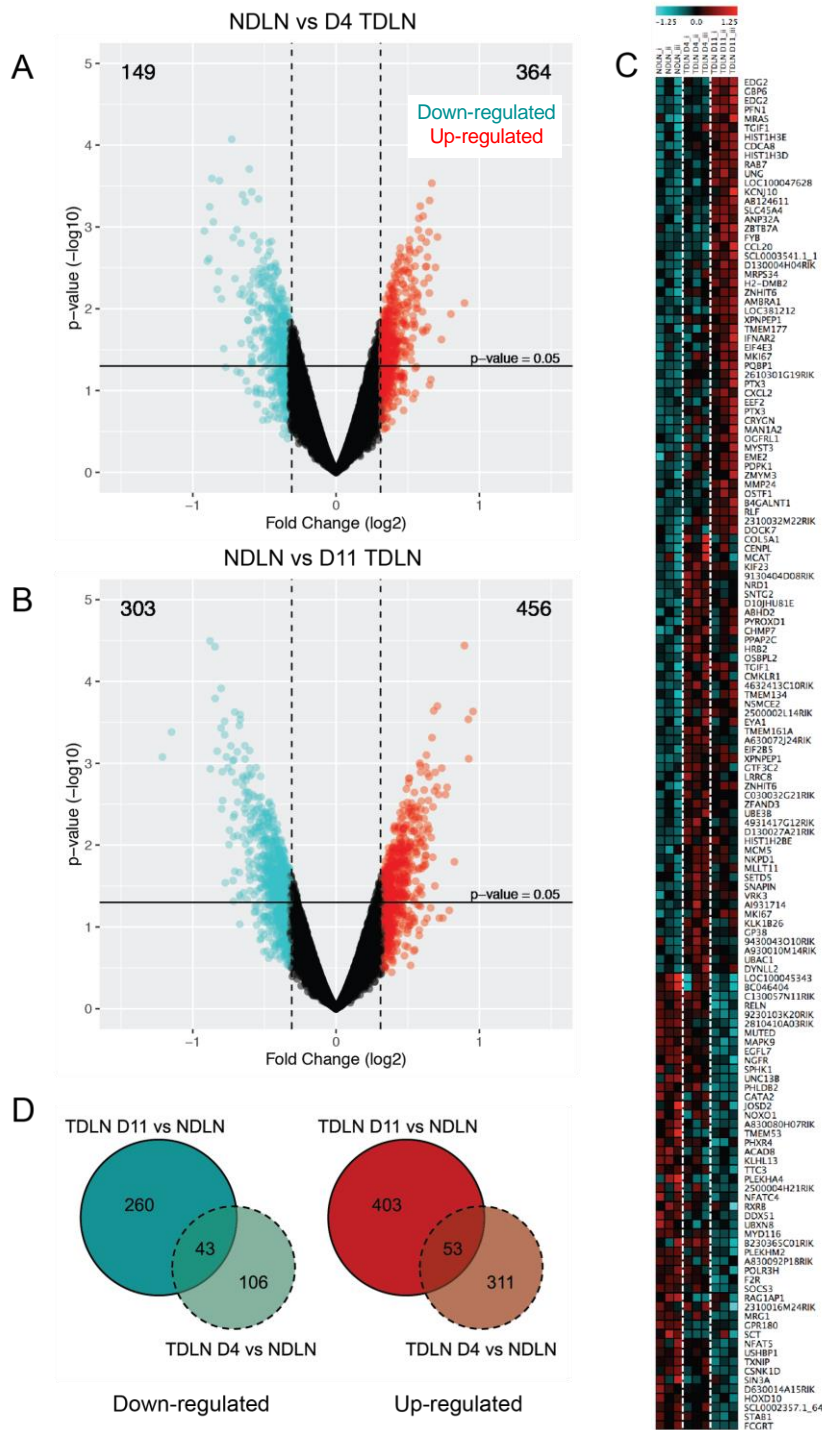


Figure 3.7. TDLN-derived LECs undergo time-specific transcriptional changes. Bioinformatic analysis was conducted on microarray data from LECs isolated from NDNL and Day 4 and Day 11 TDLNs from B16-F10 tumour bearing mice. Volcano plots show gene targets with statistically significant expression changes with fold changes ≥ 1.25 (red) and ≤ 0.75 (cyan) represented for both Day 4 (A) and Day 11 (B) TDLNs. Fluorescent intensity values for gene targets with statistically significant expression changes were visualised using heatmaps, showing trends in expression across gene targets and time-points (C). The number of down-regulated (cyan) and up-regulated (red) gene targets overlapping between time-points is shown in Venn diagrams (D). Data shown is from one independent experiment, with pooled brachial lymph nodes from $n=2$ mice per sample (total $n=18$). All altered gene targets from (C) and (D) are listed in Appendix 1 and 2.

Of the top significantly up-regulated gene targets, *Col5a1*, pro-collagen type V α -1, with a fold change of 1.86 ($P = 0.0085$), was the highest up-regulated gene at Day 4 was, with the highest up-regulated gene at Day 11 being *Edg2*, lysophosphatidic acid receptor 2, with a fold change of 1.93 ($P < 0.001$). The highest down-regulated gene at Day 4 was *Zbp1*, Z-DNA binding protein 1, with a fold change of 0.52 ($P = 0.0011$), and at Day 11 was *Reln*, Reelin, with a fold change of 0.54 ($P = 0.0012$).

The expression of *Col5a1* by LECs has been reported, despite usual association with BECs ¹⁹³. Transcriptional profiling of lymphatics in fibrosarcoma, reported down-regulation of *Col5a1*, as well as a number of other collagen-associated molecules, such as *Col5a2*, *Col6a1*, *Col6a2* and *Col3a1*¹. This is contrary to our findings and suggests differential transcriptional changes occur in lymphatics at the primary tumour site and TDLNs, with tumour model variance acting as another confounding variable. In terms of its possible functional relevance in early TDLNs, epithelial cells in the presence of fluid sheer stress express *Col5a1*¹⁹⁴ and expression of *Col5a1* has been reported in association with HIF-1 α ¹⁹⁵. Hence, despite little reporting of *Col5a1* expression by LECs, TDLN-resident LECs may be expressing *Col5a1* as a result of altered biophysical and biochemical cues derived from the tumour. Also, colleagues have seen hypoxic signatures in early B16-F10 tumours [personal communication], suggesting that perhaps early TDLNs are experiencing distal hypoxia, with *Col5a1* expression a potential consequence.

The lysophosphatidic acid receptor 1 (LPAR1), is encoded by gene target *Edg2*, binds lysophosphatidic acid (LPA) and is well characterised to promote endothelial cell wound healing¹⁹⁶. LPA produced by platelets binds LPAR1 and regulates endothelial cell permeability, proliferation and migration through specific signal transduction pathways^{197,198}. Due to this interaction between platelets and endothelial cells, LPAR1 is considered to be an important receptor driving LPA-mediated vascular regeneration^{197,198}. Translating this to lymphatic dynamics in TDLNs, this signature is suggestive of lymphatics undergoing expansion and reprogramming in response to a wound-healing type state. As the developing tumour has been described as a “wound that never heals” ¹⁹⁹, TDLNs may be adopting a similar state.

Zbp1, initiates innate immune responses through binding of cytosolic foreign DNA and engagement of type-1 interferon signalling. In endothelial cells, *Zbp1* assists in enhanced microvascular permeability and leukocyte adhesion in response to DNA recognition²⁰⁰. Murine *Zbp1* is mostly expressed in spleen, liver and lung, however in human, expression is strongest in lymphatic tissue. Not only does this imply that down-regulated *Zbp1* expression could result in altered lymphatic permeability in TDLNs, but it also implies that type-1 interferon signalling cascades are perturbed. As type-1 interferon is associated with tissue damage sensing^{201,202}, decreased expression of *Zbp1* may result in an impaired tissue damage response in the lymphatics of TDLNs.

Reelin is encoded by gene target *Reln* and is an essential matrix molecule needed for lymphatic vessel development²⁰³, reported to act as a key signalling molecule between smooth muscle cells and lymphatic endothelial cells²⁰⁴. As expression of *Reln* is decreased in late TDLNs, this may be acting as a negative regulatory mechanism to control lymphatic expansion. Also, as smooth muscle cells have long since been known to line the lymph node capsule²⁰⁵, there is likely to be further localised regulation of lymphatic behaviour from other stromal compartments within TDLNs.

Altogether, these analyses demonstrate that LECs derived from TDLNs are responding to a plethora of biochemical and biophysical cues, and consequently undergoing significant transcriptional reprogramming, with distinct temporal changes. Top hits are indicative of altered endothelial permeability, migration and immune interactions and allude to complex signalling networks with other stromal compartments.

To gain a more precise understanding of the functional and temporal changes occurring in TDLN-derived LECs, ontology analysis of all targets with significant expression changes across both Day 4 and Day 11 TDLNs was conducted. Analysis revealed a range of altered canonical pathways (Figure 3.8), which are listed in Appendices 3 and 4.

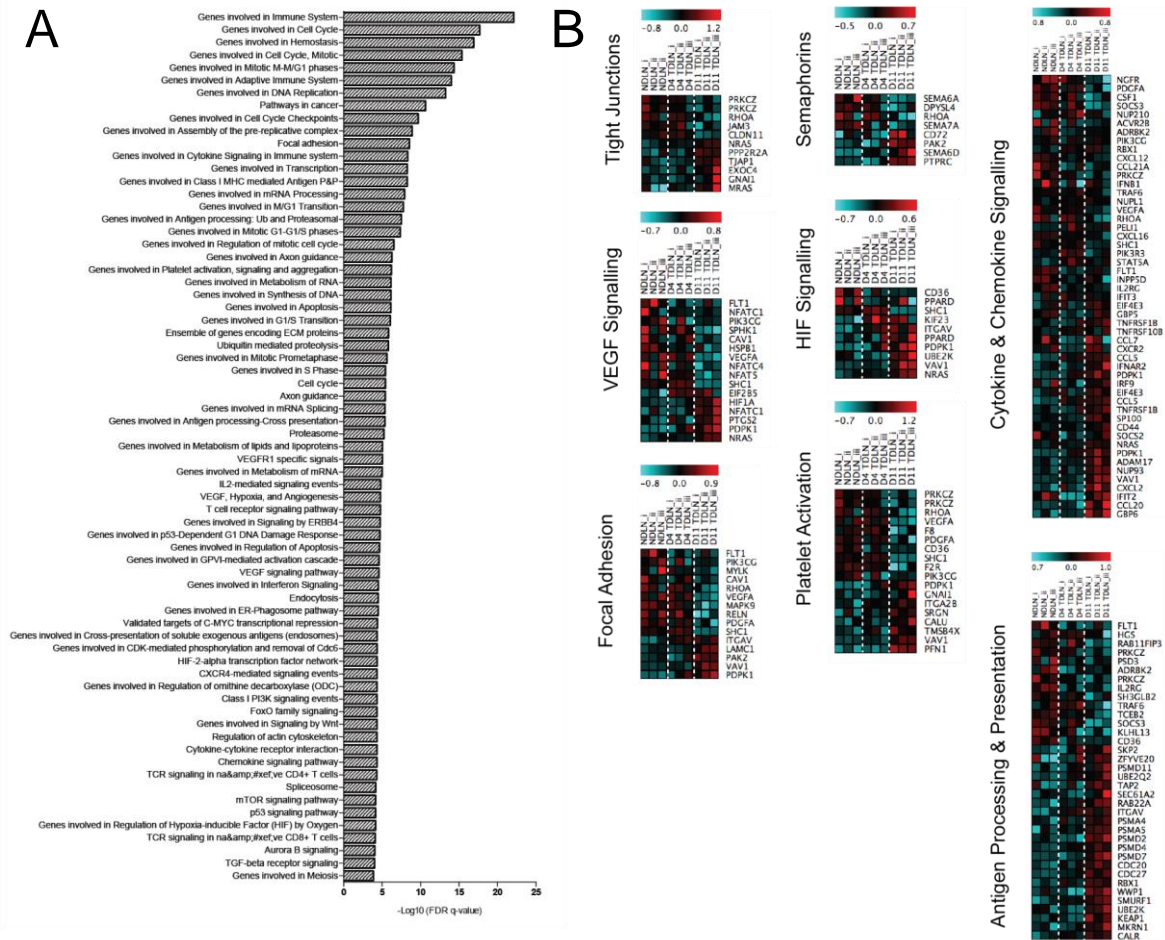


Figure 3.8. Gene targets from immune signatures and key endothelial pathways have altered expression levels in TDLN-derived LECs. Gene targets with statistically significantly expression changes from Day 4 and Day 11 TDLNs, from B16-F10 tumour bearing mice, were analysed for changes in canonical pathways, using online GSEA tools. Listed are the most represented pathways from all gene targets with statistically significantly expression changes across TDLNs, ranked according to their $-\log_{10}(\text{FDR } q\text{-value})$. (A). Fluorescent intensity values for gene targets with statistically significantly expression changes were visualised using heatmaps for canonical pathways of interest. Genes with expression fold changes ≥ 1.25 shown in red and ≤ 0.75 shown in cyan (B). Data shown is from one independent experiment, with pooled brachial lymph nodes from $n=2$ mice per sample (total $n=18$). All altered pathways and gene targets are listed in Appendix 3 and 4.

Expression of gene targets from canonical endothelial pathways, such as VEGF, Angiogenesis and Platelet Activation were altered, as well as pathways pertaining to Focal Adhesion, Tight Junctions and Hypoxia (Figure 3.8b). Across these pathways, decreased expression of *Jam3* and *Cldn11* alluded to changes in endothelial permeability or immune cell interactions, as both govern endothelial tight junction integrity, and Jam-C, encoded by gene *Jam3*, regulates the transendothelial migration of a number of immune cells^{60,61}. This not only has obvious implications for immune

cell migration and access, particularly dendritic cells, that traffic from the periphery to lymph nodes via lymphatics, but also for selective permeability of TDLNs. Altered permeability may result in greater exposure to antigen, which has implications for the anti-tumour immune response.

Changes in angiogenic growth factors, suggests that the expansion of lymphatic networks in TDLNs is being regulated transcriptionally. Specifically, endogenous expression of VEGF-A in endothelial cells has been found to maintain expression of VEGFR-2 and key vascular proteins²⁰⁶, hence down-regulation of down-stream gene target, *Vegfa*, as seen in Day 11 TDLNs, may be acting as a homeostatic regulator of lymphangiogenic expansion. Also known as a regulator of focal adhesion, down-regulation of *Vegfa* may also have implications for LEC-ECM interactions and hence lymph node lymphatic endothelium integrity. Further regulators of angiogenesis, such as *Cd36*, known as a negative regulator, and *Nras*, known to cooperate with VEGF to promote angiogenesis in hypoxic and normoxic conditions were also down-regulated, further suggesting that a complex network of signalling events govern lymphangiogenic responses in TDLNs. Of interest, is that TDLNs, as well as upstream tumours, may be hypoxic, with *Shc1* and *Itgax*, both associated with hypoxia signalling^{207,208}, up-regulated in TDLNs.

Finally, a number of immune-associated pathways were altered, with the expression of a number of targets involved in Antigen Processing and Presentation, and Cytokine and Chemokine Signalling, altered. The following gene targets were amongst the plethora of immune-associated gene targets with expression changes; Chemokines, *Cxcl2*, *Cxcl12*, *Cxcl16*, *Cxcl19*, *Ccl5*, *Ccl20* and *Ccl21*; Semaphorins, *Sem6a*, *Sema6d* and *Sema7a*; Immune Receptors, *Il2rg*, *Cd44*, *Adam17*, *Cd36*, *Ifnar2* and *Trl4*; immune signalling molecules, *Cd74*, *Calr* and many proteasomal subunits (*Psm4*, *Psm5*, *Psm4*, *Psm7* and *Psm11*). This highlighted a strong immunity signature in TDLN-derived LECs and gave convincing reason to further pursue immune functionality of TDLN-derived LECs.

To assess the relative contribution of expression changes in immune-associated pathways at individual time-points, ontology analysis was repeated for Day 4 and Day 11 gene lists. Of these time-point specific ontology pathway lists, pathways were

categorised according to their functional role, for example with *Antigen Processing and Presentation* being categorised as an '*Immunity*' pathway. Analysis revealed that 15.7% of all altered pathways at Day 4 and 20.0% at Day 11 were classified as *Immunity* pathways (Figure 3.9). Other represented pathway families included, *Cell Signalling*, *Cell Cycle*, *DNA Replication*, *Transcription*, *Metabolism*, *Apoptosis*, *Hypoxia* and *Endothelial biology*, as detailed in Appendix 5.

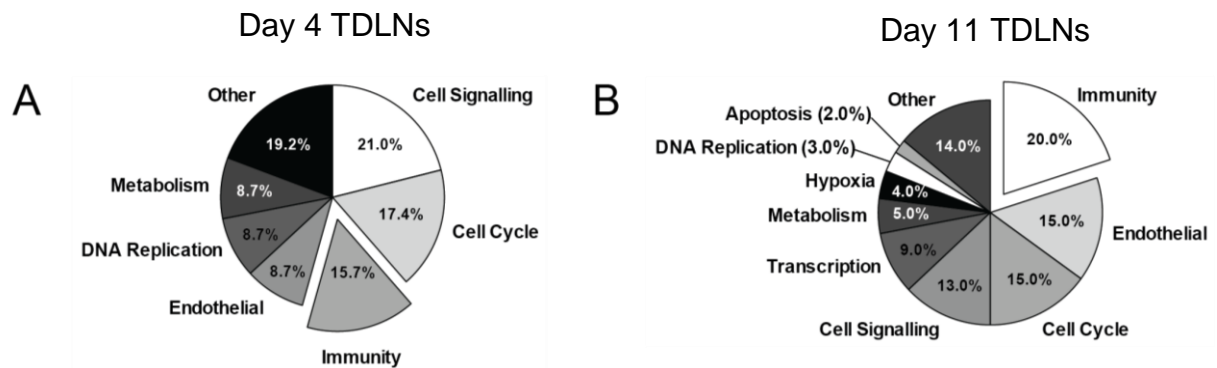
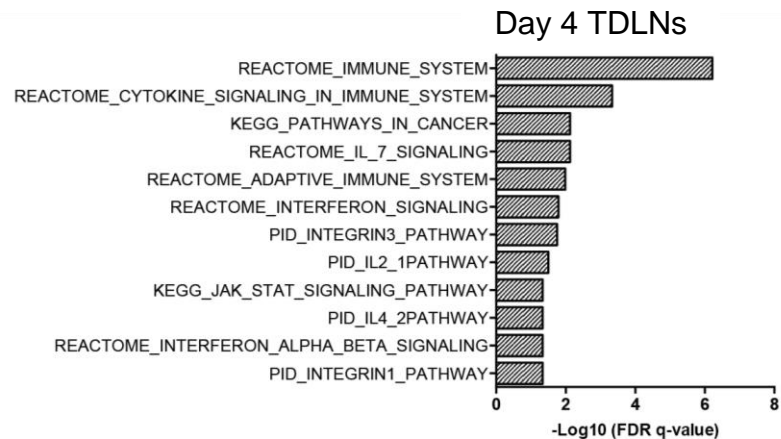


Figure 3.9. *Immunity* pathways are highly represented in early and late TDLNs, relative to other canonical pathways Significantly represented canonical pathways from GSEA analysis were manually categorised. Categorisation was based on which ontological family the individual pathway represented e.g. antigen presentation was categorised as an *Immunity* pathway. The total number of individual pathways within an ontological family was calculated as a percentage (%) of the total number of pathways altered and presented as pie charts. *Immunity* pathways are represented in both Day 4 TDLNs (A) and Day 11 TDLNs (B) and shown here in the pop-out pie chart segments. Manual categorisation of pathways is detailed in Appendix 5.

Immunity associated pathways were then visualised using bar charts, plotting transformed FDR q-values (Figure 3.10). Of the specific pathways listed, *Adaptive Immunity*, *Integrins*, *Cytokines & Chemokines (IL-4, IL-2, IFN, IL-7 and CXCR4)*, *Antigen Cross-Presentation*, *Semaphorins* and *Vascular Cell Surface Interactions*, were all identified. Aside from *Reactome_Immune System* and *Reactome_Adaptive Immune System*, which listed top in both Day 4 and Day 11 ontology analysis, *Cytokine Signalling* and *Antigen Processing and Presenting*, were the most represented *Immunity* pathways in Day 4 and Day 11, respectively.

A



B

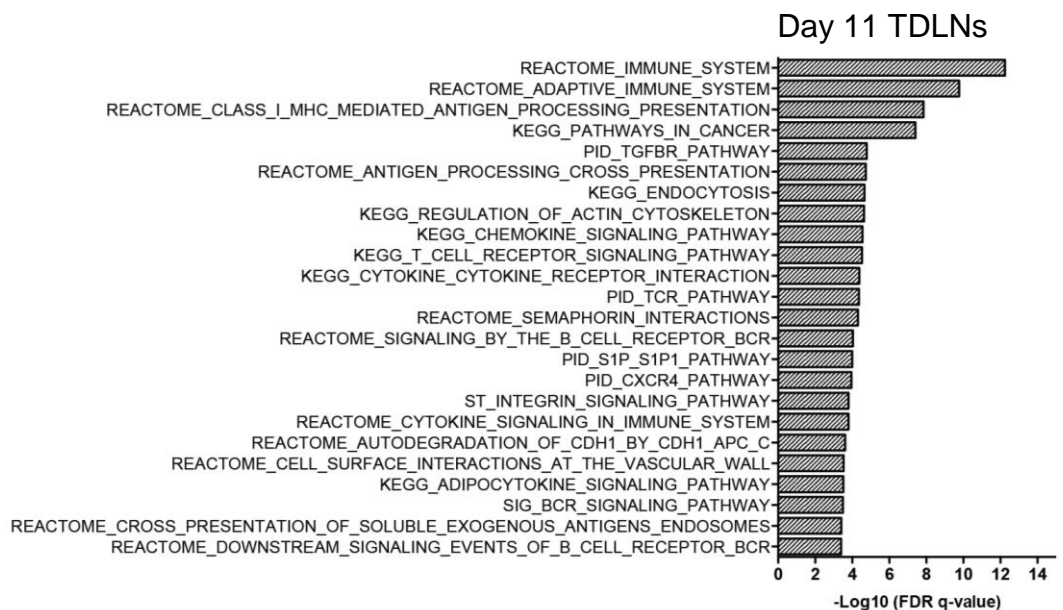


Figure 3.10. Specific *Immunity* pathways with altered gene expression profiles in TDLNs. *Immunity* pathways with altered gene expression profiles from both Day 4 (A) and Day 11 (B) TDLNs are ranked according to their $-\log_{10}(\text{FDR } q\text{-value})$, showing the most represented pathways at both time-points. Data shown is from one independent experiment, with pooled brachial lymph nodes from $n=2$ mice per sample (total $n=18$).

To investigate the specific genes assigned to *Immunity* associated pathways in a time-point dependent manner, heatmaps were created to visualise specific genes from *Immunity* pathways with altered gene expression profiles in early at Day 4 and Day 11 (Figure 3.11), as listed in Appendix 6. *Immunity* associated gene targets are listed in Appendix 6.

In addition to automated pathway analysis of TDLN gene sets, lymphatic gene targets known to be involved in specific Immunity pathways, that were absent from GSEA analyses, were manually added. For example, the stromal marker Podoplanin (or GP38 as it's also known), expressed on cancer-associated fibroblasts (CAFs), FRCs and LECs, and described to be important for dendritic cell migration, was incorporated into these heatmaps.

In Day 4 TDLNs (Figure 3.11a), key down-regulated Immunity genes included collagens *Col1a2* and *Col5a1*, as well as *Ccl21*. Collagen V forms reticular networks in a number of tissues, including the lymph node and Collagen-I is a key component of the lymph node capsule, as well as the conduits running throughout the node, which both provide key structural support. Increased collagen density is often observed in tumour-draining and metastatic lymph nodes, implying that any changes in collagen deposition in lymph nodes is driven by other stromal cells, such as FRCs. Indeed, work from our lab shows that FRCs increase their collagen production in TDLNs¹⁹¹, suggesting that LECs may not contribute greatly to structural changes in the node, with FRCs instead providing the critical building blocks for structural lymph node remodelling. LEC-derived CCL21 is an essential chemokine for dendritic cells, with a gradient across the SCS necessary to facilitate entrance of dendritic cells into the node. Once within the node, secretion by FRCs guides dendritic cells from the node edge to T-cell zones. As well as being produced by FRCs and LECs in the node, CCL21 is produced by peripheral lymphatics, providing not only a directional cue for entry but also a guidance cue for dendritic cells to reach larger collecting lymphatic vessels, whereby biophysical factors play a larger role in dendritic cell migration. CCL21 in draining lymph nodes, can hence derive from peripheral sources also. Key up-regulated Immunity genes included cytosolic DNA binding protein gene, *Zbp1*, interferon response genes such as *Ifnb1*, *Ifit2* and *Ifit3* and lymphatic marker, *Pdpr*. This suggests that lymphatic marker Podoplanin may exhibit a specific functional role in reprogrammed lymphatics, which is a novel finding, and that interferon signalling is a key transcriptional change in early TDLN lymphatics, brought on perhaps by detection of tumour DNA or danger associated molecular patterns (DAMPs) from tissue damage, draining from early developing tumours.

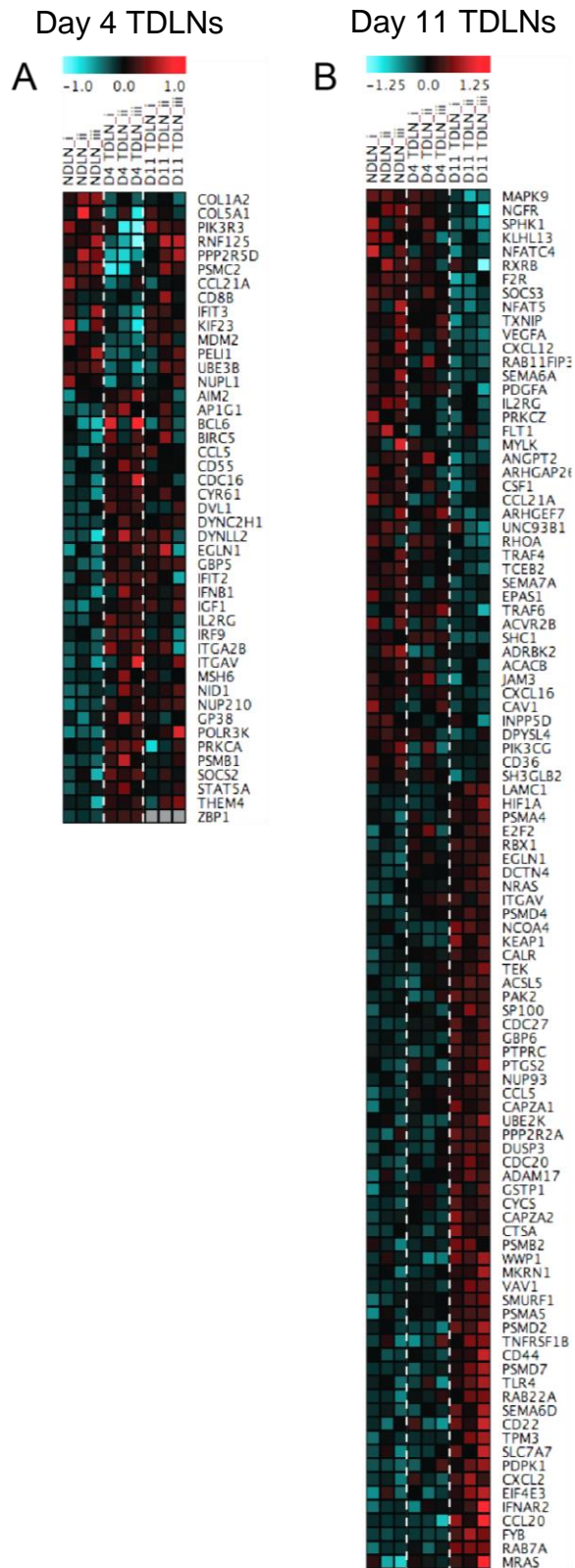


Figure 3.11. Genes associated with *Immunity* pathways with altered gene expression profiles in TDLNs. Fluorescent intensity values for *Immunity* associated gene targets with significantly altered expression levels in Day 4 TDLNs (A) and Day 11 TDLNs (B) relative to control NDNLs, were visualised using heatmaps. Genes with expression fold changes ≥ 1.25 shown in red and ≤ 0.75 shown in cyan. Data shown is from one independent experiment, with pooled brachial lymph nodes from $n=2$ mice per sample (total $n=18$). Altered gene targets are listed in Appendix 6.

In Day 11 TDLNs (Figure 3.11b), key down-regulated *Immunity* genes of interest included *Ccl21a*, *Cxcl12*, *Sema6a*, *Pdgfa*, *Angpt2*, *Cldn11* and *Jam3*. As previously described, CCL21 is a key chemokine for dendritic cell migration, governing both its peripheral entry to lymphatic vessels but also its entry to and through lymph nodes. Endothelial-derived CXCL12 has been associated with B-cell proliferation, macrophage recruitment and maintenance, and is found to be over-expressed in a number of tumours, with angiogenic characteristics^{209, 210}. Semaphorin-6A (encoded by gene, *Sema6a*), Platelet-derived growth factor-A (encoded by gene, *Pdgfa*) and Angiopoietin-2 (encoded by gene, *Angpt2*), are all soluble factor regulators of angiogenesis, with Angiopoietin-2 also identified as a regulator of endothelial cell inflammatory response, sensitizing endothelial cells towards TNF- α , which enhances immune adhesion to endothelium. A prominent signature for neovascularisation is expected due to the expansion of lymphatics in late TDLNs, which in itself could act to modulate immune cell entry due to altered immune cell interactions. Chemokines were also up regulated in Day 11 TDLNs, namely *Sem6d*, *Ccl20*, *Cxcl2* and *Ccl5*. These genes encode factors that have been described as mediators of dendritic cell activation, recruitment and migration (Semaphorin-6D and CCL20), and other leukocyte recruitment, such as T-cells, neutrophils (CXCL2) and granulocytes (CCL5). This suggests that not only is chemokine signalling perturbed in early TDLNs, but is also altered in late TDLNs, indicative of a sustained transformation in TDLNs across tumour development, and coincident impacts on the immune microenvironment.

Furthermore, gene targets *Jam3* and *Cldn11*, denoting endothelial junctional molecules Jam-C and Claudin-11, were down-regulated significantly in Day 11 TDLNs. These molecules, amongst others, are important for maintaining junctional integrity and for facilitating fluid drainage, and respond to shear stresses, the soluble milieu and migrating immune cells^{61,211,3}. Jam-C has been specifically described as a negative regulator of immune cell trafficking, implying that down-regulation in late TDLNs would result in heightened trafficking⁶¹. Jam-C has also recently been identified as a regulator of VEGF-C, promoting lymphangiogenesis and tumour metastasis. This suggests that in late TDLNs where expression of *Jam3* is down-regulated, that perhaps late TDLNs are undergoing a state of negative regulation of lymphangiogenesis²¹². In addition, the role of Jam-C in terms of immunity appears

complex with one study showing a pro-migratory function⁶⁰ and another study demonstrating knock-out resulted in heightened pro-inflammatory responses and enhanced immune trafficking through increased VCAM-1 expression²¹³. In regards to Claudin-11, little has been described in lymphatic endothelium, with other Claudin family members reported in dermal lymphatic vasculature, namely Claudin-5²¹⁴. Hence, collectively in terms junctional molecules, down-regulation has implications not only for lymphatic permeability at TDLNs but also for immune trafficking and lymphangiogenesis.

Interestingly, many antigen processing-associated gene targets denoting proteasomal subunits (*PsmA4*, *PsmA5*, *PsmD2*, *PsmD4*, *PsmD7*), RAB proteins and Calreticulin were up-regulated in Day 11 TDLNs. This may imply that lymphatic endothelial cells of TDLNs acquire enhanced antigen processing and presenting functions, which would have direct ramifications on T-cell priming and other antigen pathways reported to occur in the lymph node, such as antigen archiving and transfer¹²⁰. Genes encoding co-stimulatory molecules, *Cd80* and *Cd86*, which are required by professional APCs to prime antigen-specific T-cell responses, were detected by the microarray, demonstrating expression at gene level in LN-LECs. Expression of these markers, were however unchanged in Day 4 or Day 11 TDLNs with p-values >0.05 (Day 4 TDLN Fold Change = 0.94; Day 11 TDLN Fold Change = 1.05). This is contrary to literature stating low-undetectable protein expression levels of CD80 and CD86 in LN-LECs¹²².

Overall, these genes primarily describe a strong immune signature for TDLN-derived LECs, with data suggesting potential DNA-sensing in early TDLNs, enhanced antigen processing and presentation in late TDLNs and a significant change in immune interactions through expansion of lymphatic networks and altered soluble milieu. Specifically, altered chemokine signalling in both Day 4 and Day 11 TDLN-derived LECs, suggests this a consistent transformation, across the lymphatic compartment and throughout tumour development. With a plethora of chemokines altered, this data suggests LECs may play a role in migration of a number of immune populations, with altered expression likely having an impact of migratory behaviour of many immune cells. With accompanying changes to expression of Podoplanin, which is a novel physical regulator of immune cell migration, and potentially altered lymphatic permeability, these changes suggest not only soluble modulation of immune migration

by LECs, but also a physical involvement. With similar changes observed in FRCs¹⁹¹, this data demonstrates that factors derived from the tumour microenvironment affect similar axes across stromal compartments. Whether these factors enhance or perturb expression is hence dependent on which stromal compartment and on the time-point, be it early or late in tumour development. It is also likely that certain early and late changes are functionally linked, with early changes precluding late changes. This would require further investigation but would shed light on the complex functional interactions of stromal compartments, both in steady state and in response to factors derived from the tumour microenvironment.

3.3.3 Verification of microarray identified targets of interest

Assessing the transcriptional changes across both Day 4 and Day 11 TDLN-derived LECs, early immune signatures alluded to changes in critical gene targets associated with lymphatic permeability and immune trafficking. We hence chose to verify *Cdh5*, *Cldn11*, *Jam3*, *Ccl21* and *Pdpr*.

Firstly, we verified junctional molecule gene targets, *Cdh5*, *Cldn11* and *Jam3*, as decreased expression in TDLN lymphatics implies disrupted permeability and enhanced leakiness, which has implications for access of antigen and trafficking immune cells into TDLNs (Figure 3.12). In the microarray, no significant change was seen in *Cdh5*, with a down-regulated fold-change of 0.88 and p-value of 0.40 in Day 11 TDLNs relative to control NDNLs. Whereas, *Cldn11* and *Jam3* were both significantly down-regulated, with a fold-change of 0.74 and 0.73 and p-values 0.01 and 0.02, respectively. Using qRT-PCR, we were able to recapitulate the decreasing trends in Day 11 TDLNs seen for *Cldn11* and *Jam3*, with statistically significant decreases seen in *Cldn11* expression at Day 4 and *Jam3* expression at Day 11. Fluctuating changes were seen across TDLNs in *Cdh5* expression, however no significant changes were found, further recapitulating trends seen in the microarray. This collectively suggests that certainly at an RNA level, expression of junctional molecules in LN-LECs is indeed perturbed in TDLNs, with likely temporal changes through tumour development.

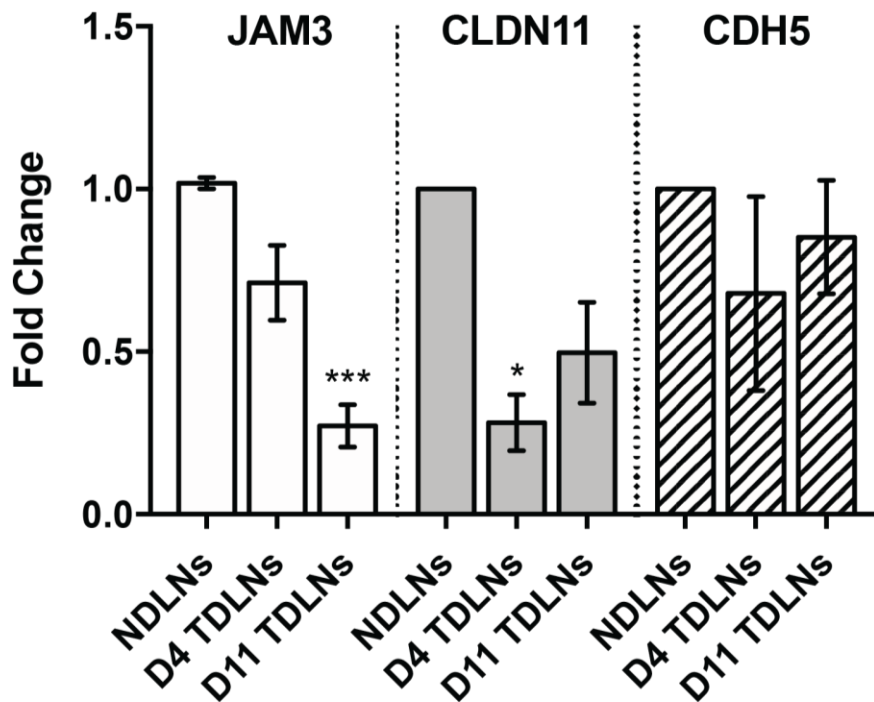


Figure 3.12. Verification of LN-LEC RNA expression trends of junctional molecules. qRT-PCR was conducted on LN-LECs samples isolated from control NDNLs, Day 4 TDLNs and Day 11 TDLNs. TaqMan™ probes against JAM3, CLDN11 and CDH5 were used to detect changes in junctional molecule expression. Shown is data from two independent experiments, with n=4 NDNLs and n=5 Day 4 TDLNs and n=5 Day 11 TDLNs. Data presented as mean ± SEM. Statistical significance was calculated using One-way ANOVA ($P \leq 0.05$).

As CCL21 is a critical chemokine for immune priming dendritic cells, down-regulation of CCL21 expression in LECs has many implications for dendritic cell migration. Altered expression of CCL21, by LN-LECs in particular, could have direct impact on dendritic cell migration across the subcapsular sinus, as it is there that LEC-established chemokine gradients govern traversing dendritic cells. Immunofluorescent staining of CCL21 in early TDLNs, showed no visible change in CCL21 distribution or expression, with CCL21 seen universally expressed in the capsule, across conduits, and on vascular venules (Figure 3.13). However, as CCL21 can drain via lymphatic vasculature from peripheral tissue and is also produced by FRCs in lymph nodes, we are merely describing here the total CCL21 content in lymph nodes rather than production. This suggests that CCL21 is present in early TDLNs and appears consistently distributed, hence despite transcriptional down-regulation in LECs,

CCL21 within the early TDLN is intact. Interestingly colleagues described a loss of CCL21 RNA expression in FRCs derived from Day 11 TDLNs, which further suggests that aberrant organ-wide CCL21 expression is a feature of many stromal cell subsets, in TDLNs from later stages as well as early stages of tumour development. As this work did not quantify CCL21 protein expression, as it would be non-specific to lymphatic derived CCL21, further work is required to quantify changes in CCL21 protein expression and secretion across stromal populations in TDLNs from different stages of tumour development.

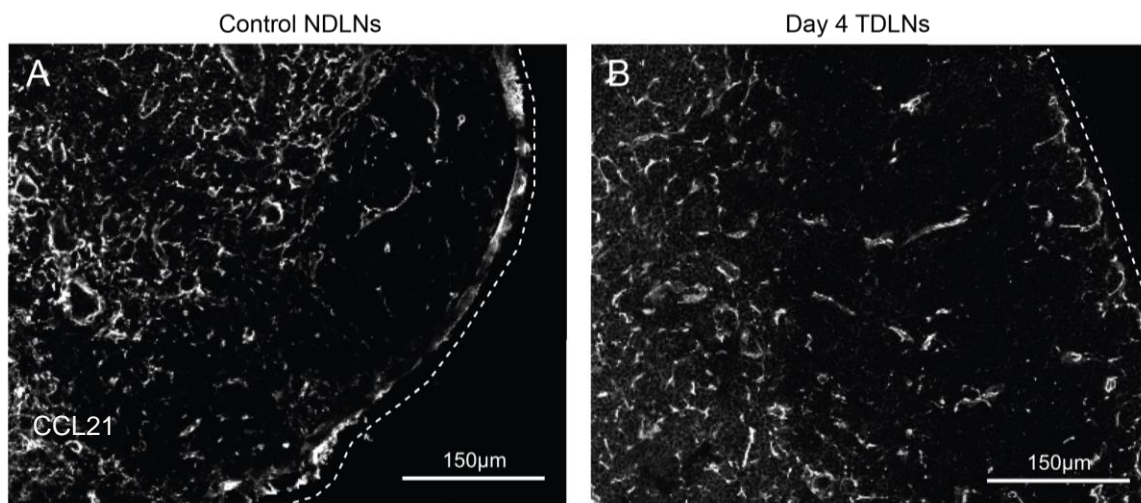


Figure 3.13. CCL21 protein expression is unaltered in early TDLNs. Representative control NDNLs (A) and Day 4 TDLNs (B), from B16-F10 tumour-bearing mice, were immunofluorescently stained for CCL21 (grey). Regions of interest were imaged at 20x magnification using confocal microscopy. Dotted white lines highlight the edge of the lymph node and scales represent 150µm. Shown are representative FOVs from two independent experiments, across n=6 NDNLs and n=6 Day 4 TDLNs.

Our final gene target of interest, which was significantly up-regulated in LECs derived from early TDLNs, is stromal marker, Podoplanin. Described as essential for dendritic cell migration along FRC networks in lymph nodes, we were interested to explore the expression of LEC-derived Podoplanin, with the hypothesis that changes in expression could influence dendritic cell migration. Immunofluorescent analysis of Podoplanin in both subcapsular sinus and medullary regions appeared unchanged between control NDNLs and TDLNs (Figure 3.14).

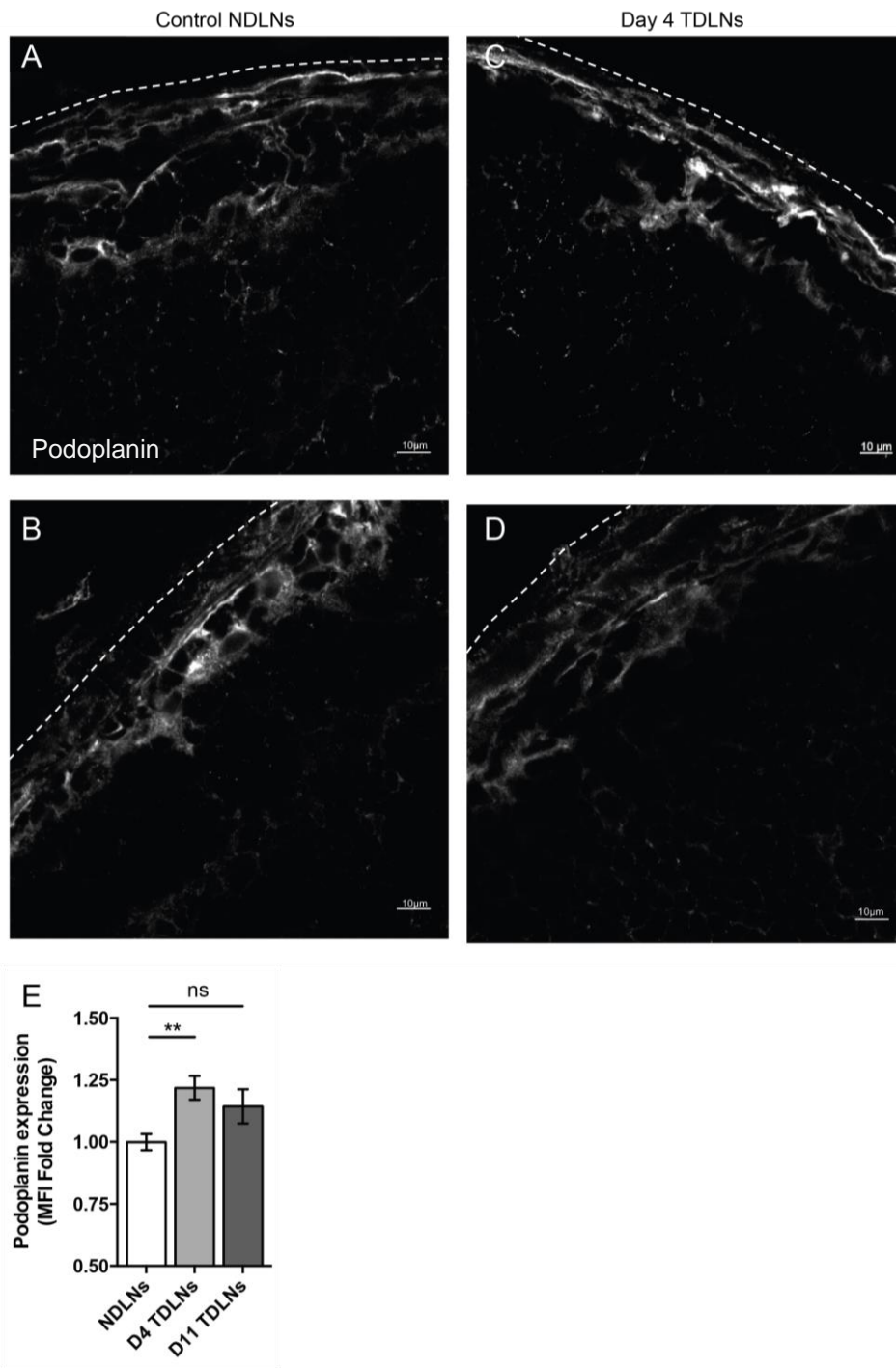


Figure 3.14. Podoplanin protein expression is upregulated on early TDLN-derived LECs. Control NDNLs (A, B) and Day 4 TDLNs (C, D) from B16-F10 tumour-bearing mice were immunofluorescently stained for Podoplanin (grey). Regions of interest were imaged at 63x oil magnification using confocal microscopy. Dotted white lines highlight the edge of the lymph node and scales represent 10µm. Shown are representative FOVs from subcapsular sinus regions from five independent experiments, with n=12 control NDNLs, n=13 Day 4 TDLNs (A-D). Control NDNLs and TDLNs from B16-F10 tumour-bearing mice were assessed for Podoplanin expression using flow cytometry (E). Fold changes in geometric mean fluorescent intensity (gMFI) were calculated relative to control NDNLs per independent experiment. Shown is data from n=6 independent experiments, with n=22 NDNLs and n=20 Day 4 TDLNs. Data presented as mean ± SEM. Statistical significance was calculated using One-way ANOVA ($P \leq 0.05$).

However, when assessed using flow cytometry, LEC-specific Podoplanin expression in early (Day 4) and late TDLNs (Day 11), a significant increase in expression at Day 4 was seen (NDLNs Mean Fold Change, 0.99 ± 0.03 ; Day 4 TDLNs Mean Fold Change, 1.21 ± 0.04) (Figure 3.14). As Podoplanin is up-regulated also in FRCs derived from late TDLNs (Day 11)¹⁹¹, our data further suggests a global change in stromal cell expression of Podoplanin. This also identifies Podoplanin as a potent responder to factors derived from the tumour microenvironment, with Podoplanin up-regulated in LECs of early TDLNs and FRCs in late TDLNs.

*3.3.4 Changes in expression of key gene targets correlate with dendritic cell marker, *Itgax*, in human melanoma lymph nodes*

In recent publications, the TCGA Cutaneous Melanoma dataset has been used to investigate the role of lymphangiogenesis in immune modulation^{190,189}. While these studies have employed such datasets to explore the role of lymphangiogenesis in primary tumour immune infiltrate and relative responsiveness to immunotherapy, lymph node samples from this dataset have so far been neglected. Thus, lymph node samples serve as a useful resource to answer questions pertaining to immune kinetics in the lymph node itself. We hence used this dataset to explore lymphatic-immune crosstalk in TDLNs, in particular communication between lymphatics and dendritic cells.

Expression data from only lymph node samples was accessed and analysed for correlative patterns between targets identified in our microarray, as well as lymphatic markers *Pdpn*, *Prox1* and *Lyve1*, and *Itgax*, which denotes the dendritic cell marker CD11c. *Itgax* expression data was categorised into lo-mid-hi expression as described in methods and plotted against gene target mRNA expression. This highlighted that of our top gene targets and lymphatic markers, *Pdpn* and *Zbp1* significantly correlated with *Itgax* expression ($P \leq 0.05$) (Figure 3.15a). This identified a clinically relevant target from our murine dataset and suggests Podoplanin as a possible mediator of dendritic cell mediated immunity and migration. Regarding Immunity-associated targets, *Ccl20* positively correlated with *Itgax* expression, suggesting this chemokine as essential in dendritic cell migration in human melanoma (Figure 3.15b). Interestingly, a negative

correlation could be seen for *Sema6d*, identifying perhaps a lymphatic-derived negative regulator of dendritic cell immunity.

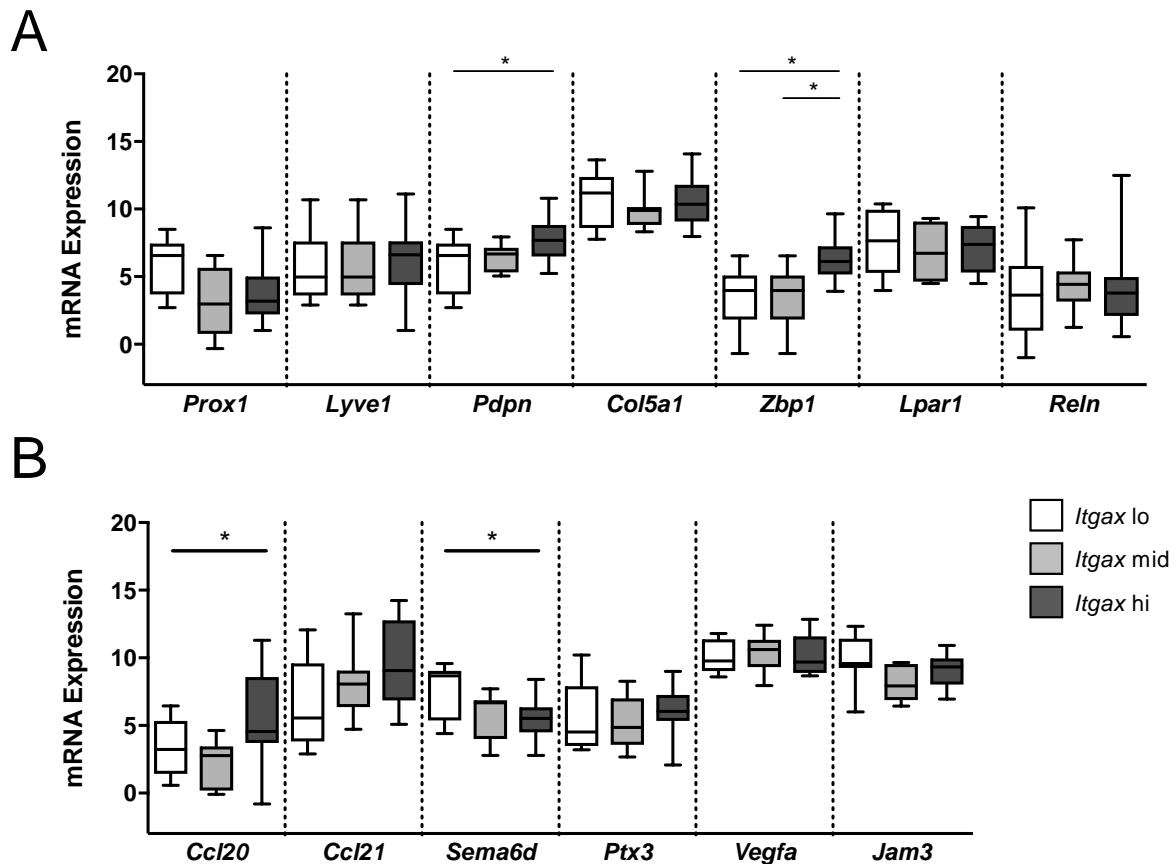


Figure 3.15. Microarray identified gene targets of interest correlate with dendritic cell marker, *Itgax*, in human melanoma. mRNA expression data, from 160 lymph node human melanoma samples, was accessed from online TCGA databases. Shown is mRNA expression of key gene targets (y-axis) categorized relative to lymph node sample expression of dendritic cell marker, *Itgax*. Box plots represent the range of gene target expression within samples exhibiting low, medium or high *Itgax* expression (white = *Itgax*-lo; light grey = *Itgax*-mid; dark grey = *Itgax*-hi). Data shown is presented as 25th to 75th percentiles box plots, with 5-95th percentile whiskers and median line shown. Statistical significance was calculated using One-way ANOVA ($P \leq 0.05$).

Collectively, this data provides translational application of our murine microarray dataset, confirming that gene targets altered in TDLN-derived LECs, may indeed have an important role in dendritic cell mediated immunity. Many gene targets identified in the microarray however showed no correlative link with dendritic cells, implying a lack of functionality in human melanoma. Of particular interest, Podoplanin, which was identified from our microarray data and verified to be up-regulated in early TDLNs, was one of few targets significantly correlated with dendritic cell marker, highlighting it as one of the more plausible targets to pursue in further experiments.

3.4. Discussion

Lymphangiogenesis is a well-established characteristic of tumour development and progression, with a significant body of evidence highlighting its association with lymph node metastasis and poor patient survival in a many human tumours, including melanoma and breast cancer^{127,126,130,134}. More recently, lymphatics have been postulated to play a more active role in the tumour microenvironment than previously thought, with remodelling and expansion of the lymphatic network associated with tumour immune landscapes. The contribution of lymphangiogenesis to the immune composition and function of associated TDLNs is somewhat less clear. Hence, we wished to explore further the functional contribution of lymphatics in the tumour microenvironment including TDLNs, using melanoma as our model of choice, due to its highly immunogenic nature.

In line with published work^{127,191}, we first confirmed that expanded lymphatic networks were established in tumour-draining brachial lymph nodes of B16.F10 tumours. Day 4 TDLNs exhibited varying degrees of lymphangiogenic responses, indicating an early transitional phase in response to the tumour, unlike later TDLNs, where Day 11 consistently detected extensive lymphatic expansion. Interestingly, in early TDLNs, the bulk of lymphangiogenesis occurred in capsular vessels rather than those of deeper sinuses, potentially alluding to a specific functional need for more vessels at the node periphery. When looking at primary lesions in the dermis from induced Tyr^{CreER}Braf^{CA}Pten^{lox} mice (Figure 3.6), an increase in the number of lymphatic vessels was observed even from the earliest pre-malignant lesions, suggesting that the lymphangiogenic programme is initiated early in tumour development, and is likely key for communication with downstream lymph nodes. Further work is needed to assess the transcriptional profiles of lymphatics derived from both B16-tumours and Braf-tumours, with matched draining lymph nodes over time. This could be achieved through isolating lymphatics from pooled tumours by FACS and conducting a microarray or single-cell sequencing. If matched with proteomic analysis, this would identify not only transcriptional signatures but also proteomic signatures, which are site-specific in tumour development. This analysis would also give an indication of upstream drivers of lymph node changes, which is currently lacking in this work and in the field's understanding of LN transformation in response to tumour

microenvironment derived factors. This further suggests that lymphatics of TDLNs respond to early factors derived from the evolving tumour microenvironment, giving rise to a fully expanded lymphatic network in late TDLNs. The kinetics of lymph node lymphatic expansion is poorly understood, so not only did this act as verification that there is a lymphangiogenic response in our models, but also that this is an early event in tumour development. This is particularly pertinent when considering therapeutic targeting of metastasis via inhibition of lymphangiogenic signals, as this data suggests perhaps the optimal window for blocking lymphangiogenesis is in early stages of tumourigenesis. Also, as VEGF-C mediated lymphangiogenesis has been shown to be associated with an immune suppressive tumour infiltrate¹⁹⁰; anti-lymphangiogenic therapy is likely to have an effect on immune dynamics in TDLNs also. As TDLNs act as the hub for immune response initiation, lymphangiogenesis may have a prominent effect on the priming of immune responses in early TDLNs. This could then set the scene for a developing tumour, skewing the immune response either in favour of or against tumour progression. Hence, application of anti-lymphangiogenic therapy must consider temporal and spatial effects on the immune response, with characterisation of immune changes in the primary tumour and TDLNs, at early and more developed time-points required. Adding further complexity to the matter is a recent finding, that VEGF-C mediated lymphangiogenesis also dictates susceptibility of a tumour to immunotherapy. Whereas it was hypothesised that anti-lymphangiogenic therapy would reduce risk of metastasis and perturb infiltration of suppressive immune cells, it was found in this study that lymphangiogenic tumours were in fact more sensitive to immune therapy, with better tumour rejection, reduced metastasis, epitope spreading and re-challenge protection reported¹⁸⁹. As we see lymphangiogenesis early on in tumour development, in both primary tumours and TDLNs, this finding is intriguing and suggests that perhaps early administration of immune therapy to lymphangiogenic tumours may indeed have a positive impact on the anti-tumour immune response. By suggesting that lymphangiogenesis is a critical parameter in successful immune priming by immune therapy, it may be the case that lymphangiogenesis directly influences immunity by facilitating better immune cell trafficking delivery of tumour antigen to TDLNs. Indeed, it is already known that lymphatics archive tumour antigen and directly modulate tumour-antigen specific CD8 T-cells¹⁸⁸. Hence, as lymphangiogenesis plays a critical role in tumour development and has perhaps a complex role in the anti-tumour immune response, it is essential to better define how

lymphatics directly modulate immunity in the tumour microenvironment. As lymph nodes communicate with tumours from early stages of development and mount immune responses, it is critical to specifically understand early lymphatic contributions in the lymph node. Hence, in order to determine how TDLN lymphatics functionally respond to factors derived from the early developing tumour microenvironment, we identified the transcriptional changes occurring in lymphatic endothelial cells from pre-metastatic TDLNs.

As well as changes in expression of gene targets from a number of canonical endothelial biology and cell cycle pathways, transcriptional profiling revealed expression changes of gene targets associated with pathways pertaining to immunity. Both in early and late TDLNs, expression of gene targets from immunity-associated pathways were altered, confirming that lymphatics were indeed functionally changed in response to factors derived from the tumour microenvironment, in favour of immune modulation. Gene targets of interest that were altered encompassed endothelial permeability, chemokine signalling and immune interactions, with expression of key dendritic cell migration factors altered. With greater lymphatic coverage of the node, expanded lymphatics provide a better network for immune cell access, which twinned with potential changes in permeability, has implications not only for immune cell access, but also dissemination of soluble factors and antigen. Characterised as amateur APCs, with the ability to archive and present antigen, TDLN-derived LECs are perhaps not only passively supplying more antigen to TDLNs through heightened permeability, but also actively processing and presenting antigen to interacting immune cells. Furthermore, disruption of migratory cues, resulting from down-regulated chemokine expression, could cause changes to localised chemokine gradients. Collectively, we have confirmed the role of LECs in immunity, showing an active role in immune modulation in the form of immune receptors, antigen processing and presentation and chemokine expression. However, our novel contribution to the understanding of lymphatic immunology is the capacity for these roles to be altered by factors derived from the tumour microenvironment, with unique functionality of TDLN-LECs defined.

We further investigate for the first time, TDLN data from patient TCGA repositories. Due to links between dendritic cell behaviour and immunity, and lymphangiogenesis

we focused on the association between microarray defined top hits and dendritic cell marker, ITGAX. Having verified up-regulation of Podoplanin protein expression in TDLN-derived LECs and hence hypothesising a role for Podoplanin in modulation of immune interactions, positive correlation with ITGAX expression in human patient TDLNs, was encouraging. This confirmed a potential role for Podoplanin in dendritic cell infiltrate in human melanoma-derived TDLNs, suggesting not only a role for Podoplanin in murine models, but also identifying it as a clinically relevant gene target. Surprisingly, CCL21A and JAM3, which are well defined mediators of migration and physical immune cell interactions with endothelium, did not correlate with ITGAX expression. Whereas these factors are known to be critical for dendritic cell movement in basal and inflammatory settings, these factors may be of less importance in human TDLNs. Other lymphatic markers and top up- and down- regulated hits in our microarray also did not significantly correlate with ITGAX expression, suggesting perhaps independent roles in human melanoma. Technical issues could also explain a lack of detection, as bulk tissue would have been used for this analysis. As LECs and migratory DCs are a small composite of the lymph node, perhaps only stronger correlative signatures were detected, with weaker associations undetected.

Overall, this data indicates that not only are lymphatics in TDLNs expanding in response to factors derived from the tumour microenvironment but are also undergoing key pre-metastatic transcriptional alterations that likely have significant ramifications for the anti-tumour response, in particular dendritic cell mediated immunity. We hypothesise that the physical and soluble interactions between dendritic cells and lymphatic endothelial cells are modified early on in tumour development, although whether they are enhanced or perturbed is currently unclear. As the soluble cues driving dendritic cell mobility are well characterised in the literature, focus will be given to investigating the physical interactions between these cells. We will determine how these physical interactions are altered in TDLNs and what mechanisms drive these interactions, focusing on key hits from the microarray, namely Podoplanin, which we hypothesise to play a critical role in this process.

CHAPTER 4

RESULTS

4. Determining the interactions between DCs and LECs in TDLNs

4.1. Introduction

In recent years, there has been a surge of interest towards the potential use of dendritic cells in cancer immunotherapy, aiming to manipulate the immune-priming functionality of dendritic cells, creating 'vaccines' by pulsing with tumour antigen. As the immune system is suppressed in the tumour microenvironment, these studies sought to use dendritic cell-based vaccines to re-establish a potent anti-tumour immune response. Due to the immunogenic nature of melanoma, many of these trials have been conducted in patients diagnosed with metastatic melanoma. These efforts however have had limited efficacy, with variable responses in patients^{215,216}. Due to the complexity of mounting an immune response, there are a number of confounding factors that could contribute to the inefficiencies of dendritic cell vaccines. Not only must dendritic cells be sufficiently and precisely prepared prior to patient vaccination, but also, there are a number of in-situ hurdles. The main hurdle in priming an anti-tumour response is migration. Dendritic cells must acquire a migratory phenotype and interact with a number of stromal cells to exit the tumour and reach tumour-draining lymph nodes via the lymphatics. In addition, they must migrate through lymph nodes towards T-cell zones for immune cell priming. A recent study has indeed shown that a significant number of total vaccinated dendritic cells remain in the tumour itself rather than migrating²¹⁷. This has hence been an important area for research, with much work exploring the soluble and physical cues needed for dendritic cell migration in healthy and diseased states. A particular knowledge area lacking and poorly understood is the relative contribution of non-immune stromal cells. Dendritic cell migration along lymphatic vasculature is well characterised in resting and inflammatory states with ICAM-1, VCAM-1, LYVE-1 and CCL21^{16, 52, 55,63}, all identified as essential mediators of migration. In specific regard to lymph nodes, as well as CCL21 signalling, Podoplanin was recently identified as a mediator of dendritic cell migration along FRC conduits in lymph nodes, facilitating access to T-cell zones in resting and inflammatory states⁷⁷. However, there remains a lack of mechanistic research into the migratory patterns of dendritic cells in the wider tumour microenvironment, and their interactions with stromal cells on route to tumour-draining

lymph nodes. The primary stroma that dendritic cells interact with when trafficking from the periphery to respective draining LNs is the lymphatic vasculature. In Chapter 3, we identified a number of gene targets associated with immune pathways with altered expression levels in LECs of tumour-draining lymph nodes; multiple factors pertained to dendritic cell interactions. In light of these findings and the current knowledge gaps in dendritic cell biology and dendritic cell-mediated cancer therapy, we sought to take these observations forward to determine the interactions between lymphatic endothelial cells and dendritic cells in tumour-draining lymph nodes.

4.2. Methods

4.2.1. *In vivo dendritic cell migration assay*

To assess localization of tumour-derived migrated DCs LNs from tumour-bearing mice, control NDLNs and Day 5 TDLNs were retrieved from mice that had been TRITC painted, as described in Section 2.3. Lymph nodes were then processed for flow cytometry analysis and confocal imaging.

For flow cytometry, lymph nodes were digested as previously described in Section 2.2 and prepared for flow cytometry as described in Section 2.8. Single cell suspensions were stained with Pacific Blue-conjugated CD8a, 488-conjugated CD103, PeCy7-conjugated CD11c, APC-conjugated MHCII and APC-Cy7-conjugated CD11b. Details of all antibodies used are listed in Table 2.10. Samples were run on the LSR BD Fortessa™ flow cytometer as described in Section 2.8, with TRITC detected using the 488nm laser and 532/561nm filter. Quantification of TRITC+ dendritic cells in each lymph node was conducted using offline FlowJo® software, gating on CD11c+ cells within singlets. TRITC+ dendritic cells were gated within specific dendritic cell subpopulations gating on CD11b+, CD8a+ or CD103+ populations within total CD11c+ cells. Raw counts per lymph node and respective percentages were exported into Microsoft Excel.

For immunofluorescent imaging, LNs were processed for histology using methods outlined in Section 2.9, stained for LYVE-1 and Podoplanin and nuclei counterstained with DAPI (1: 10,000) for confocal microscopy. Whole tile-scans at 20x magnification and 1024 resolution were taken of whole nodes. Quantification of TRITC+ cells within the subcapsular sinus was conducted using HALO™ image analysis software. The node was partitioned digitally, with the 'Total Lymph Node Area' defined using the DAPI counterstain to mark out the perimeter of the node. The 'Outer Region' was defined as area $\leq 150\mu\text{m}$ from the edge of the node and the 'Inner Region' was defined as area $\geq 150\mu\text{m}$ from the edge (Figure 4.1a). A TRITC quantification mask was manually set-up, ensuring that only TRITC+ cells were detected using this mask (Figure 4.1b). Automated analysis of each defined area then detected specific TRITC+ cells within each part of the node. Automated analysis yielded data for the following

parameters, Total Lymph Node Area (mm²); TRITC Area Coverage (mm²); TRITC Coverage (% of Area). In conclusion, this method enabled us to compare the relative distribution of TRITC cells in NDLN and early TDLNs.

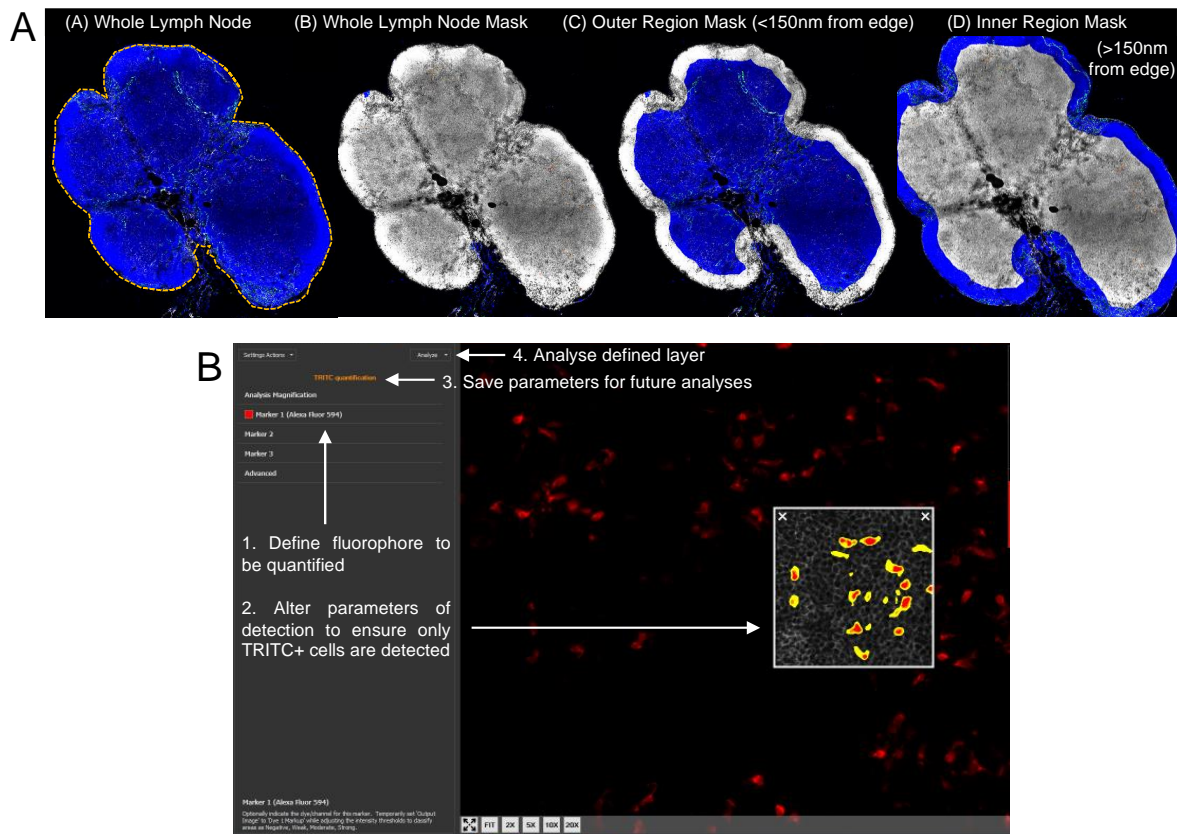


Figure 4.1. Schematic outlining methods of quantifying TRITC+ cells. For quantification of TRITC coverage in different compartments of the lymph node, a detection perimeter was defined in HALO™ image analysis software and detected, with outer and inner regions defined on distance from the edge (A). To detect TRITC+ only cells, a detection mask for AlexaFluor594 was created. Each regional mask (Whole LN, Inner Region, Outer Region) was then analysed using the TRITC detection mask (B). Settings were saved and used for future analyses.

4.2.2. *In vitro* characterisation of lymphatic endothelial cells

To characterise LECs cultured *in vitro*, cells were cultured on collagen-coated circular coverslips (12mm diameter) in 24-well plates and cultured until a monolayer was formed. For characterisation using flow cytometry, cells were processed according to methods outlined in Section 2.8 and stained with biotin-conjugated anti-LYVE1, PE-conjugated ESAM, APC-conjugated anti-Podoplanin, 488-conjugated anti-CD31, 488-conjugated anti-ICAM1, 488-conjugated anti-VCAM1. For LYVE-1, staining with fluorescent conjugated streptavidin was conducted for a further 30 minutes, followed

by further washes with PBS. Details of all antibodies used are listed in Table 2.10. Cells were then processed on the LSR BD Fortessa™ flow cytometer as described in Section 2.8. For ICAM/VCAM measurements by flow cytometry, cells were also treated with TNF-alpha (100ng/ml) at 37°C for 18 hours.

For immunofluorescent characterisation, cells were processed according to methods outlined in Section 2.9 and stained with rabbit primary antibodies against PROX-1. Cells were then stained with fluorescently conjugated anti-rabbit secondary antibodies. Details of all antibodies used are listed in Table 2.11.

4.2.3. Quantification of dendritic cell morphology

To quantify changes in dendritic cell morphology upon physical interaction with CCM or TCM-conditioned LECs, the number of cellular protrusions, cell area and the sphericity of each cell was quantified using image analysis software *FIJI* (Figure 4.2). Having set the scale accordingly, measurement of the shortest and longest length allowed for manual calculation of the sphericity index ($SI = \text{shortest length} / \text{longest length}$) (Figure 4.2a). Protrusions were also manually calculated, with a protrusion defined by a clear dendrite extension (Figure 4.2b). Cell area was measured by manually drawing around the edge of each cell, providing a 2D area measurement (Figure 4.2c).

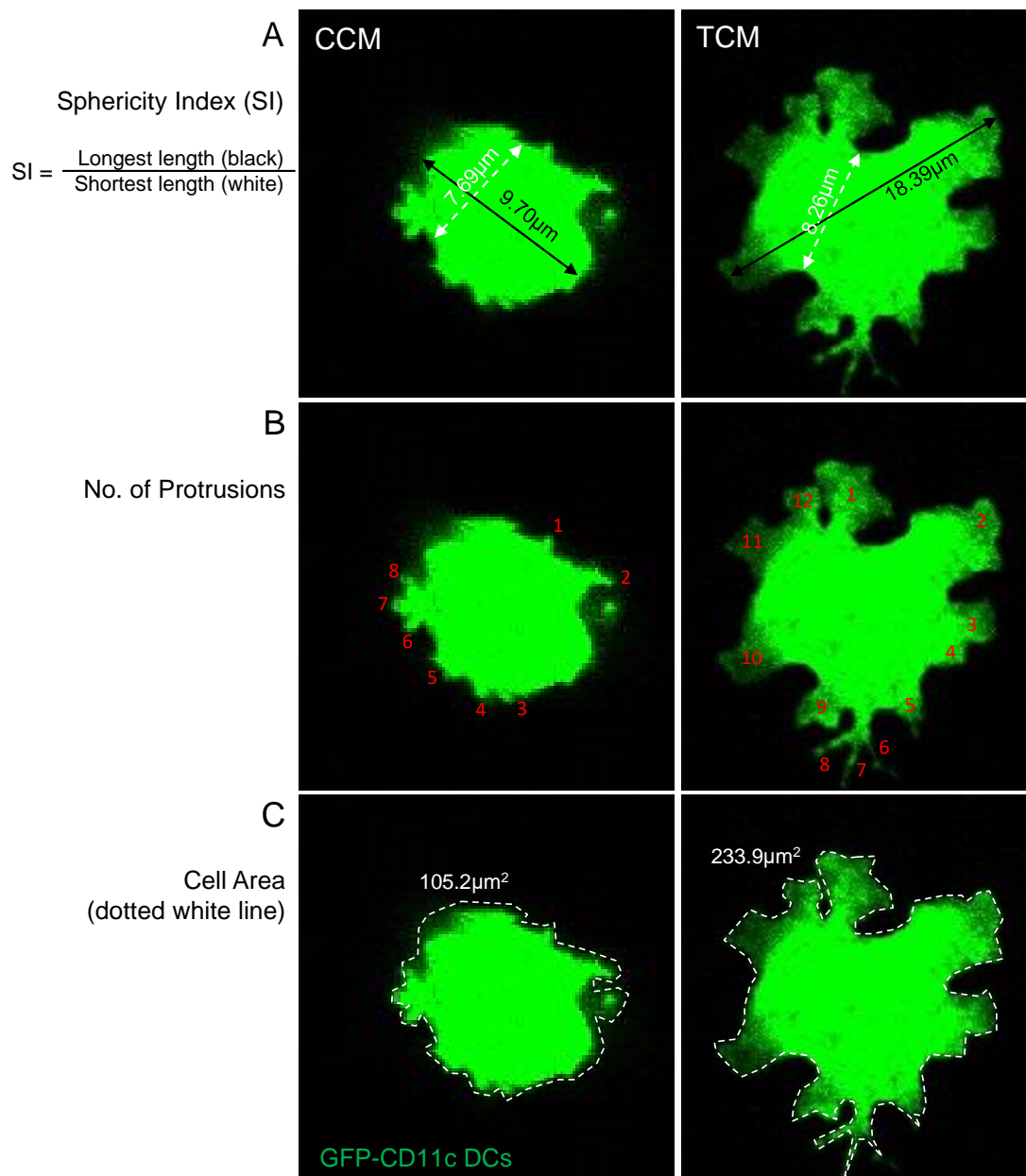


Figure 4.2. Schematic outlining methods of quantifying morphological features of DCs. For quantification of sphericity index, the shortest and length of each cell was defined and calculated using the equation stated (A). The number of protrusions per cell were manually counted, as shown in red (B). The cell area was calculated by manually drawing around each cell (dotted white line) (C).

4.2.4. *In vivo* characterisation of lymphatic networks in dermal ear sheets

For staining of lymphatic vessels in wholemount ears, dermal ear sheets were processed in accordance to methods outlined in Section 2.9.3. Ear sheets were stained with rabbit anti-LYVE1, rat anti-CD31 and Syrian hamster anti-Podoplanin, followed by fluorescent-conjugated anti-rabbit and anti-rat secondary antibodies. Ear sheets were then treated with RapiClear® to enhance visual clarity when imaging, following the protocol described in Section 2.9.3. Ear sheets were then imaged using confocal microscopy. With multiple z-stacks taken per ear sheet across regions of interest, at a magnification of 20x and resolution of 1024 x 1024.

4.2.5. *Measurement of Podoplanin expression by flow cytometry*

For assessment of Podoplanin expression in PDPN-FL tissues, lymph nodes and ears were digested in accordance to methods outlined in Section 2.2 and processed for flow cytometry as described in Section 2.8. Single cell suspensions were stained with 488-conjugated anti-CD31, PeCy7-conjugated anti-CD45, APC-conjugated anti-Podoplanin and Biotin anti-LYVE1. Secondary steps were conducted using APC-Cy7-conjugated streptavidin antibodies. Cells were then processed on the LSR BD Fortessa™ flow cytometer as described in Section 2.8. To assess Podoplanin expression specifically on lymph node lymphatic endothelial cells, the geometric mean fluorescent intensity of Podoplanin within the CD45- CD31+ LYVE1+ population was calculated.

For *in vitro* dermal lymphatic endothelial cells, samples were retrieved from culture and stained for Podoplanin as per methods outlined in Section 2.8. Cells were stained with violet viability dye and APC-conjugated anti-Podoplanin and processed on the LSR BD Fortessa™ flow cytometer as described in Section 2.8. The geometric mean fluorescent intensity of Podoplanin, within total viable cells, was calculated for control and TCM treated samples. Fold changes were calculated relative to control samples.

4.3. Results

4.3.1. Differential migratory patterns of dendritic cells in early TDLNs

To determine whether the interactions between lymphatic endothelial cells and dendritic cells are altered in early TDLNs, imaging of lymph nodes from TRITC-painted mice was employed. The use of TRITC 'paint' is an established method to assess migratory behaviour of dendritic cells^{218, 219, 220}. The sensitising TRITC paint applied to the skin upstream of lymph nodes, where upon crossing the epithelial barrier, migratory dendritic cells take up the agent and migrate to draining lymph nodes. We used this method to assess any differences in lymph node localisation and infiltration of TRITC dendritic cells coming from early tumours.

To highlight the localisation of migrated dendritic cells relative to lymphatics, lymph nodes were also stained with lymphatic marker, LYVE-1. In both NDNLs and early TDLNs, TRITC dendritic cells could be seen in the nodes, demonstrating that skin and tumour-derived dendritic cells had indeed migrated from early tumour sites in response to stimulation. In control NDNLs, TRITC dendritic cells were observed primarily in the inner cortex, with very few detected within the outer region or subcapsular sinus of the node (Figure 4.3a). In contrast, although many TRITC dendritic cells were found in the inner cortex of early TDLNs, a significant accumulation of cells was detected in the outer regions and subcapsular sinuses of the nodes (Figure 4.3b-d).

To determine the extent of differential localisation between NDNLs and TDLNs, the distance TRITC dendritic cells had migrated from the edge of the node was quantified. Multiple measurements were taken per node, demonstrating a range of 136.0µm to 258.9µm, with an average of 198.5µm ± 17.4µm in control NDNLs and 105.9µm to 230.1µm in Day 4 TDLNs, with an average of 150.5µm ± 27.6µm (Figure 4.4a). These control measurements acted as a cut-off range for further automated measurements, highlighting that most TRITC dendritic cells migrate >150µm into lymph nodes in control settings.

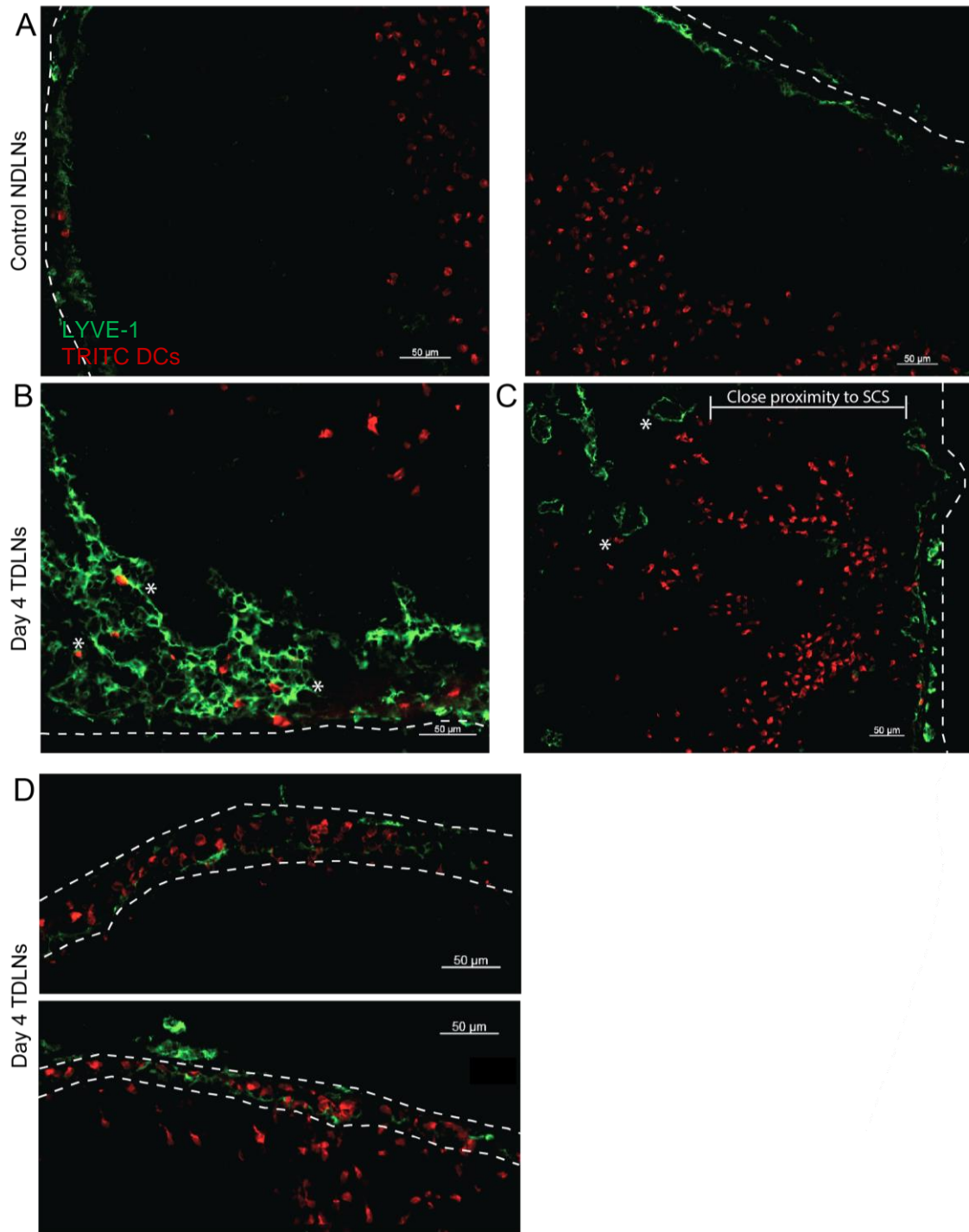


Figure 4.3. Migratory TRITC+ DCs cluster in outer regions of early TDLNs in association with subcapsular lymphatics. Control NDNLNs (A) and Day 4 TDLNs (B-D) from B16-F10 tumour-bearing mice were immunofluorescently stained with LYVE-1 (green) with periphery-derived migratory dendritic cells marked with TRITC (red). Regions of interest were imaged at 20x magnification using confocal microscopy. Shown are representative FOVs from n=5 independent experiments, with n=9 NDNLNs and n=18 Day 4 TDLNs. Dotted lines define the lymph node edge (A) and subcapsular sinuses (B). Scale bars represent 50µm.

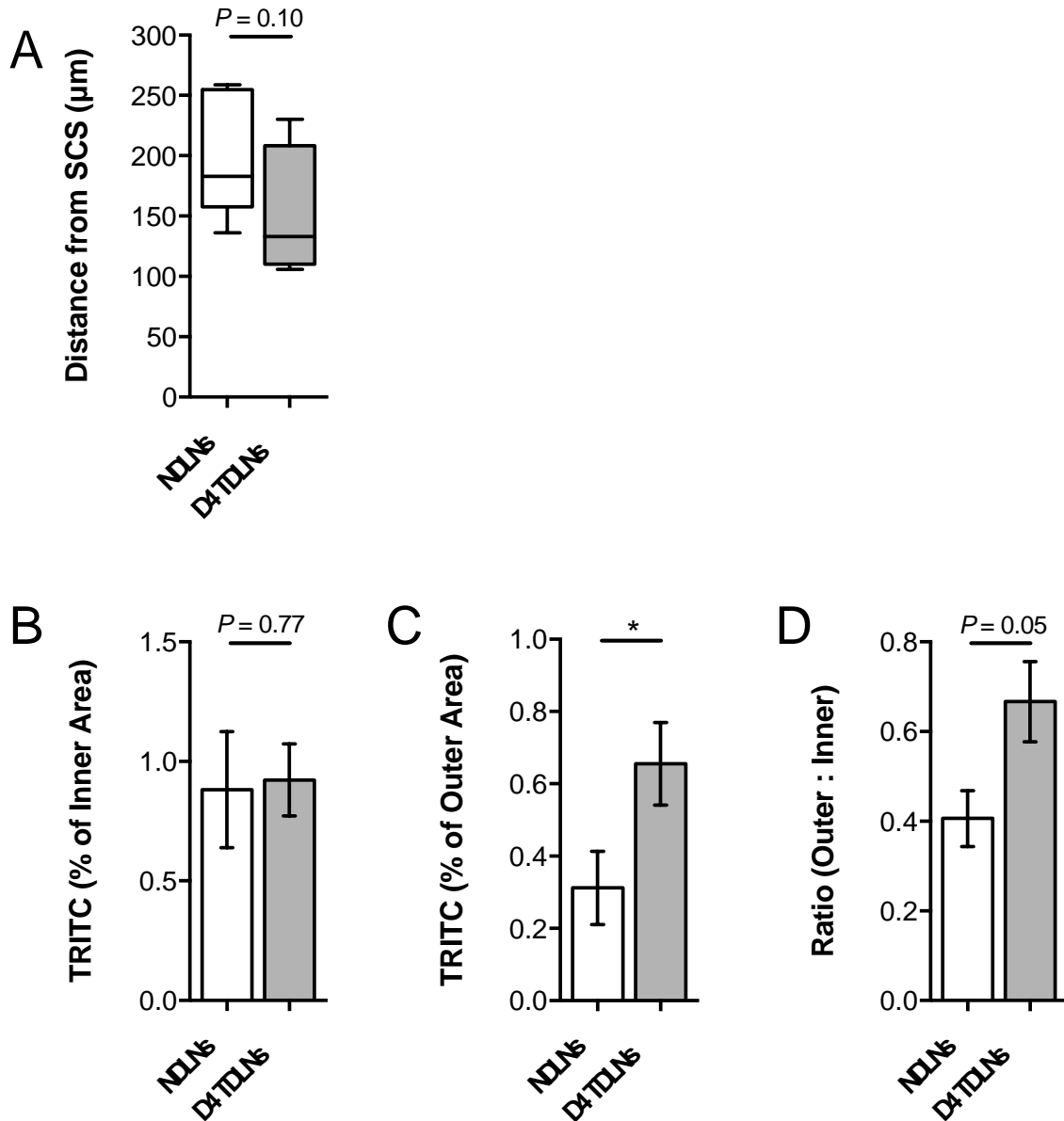


Figure 4.4. Increased clustering of migratory TRITC+ DCs in outer regions of early TDLNs. Control NDLN6 and Day 4 TDLN6 from B16-F10 tumour-bearing mice painted with TRITC were tile scan imaged at 20x magnification using confocal microscopy. Whole lymph node images were analysed using offline image analysis software. The distance of TRITC+ cells from the edge of the lymph node was manually measured (A) and the quantification of TRITC coverage as a percentage of inner and outer lymph node areas was calculated using Halo™ software (B,C). The inner lymph node was defined as >150µm from the edge of the lymph node (B) and the outer lymph node area was defined as within ≤150µm from the edge of the lymph node (C). Manual ratio calculations of outer to inner TRITC coverage was calculated using data from B and C (E). Shown is data from n=3 independent experiments with n=8 control NDLN6 and n=4 Day 4 TDLN6 (A), and n=5 independent experiments with n=9 NDLN6 and n=18 Day 4 TDLN6 (B-D). Data presented as 25th to 75th percentiles box plots, with 5-95% percentile whiskers and median line shown (A). Data presented as mean ± SEM (B-D). Statistical significance was calculated using the Mann Whitney test ($P \leq 0.05$).

To more precisely quantify spatial distribution of TRITC dendritic cells the relative localisation was determined using image analysis software, as per methods outlined above in Section 4.2. Nodes were partitioned based on previously defined parameters, with the 'outer region' defined as $<150\mu\text{m}$ from the edge and the 'inner region' defined as $>150\mu\text{m}$. The area of each node covered by TRITC positive cells, relative to inner and outer nodal regions, was calculated as a percentage of the area or as total area coverage. There was no difference between NDLNs and early TDLNs, in terms of TRITC coverage in the inner nodal regions. (Figure 4.4b), with TRITC coverage averaging $0.88\% \pm 0.24\%$ in control NDLNs and $0.92\% \pm 0.15\%$. However, an increase in the percentage of TRITC coverage within the outer nodal regions was seen, with an average percentage coverage of $0.31\% \pm 0.10\%$ in control NDLNs and $0.65\% \pm 0.11\%$ in Day 4 TDLNs (Figure 4.4c). The ratio of outer to inner TRITC coverage was hence increased with the average ratio of outer coverage to inner coverage calculated as 0.40 ± 0.06 in control NDLNs and 0.66 ± 0.08 in Day 4 TDLNs, as expected (Figure 4.4d). Overall, this demonstrates a quantifiable change in TRITC dendritic cell localisation in the TDLNs of early tumours, with an outer clustering phenotype observed.

To assess whether the change in migration of TRITC dendritic cells was restricted to localisation or whether numbers of migratory dendritic cells were also altered, flow cytometry was carried out on whole lymph nodes. Using the gating strategy outlined in Figure 4.5 (NDLN vs TDLN gating in Appendix 7), we first observed a significant increase in lymph node cellularity, with average cellularity between control lymph nodes and Day 4 TDLNs increasing by 2.5-fold (Control LNs Average, $0.61 \times 10^6 \pm 0.16$; Day 4 TDLNs Average, $1.53 \times 10^6 \pm 0.16$) (Figure 4.6a). This trend is in line with published work¹⁹¹ and previously described findings in Chapter 3. Upon gating within CD11c+ singlets, an increasing trend in the number of CD11c+ dendritic cells could be seen with the average count per node fold-change calculated in control LNs as 1.00 ± 0.18 and in Day 4 TDLNs as 1.94 ± 0.27 (Figure 4.6a). Although with increases in whole lymph node cellularity, this equated to an overall significant decrease in the percentage of CD11c+ dendritic cells, relative to singlets (Control LNs Average, $6.8\% \pm 1.0$; Day 4 TDLNs Average, $4.25\% \pm 0.4$) (Figure 4.6c).

Gating specifically on subpopulations within total CD11c DCs revealed similar trends with the count per node fold-change increased in CD8a, CD11b and CD103 DCs (Figure 4.6d-f). Relative to total CD11c DCs however, percentages were unchanged in CD8a subpopulations but significantly decreased in CD11b and CD103 subpopulations (CD11b, Control NDLNs - $81.6\% \pm 2.9$ and Day 4 TDLNs - $68.8\% \pm 3.4$; CD103, Control NDLNs - $16.7\% \pm 1.0$ and Day 4 TDLNs - $11.8\% \pm 0.7$) (Figure 4.6g-i).

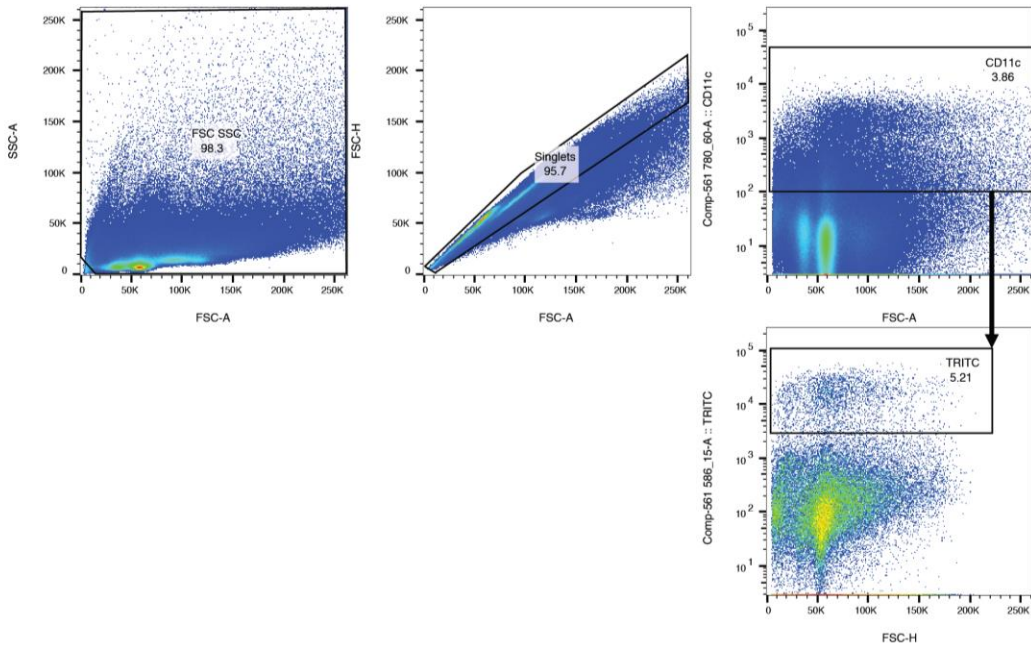
TRITC+ migratory CD11c+ dendritic cells revealed similar trends, with increases both in the number and percentage of TRITC+ cells (Figure 4.7a-d). Average count per node fold-changes yielded significant increases in total TRITC+ CD11c+, with almost significant increases seen in migratory populations, CD11b and CD103. Average count per node fold-changes in Day 4 TDLNs relative to control NDLNs, were 1.99 ± 0.33 in TRITC+CD11c+, 1.71 ± 0.27 in TRITC+CD11b+ and 2.15 ± 0.46 in TRITC+CD103+ subpopulations (Figure 4.7e-g). A statistically significant increase in the TRITC count fold-change in resident CD8a+ populations was also seen, however as the number of TRITC+ cells detected in this population was <50 per node, this is an insignificant contribution to the overall trends of migratory DCs. As a percentage of the total subpopulation, e.g. TRITC as a percentage of CD8, trending increases could be seen across CD8, CD11b and CD103 populations, however with no statistically significant changes (Figure 4.7i-l). Reconciling the increase in count of TRITC+ CD11c+ (Figure 4.7a) with the decrease in the percentage of CD11c+ relative to singlets (Figure 4.6c), this data suggests the increase in TRITC+ CD11c+ DCs in early TDLNs is not sufficient to compensate for the rapidly expanding node, as shown in Figure 4.6a, resulting in the overall decrease in the percentage of CD11c+ DCs seen.

Firstly, this data defines TRITC+ cells as predominantly expressing CD11b and CD103, confirming TRITC+ cells present in the LN as migratory DCs. Secondly, this data collectively demonstrates that increases in total CD11c were partially accounted for by increases in migratory populations. Finally, these findings overall describe a definitive and significant increase in lymph node cellularity in Day 4 TDLNs, which is accompanied by changes in dendritic cell composite, with increasing numbers of total and migratory CD11c+ dendritic cells. Hence in addition to delocalisation, there appear

to be changes in the dynamics of influx from the periphery as well as intrinsic changes to resident populations.

Overall, from both the immunofluorescent and flow cytometry analysis, we concluded that in early TDLNs, there is enhanced migration of dermal derived dendritic cells, comprised mostly of CD11b+ subsets. These migratory dendritic cells, upon arrival at early TDLNs, accumulate at the edge of the lymph node within the subcapsular sinus. This suggests an important role for lymphatics in the migration of tumour-derived dendritic cells, posing the question as to whether they are perturbing or promoting tumour-derived dendritic cell mediated immunity.

A



B

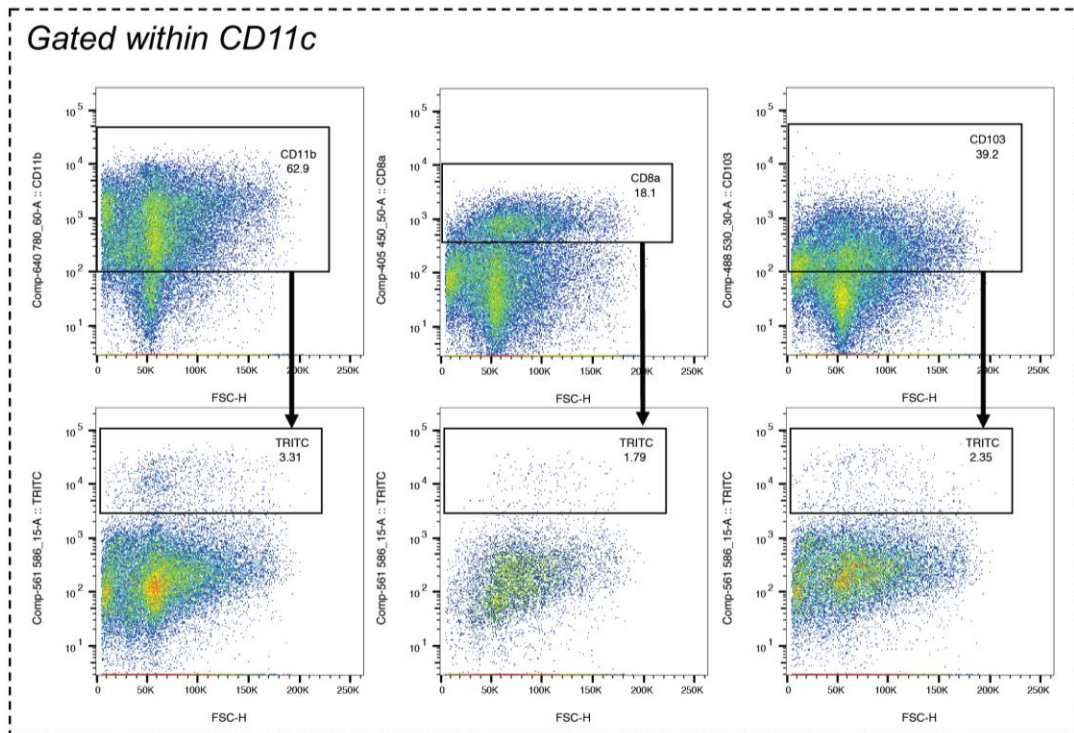


Figure 4.5. Gating strategy for dendritic cell profiling in TDLNs from TRITC painted tumours. Representative gating strategy to identify dendritic cell populations. Total CD11c+ dendritic cell populations and migratory CD11c+ TRITC+ highlighted within gates shown in (A). Within total CD11c+ dendritic cell populations, sub-populations were gated on CD8a+, CD11b+ and CD103+, with TRITC denoting migratory dendritic cells within each sub-population. Full gating for NDLN vs Day 4 TDLN is detailed in Appendix 7.

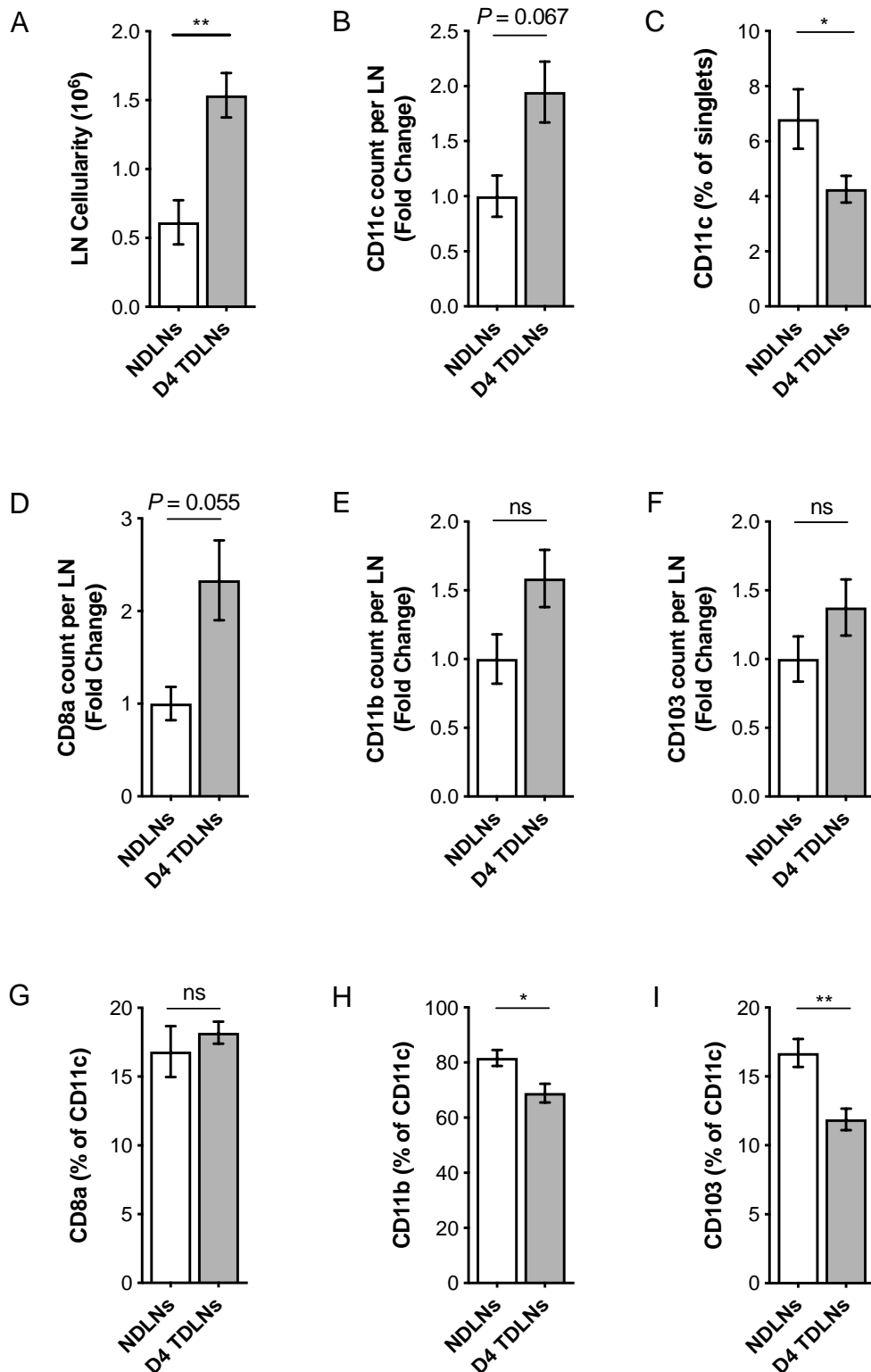


Figure 4.6. Lymph node cellularity and dendritic cell counts is increased in early TDLNs. Using flow cytometry, NDLNs and TDLNs were analysed for total lymph node cellularity (A), total CD11c dendritic cells in terms of total count and as a percentage of singlets (B,C). Quantification of subpopulations of dendritic cell – CD8a, CD11b, CD103, in terms of count fold-change (D-F) and percentage of total CD11c DCs (G-I). Shown is data from three independent experiments, with n=7 Control NDLNs and n=13 Day 4 TDLNs. Data presented as mean \pm SEM. Statistical significance was calculated using the Mann-Whitney test ($P \leq 0.05$).

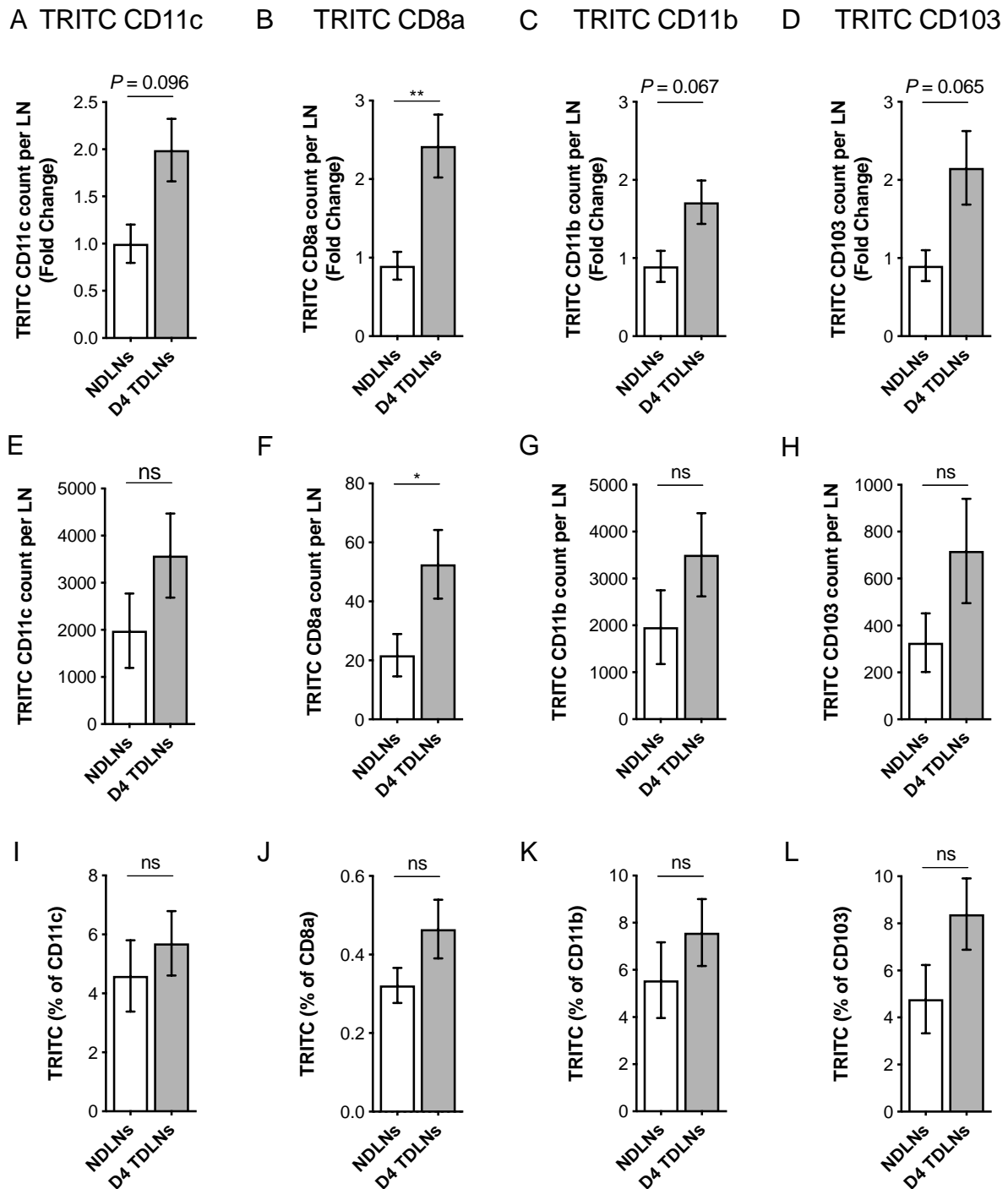


Figure 4.7. Altered profiles of TRITC+ dendritic cell subpopulations in early TDLNs. Using flow cytometry, TRITC+ CD11c DCs and subpopulations of dendritic cells – CD8a, CD11b, CD103, in NDNLNs and TDLNs were analysed for subset count fold-change (A-D), raw count per lymph node (E-H), and TRITC percentage of subset (I-L). Shown is data from three independent experiments, with $n=7$ Control NDNLNs and $n=13$ Day 4 TDLNs. Data presented as mean \pm SEM. Statistical significance was calculated using the Mann-Whitney test ($P \leq 0.05$).

4.3.2. Murine LECs express canonical endothelial markers

To investigate the consequences of accumulation within the SCS, and how lymphatics may impact dendritic cell migration into the node, a simple *in vitro* model using LECs (LECs) and isolated DCs was developed. Firstly, we characterised expression profiles of LECs grown on collagen-coated plates (Figure 4.8).

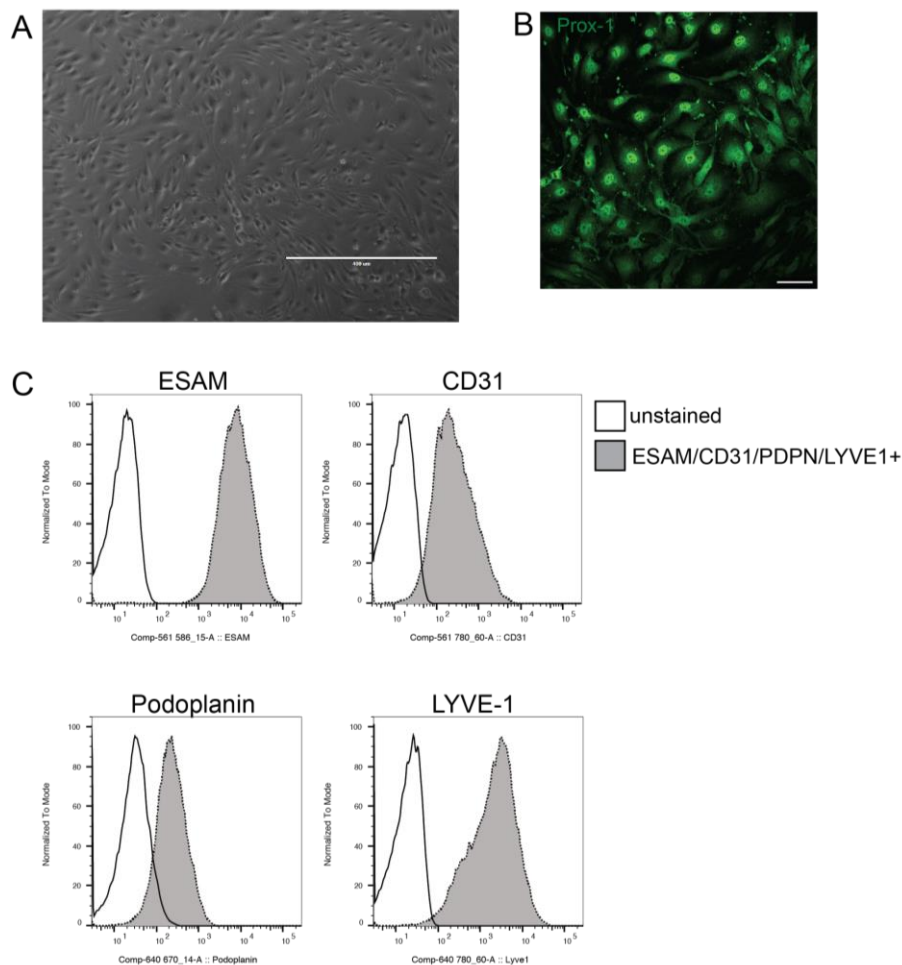


Figure 4.8. *In vitro* LECs express canonical lymphatic markers and lymphatic transcription factor, PROX-1. Primary LECs were grown *in vitro* on collagen-coated plates (50µg/ml) until a monolayer had formed and imaged using phase-contrast. Scale bars represent 400µm (A). Primary LECs were grown on collagen-coated glass coverslips until a monolayer had formed and immunofluorescently stained for lymphatic marker and transcription factor, PROX-1 (green). Cells were imaged at 20x magnification using confocal microscopy. Scale bars represent 100µm (B). Primary LECs were grown *in vitro* on collagen-coated plates (50µg/ml) until a monolayer had formed, and stained with fluorescently-conjugated antibodies for flow cytometry, assessing the expression of lymphatic surface markers (CD31, ESAM, Podoplanin and LYVE-1). Unstained cells were processed as controls and used to set the threshold for negative expression (white peaks). Positive expression of these markers is denoted by a shift in the histogram peak relative to controls (grey peaks) (C).

Phase contrast imaging revealed classic “cobble-stone” morphology (Figure 4.8a), with confocal microscopy showing prominent expression of lymphatic transcription factor, PROX-1 (Figure 4.8b). Flow cytometry also showed positive expression of lymphatic markers ESAM, CD31, Podoplanin and LYVE-1 (Figure 4.8c), with ESAM and LYVE-1 expressed to a higher extent than CD31 and Podoplanin.

4.3.3. Enhanced physical interactions between DCs and LECs *in vitro*

Having established their expression profile, LECs were used for co-culture interactions assays. Cells were cultured on collagen-coated plates until a monolayer was formed, and splenic GFP-CD11c added to assess the physical interactions between the two cell types (Figure 4.9).

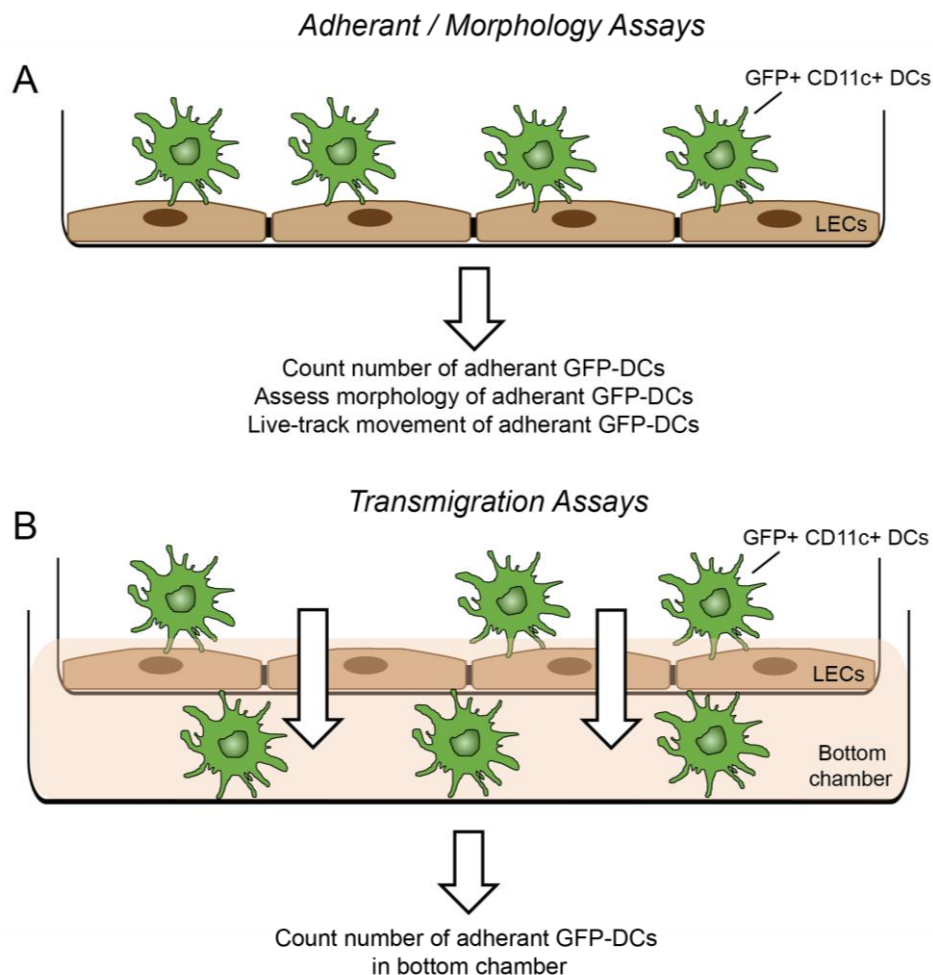


Figure 4.9. Schematic of *in vitro* dendritic cell assays used to assess lymphatic interactions. Adhesion assays used to count number of adherent GFP-DCs and assess morphological changes (A). Transmigration assays used to count number of GFP-DCs in bottom chamber (B). GFP+ dendritic cells (GFP-DCs).

Physical interactions were assessed by a) adhesion to a monolayer, b) morphological changes when interacting with a monolayer, c) transmigration across an endothelial monolayer grown on transwells and d) movement across a monolayer. This recapitulated the physical interactions that occur at the subcapsular sinus, when arriving migratory DCs bind to and traverse the lymphatic lining in order to enter the lymph node. LECs were pre-treated with TCM for 48hrs to recapitulate the short-term exposure that lymphatics undergo in early TDLNs over the 4-days post tumour cell inoculation and TCM was derived from the same B16-F10 tumour cells injected *in vivo*.

Indeed, when co-cultured with TCM-conditioned LECs the number of protrusions per cell was significantly increased, with an average of 3.5 ± 0.4 DC protrusions in control treated conditions and 5.6 ± 0.82 in TCM treated conditions (Figure 4.11a,b). Appearance of dendrites is associated with maturity, transmigration and antigen uptake and presentation^{222,77}. Dendritic cells cultured with TCM-conditioned LECs were also larger, with an average DC area of $67.7\mu\text{m}^2 \pm 6.3$ in control treated conditions and $93.1\mu\text{m}^2 \pm 11.5$ in TCM treated conditions. (Figure 4.11a,c). This did not represent a statistically different change. Upon quantification of sphericity, i.e. the degree of morphological change from initial spherical appearance, there was no difference between conditions either with an average sphericity index of 0.58 ± 0.04 in control treated conditions and 0.56 ± 0.03 in TCM treated conditions (Figure 4.11a,d).

Interestingly, whilst these cells seemed more adherent and exhibited anchorage phenotypes morphologically, they were less motile. Using a transwell system, the number of GFP+ CD11c+ dendritic cells that migrated across an endothelial monolayer akin to the subcapsular sinus floor, into the bottom chamber was quantified. An average of $38 \text{ cells} \pm 8.0$ per field of view had migrated across control treated endothelium, whereas only $19 \text{ cells} \pm 1$ per well migrated across TCM-conditioned endothelium (Figure 4.12). A 50% decrease in migration in the presence of more, stronger interactions implies TCM-conditioned endothelium impairs DC movement. Indeed, upon assessment of motility across a lymphatic monolayer using live-cell tracking over an hour, cells were more stationary. Offline analysis of live-cell tracking showed the movement of DCs from their preliminary position had a more limited range in TCM treated conditions, compared to control treated conditions (Figure 4.13a).

Upon quantification this translated to some significant changes in motility, with the speed of DC movement, the length of trajectory and the distance of DC movement from their starting position all significantly reduced in the presence of TCM conditioned LECs.

As all assays were conducted over a 1-hour duration in culture with treated lymphatic endothelial cells, these findings demonstrate that over this duration, DCs anchor down and adhere to TCM-conditioned lymphatic endothelium more than they do with control treated lymphatic endothelium; with indicative morphological changes. The function consequence of this is reduced transmigration and motility.

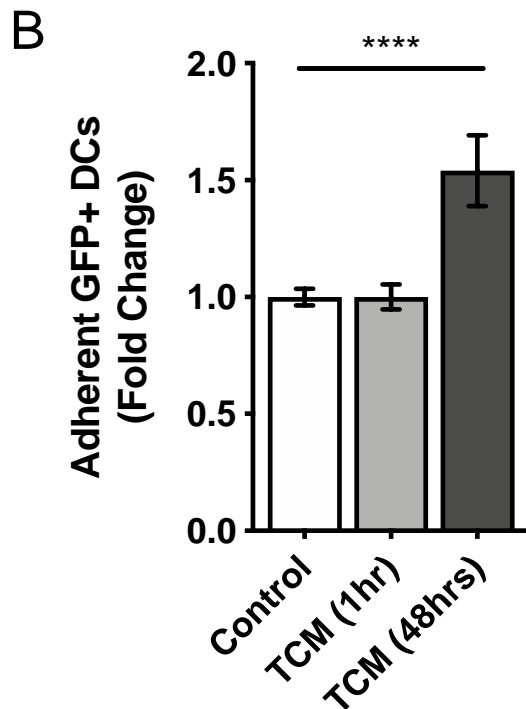
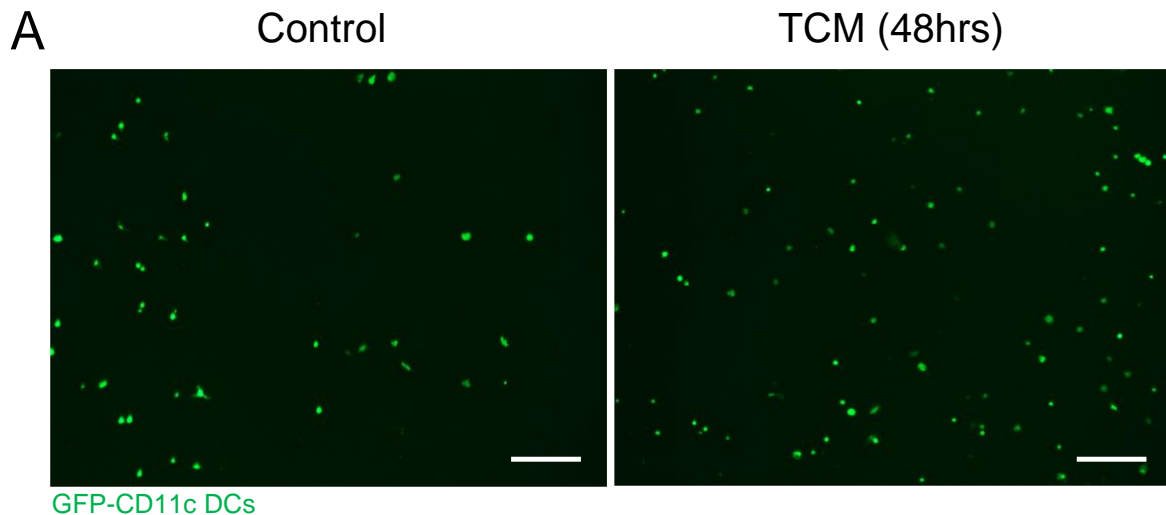


Figure 4.10. Enhanced adhesion of dendritic cells to TCM-conditioned LECs *in vitro*. GFP-DCs were co-cultured with LECs grown on collagen-coated plates (50µg/ml) and conditioned with tumour-conditioned media (TCM) for 1hour or 48hours prior to co-culture. GFP-DCs adhered to monolayers of LECs imaged using the EVOS® system. Representative FOVs shown and scale bars represent 200µm (A). Adherent GFP+ cells were manually counted using *FIJI* image analysis software. Raw counts were normalised relative to control samples within independent experiments to calculate fold changes in adherent GFP-DCs (B). Shown is data from n=4 independent experiments with n=77 Control; n=29 TCM (1hr); n=17 TCM (48hrs). Data presented as mean ± SEM. Statistical significance was calculated using One-way ANOVA ($P \leq 0.05$).

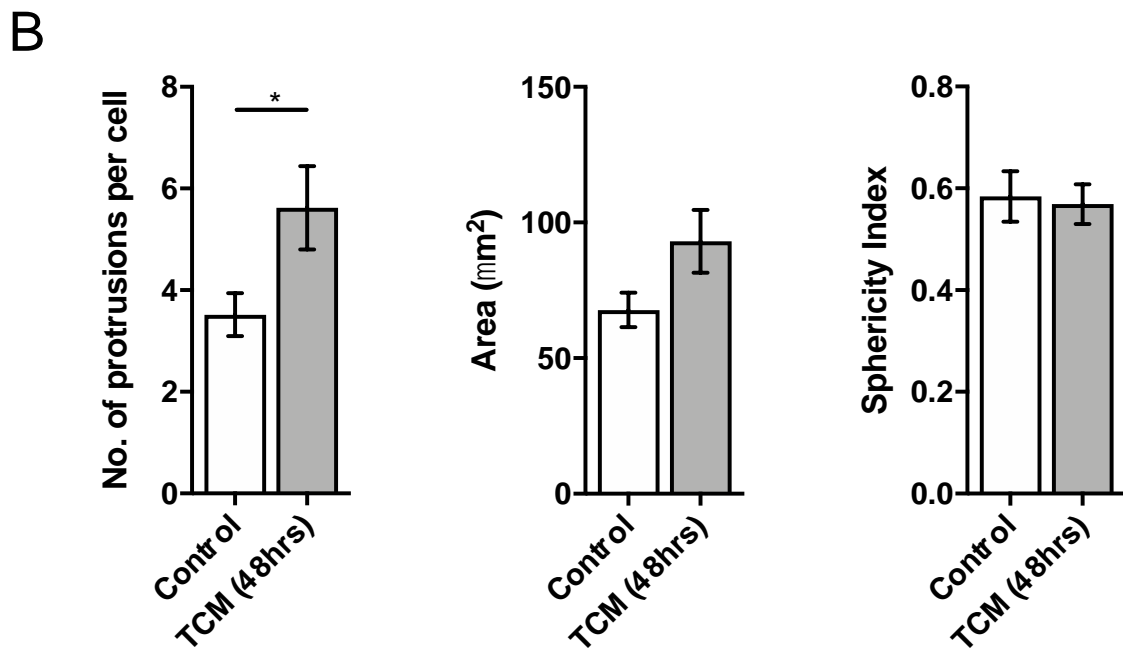
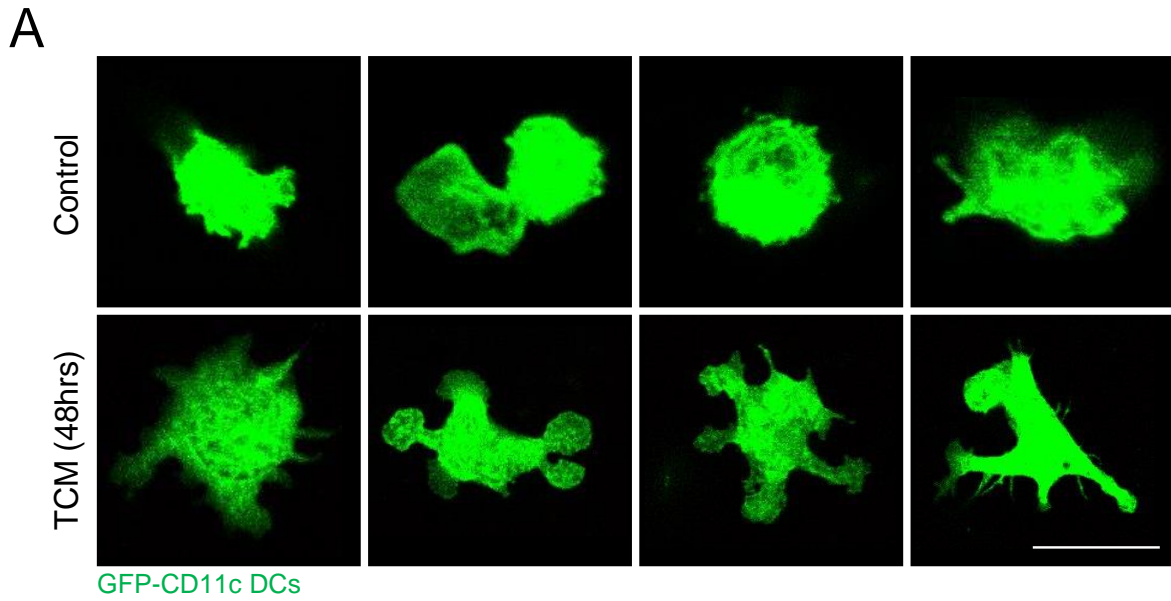


Figure 4.11. Altered dendritic cell morphology upon co-culture with TCM-conditioned LECs *in vitro*. GFP-DCs co-cultured with LECs on coverslips, fixed and imaged using confocal microscopy. Representative GFP-DCs from co-cultures with control or TCM-conditioned LECs. Scale bars represent 10 μ m (A). Manual counts of protrusions per cell (left) and measurements of area (middle), and sphericity index (right) (B). Shown is data from n=2 independent experiments with n=18 Control; n=12 TCM. Data presented as mean \pm SEM. Statistical significance was calculated using Student t-tests ($P \leq 0.05$).

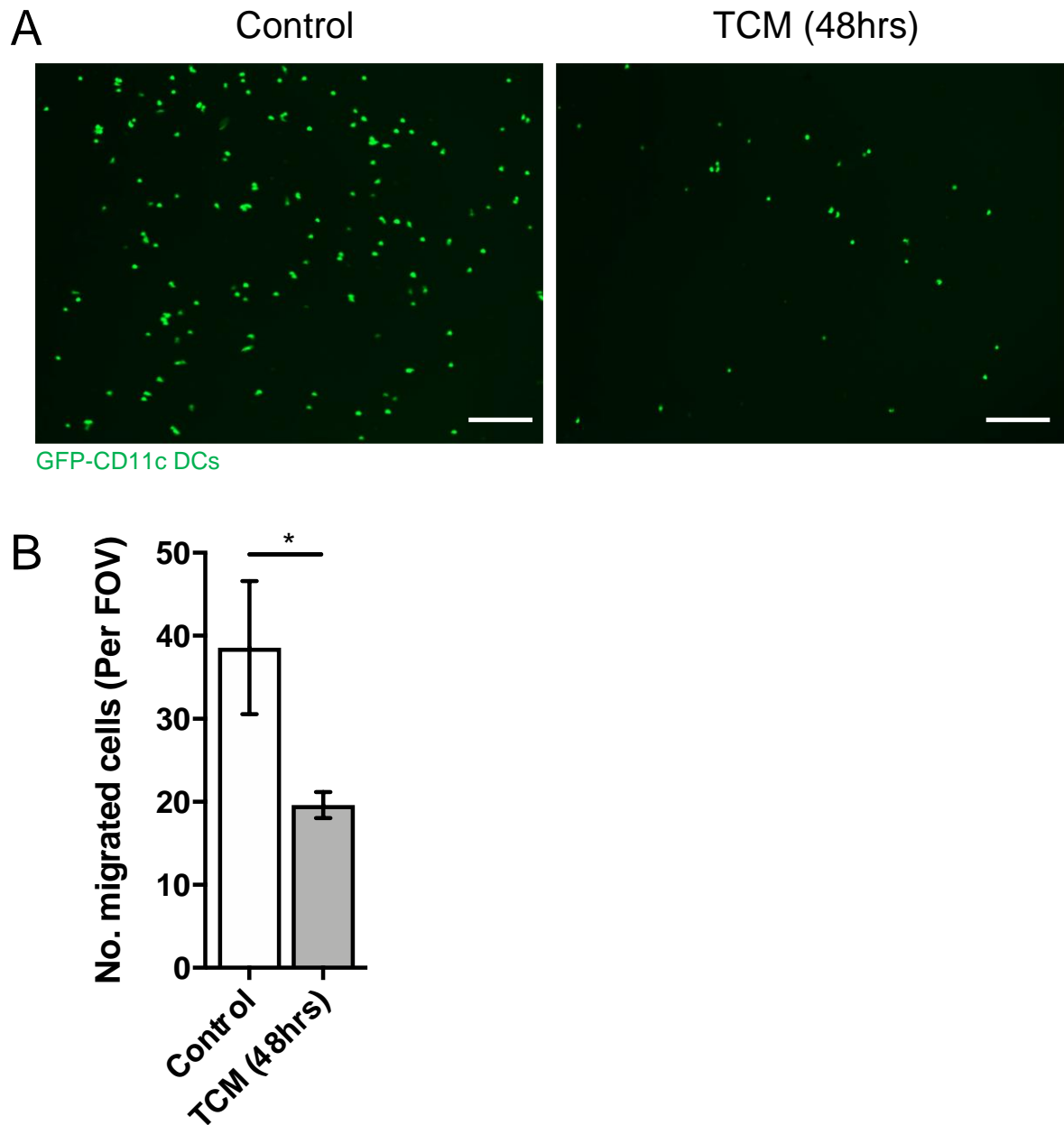


Figure 4.12. Perturbed transmigration of dendritic cells across TCM-conditioned LECs *in vitro*. GFP-DCs were co-cultured with LECs grown on collagen-coated transwell inserts (50µg/ml) and conditioned with tumour-conditioned media (TCM) for 48hours prior to co-culture. Migrated GFP-DCs were imaged using the EVOS® system. Representative FOVs shown and scale bars represent 200µm (A). Migrated GFP+ cells were manually counted using *FIJI* image analysis software. Data shown is the number of migrated DCs per FOV, calculated by manual counting of the number of GFP+ DCs in the bottom chamber of each well (B). Data shown is from n=2 independent experiments with n=16 Control; n=17 TCM (48hrs) and presented as mean ± SEM. Statistical significance was calculated using Student t-tests ($P \leq 0.05$).

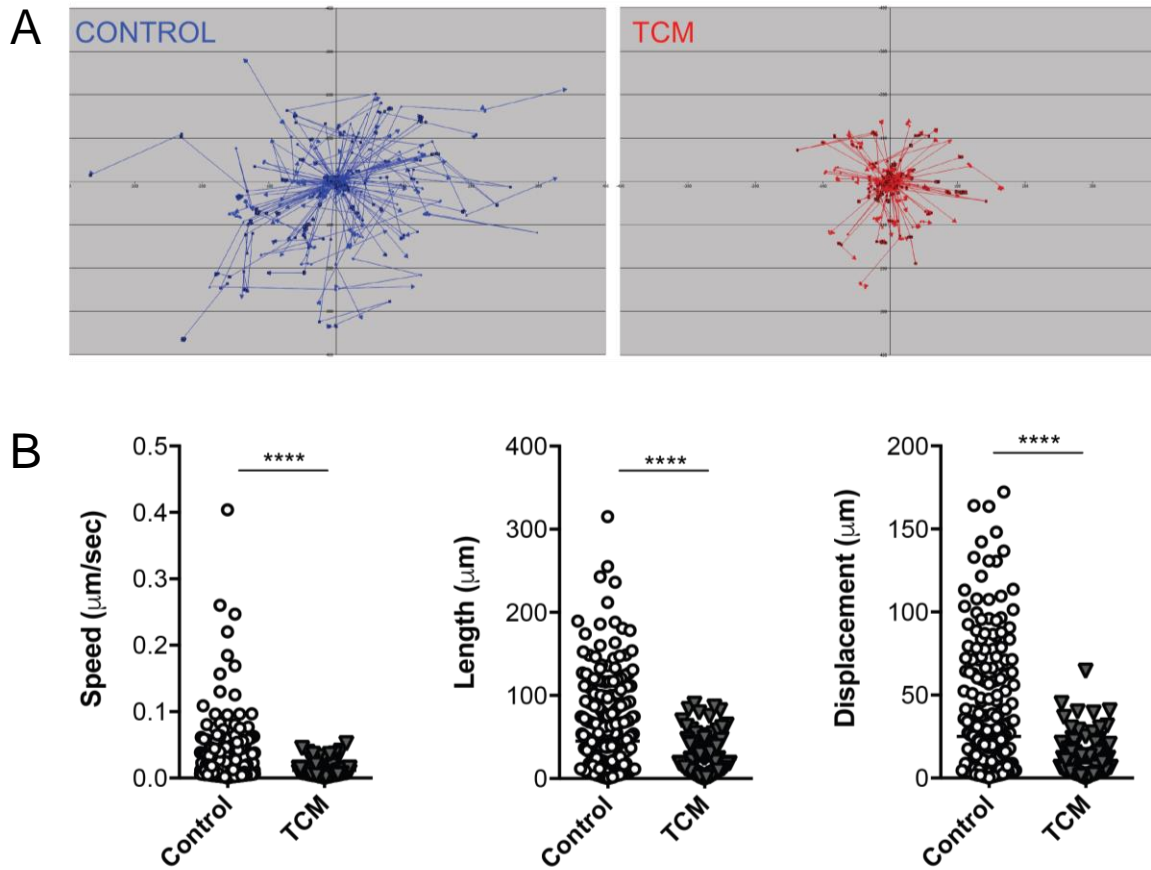


Figure 4.13. Perturbed motility of dendritic cells across TCM-conditioned LECs *in vitro*. GFP-DCs were co-cultured with LECs conditioned with tumour-conditioned media (TCM) for 48 hours prior to co-culture. GFP-DCs adhered to monolayers of LECs were tracked using live-imaging over a duration of 1 hour. Offline data analysis produced spider-plots to visualise motility of DCs during the experiment (A) and quantified motility in terms of speed, length of trajectory and displacement (B). Shown is data from $n=2$ independent experiments. Data presented as mean \pm SEM. Statistical significance was calculated using Student t-test ($P \leq 0.05$).

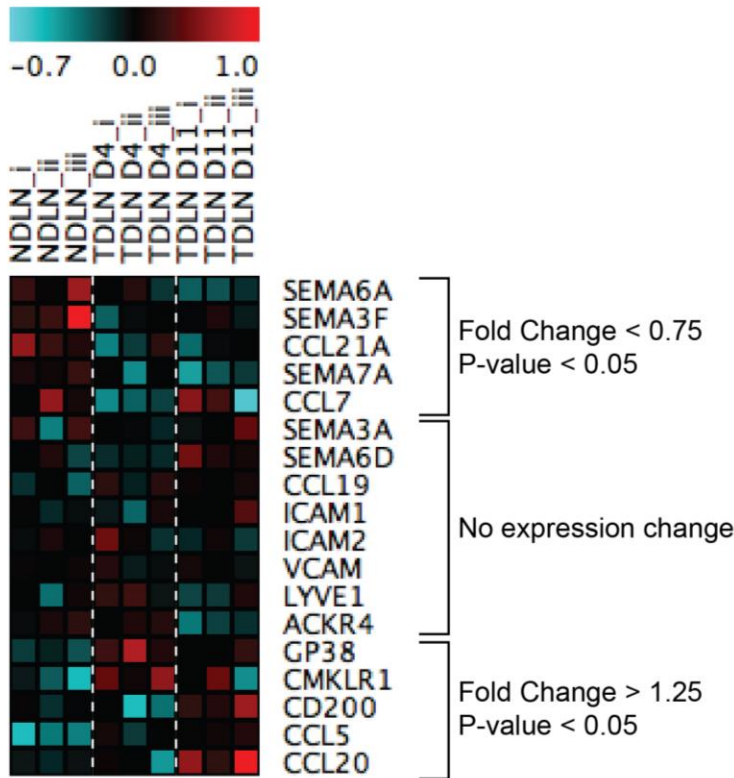
4.3.4 Microarray identified candidate gene targets for altered LEC-immune interactions *in vivo*

To visualise changes in soluble and membrane-bound factors involved in LEC-immune interactions, we analysed our microarray data acquired from LECs derived from NDLENs and TDLENs (see Methods 3.22), to determine expression trends in molecular targets known to be involved in immune cell adhesion, migration and lymphatic interactions (Figure 4.14a). To visualise the changes in expression of these factors, heatmaps were created based on fold change or statistical significance to eliminate bias (Figure 4.14a). Several factors were unchanged in their expression profiles, with chemokine signaling factors, CCL19 and CCRL1 and cell-adhesion molecules, ICAM-1, ICAM-2, VCAM-1 and LYVE-1, all showing no difference in fold change expression in both Day 4 and Day 11 TDLEN-derived LECs (Figure 4.14b). This demonstrates that factors derived from early developing B16-tumours may not regulate canonical integrin-dependent pathways and LYVE-1, recently identified to have cell adhesion properties⁵². As we observed a difference in dendritic cell-lymphatic interactions *in vivo* and *in vitro*, we concluded that these factors are hence unlikely to be responsible for tumour-driven prolonged interactions between dendritic cells and lymphatic endothelial cells. The same conclusion was drawn for CCL19 and CCRL1; eliminating CCL19 signalling and chemokine scavenging as a means of altered dendritic cell localisation in early TDLENs.

Of the factors reported to be required for dendritic cell migration, expression of neither Semaphorin-3A nor Semaphorin-7A were altered in early TDLENs (Figure 4.14), despite significantly decreased expression of Semaphorin-7A in late TDLENs (Day 11 TDLENs Fold Change = 0.72, $P = 0.005$). This suggests that disrupted expression of Semaphorin-7A may impact dendritic cell migration and localisation in nodes at later stages of tumours development, however is unlikely to be responsible for changes in dendritic cell-lymphatic endothelial interactions in early TDLENs. Of the up- and down-regulated chemokines, CCL21 was down regulated in both Day 4 and Day 11 TDLENs (Day 4 TDLENs Fold Change = 0.74, $P = 0.024$; Day 11 TDLENs Fold Change = 0.71, $P = 0.009$) (Figure 4.14b). As CCL21 is critical for migration, decreased expression in TDLENs could indeed contribute towards delocalisation of dendritic cells. However, as shown in Chapter 3, CCL21 expression could be detected in all stromal compartments

of Day 4 TDLNs, despite significant changes in CCL21 RNA expression by LECs in TDLNs. Total CCL21 expression may hence not be perturbed to the extent needed to drive changes in dendritic cell interactions with lymphatics at the lymph node periphery. Also, in early TDLNs Podoplanin (*Gp38*) and Chemerin receptor (*Cmklr1*) were both significantly up-regulated (Day 4 TDLNs: *Gp38* Fold Change = 1.44, $P = 0.005$ and *Cmklr1* Fold Change = 1.54, $P = 0.003$) (Figure 4.14b). As Podoplanin has recently been reported to contribute to FRC-dependent dendritic cell mobility once within lymph nodes^{77,235}, we were intrigued by the expression changes in early TDLN-derived LECs. Furthermore, as shown in Chapter 3, increases in RNA expression were validated at a protein level using flow cytometry.

A Immune Interactions



B

Gene Target	Gene Name	Day 4 TDLNs		Day 11 TDLNs	
		Fold Change	P-value	Fold Change	P-value
<i>SEMA3A</i>	Semaphorin-3A	0.95	0.240	0.99	0.850
<i>SEMA3F</i>	Semaphorin-3F	0.67	0.024	0.69	0.022
<i>SEMA6A</i>	Semaphorin-6A	0.93	0.570	0.96	0.369
<i>SEMA7A</i>	Semaphorin-7A	0.89	0.290	0.72	0.005
<i>CCL5</i>	Chemokine ligand-5	1.30	0.009	1.30	0.012
<i>CCL7</i>	Chemokine ligand-7	0.71	0.018	0.87	0.573
<i>CCL19</i>	Chemokine ligand-5	1.16	0.109	1.04	0.686
<i>CCL20</i>	Chemokine ligand-20	0.97	0.277	1.49	0.013
<i>CCL21</i>	Chemokine ligand-21	0.74	0.024	0.71	0.009
<i>CD200</i>	OX-2 membrane glycoprotein	0.67	0.011	1.24	0.036
<i>ICAM1</i>	Intracellular adhesion molecule 1	0.97	0.733	1.09	0.402
<i>ICAM2</i>	Intracellular adhesion molecule 2	1.06	0.580	0.89	0.188
<i>VCAM1</i>	Vascular cell adhesion molecule 1	1.00	0.228	0.95	0.427
<i>LYVE1</i>	Lymphatic vessel endothelial hyaluronan receptor 1	1.17	0.133	0.99	0.887
<i>ACKR4</i>	Atypical chemokine receptor 4	1.02	0.593	0.86	0.095
<i>GP38</i>	Podoplanin	1.44	0.005	1.13	0.203
<i>CMKLR1</i>	Chemerin chemokine-like receptor 1	1.54	0.003	1.13	0.394

Figure 4.14. Microarray data of gene targets involved in immune cell interactions. Fluorescent intensity values for gene targets with significantly altered expression levels in Day 4 TDLNs and Day 11 TDLNs relative to control NDNLNs, were visualised using heatmaps. Genes with expression fold changes ≥ 1.25 shown in red and ≤ 0.75 shown in cyan (A). Tabulated fold change and p-values for each gene target shown in the heatmap (B). Data shown is from one independent experiment, with pooled brachial lymph nodes from n=2 mice per sample (total n=18).

4.3.5. Dendritic cells interact with Podoplanin expressing lymphatic endothelium in lymph nodes *in vivo*

To assess whether migratory dendritic cells come into physical contact with Podoplanin in the subcapsular sinus, high magnification confocal microscopy was conducted on control NDNLs and Day 4 TDLNs from TRITC painted mice where less TRITC+ dendritic cells were found in the outer regions and subcapsular sinus of control NDNLs than Day 4 TDLNs. TRITC+ dendritic cells were observed in direct contact with areas of the subcapsular sinus that were strongly positive for Podoplanin (Figure 4.15). Expression was detected on the ceiling and floor of the sinus, and on the strands connecting the ceiling and floor (Figure 4.15). On all Podoplanin positive regions of the sinus, TRITC+ dendritic cells could be seen interacting with the ceiling, the floor and sinus strands (Figure 4.15).

4.3.6 Tumour-derived factors drive up-regulation of Podoplanin protein expression and consequent adhesion of dendritic cells to lymphatic endothelial cells *in vitro*

Having identified a physical interaction between DCs and LECs at the subcapsular sinus, of both resting and early TDLNs, and shown the up-regulation of Podoplanin at both an RNA and protein level, we investigated whether Podoplanin could be driving prolonged physical interactions *in vitro*. Indeed at 48-hours, Podoplanin expression was up-regulated in LECs treated with TCM. *In vitro* cultures treated with TCM for 5hrs and 72hrs, the fold change in expression of Podoplanin was 0.85 ± 0.14 and 1.60 ± 0.11 , respectively. Whereas in LECs treated with 48hrs, the fold change in expression of Podoplanin was 6.19 ± 2.72 (Figure 4.16a). To ensure that TCM was not inducing the up regulated expression of other cell adhesion molecules known to bind DCs, TCM or TNF- α (100ng/ml) was added to cultured cells, and cells processed for flow cytometry for expression of CAMs. Treatment dramatically increased the expression of VCAM-1, with a lesser affect observed with ICAM-1. Cultures treated with TCM showed no up-regulated expression of VCAM-1 and ICAM-1 relative to control treated wells (Figure 4.16b). This suggested that B16-F10 derived TCM, did not induce altered VCAM-1 and ICAM-1 expression in our *in vitro* system, and further suggests a lack of sufficient levels of factors that induce VCAM-1 and ICAM-1 expression.

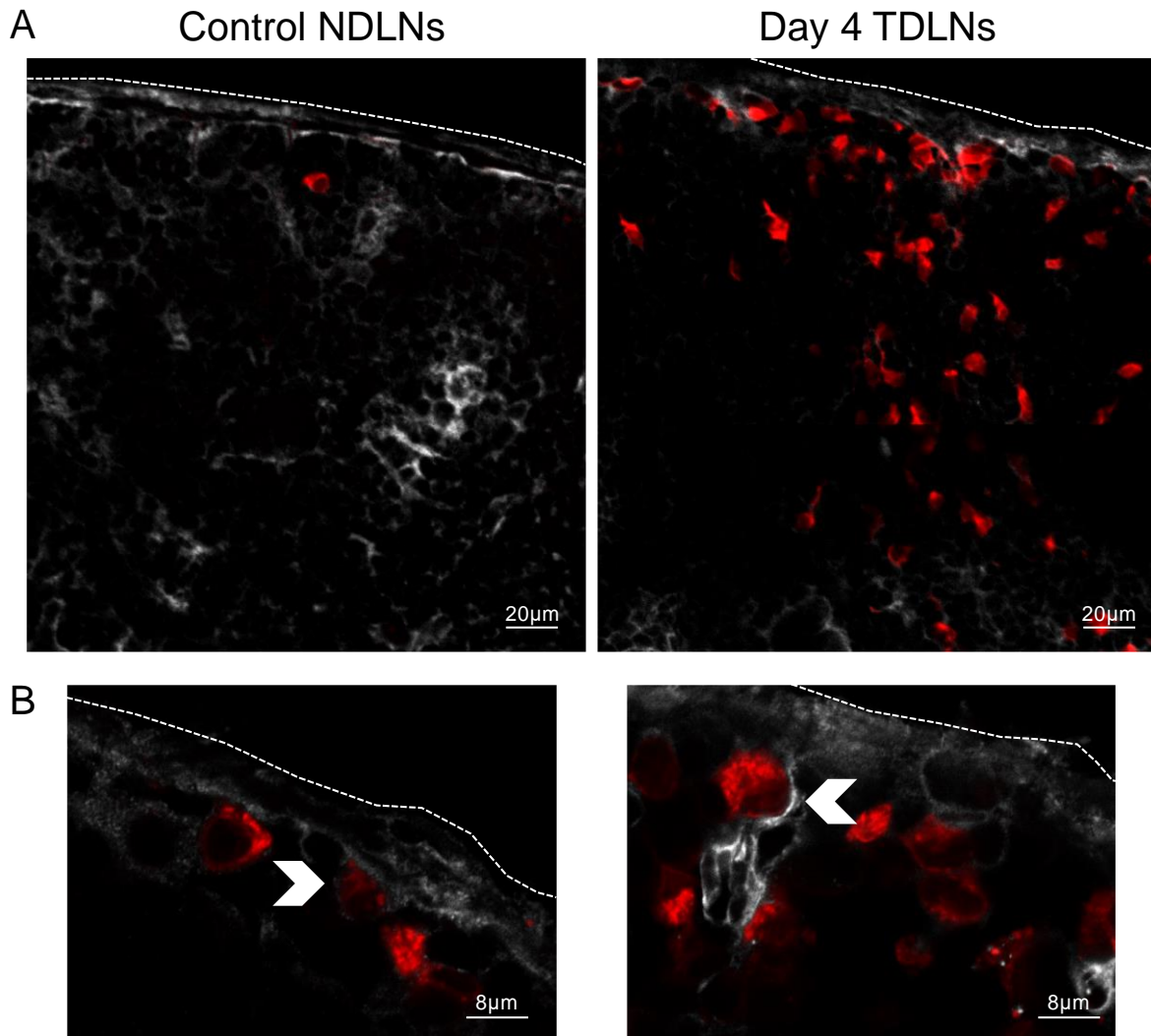


Figure 4.15. Immunofluorescent imaging of TRITC+ DCs in the subcapsular sinus of LNs. Control NDNLNs and Day 4 TDLNs derived from B16-F10 tumour bearing mice, painted with TRITC. Lymph nodes were immunofluorescently stained for Podoplanin (white) and TRITC DCs (red), and imaged using confocal microscopy at 20x (A) and 63x oil (B) magnification. Few TRITC DCs can be seen in the subcapsular sinus of control NDNLNs (A, left panel) and clusters of TRITC DCs seen in the subcapsular sinus of Day 4 TDLNs (A, right panel). Those seen in the subcapsular sinus can be seen to interact with Podoplanin positive regions (arrowheads) in both Control and Day 4 TDLNs (B). Shown are representative FOVs from n=5 independent experiments with n=9 NDNLNs and n=18 Day 4 TDLNs. Scale bars represent 20µm (A) and 8µm (B).

To confirm the role of Podoplanin in physical interactions between DCs and LECs, *in vitro* cultures were treated with Podoplanin blocking antibody clone 8.1.1, which has previously been used for *in vivo* blocking experiments²³⁶. As we had hypothesised that Podoplanin was driving prolonged physical interactions, with a dominant adhesion and anchorage phenotype, we assessed adhesion of GFP+ DCs to LECs *in vitro* in

resting conditions in the presence of Podoplanin blocking antibody (Figure 4.17a). We saw a significant reduction in adherence of GFP+ DCs, with fold-changes in control treated LECs averaging 1.00 ± 0.03 and in anti-Podoplanin treated LECs averaging 0.71 ± 0.06 (Figure 4.17b). Full gating strategies stated in Appendix 8.

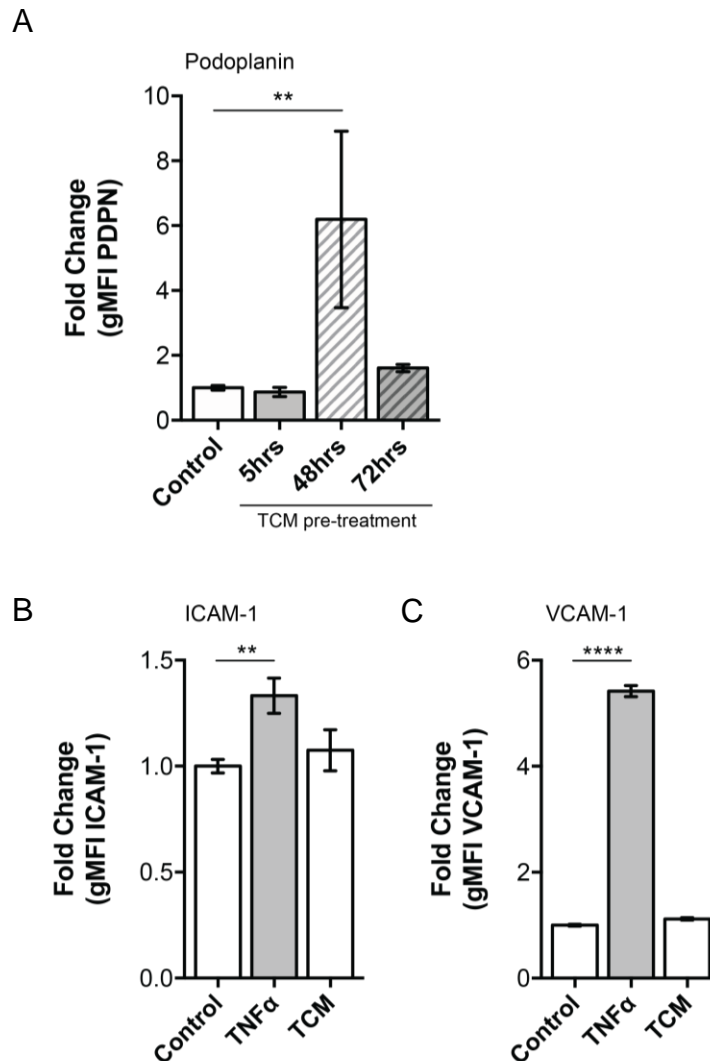


Figure 4.16. Enhanced Podoplanin expression in LECs treated with TCM for 48hrs *in vitro*. Primary LECs cultured in collagen-coated plates and treated with 50% B16-F10 derived TCM for 5-72hrs or recombinant TNF α (100ng/ml) overnight. Cells were retrieved from culture and stained with fluorescently-conjugated antibodies for flow cytometry, assessing Podoplanin (A), ICAM-1 (B) and VCAM-1 (C) surface expression. Unstained cells were processed as controls and used to set the threshold for negative expression. Fold changes in geometric mean fluorescent intensity (gMFI) were calculated relative to control untreated LECs per independent experiment. Data shown is representative of n=3 independent experiments with n=6-10 samples per group. Data is shown \pm SEM. Statistical significance calculated using the Kruskal-Wallis test.

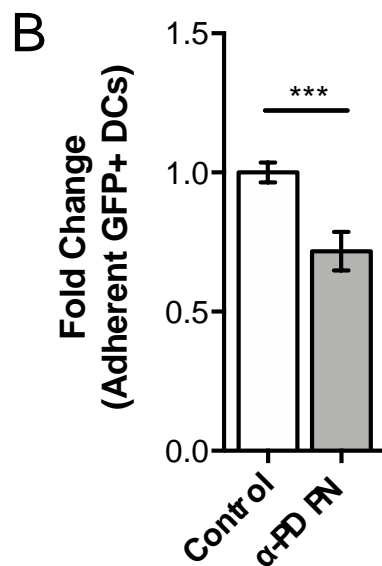
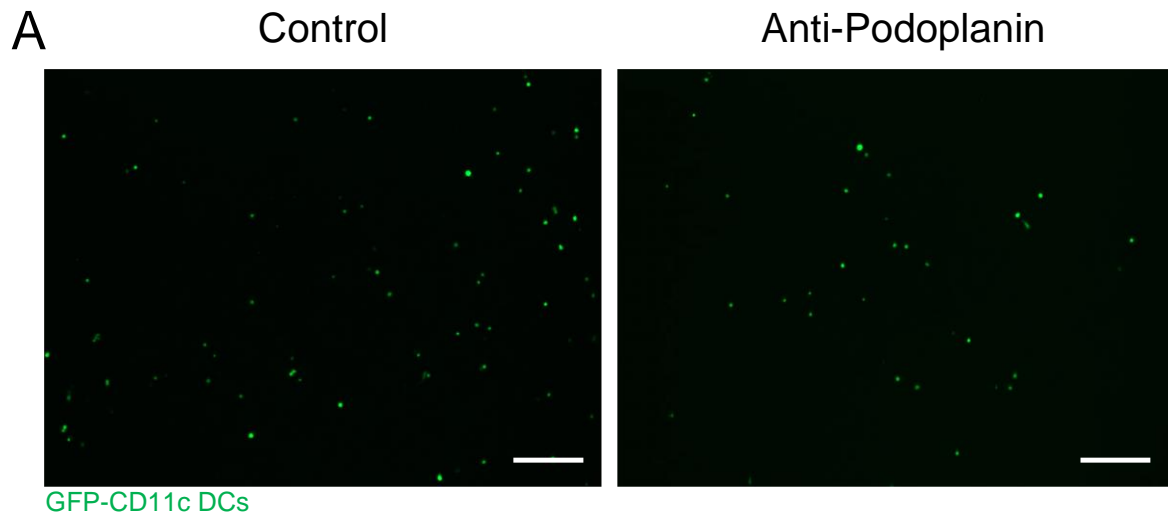


Figure 4.17. Podoplanin blockade inhibits DC adhesion to LECs *in vitro* in resting conditions. GFP-DCs were co-cultured with LECs grown on collagen-coated plates (50µg/ml) and conditioned with tumour-conditioned media (TCM) for 48hours prior to co-culture. GFP-DCs adhered to monolayers of LECs imaged using the EVOS® system. Representative FOVs shown and scale bars represent 200µm (A). Adherent GFP+ cells were manually counted using *FIJI* image analysis software, and the fold changes in adherent GFP-DCs calculated using raw counts normalised to control samples within independent experiments (B). Data shown is from n=3 independent experiments with n=76 Control; n=24 anti-Podoplanin. Data presented as mean ± SEM. Statistical significance was calculated using the Student t-test ($P \leq 0.05$).

To determine whether splenic DCs used throughout these assays, expressed the described ligand of Podoplanin, CLEC-2, we processed spleens and lymph nodes using flow cytometry to assess surface expression of CLEC-2 on CD11c+ DCs.

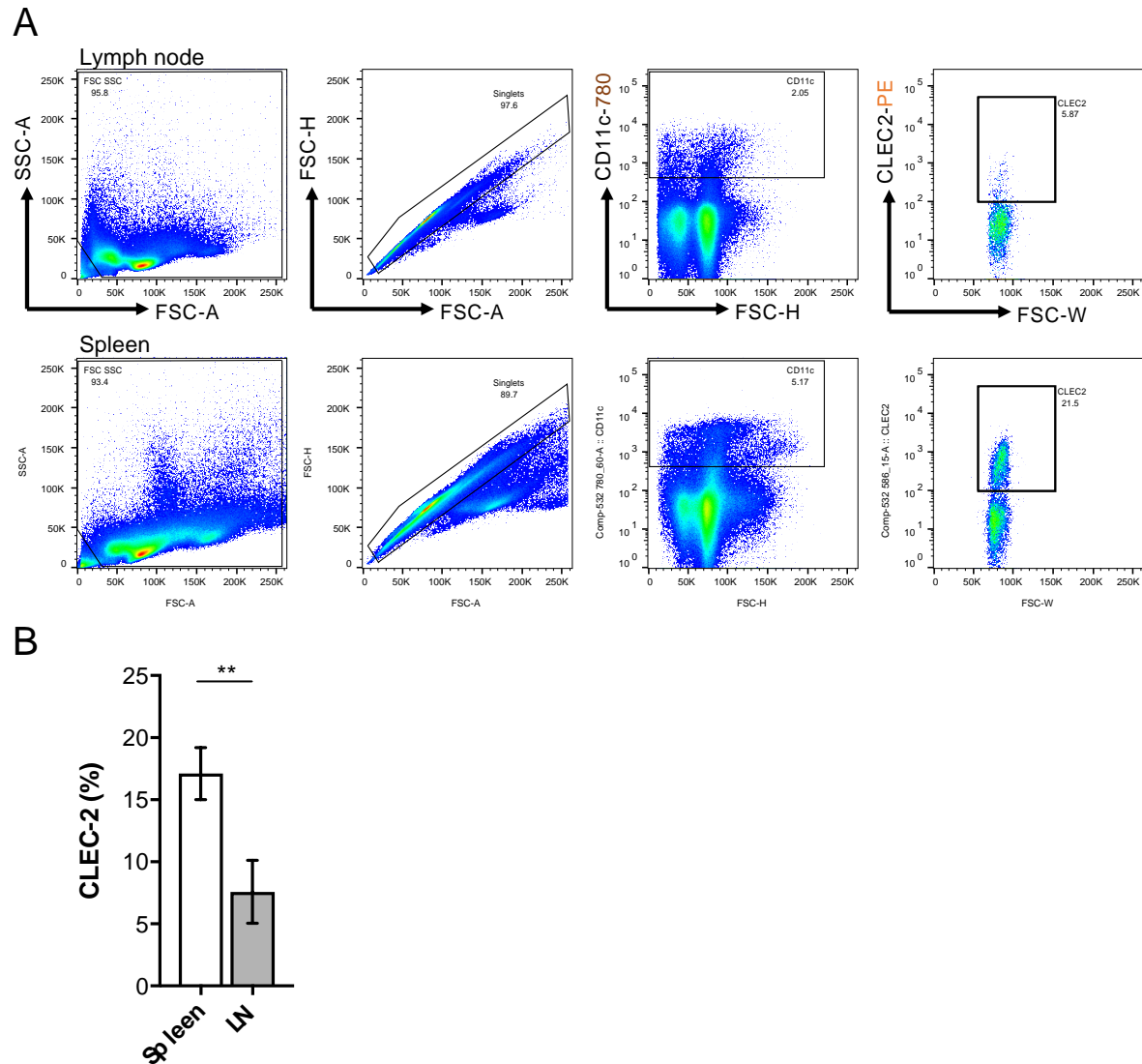


Figure 4.18. CLEC-2 is expressed in DCs derived from spleen and lymph nodes. Spleens and lymph nodes derived from wild-type C57BL/6 mice were digested and samples stained with fluorescently-conjugated antibodies for flow cytometry to assess surface expression of CD11c and CLEC-2. Unstained cells were processed as controls and used to set the threshold for negative expression. CLEC-2 positive cells gated within total CD11c DCs in splenic and lymph node samples (A). Data shown is percentage of CLEC-2 positive expression in populations within total CD11c DCs (B). Data shown is representative of n=3 independent experiments with n=7 Spleens; n=7 Lymph Nodes. Data is shown \pm SEM. Statistical significance calculated using the Mann Whitney test ($P \leq 0.05$).

As a comparison and to see whether lymph node DCs expressed CLEC-2, resting lymph nodes were also processed for flow cytometry. In splenic samples, a defined population of CLEC2+ cells could be seen within CD11c+ DCs, whereas in lymph nodes a less well-defined population could be seen (Figure 4.18a). Upon quantification of the percentage of CLEC2+ populations within CD11c+ DCs, an average of $17.11\% \pm 2.09$ of CD11c+ DCs expressed CLEC2+ in splenic samples and $7.58\% \pm 2.52$ in lymph node samples (Figure 4.18b). This confirms that splenic DCs used throughout these assays do indeed express CLEC-2 and hence have the capacity to physically interact with and bind to Podoplanin expressing LECs *in vitro*.

4.3.7 *In vivo blockade of Podoplanin inhibits dendritic cell migration into lymph nodes*

To investigate further the role of Podoplanin in dendritic cell migration in the extended tumour microenvironment, we inhibited Podoplanin along the drainage pathway using subcutaneous administration of blocking antibody clone 8.1.1 as previously described in literature²³⁶. To avoid effects of Podoplanin blocking on lymphatics, tumour cells and fibroblasts at the tumour site and thus potentially impairing DC trafficking away from the tumour, we instead injected blocking antibody subcutaneously into the front leg, to ensure rapid delivery of antibody to the downstream draining brachial lymph node. Blocking antibody was administered daily to maintain inhibition of Podoplanin throughout the experiment, having allowed 24 hours for inoculated tumour cells to settle at the injected site. Tumours were painted with TRITC, using previously described protocols, and lymph nodes harvested 18 hours later for histology and flow cytometry analysis.

In TDLNs derived from TRITC painted tumours, TRITC+ cells were detected in TDLNs in both control IgG and blocking antibody treated conditions. Importantly however, the lymphatic expansion phenotype observed in early TDLNs was retained in mice treated with IgG controls or blocking antibody. Localisation of TRITC+ cells could be seen at the subcapsular sinus and in regions of lymphatic expansion in both IgG and blocking antibody treated conditions, however the extent of TRITC infiltrate across FOVs appeared reduced in comparison to previously imaged Day 4 TDLNs (Figure 4.19). This could be due to both IgG and blocking antibodies perturbing overall infiltrate of

TRITC+ DCs, which would explain the overall lack of TRITC+ cells seen in these FOVs.

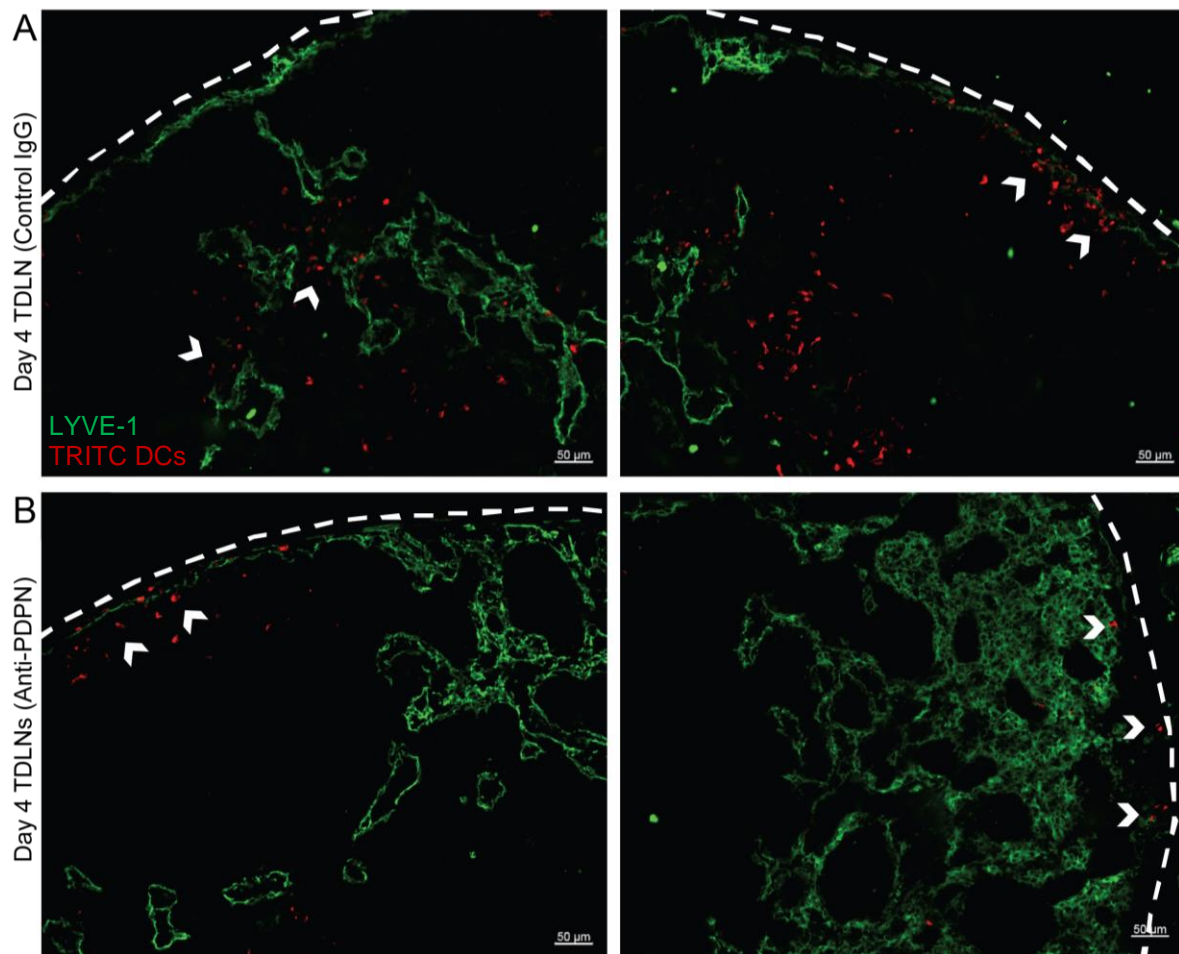


Figure 4.19. *In vivo* Podoplanin blockade does not alter migratory dendritic cell localisation in LNs. Day 4 TDLNs from B16-F10 tumour-bearing mice injected subcutaneously daily with IgG control (A) or anti-Podoplanin blocking antibody (B) at a concentration of 1mg/ml in 50μl of sterile PBS. Samples were immunofluorescently stained with LYVE-1 (green) with periphery-derived migratory dendritic cells marked with TRITC (red). Shown are representative FOVs from n>3 independent experiments, with n>10 LNs imaged across all groups. Lymph node edge (dashed white line). Dotted lines define the lymph node edge and white arrowheads indicate TRITC localisation relative to lymphatic regions. Scale bars represent 50μm.

To determine whether IgG and blocking antibodies did indeed significantly reduce the overall infiltrate of TRITC+ DCs, control NDNLs and early TDLNs, from matched animals, were processed for flow cytometry. Similarly, to previous experiments, lymph nodes were stained for CD11c, CD8a, CD11b and CD103 to discern trends in specific DC populations. Across conditions, lymph node cellularity was not significantly altered, except for in Day 4 TDLNs treated with anti-Podoplanin blocking antibody (Figure

4.20a). Global assessment of CD11c, in terms of count and percentage of singlets showed similar trends, with the fold-change count per lymph node also showing highest levels in anti-Podoplanin blocking antibody treated Day 4 TDLNs (Figure 4.20b,c). Similar to previous findings (Figure 4.7), the infiltrate of migratory DC subsets was increased in D4 TDLNs versus NDNLs in PBS treated conditions (Figure 4.21). However, neither treatment with IgG nor anti-Podoplanin blocking antibody appeared to reverse this increased trend. Whether TRITC infiltrate was assessed by counts (Figure 4.21) or as a percentage of a population (Figure 4.22), there were no significant changes across conditions.

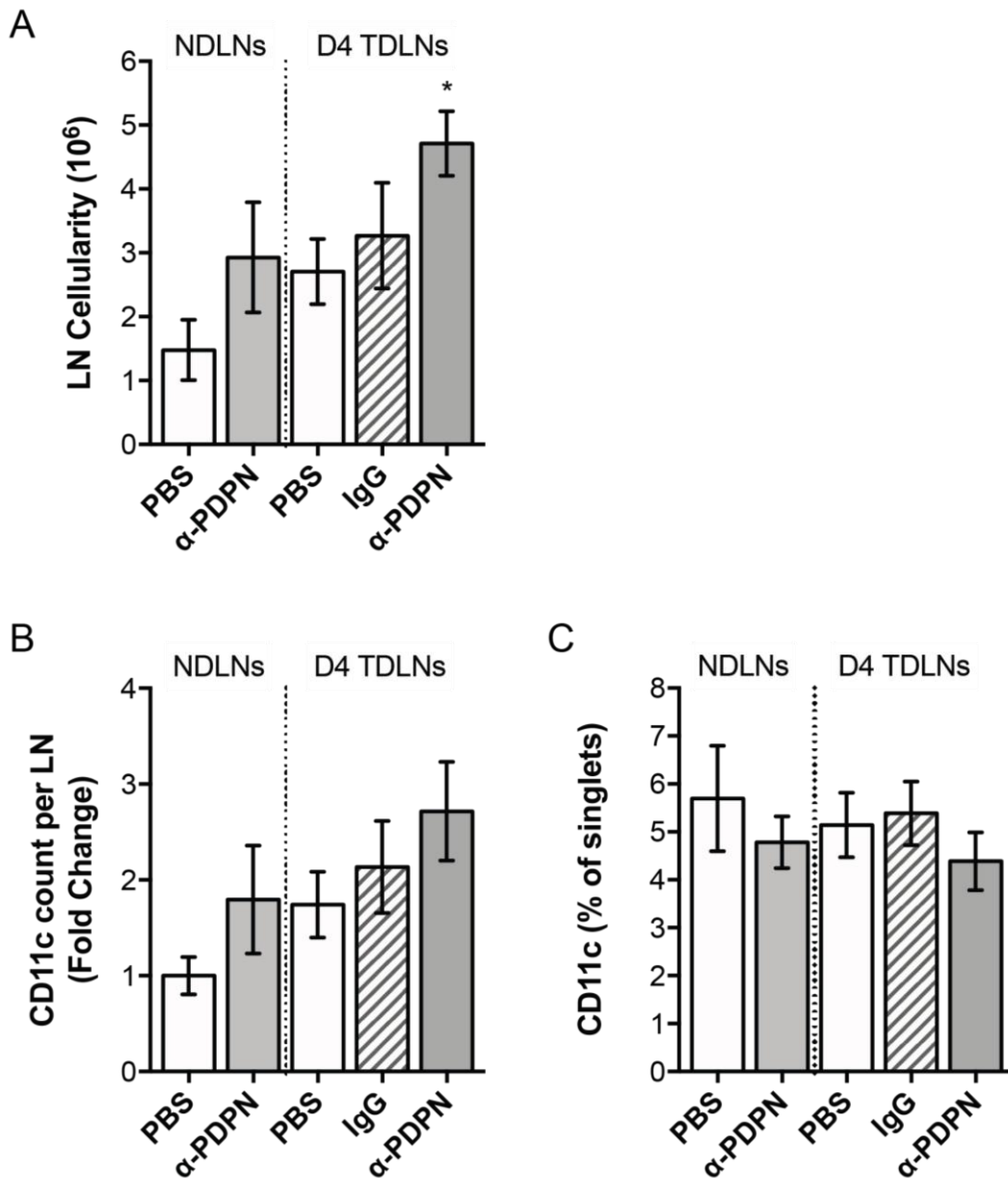


Figure 4.20. Podoplanin blockade does not significantly alter dendritic cell counts in early TDLNs. NDLNs and Day 4 TDLNs from B16-F10 tumour-bearing mice, injected subcutaneously daily with IgG control or anti-Podoplanin blocking antibody at a concentration of 1mg/ml in 50µl of sterile PBS. Samples were digested and stained with fluorescently-labelled antibodies for flow cytometry, assessing expression of DC surface marker, CD11c. Data shown is total lymph node cellularity (A), total CD11c DCs, as expressed by count fold-change (B) and as a percentage of singlets (C). Shown is data from n=2 independent experiments, with n=4 PBS NDLNs; n=4 anti-PDPN NDLNs; n=6 PBS Day4 TDLNs; n=6 IgG Day4 TDLNs; n=6 anti-PDPN Day4 TDLNs. Data presented as mean ± SEM. Statistical significance was calculated using the Kruskal-Wallis test, with $P \leq 0.05$ when compared to PBS treated control NDLNs.

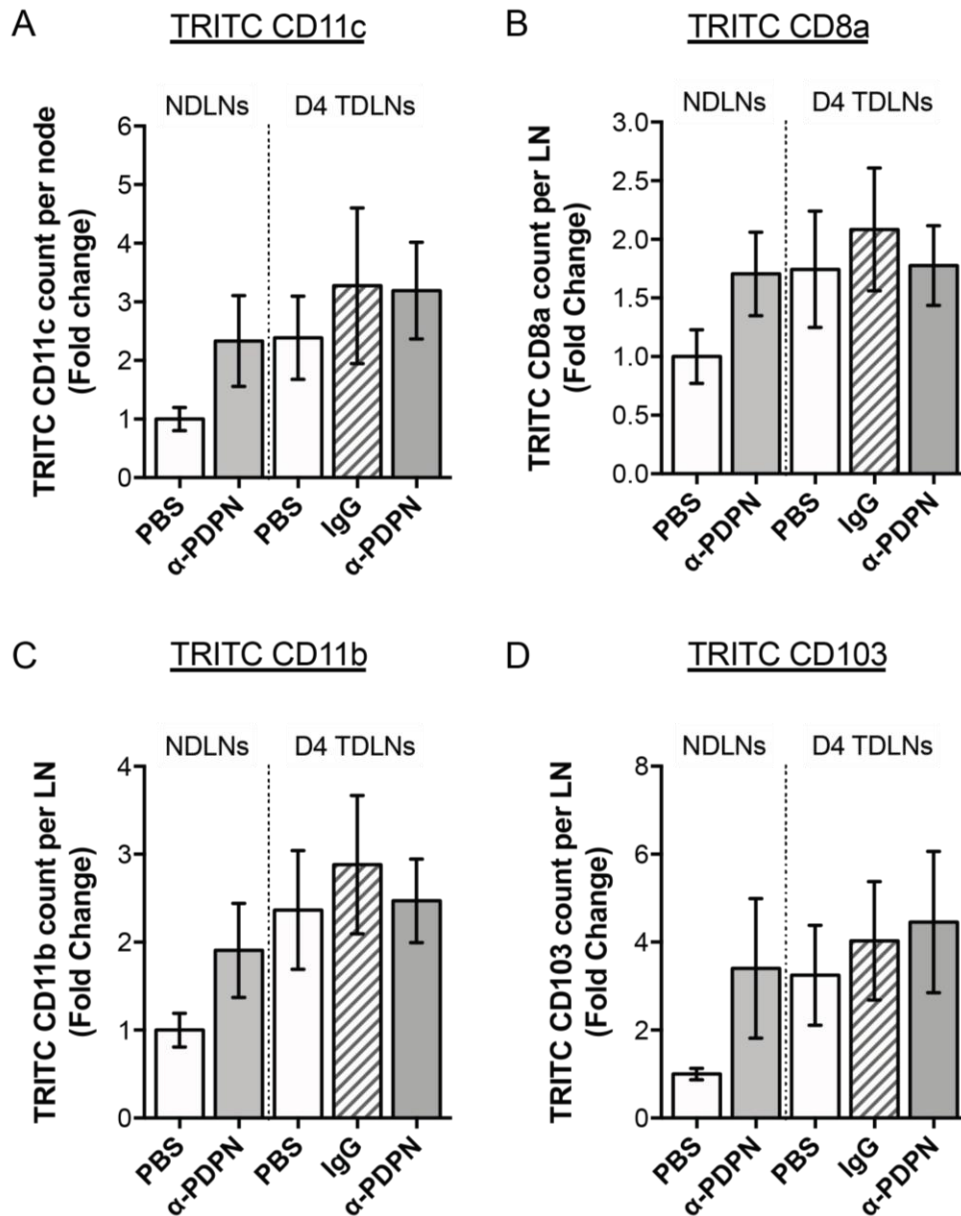


Figure 4.21. Podoplanin blockade does not significantly alter total counts of migratory TRITC DC infiltrate in early TDLNs. NDNLs and Day 4 TDLNs from TRITC painted B16-F10 tumour-bearing mice, injected subcutaneously daily with IgG control or anti-Podoplanin blocking antibody at a concentration of 1mg/ml in 50µl of sterile PBS. Samples were digested and stained with fluorescently-labelled antibodies for flow cytometry, assessing expression of DC surface markers, CD11c, CD8a, CD11b and CD103. Data shown is total TRITC CD11c (A), TRITC CD8a (B), TRITC CD11b (C) and TRITC CD103 (D), expressed by count fold change. Shown is data from n=2 independent experiments, with n=4 PBS NDNLs; n=4 anti-PDPN NDNLs; n=6 PBS Day4 TDLNs; n=6 IgG Day4 TDLNs; n=6 anti-PDPN Day4 TDLNs. Data presented as mean ± SEM. Statistical significance was calculated using the Kruskal-Wallis test, with $P \leq 0.05$ when compared to PBS treated control NDNLs.

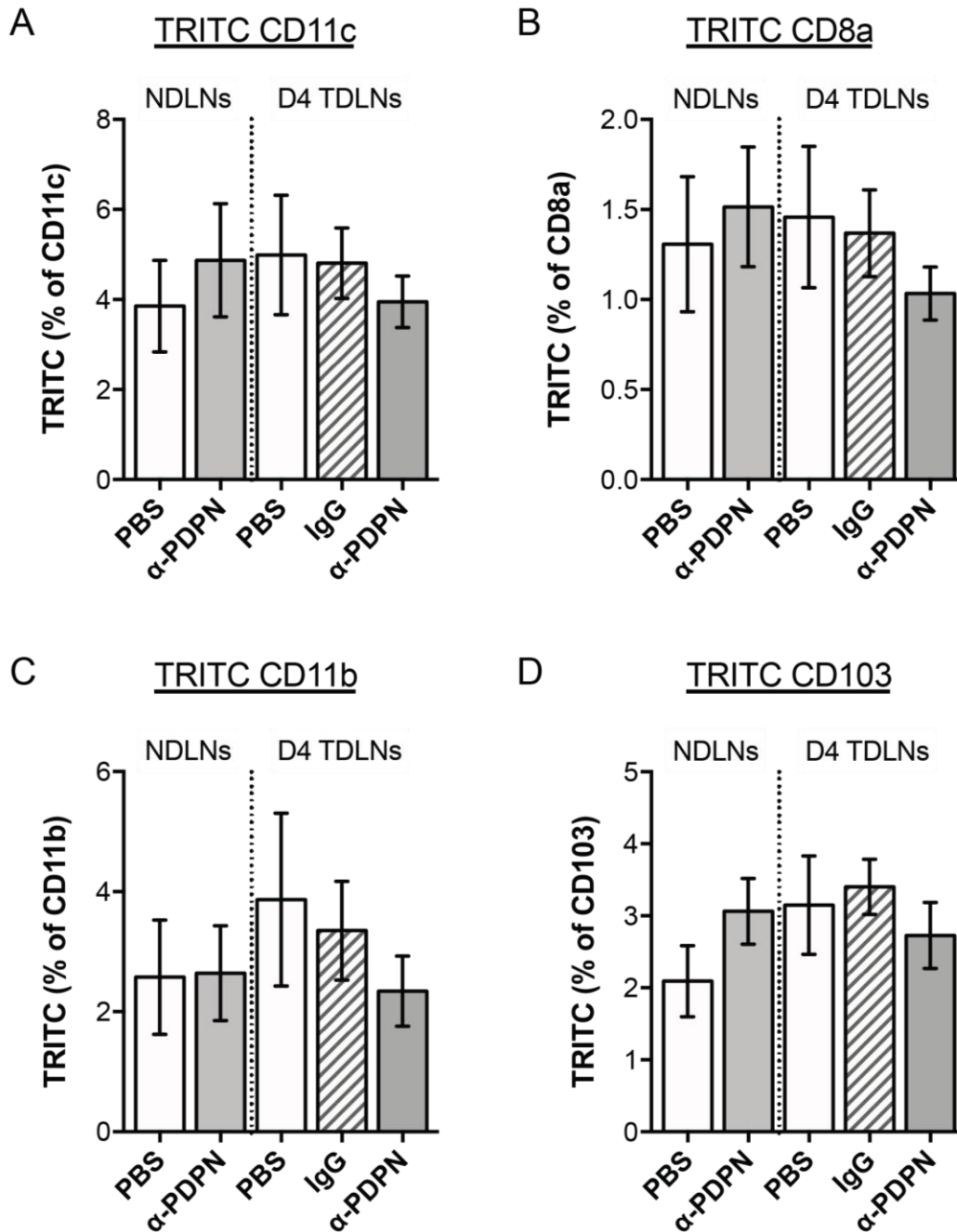


Figure 4.22. Podoplanin blockade does not significantly alter the percentage of migratory TRITC DC infiltrate in early TDLNs. NDNLs and Day 4 TDLNs from TRITC painted B16-F10 tumour-bearing mice, injected subcutaneously daily with IgG control or anti-Podoplanin blocking antibody at a concentration of 1mg/ml in 50 μ l of sterile PBS. Samples were digested and stained with fluorescently-labelled antibodies for flow cytometry, expression of DC surface markers, CD11c, CD8a, CD11b and CD103. Data shown is TRITC cells, expressed as a percentage of total CD11c (A), CD8a (B), CD11b (C) and CD103 (D). Shown is data from n=2 independent experiments, with n=4 PBS NDNLs; n=4 anti-PDPN NDNLs; n=6 PBS Day4 TDLNs; n=6 IgG Day4 TDLNs; n=6 anti-PDPN Day4 TDLNs. Data presented as mean \pm SEM. Statistical significance was calculated using the Kruskal-Wallis test, with $P \leq 0.05$ when compared to PBS treated control NDNLs.

As migratory DC infiltrate, as shown by TRITC CD11c count per lymph node, in early TDLNs in untreated LNs were increased relative to control NDNLs, blockade of Podoplanin was expected to inhibit the ingress of DCs. This data however shows that subcutaneous administration of blocking antibody, using this regime and particular antibody concentrations, does not induce significant changes in migratory DC infiltrate in early TDLNs.

4.3.8 Dendritic cell migration is perturbed in Podoplanin-flox mice

As little was seen in the in vivo blockade model, we further applied the TRITC tumour model to ears of tumour-bearing PDPN-FL mice, as the ear is very lymphatic rich and hence we expected to see an exaggerated impact of perturbed Podoplanin signalling on DC trafficking to TDLNs. In this case, draining cervical lymph nodes were collected for analysis, as they lay downstream of the tumours implanted in the ears. We TRITC painted wild type, heterozygous and homozygous PDPN-FL mice inoculated with subcutaneous B16-F10 tumours.

Firstly, lymphatic vasculature integrity was assessed using immunofluorescent imaging. By staining for lymphatic marker, LYVE-1, and CD31, which is highly expressed in blood vasculature; lymphatic vessels in both wild type and homozygous PDPN-FL mice displayed undisrupted networks, with no visible alteration in branching or vessel morphology (Figure 4.23a). Furthermore, the blood and lymphatic vasculature appeared visibly separate in both wild type and homozygous mice. Upon assessment of Podoplanin expression, wild type mice exhibited expected expression patterns with Podoplanin detected throughout the vasculature and at valves. Heterozygous mice appeared to be moderately affected by loss of an allele, with similar expression patterns seen across the vasculature, suggesting one allele is sufficient for Podoplanin protein translation. As expected in homozygous mice, Podoplanin staining was undetectable (Figure 4.23b), with positive Podoplanin expression detected in heterozygous ears but to a lesser extent. This characterisation led us to conclude that lymphatic vasculature was intact and Podoplanin knockout did not affect expression of other markers such as LYVE-1. Therefore, any changes in

dendritic cell migration seen in this model, could be attributable to perturbed Podoplanin expression.

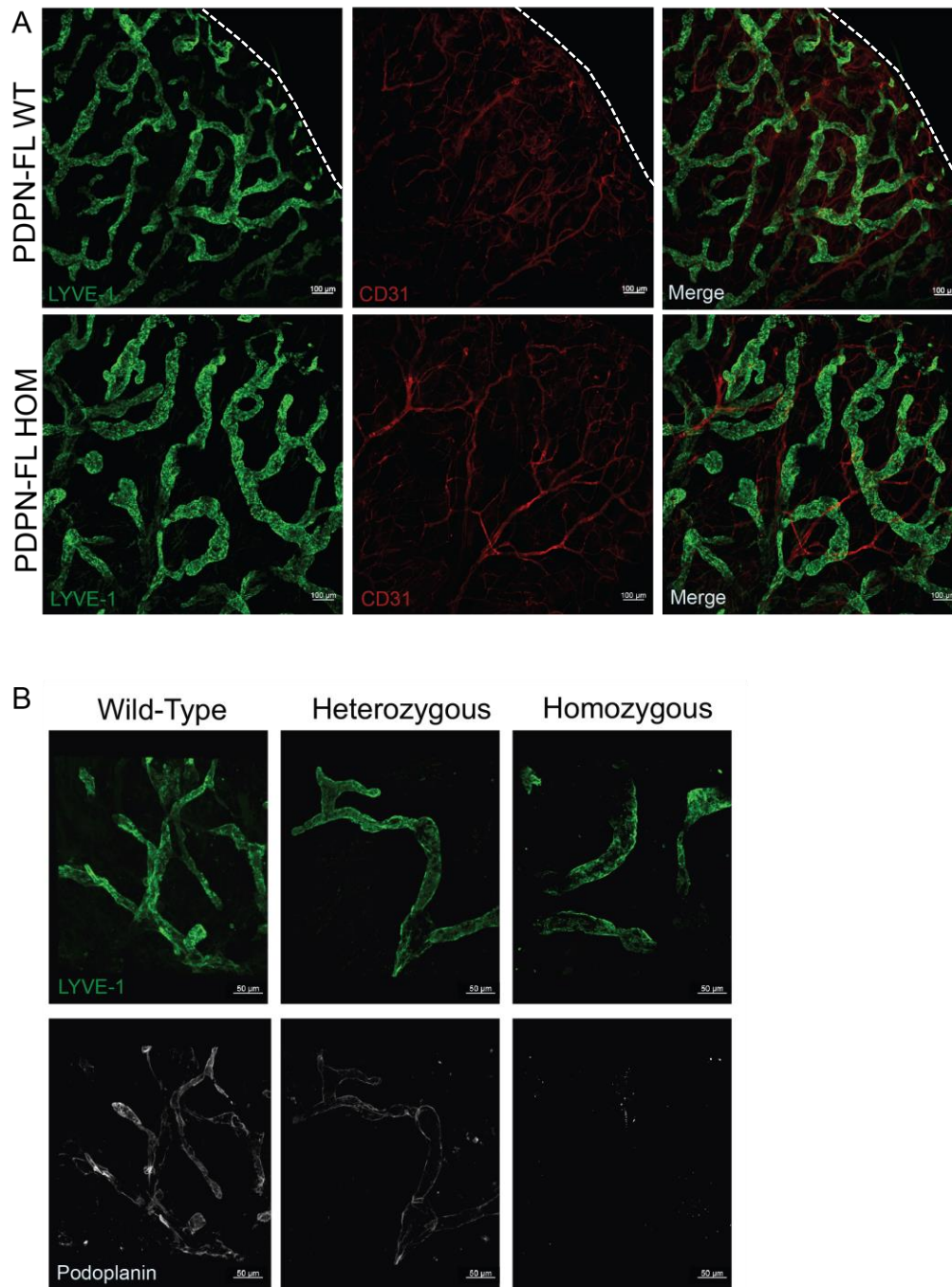


Figure 4.23. Characterisation of lymphatic networks and Podoplanin expression in ear dermis from PDPN-FL mice. Ear dermal sheets from PDPN-FL mice of wild type, heterozygous and homozygous genotypes were immunofluorescently stained for lymphatic surface markers, LYVE-1 and Podoplanin, and blood vasculature surface marker, CD31. Samples were imaged at 20x magnification using confocal microscopy. Representative FOVs showing lymphatic and blood vasculature in PDPN-FL wild-type (WT) and homozygous (HOM) ear dermal sheets. Scale bars represent 100µm (A). Representative FOVs showing Podoplanin expression in lymphatic vessels as defined by LYVE-1 expression. Scale bars represent 50µm (B). Shown are images from n>3 independent experiments. White dotted lines represent edge of the ear dermal sheet.

Similarly, to previous analysis on PDPN-FL mice, TDLNs from wild type, heterozygous and homozygous PDPN-FL mice were taken from tumour-bearing mice for flow cytometry analysis of dendritic cell markers, CD11c, CD8a, CD11b and CD103. As expected in heterozygous mice, lymph node cellularity was unaltered (Figure 4.24a) and little change could be seen across overall dendritic cell counts, expressed either as count fold-change or as a percentage (Figure 4.24b,c). This trend was reflected in subsets, which also showed little change in total numbers of CD8a, CD11b and CD103 DCs (Figure 4.24d-i). In homozygous mice however, total counts per lymph node were significantly reduced in total CD11c DCs (Figure 4.24b) as well as subset specific DCs (Figure 4.24d-f), with the most prominent reduction seen in CD11b DCs (Figure 4.24e). This was not however reflected in calculations of relative percentage composite, with the percentage of CD8a, CD11b and CD103 as a percentage of total CD11c was unchanged across genotypes (Figure 4.24g-i). Upon specific assessment of TRITC+ DCs, decreased trends in the counts and relative percentages of DC subsets was seen in heterozygous PDPN-FL mice, with numbers almost entirely ablated in homozygous PDPN-FL mice (Figure 4.25). Whether TRITC was assessed within total CD11c DCs or within specific CD8a, CD11b or CD103 populations, TRITC detection was significantly perturbed.

This collectively shows a substantial effect of Podoplanin knockout on DC trafficking in tumour-bearing mice, whereby migration of tumour-derived DCs, denoted by TRITC expression, was dramatically reduced in PDPN-FL homozygous mice.

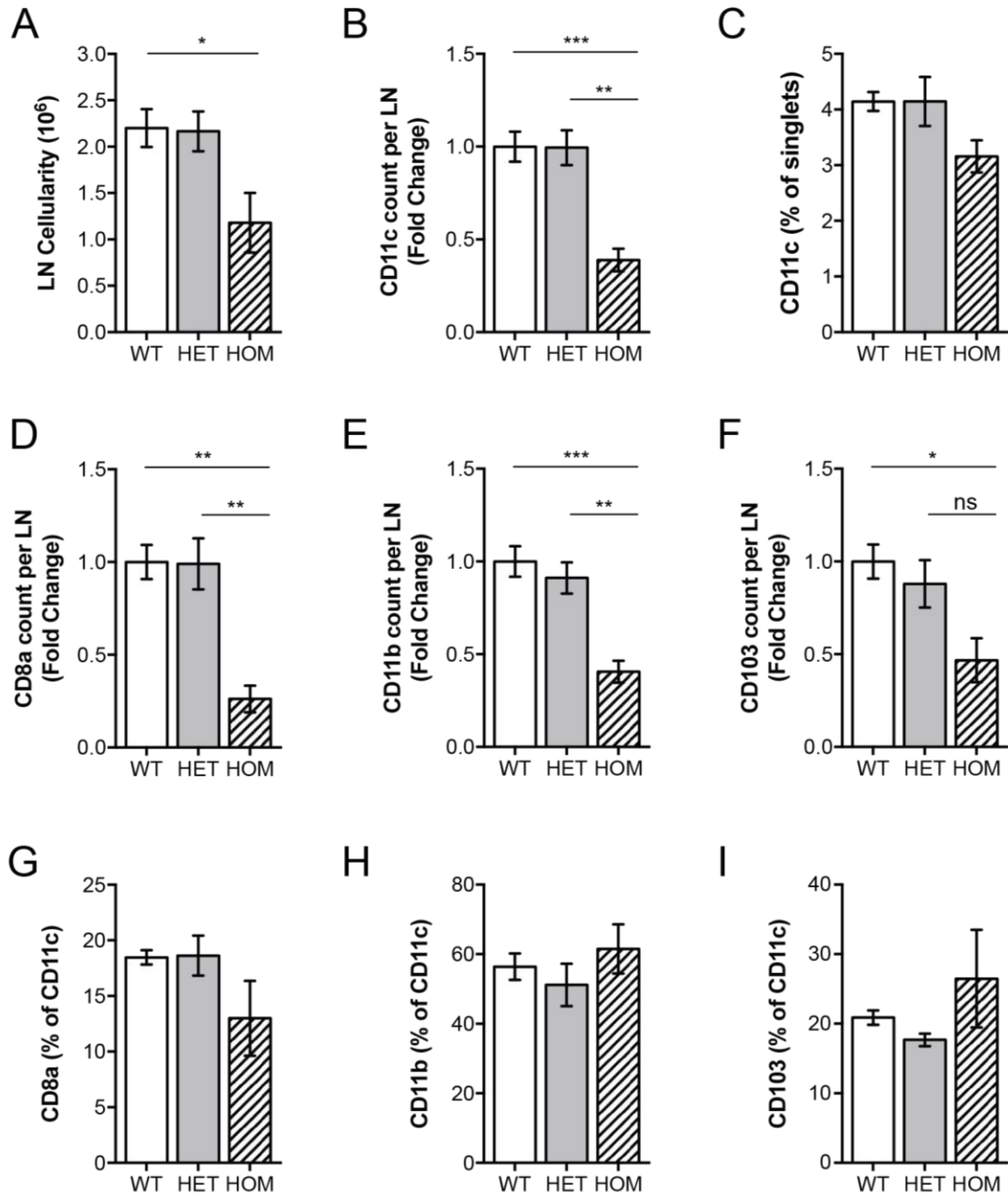


Figure 4.24. Dendritic cell composite and lymph node cellularity is altered in PDPN-FL homozygous mice. NDlns and Day 4 TDLNs Day 4 TDLNs from B16-F10 tumour-bearing PDPN-FL mice. Samples were digested and stained with fluorescently-labelled antibodies for flow cytometry, assessing expression of DC surface markers, CD11c, CD8a, CD11b and CD103. Data shown is total lymph node cellularity (A), total CD11c dendritic cells, as expressed by count fold-change (B) and as a percentage of singlets (C), and CD8a (D,G), CD11b (E,H) and CD103 (F,I) infiltrate as shown by count fold-change. Shown is data from n=2 independent experiments, with n=10 wild-type LNs; n=6 heterozygous LNs; n=4 homozygous LNs. Data presented as mean \pm SEM. Statistical significance was calculated using One-way ANOVA ($P \leq 0.05$). WT: PDPN-FL wild-type; HET: PDPN-FL heterozygous; HOM: PDPN-FL homozygous.

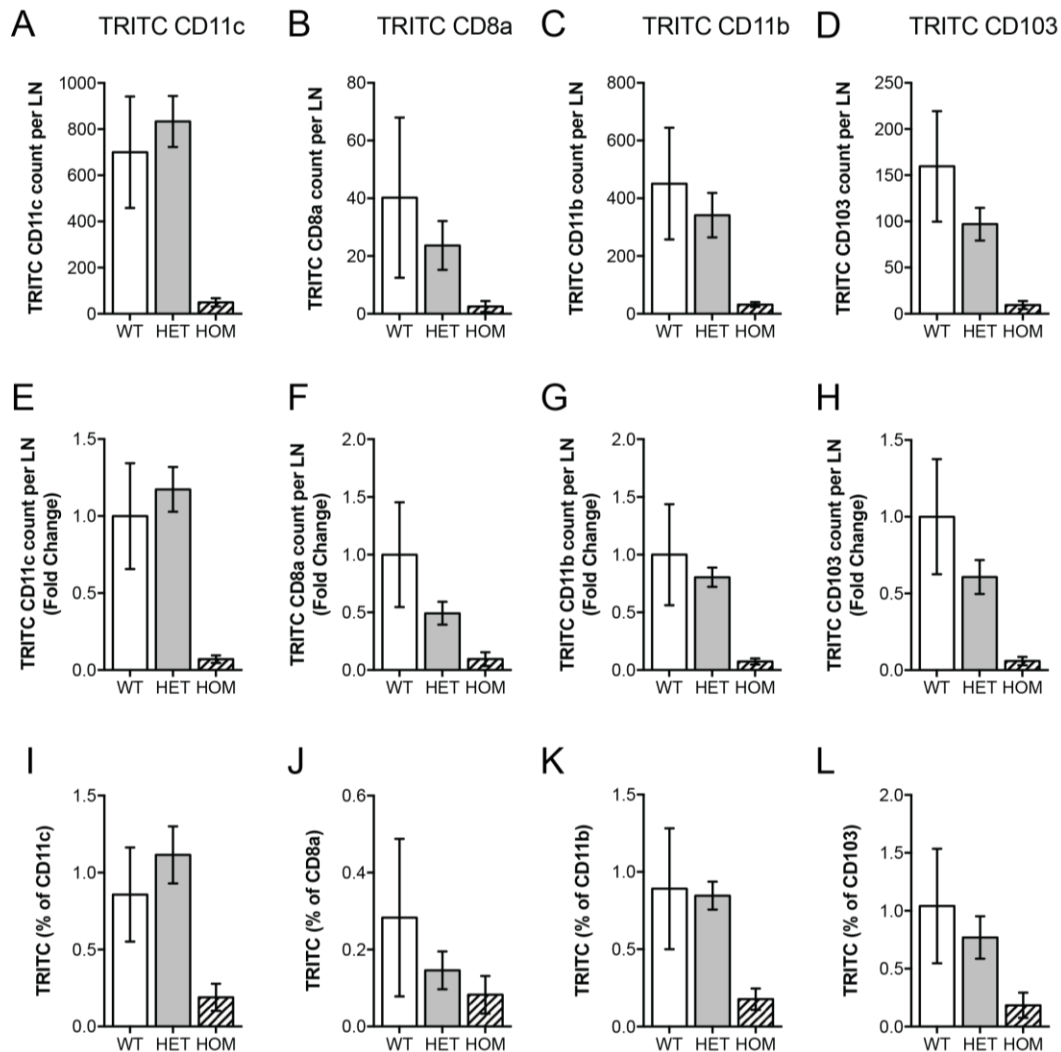


Figure 4.25. Migratory dendritic cell infiltrate is altered in PDPN-FL homozygous mice. NDLNs and Day 4 TDLNs from TRITC painted B16-F10 tumour-bearing PDPN-FL mice. Samples were digested and stained with fluorescently-labelled antibodies for flow cytometry, assessing expression of DC surface markers, CD11c, CD8a, CD11b and CD103. Data shown is TRITC count per lymph node relative to DC subset (A-D), TRITC count fold-change relative to DC subset (E-H) and percentage of TRITC+ cells relative to DC subset (I-L). Shown is data from n=2 independent experiments, with n=10 wild-type LNs; n=6 heterozygous LNs; n=4 homozygous LNs. Data presented as mean \pm SEM. Statistical significance was calculated using One-way ANOVA ($P \leq 0.05$). WT: PDPN-FL wild-type; HET: PDPN-FL heterozygous; HOM: PDPN-FL homozygous.

To determine the levels of Podoplanin expression in LECs across genotypes in LNs and ears, samples were stained with CD45, LYVE-1 and CD31, to allow for gating on CD45- LYVE1+ CD31+ populations (Figure 4.26a). In both LNs and Ears reduced Podoplanin expression was seen in heterozygous samples, with a more dramatic reduction in Podoplanin expression was seen in homozygous samples. In LNs, the

average gMFI of Podoplanin in LYVE1+ CD31+ cells was 312.8 ± 45.9 in wild type LNs, 179.5 ± 40.0 in heterozygous LNs and 100.5 ± 40.5 in homozygous LNs (Figure 4.26b). In comparison to expression of Podoplanin in ears, which was overall much higher than LN expression, the average gMFI of Podoplanin in LYVE1+ CD31+ cells was 9946.4 ± 1452.5 in wild type LNs, 4656.4 ± 948.8 in heterozygous LNs and 8.02 ± 3.07 in homozygous LNs (Figure 4.26b). From these values, it can be concluded that the knockdown of Podoplanin appears more affective in peripheral tissue sites than in lymph nodes.

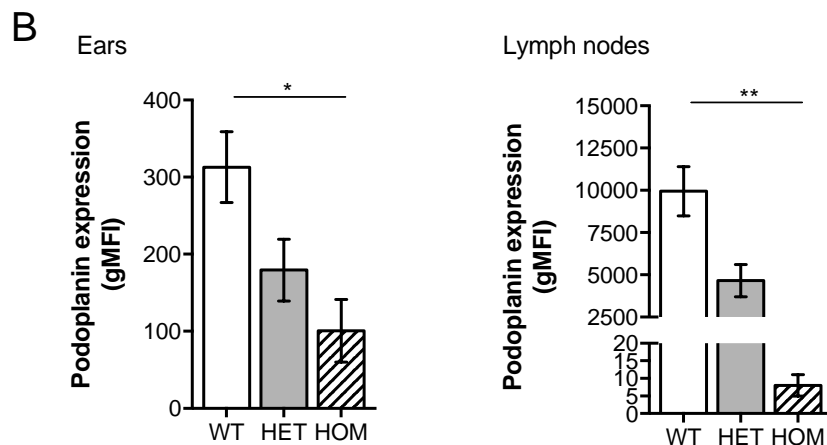
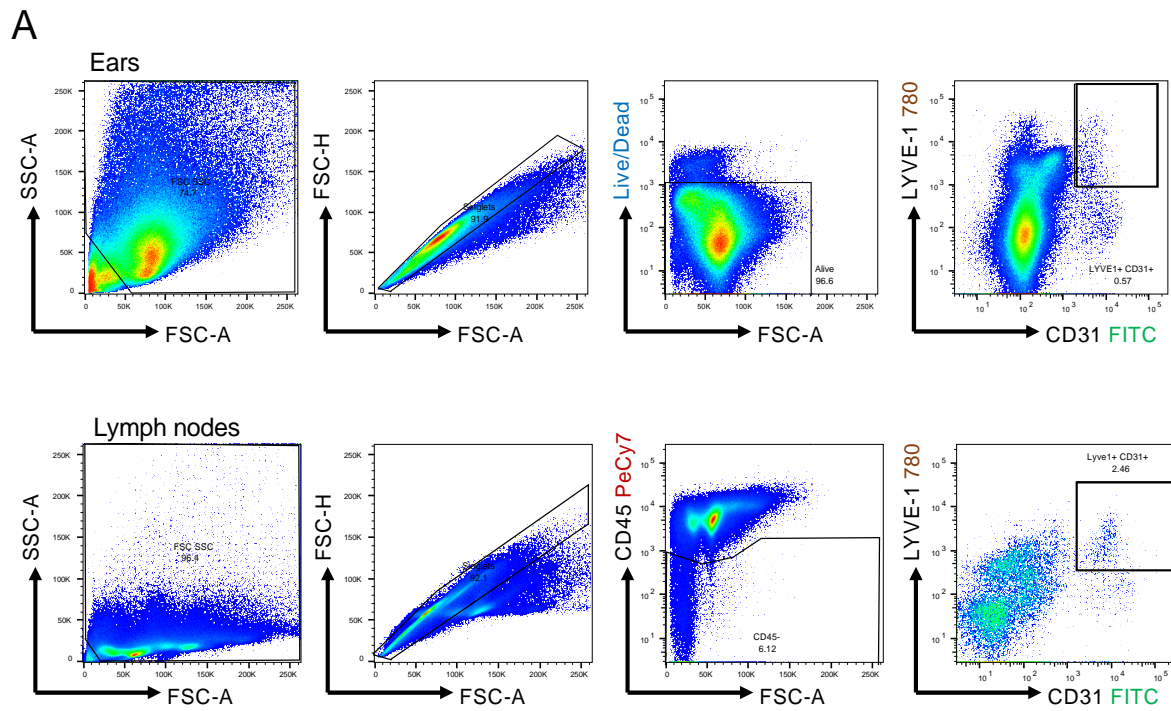


Figure 4.26. Podoplanin expression is perturbed in lymph nodes and ear dermis from heterozygous and homozygous PDPN-FL mice. Using flow cytometry, Tumour-bearing ear dermis (A, top panel) and cervical TDLNs (A, bottom panel) were analysed for Podoplanin expression, assessing the geometric fluorescent intensity in CD45- LYVE1+ CD31+ populations (A,B). Shown is data from $n > 3$ independent experiments with $n = 7$ WT; $n = 11$ HET; $n = 2$ HOM (ears) and $n = 8$ WT; $n = 6$ HET; $n = 3$ HOM (lymph nodes). Data presented as mean \pm SEM. Statistical significance was calculated using One-way ANOVA ($P \leq 0.05$).

4.4. Discussion

Lymphangiogenesis has been shown to promote immune infiltrate at the primary tumour^{188,189}, however little is known of the functional consequences at the TDLN where observations have been limited to the context of well-established tumours rather than at earlier stages of development. We hence set out to determine the functional impact of lymphatics in early TDLNs on immunity, with a specific focus on their role in dendritic cell trafficking.

As particular subsets of migratory dendritic cells have been described to carry tumour antigen, it was pertinent to define the composite of lymph node dendritic cells further. Using gating strategy defined in dendritic cells were subcategorised into CD11c+ CD8a+, CD11c+ CD11b+ and CD11c+ CD103+. The CD11c+ CD8a+ population denotes the lymph node resident dendritic cells, which do not migrate, and hence were expected to be TRITC negative. The CD11c+ CD11b+ population denotes the majority of migratory dendritic cells, with both **epidermal** and **dermal** populations found to express low-to-high levels. Finally, the CD11c+ CD103+ population denotes a subset of migratory **dermal** dendritic cells, which recently were described as critical primers of anti-tumour immunity, carrying melanoma tumour antigen to TDLNs, whereby they directly activate effector T-cells²²¹.

Confocal analysis of early TDLNs found that migratory DCs cluster in lymphatic dense regions and at the subcapsular sinus, with the distance migrated into TDLNs lower than for control NDLNs. This was supported by quantification of the relative distribution of migratory DCs in subcapsular and cortical of the node showing preferential delocalisation of migratory DCs to subcapsular regions in early TDLNs. This analysis suggested that dendritic cells remained closer to the LN periphery, suggesting that migratory dendritic cells were indeed not entering as far into early TDLNs than in control NDLNs. In light of transcriptionally altered lymphatic permeability, this suggests other factors may be influencing migration of DCs, as despite potential enhanced leakiness migratory DCs are being retained at the edge of the node.

As LNs are insufficient for yielding a significant number of LECs to grow up *in vitro*, skin-derived LECs were purchased and used to verify *in vivo* observations. Despite

likely being functionally distinct from LN-derived LECs, *in vitro* assays did mimic *in vivo* observations whereby DCs underwent prolonged interactions with TCM-conditioned LECs, as measured by adhesion, mobility and transwell migration. These *in vitro* assays suggested that the clustering seen at lymphatic-rich subcapsular sinuses in early TDLNs may be governed by changes in the adherent properties of tumour-conditioned lymphatic endothelium. This results in prolonged physical interactions with incoming DCs that need to traverse the sinus to enter the lymph node. We hence describe a novel finding, in lymphatic-driven changes in DC migration behaviour in early TDLNs, that is likely modulated by factors draining from early developing tumours at the primary site. Morphological changes were further suggestive of an anchorage phenotype, implying that conditioning of LECs with TCM promoted physical interactions between LECs and DCs. These *in vitro* findings shed some light on the potential mechanisms underpinning the clustering phenotype *in vivo*, suggesting that migratory DCs physically interact more with lymphatics in early TDLNs which inhibits or delays migration into the node. This data is not the first to describe physical interactions with subcapsular sinus lymphatics upon entry to LNs but is the first to describe perturbed interactions in TDLNs. As these findings are also in early TDLNs, we further propose a potential novel mechanism for altered DC migration at early stages of tumour development. However, as this analysis has been conducted in static states, using section lymph nodes retrieved at a specific time-point, this does not provide any kinetic data. The observation of DCs failing to reach deeper into Day 4 TDLNs, may just be question of timing. There is yet to be any kinetic analysis of DC migration in TDLNs, revealing an area for future work, whereby live tracking of DCs, arriving at TDLNs from different time-points in tumour development, would determine whether migration is perturbed overall or whether kinetic dynamics are altered. The latter could still indeed be of functional significance, as delayed entry and prolonged presence in contact with tumour-conditioned lymphatics at the TDLN sinus may indeed influence DC immunity through further conditioning by LECs of DCs in contact; as is explored in Chapter 5.

In order to derive a molecular mechanism driving this interaction, we explored the microarray gene target list, to identify candidates in early TDLNs. Of the molecules reported to be involved in immune migration, the expression of canonical markers such as ICAM and VCAM were unchanged in Day 4 or Day 11 TDLNs. TCM-treatment of

LECs *in vitro* also failed to up-regulate these markers, suggesting expression of ICAM and VCAM is unresponsive to tumour-derived factors both *in vitro* and *in vivo*, presenting them as unlikely contenders for the altered immune interactions. Podoplanin however emerged as a strong candidate, with RNA and protein expression up-regulated in LECs derived from early TDLNs (Figure 3.14 and 4.14). Considering the newly identified role of Podoplanin as an adhesion molecule for migrating dendritic cells and verified expression changes in Day 4 TDLN-derived LECs, at both RNA and protein levels, we hypothesized that Podoplanin up-regulation is a critical alteration in early TDLNs that could contribute to prolonged dendritic cell interactions with lymphatic stroma. Immunofluorescent imaging also demonstrated DC interaction with Podoplanin positive lymphatics upon entry to lymph nodes, suggesting Podoplanin to be important for incoming immune cells traversing the subcapsular sinus. In some instances, we also saw cup-like structures around TRITC+ dendritic cells, implying Podoplanin may also mediate transmigration across the lymphatic endothelium lining of the node. Literature supported the notion of Podoplanin as a mediator of DC migration, with recent studies demonstrating knockout of Podoplanin and reciprocal CLEC-2 ligand as having an inhibitory effect on lymphatic vessel entry at the periphery and on lymph node migration^{77,237}. Ligation of CLEC-2 has also been reported to drive morphological changes similar to those observed here *in vitro*, with changes in the number of protrusions associated with CLEC-2 engagement. Hence, if DCs were interacting with Podoplanin expressed on the surface of LECs through CLEC-2, such morphological changes are expected. As splenic DCs were shown to express CLEC-2, we concluded that CLEC-2 ligation of Podoplanin was likely to be the mechanism driving enhanced adhesion *in vitro*. B16-derived TCM-induced up-regulation of Podoplanin *in vitro* and DC adhesion to LEC monolayers was impaired following Podoplanin blockade, further supporting a role for Podoplanin in mediating physical interactions between DCs and LECs and a role for tumour-derived factors in regulating that interaction through up-regulation of Podoplanin expression. This further suggests that prolonged exposure to B16-derived factors *in vivo* can indeed modulate Podoplanin expression on TDLN-lymphatics, resulting in altered DC interactions and migration. However, the reduced proportion of CD11c+ DCs expressing CLEC-2 in the lymph node samples suggests lymph node-DCs may not express CLEC-2 to a similar degree. As lymph nodes are predominantly comprised of resident DCs however and the literature alludes to CLEC-2 being a facilitator of migration expressed by mature

DCs, resident DCs are unlikely to express CLEC-2. Furthermore, as the number of migratory DCs in resting lymph nodes makes up a small proportion of the overall population, the level of CLEC-2 detection is expected to be low.

Future work using Podoplanin knock-out LECs *in vitro*, would better determine whether Podoplanin is exclusively required for DC adhesion and prolonged interactions. This would need to be conducted with control treated and TCM treated LECs to investigate whether other cell adhesion molecules contributed to this adhesion phenotype. Alternatively, these experiments could also be conducted using CLEC-2 knockout DCs, as used in the literature with FRC adhesion assays⁷⁷.

To further establish whether this axis and consequent DC migration could be modulated, *in vivo* blockade and genetic models were used. Across both methods of targeting Podoplanin expression, individual experiment repeats exhibited a degree of variation. This was evident particularly in antibody-mediated Podoplanin blockade experiments, whereby upon combining data from repeated experiments, clear trends showing significantly reduced DC migration from initial experiments, could no longer be seen. The high variability in these experiments could be due to variable systemic effects of the antibody, as Podoplanin is expressed by other cell types, such as fibroblasts. Variability was particularly seen in flow cytometry experiments, with no significant changes observed in the number of infiltrating TRITC+ DCs in NDlns and TDLNs across time-points and DC subsets when comparing LNs from control treated to anti-Podoplanin treated mice. Despite this, immunofluorescent imaging of TDLNs derived from mice receiving Podoplanin blockade treatment suggested an overall decrease in migratory DCs reaching nodes, with some clustering at the lymphatic sinus still observed.

Of interest in these blockade experiments was the significant increase in the LN cellularity in Day 4 TDLNs treated with anti-PDPN, which could be masking accurate quantification of the number of DCs migrated into TDLNs. This phenomenon was previously described in resting LNs in relation to Podoplanin engagement in LN-FRCs, whereby administration of anti-PDPN blockade antibody resulted in LN expansion²³⁵. The study described a mechanism by which Podoplanin induced RhoA-dependent FRC stretching, caused by physical interactions with CLEC-2 expressing DCs²³⁵. This

study contributed to the mechanistic understanding of LN expansion in adaptive immunity and supports this work by confirming that CLEC-2 expressing DCs can and do interact with Podoplanin expressing stromal cells in LNs. As the aforementioned study demonstrated that the same DCs which initiate immunity through T-cell priming, also initiate LN remodelling, future work should look in more detail at the functional implications of active or perturbed Podoplanin-CLEC2 signalling between DCs and LECs in TDLNs, focusing on overall LN reorganisation and implications for tumour progression and LN metastasis.

As antibody blockade delivered such variable results across independent experiments using the shoulder injectable model and artificially expanded TDLNs, the Podoplanin-flox mouse model was used in conjunction with a site-administration change from the shoulder to lymphatic-rich ear dermis. Control mice homozygous for Podoplanin knockout demonstrated clear ablation of protein expression in lymphatic-rich ear dermis, visualised using immunofluorescent imaging. This was supported by flow cytometry assessment of protein expression, showing that both in ear dermis and downstream cervical lymph nodes, protein expression was significantly reduced in LECs from both sites. Using this model, flow cytometry data provided evidence that migration into TDLNs was significantly reduced only in homozygous knockout tumour-bearing mice, with dramatic reductions in TRITC+ DC infiltrate detected in cervical TDLNs from early ear tumours. This is in line with published work showing lymphatic-specific knockout of Podoplanin substantially decreases migration of peripheral DCs to local draining lymph nodes in resting conditions²³⁷, and that it perturbs DC capacity to engage Podoplanin on peripheral lymphatic vessels; hence preventing entry⁷⁷. Despite reduced levels of LN cellularity, which could explain to a degree the decrease in TRITC detection in early TDLNs, the levels to which lymph node cellularity was altered, is unlikely to account for the almost complete ablation of TRITC+ infiltrate. Hence, as lymphatic vasculature was visibly intact and other markers such as LYVE-1, which facilitates DC migration, were unaffected by knockout; we can conclude from this data that Podoplanin does indeed facilitate DC migration in the tumour microenvironment. Future experiments should utilise lymphatic specific knockdown models, under promoters such as PROX-1 or LYVE-1, which would enable LEC specific knockdown without affecting global vasculature changes and lymph node architecture.

Interpreting the results here in conjugation with the aforementioned literature, it is possible that disrupted DC migration in our homozygous knockout mice may be partly due to peripheral Podoplanin knockout. Further investigation is hence needed, to define peripheral interactions with lymphatics at the primary tumour site to elucidate the role of Podoplanin beyond the TDLN and analysis of matched ears from these samples would provide insight into whether migratory DCs were incapable of entering peripheral lymphatics of homozygous mice. Despite the non-specific targeting of Podoplanin in these *in vivo* models, our data is the first to translate the functional role of the Podoplanin-CLEC2 axis in DC trafficking in a tumour setting, suggesting this axis to be critical for DC migration in the tumour microenvironment, as well as resting and inflammatory states. Furthermore, as the number of viable heterozygous and homozygous mice that survived per litter as low, these experiments were not conducted in control settings. Hence, these experiments hence need to be repeated in lymphatic-specific Podoplanin knock-out mice in control and tumour-bearing conditions, with a robust number of mice from wild-type, heterozygous and homozygous backgrounds to verify DC migratory patterns in all biological contexts. This would also provide insight into whether patterns of perturbed DC migration in Podoplanin-knockout mice is dependent on a tumour state or occurs generally in resting states also. Finally, these experiments would also provide an opportunity to see whether Podoplanin is a major player in DC migration, or whether chemokines, such as CCL21, and molecules, such as CCRL1, are the primary governors of DC migration. As Podoplanin would be knocked out in these experiments, any perturbations to expression of other factors, would highlight their importance in DC migration, independent of Podoplanin expression.

Another critical aspect explored in these experiments is the implication for subset-specific DC trafficking. In both B16-F10 and *Braf*^{V600E}/*Pten* melanoma models, CD103+ dermal DCs at the primary tumour site have been described to be the dominant migratory subpopulation carrying tumour antigen to TDLNs, with CD103+ DCs further found to induce anti-tumoural T-cell responses²²¹. Expansion of this subset was further found to enhance efficacy of checkpoint therapies with anti-PD-L1²²¹. In our model, the infiltration of migratory CD11b and CD103 dermal DCs was increased in early TDLNs in terms of total count, which also manifested as an overall increase in the percentage of total migratory DCs. Although not significant, these

findings suggest that indeed in early TDLNs, dermal DCs are responding to the developing tumour through enhanced trafficking to TDLNs. In terms of the effect of Podoplanin on these trends, little affect could be seen through blockade treatments. However, in homozygous knockout mice, the number of migratory DCs detected in early TDLNs was ablated. As described above, this could be due to poor entry of DCs at the primary site, rather than a specific role of Podoplanin at the sinus of TDLNs and could also be driven by overall reduced nodal cellularity and defective lymph node architecture, as is seen in global Podoplanin knockout mice.

To hence specifically determine the influence of Podoplanin on subset specific migration, DCs derived from reporter mice with GFP expressed under CD11b or CD103 promoters could be injected into wild-type mice to assess whether these subsets preferentially interact with lymphatic expressed Podoplanin. This would also need to be conducted in conjunction with lymphatic specific Podoplanin knockout mice on a tumour background to elucidate the role of lymphatic Podoplanin on dermal DC trafficking in the tumour microenvironment.

In summary, these findings act as an evidence base for Podoplanin mediated DC trafficking in basal settings as well as the tumour microenvironment. We further show that current *in vivo* models are insufficient to adequately assess the relative contribution of Podoplanin in DC migration in TDLNs, with lymphatic specific knockout models needed. We do however demonstrate that DCs in early stages of tumour development are mobilised and furthermore that their route is heavily reliant on lymphatics. We show lymphatics in the tumour microenvironment are conditioned by factors derived from the tumour microenvironment with implications for DC trafficking in early TDLNs and hence propose lymphatics as critical regulators of DC-mediated immunity in the early developing tumour. As therapies utilising DC vaccines to promote anti-tumour immunity assume efficient trafficking to TDLNs, we propose the role of non-immune stroma, in particular lymphatics, must be considered in conjunction. A deeper mechanistic and kinetic understanding of DC trafficking and their interactions with other stromal cells in the tumour microenvironment is hence needed to improve DC-based therapies.

CHAPTER 5

RESULTS

5. Determining the role of lymphatic-DC cross-talk in T-cell priming in TDLNs

5.1. Introduction

The process of DC-mediated T-cell priming is complex. For a dendritic cell to initiate an appropriate T-cell response, it must be mature and activated, characterised through expression of CD40, CD80, CD86 and MHC-II. They must also express an array of cytokines permissive of T-cell responsiveness, such as IL-12 which promotes T-cell expansion and cytokines such as IL-4, IL-6, IL-10 and TGF- β , which determine the differentiation of naïve T-cells. To prime effective antigen-specific T-cell responses, antigen must be taken up, processed correctly and presented on MHC Class-I and Class-II to CD8+ and CD4+ T-cells respectively. Concurrent interaction of T-cell expressed CD28 with DC-expressed molecules, CD80 and CD86, drives a co-stimulatory signal that sustains T-cell activation. With specific regard to migratory DCs and their role in T-cell priming in lymph nodes, their location within the node is also critical to successfully mounting an immune response. Upon arrival, DCs must traverse the subcapsular sinus and travel along FRC conduits to reach T-cell zones in the lymph node cortex. This is heavily dependent on the correct chemotactic cues and molecular facilitators of migration, such as CLEC-2 expression⁷⁷. There hence exists a biological “tool-box” for T-cell priming, with dendritic cells needing molecular tools to physically reach T-cells and uptake, process and present antigen, which all effectively mount an antigen-specific T-cell response.

In the context of cancer, the anti-tumour immune response is understood to be disrupted, leading to poor recognition and clearance of tumour cells. Immune tolerance in the melanoma tumour microenvironment is known to be driven by immunosuppressive molecules, namely PD-L1 and CTLA-4 expressed on tumour, immune and stromal cells¹⁷³. PD-L1 induces T-cell exhaustion and apoptosis through ligation of receptor PD-1¹⁶⁷, and CTLA-4 out-competes CD28 for ligation of CD80 and CD86¹⁶⁸, acting as a negative regulatory molecule for T-cells. The over-representation of these molecules in melanoma^{158,173,285} has led to a flurry of recent clinicals, with much success achieved with the anti-CTLA4 drug, Ipilimumab, and anti-PD-1 drug, Nivolumab, in late stage melanoma patients^{286,287,288}. Other molecules

such as tryptophan enzyme, IDO^{158,159,175} and cytokine, TGF β ^{171,172,176}, also promote T-cell deletion and the expansion of regulatory T-cells in the melanoma tumour microenvironment, demonstrating the complexity of mechanisms involved in establishing and maintaining immune tolerance in the tumour microenvironment.

Much of this research however, has been conducted in late stages of tumour development and human disease, with little knowledge of how pro-tumour immune tolerance develops in early stages of the disease. In recent years, lymphatic endothelial cells have been identified as novel regulators of immunity and dendritic cell function^{105,106,107,16,114,118,122} in basal and inflammatory conditions. As we have shown in previous chapters that lymphatics are transcriptionally altered in early TDLNs (Chapter 3) and exhibit altered physical interactions with tumour-derived migratory DCs, we sought to determine whether these early lymphatic changes could have other immune consequences in the context of T-cell priming and responses. As there is still a paucity of research in the context of the dynamics of lymphatic-mediated immunity in TDLNs of early disease, this is a novel line of investigation and will shed light on our understanding of anti-tumour immunity in early stages of disease.

5.2. Methods

5.2.1. *In vitro* antigen transfer assays

For assessment of antigen transfer from LECs to DCs, an *in vitro* antigen transfer assay was developed. As described in Section 2.10, LECs pulsed with OVA antigen and co-cultured with splenic GFP⁺ CD11c⁺ DCs. After 1 hour of co-culture, non-adherent DCs in the media and adherent DCs and LECs were processed for flow cytometry. To establish uptake of OVA by DCs cultured alone, bulk DCs were seeded at a density of 5×10^5 in the presence or absence of fluorescent conjugated OVA (100 μ g/ml), in round-bottom 96-well plates. DCs were incubated with OVA at 37°C for 15 minutes. Samples were stained with PeCy7-conjugated anti-CD11c (1:300) at 4°C for 20 minutes, to allow OVA uptake to be quantified specifically in GFP⁺ CD11c⁺ DCs using flow cytometry. The percentage of OVA⁺ DCs within GFP⁺ CD11c⁺ populations and the geometric mean fluorescent intensity of 647-OVA was calculated offline using FlowJo® software. The protocol for antigen pulsing lymphatic endothelial cells followed a protocol optimised by colleague Dr. Matt Lakins¹⁷³. When establishing the ratio of DCs to LECs, the ratio used for adhesion assays was used, as stated in Section 2.10.4. In previous adherence assays, 1hr co-culture durations were used, and to ensure this was sufficient duration for any antigen transfer, 1hrs and 2hr incubations were trialed during assay optimisation, as shown in Appendix 10.

5.2.2. *In vitro* T-cell proliferation assays

To measure T-cell priming by lymphatic conditioned DCs, OT-1 T-cells were used for *in vitro* proliferation assays. Assays were set-up as stated in Section 2.10.6, with DCs co-cultured with OVA-pulsed LECs before being transferred to co-cultures with T-cells. Co-cultures were incubated at 37°C for 72 hours in round-bottom 96-well plates before centrifugation at 2000rpm for 1 minute. Samples were then stained with Live/dead violet at 4°C for 10 minutes, followed by primary antibodies; BV780-conjugated anti-CD8a and biotin-anti-PD1 (followed by APC-Cy7-conjugated streptavidin) at 4°C for 20 minutes. As OT-1 T-cells were stained with CFSE prior to co-culture, proliferated T-cells were detected using flow cytometry. The percentage of proliferated cells within

total viable CD8a+ T-cells, the percentage of viable cells within total CD8a+ T-cells and percentage expression of death ligand receptor, PD1, was calculated offline using FlowJo® software. The protocol for T-cell co-culture with antigen-presenting cells and CFSE staining followed a protocol optimised by colleague Dr. Matt Lakins¹⁷³. The ratio of DCs:Tcells (1:10) was informed by literature.

5.2.3. *In vivo lymphatic endothelial cell antigen assays*

For assessment of antigen uptake and processing *in vivo*, FITC-OVA and DQ-OVA were injected subcutaneously in control and tumour-bearing mice as outlined in Section 2.10, with an explanation of how these OVA conjugates work in Section 2.10.2. Brachial LNs from control and tumour-bearing mice injected with FITC-OVA were processed for immunofluorescent imaging to observe localisation of OVA. In addition, LNs were retrieved for flow cytometry analysis for more detailed analysis of OVA uptake and DQ-OVA processing across lymph node compartments.

For immunofluorescent imaging of OVA localisation, control NDNLs and Day 4 TDLNs were isolated and prepared as per methods in Section 2.9. Sections were stained with primary rabbit anti-LYVE1 at 4°C overnight, followed by secondary staining with 594-conjugated donkey anti-rabbit at room temperature for 1 hour. FITC-OVA positive cells were detected using the 488nm laser. Whole lymph node tile scans and images of regions of interest were taken as per Section 2.9. Details of all antibodies used can be found in Table 2.11.

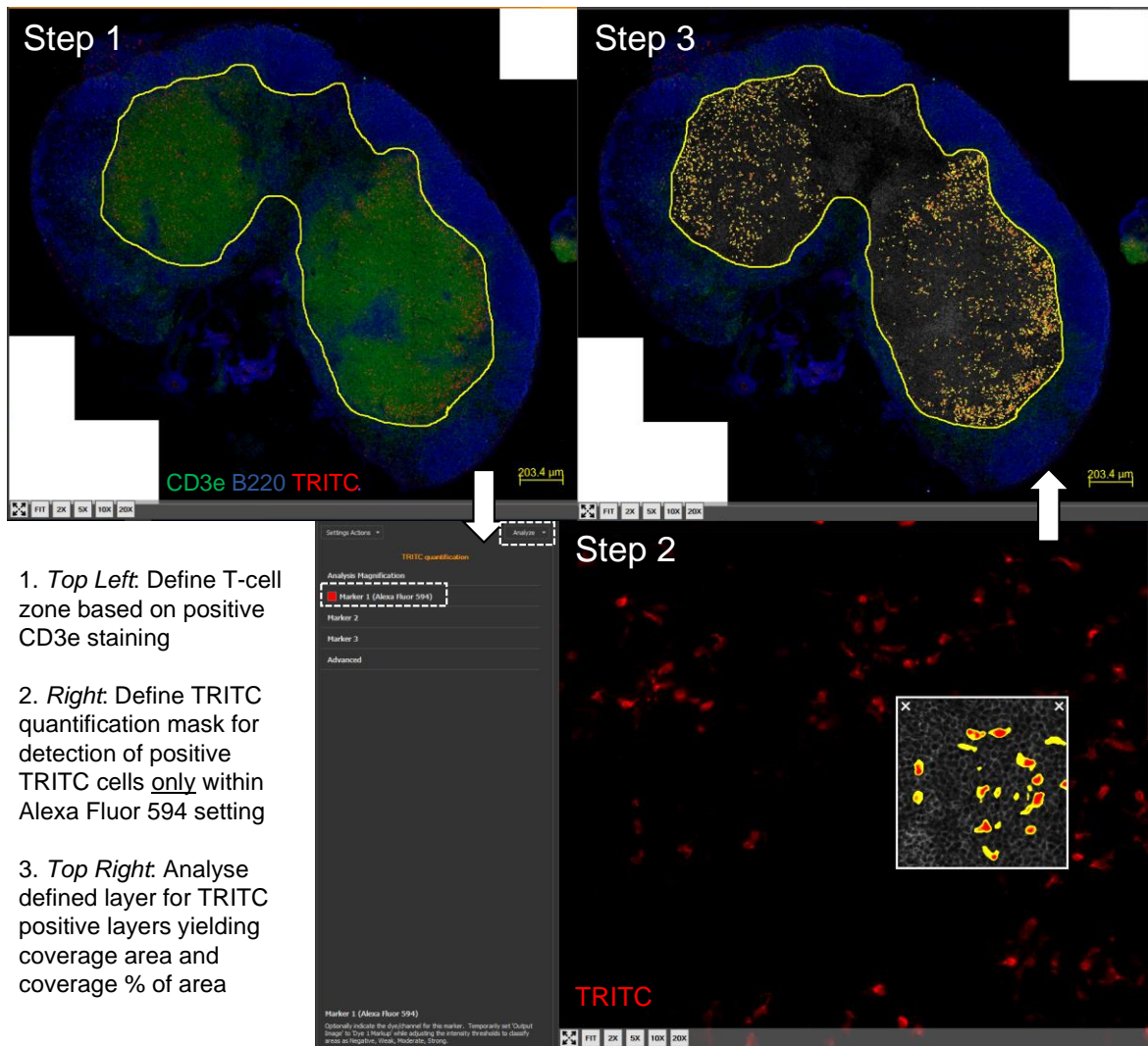
For flow cytometry analysis of FITC-OVA uptake and DQ-OVA processing, control NDNLs and Day 4 TDLNs were isolated and digested as per methods described in Section 2.2. To assess distribution of FITC-OVA and DQ-OVA across lymph node compartments, samples were stained with 450-conjugated anti-CD11c, PeCy7-conjugated anti-CD31, APC-conjugated anti-Podoplanin and APC-Cy7-conjugated anti-CD45 at 4°C for 30 minutes. This identified both dendritic cell and non-immune stromal cell uptake of FITC-OVA and relative DQ-OVA processing capacity. Details of all antibodies used can be found in Table 2.10.

5.2.4. In vivo antigen transfer assays

As described above in Section 5.2.3, mice were injected with DQ-OVA. To assess whether incoming dendritic cell populations processed lymph node derived antigen, control and tumour-bearing mice injected with DQ-OVA, were also painted with TRITC. This was carried out as per methods described in Section 2.3 DQ-OVA was injected in the front leg to ensure rapid delivery of OVA to draining brachial lymph nodes, followed by TRITC painting. As for DQ-OVA assays conducted without TRITC painting, lymph nodes were digested and processed for flow cytometry as described in Section 2.8 and stained with 450-conjugated anti-CD11c, PeCy7-conjugated anti-CD31, APC-conjugated anti-Podoplanin and APC-Cy7-conjugated anti-CD45. TRITC was detected using the 561nm laser. The percentage of total DQ-OVA+ cells and the geometric mean fluorescent intensity of DQ-OVA, within TRITC+ populations, was calculated offline using FlowJo® software. Details of all antibodies used can be found in Table 2.10.

5.2.5. In vivo imaging of T-cell zone localisation of migratory dendritic cells

To visualise localisation of migratory dendritic cells relative to T-cells, control NDNLNs and early Day 4 TDLNs were TRITC painted, as described in Section 2.3 LNs were processed for histology as described in Section 2.9 and sections were then stained with Syrian Hamster anti-CD3e and Rat anti-B220 at 4°C overnight, followed by incubation with 488-anti-Syrian Hamster and 405-anti-Rat secondary antibodies at room temperature for 1 hour. Whole lymph node images were taken in accordance to Section 2.9, obtaining 20x tile scan images of regions of interest within T-cell and B-cell zones. For manual review of each tile scan image, Zen image analysis software was used. For quantitative image analysis of TRITC coverage within T-cell zones, HALO™ software (PerkinElmer, USA) was used. Using CD3e positive staining that stains T-cells, T-cell zones were defined, and a mask created to detect TRITC positive regions within that defined area (Figure 5.1). TRITC coverage was defined as both total area coverage (μm^2) and percentage coverage of total area. Details of all antibodies used can be found in Table 2.11.



1. *Top Left*: Define T-cell zone based on positive CD3e staining

2. *Right*: Define TRITC quantification mask for detection of positive TRITC cells only within Alexa Fluor 594 setting

3. *Top Right*: Analyse defined layer for TRITC positive layers yielding coverage area and coverage % of area

Figure 5.1. Method of TRITC quantification within T-cell zones. Using HALO™ image analysis software whole lymph node tile scans were uploaded and T-cell zones defined using the hand-draw tool and CD3e positive staining (1). Then parameters for the TRITC detection mask were defined and could be edited by clicking the Marker 1 Alexa Fluor 594 (large white dashed box). A region of interest box then appeared overlaid on the section (white box) showing which cells are being detected as TRITC positive. Outlines of TRITC negative cells were defined in grey, allowing for clear distinction of positively stained cells (2). Once parameters of detection were defined, the TRITC detection mask was applied to the defined T-cell zone by clicking “Analyse” in the top left corner of the screen (small white dashed box). All TRITC positive cells within the T-cell zone are detected (3).

5.2.6. *In vivo* characterisation of stromal and immune cells in TDLNs

Migratory DCs were profiled using the PCR Profiler Array, as described in Section 2.7. The PD1-PDL1 axis was also quantified in early TDLNs. Lymph nodes were retrieved from control and tumour-bearing C57BL/6 mice and processed for flow cytometry as per methods described in Section 2.8. For characterisation of PD-L1 expression, single cells suspensions were stained with 450-conjugated anti-CD11c, APC-conjugated anti-MHCII, Biotin-conjugated anti-PDL1 and APC-Cy7-conjugated anti-CD45, to identify expression on dendritic cells. For non-immune stromal cells, single cell suspensions were stained with FITC-conjugated anti-CD31, PeCy7-conjugated anti-PDL1, APC-conjugated anti-Podoplanin and APC-Cy7-conjugated anti-CD45, identifying PD-L1 expression in FRCs, BECs and LECs. For measurement of PD1 expression, T-cells were stained with 488-conjugated anti-CD4, 421-conjugated anti-CD8a, PeCy7-conjugated anti-PD1 and APC-Cy7-conjugated anti-CD25. Single cell lymph node suspensions were stained with the above antibodies at a dilution of 1:300 at 4°C for 30 minutes, followed by incubation with streptavidin anti-biotin secondary antibodies at 4°C for 30 minutes. In addition, trends in FoxP3 positive Tregs was determined by staining single cell suspensions with 647-conjugated anti-FoxP3. Details of all antibodies used can be found in Table 2.10.

5.3. Results

5.3.1. Migratory DCs are differentially localised in cortical regions of early TDLNs

As introduced previously, effective T-cell priming relies on APCs reaching the T-cell zone in LNs to enable interactions between antigen-bearing APCs and T-cells. The dynamics of T-cell interactions with migratory DCs in early TDLNs is however relatively unknown, thus the TRITC model was used to determine where in early TDLNs, migratory DCs localised to. In Chapter 4 we showed that migratory TRITC DCs cluster within the subscapular sinus and fail to migrate as far into early TDLNs as in NDLNs (Figure 4.3) leading to the hypothesis that prolonged interactions with lymphatics at the sinus may perturb access to the T-cell zone. We therefore aimed to determine the specific localisation of migratory TRITC DCs in relation to T-cell zones, using confocal microscopy to map localisation. Upon assessment of migratory DC localisation, TRITC positive DCs could be seen across T-cell zones in resting NDLNs (Figure 5.2a). In Day 4 TDLNs, TRITC positive DCs could also be seen in T-cell zones, however quantification of coverage of migrated DCs in T-cell zones, revealed markedly reduced DC content both by area and percentage, despite consistent total areas of T-cell zones (Figure 5.2b). The total area of the T-cell zones in both Control NDLNs and Day 4 TDLNs averaged $1.81 \times 10^6 \mu\text{m}^2 \pm 0.25$ and $1.80 \times 10^6 \mu\text{m}^2 \pm 0.21$, respectively. TRITC coverage however was dramatically reduced although not significant with TRITC DCs covering an average of $0.87 \times 10^5 \mu\text{m}^2 \pm 0.31$ and $0.36 \times 10^5 \mu\text{m}^2 \pm 0.11$ of T-cell zones in Control NDLNs and Day 4 TDLNs, respectively. In terms of percentage, this calculated to be an average fold-change of 0.36, meaning an overall decrease in the percentage coverage of TRITC DCs in T-cell zones. A potential reason for this lies in the observed clustering of migratory DCs at the base of B-cell follicles at the Tcell-Bcell margin and in surrounding subcapsular sinuses in Day 4 TDLNs (Figures 5.3 and 5.4). Findings reported by colleagues, demonstrate immune cells cluster in similar localities in Day 11 TDLNs, which transpired to be HEV regions, as confirmed by positive peripheral lymph node addressin (PNAd) expression¹⁹¹. These results appear to support this, although PNAd staining in conjunction with TRITC would be needed to confirm.

Collectively this demonstrates that TRITC-carrying migrated DCs that do reach the T cell zone of early TDLNs localise differently in comparison to resting NDLNs. The

functional relevance of altered and reduced coverage is not clear, but further investigation into the dynamics of contacts made between T-cells and migratory DCs that reach T-cell zones, in early TDLNs, would provide critical insight into the functional implications of this observation. Also, investigation into the kinetics of DC migration in TDLNs would shed light on the functional significance of prolonged interactions with lymphatics at the TDLN subcapsular sinus.

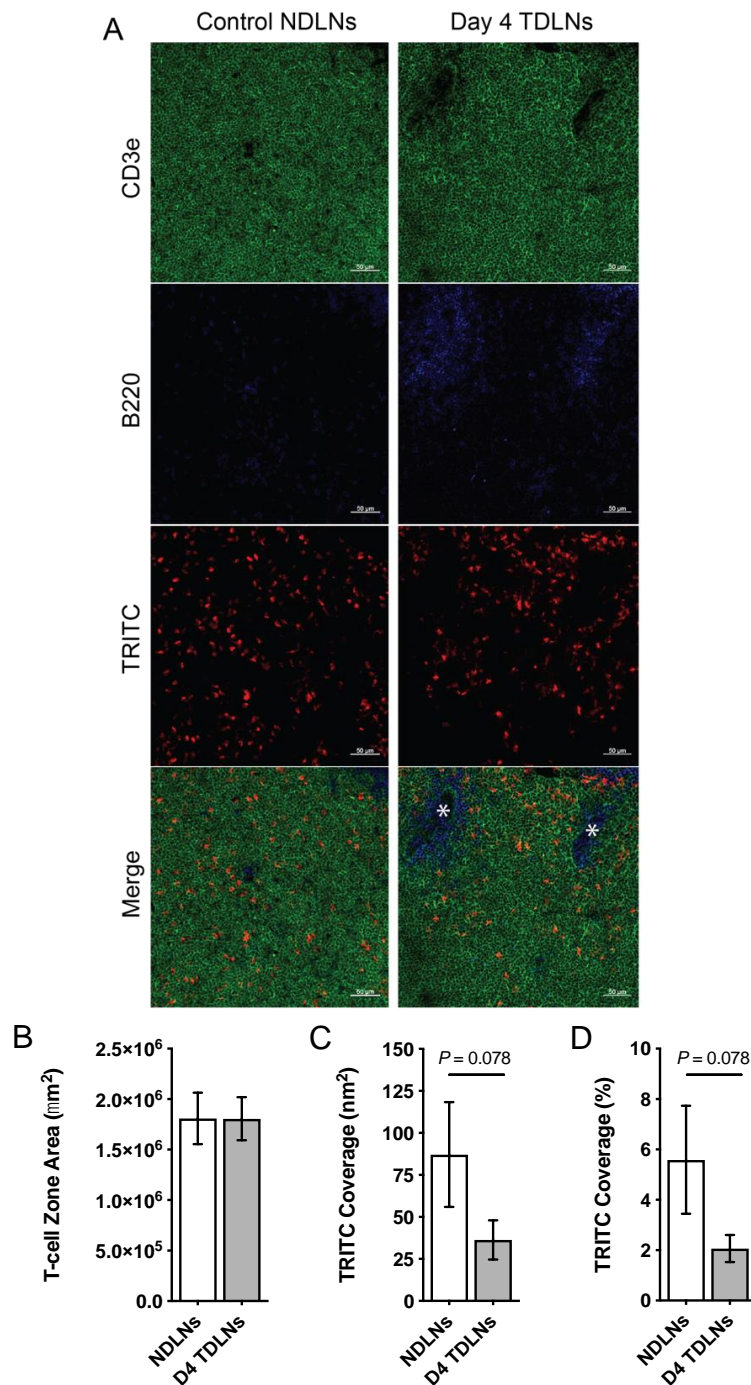


Figure 5.2. Migratory DCs are delocalised in T-cell zones of Day 4 TDLNs. Control NDLNs and Day 4 TDLNs from TRITC painted B16-F10 tumour-bearing mice were immunofluorescently stained with CD3e (green) and B220 (blue) with periphery-derived migratory dendritic cells marked with TRITC (red). Whole lymph node tile scans were taken at 20x magnification using confocal microscopy. Images shown are representative regions of interest, demonstrating TRITC+ DCs in T-cell zones in control NDLNs (A, left panel) vs Day 4 TDLNs (A, right panel), with infiltrating B-cells identified (*). Scale bars are representative of 50µm (A). Whole lymph node images were analysed offline using HALO™ software, with quantification of the area of T-cell zones (B), total TRITC coverage (C) and TRITC coverage as a percentage of the whole lymph node area (D). Data shown is representative of n=4 independent experiments, with n=6 NDLNs and n=11 Day 4 TDLNs. Data presented as mean ± SEM. Statistical significance was calculated using the Mann-Whitney test, with *P* ≤ 0.05.

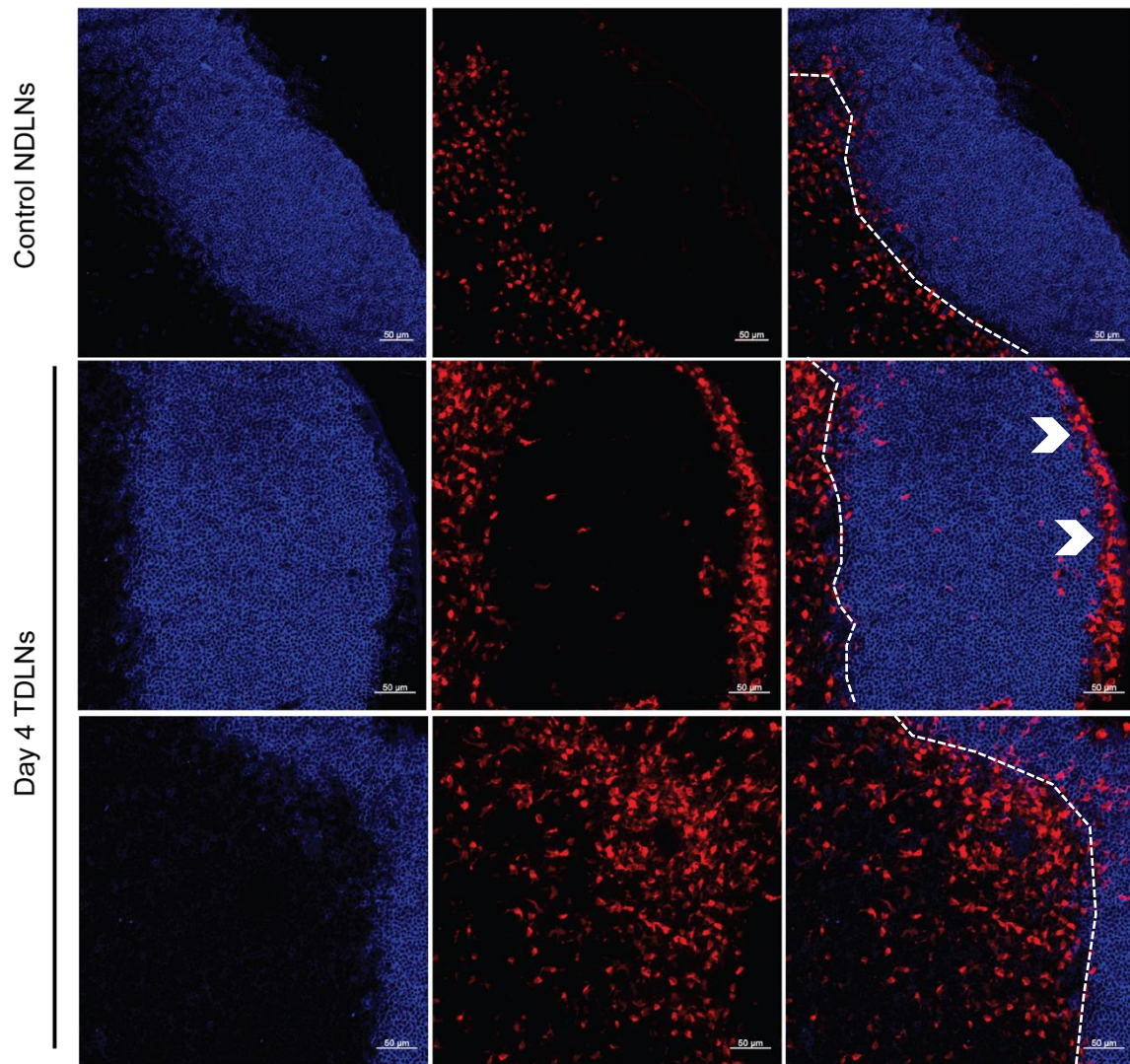


Figure 5.3. Migratory DCs are clustered around B-cell follicles in Day 4 TDLNs. Control NDLNs and Day 4 TDLNs from TRITC painted B16-F10 tumour-bearing mice were immunofluorescently stained with B220 (blue) with periphery-derived migratory dendritic cells marked with TRITC (red). Whole lymph node tile scans were taken at 20x magnification using confocal microscopy. Images shown are representative regions of interest, demonstrating TRITC+ DCs clustered around B-cell follicles, at the edge of B-cell follicles (dotted line) and in the surrounding subcapsular sinus (arrowheads). Data shown is representative of n=4 independent experiments, with n=6 NDLNs and n=11 Day 4 TDLNs.

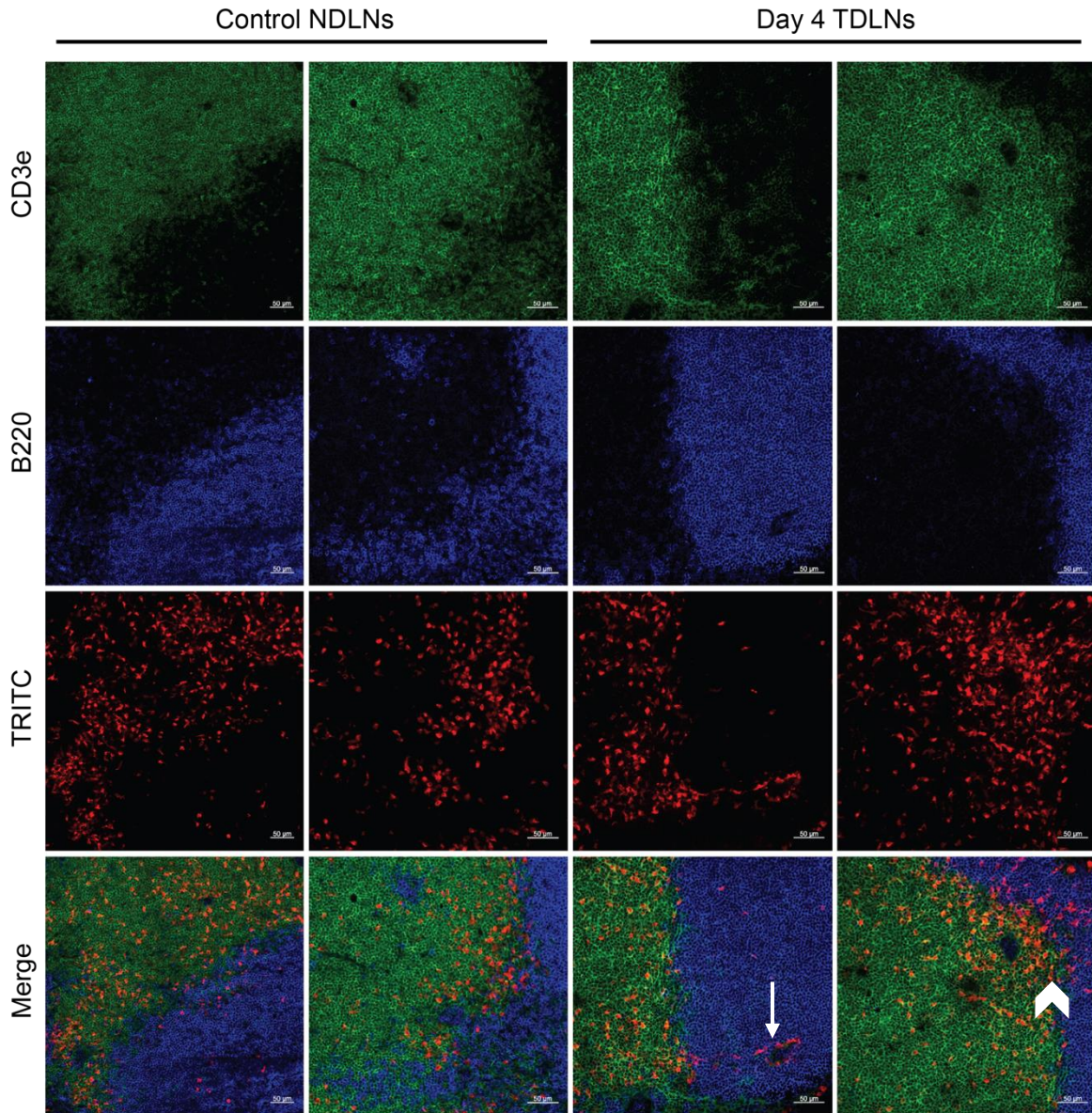


Figure 5.4. Migratory DCs are clustered at the Tcell-Bcell margins of Day 4 TDLNs. Control NDNLs and Day 4 TDLNs from TRITC painted B16-F10 tumour-bearing mice were immunofluorescently stained with CD3e (green) and B220 (blue) with periphery-derived migratory dendritic cells marked with TRITC (red). Whole lymph node tile scans were taken at 20x magnification using confocal microscopy. Images shown are representative regions of interest, demonstrating TRITC+ DCs clustered at Tcell-Bcell margins in Day 4 TDLNs (arrowheads) with some TRITC+ DCs infiltrating B-cell follicles (arrow). Scale bars are representative of 50µm (A). Data shown is representative of n=4 independent experiments, with n=6 NDNLs and n=11 Day 4 TDLNs.

5.3.2. LECs uptake and process soluble antigen *in vitro*

Having demonstrated that migratory DCs are differentially localised within T-cell zones in early TDLNs following prolonged physical interactions with LECs, we next investigated whether the said prolonged interactions with LECs were able to condition migrated DCs. As studies have shown the capacity for LECs to present antigen both *in vitro* and *in vivo*^{118,123,121,122,188}, we examined whether TDLN-LECs could use antigen scavenged to directly influence DC function. Specifically, we focussed on the concept of antigen transfer to incoming migratory DCs and potential to affect T-cell priming in TDLNs.

We first confirmed that LECs *in vitro* could indeed uptake antigen. LECs incubated in the same concentration of fluorescently conjugated OVA planned for co-culture experiments (100µg/ml), had scavenged antigen within 15 minutes (Figure 5.5a,b). On average, 89.3% ± 2.33% of total LECs per sample had taken-up OVA (Figure 5.5a,b), with an average gMFI of 12979.6 ± 4413.5 (Figure 5.5a,c).

The use of DQ-OVA confirmed that LECs could rapidly process engulfed antigen; proteolytic cleavage was detected by fluorescent signal within 15 minutes of *in vitro* (Figure 5.5d, e). In control conditions, DQ-OVA gMFI increased 2-fold from an average of 631.2 ± 145.4 at 15 minutes to an average of 1275.5 ± 47.5 at 60 minutes (Figure 5.5e). DQ-OVA gMFI did not significantly increase between 60 minutes and 75 minutes, indicating that the rate of processing plateaus after 60 minutes, potentially due to saturation. To simulate TDLN conditions, assays were also performed in TCM-conditioned LECs. Since proteasomal signatures in late TDLN-derived LECs were up-regulated, we hypothesised that antigen processing may be enhanced in the presence of TCM, however no change capacity to process engulfed antigen could be seen in the time-points examined *in vitro* (Figure 5.5e).

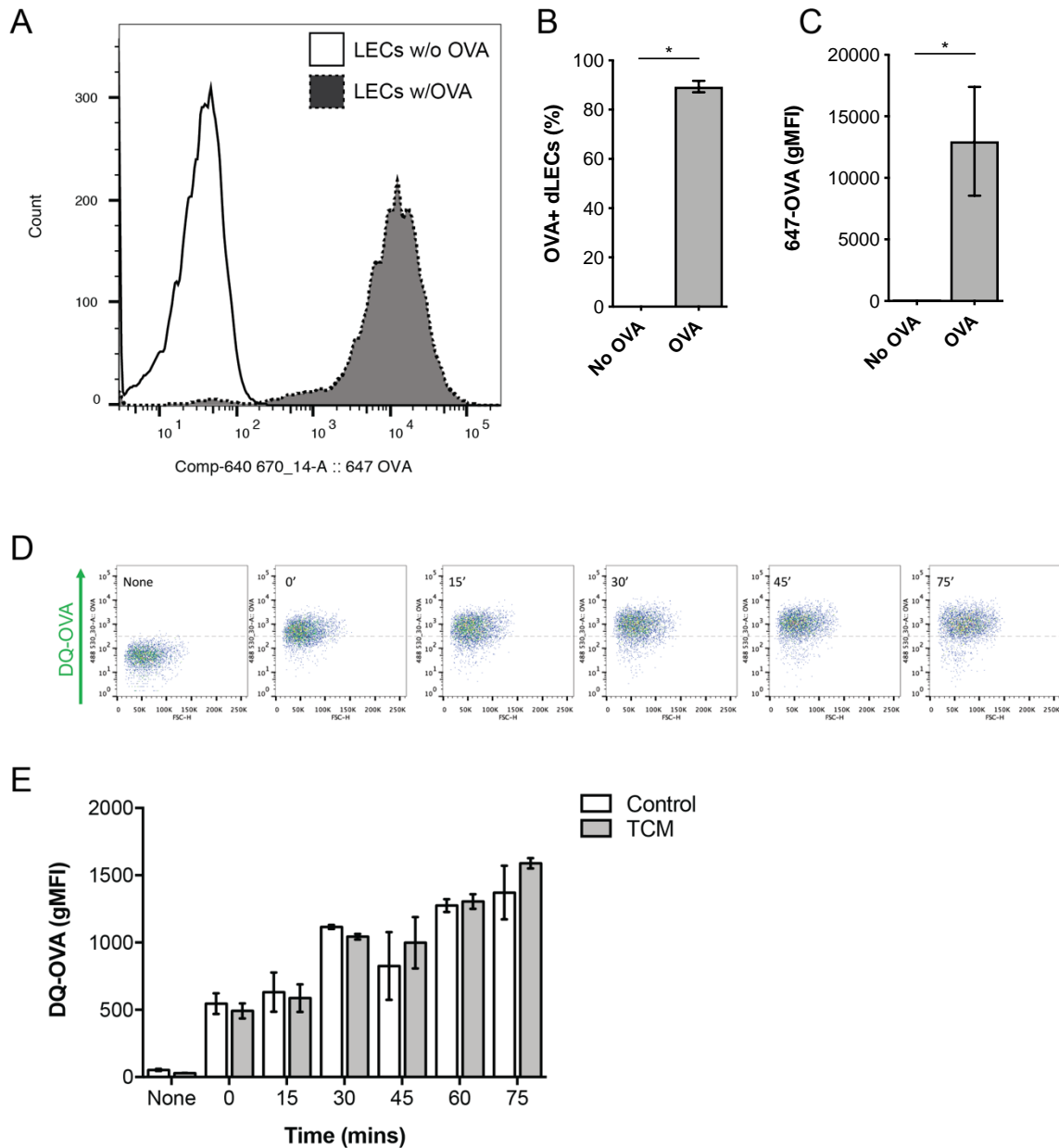


Figure 5.5. OVA uptake and processing by LECs *in vitro*. Flow cytometry was used to define OVA uptake with histograms showing a shift in fluorescence in LECs treated with OVA (w/OVA, grey peak) (A). Quantification of OVA uptake as a percentage of total LECs and geometric mean fluorescent intensity (gMFI) in LECs pulsed with and without OVA (B, C). Flow cytometry was used to define DQ-OVA processing with dot plots (D) and quantification of DQ-OVA geometric mean fluorescent intensity (gMFI) across 0-75minutes, in the presence or absence of TCM (E). Data shown represents n=2 independent experiments. Data presented as mean \pm SEM. Statistical significance was calculated using the Mann-Whitney test, with $P \leq 0.05$. Full gating strategy is detailed in Appendix 9.

5.3.3. LECs transfer antigen to CD11c dendritic cells

Having established that LECs have the capacity to uptake and process antigen *in vitro*, although tumour-derived factors did not enhance this, we then proceeded to determine physical interactions with dendritic cells would allow for antigen transfer. For this we developed an assay whereby GFP+ CD11c dendritic cells were isolated and cultured with LECs saturated with fluorescently conjugated OVA (Figure 5.6). To ensure that the only source of OVA for DCs was OVA actively taken up by LECs, cells were thoroughly washed to remove any antigen in the media. As we observed physical interactions with LECs over a 60 minutes period *in vitro*, we used the same timeframe, incubating DCs with OVA-pulsed LECs for 60 minutes at 37°C. Non-adherent DCs in suspension and adherent DCs were then retrieved for flow cytometry to detect levels of fluorescence, indicative of OVA uptake.

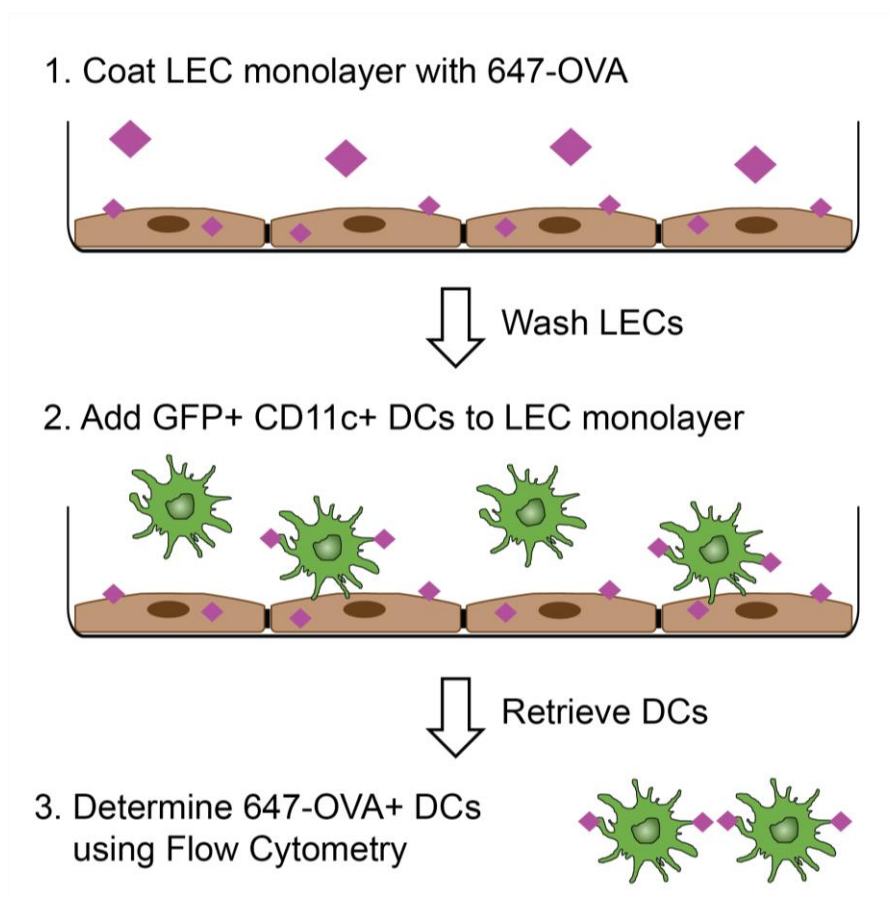


Figure 5.6. Schematic showing *in vitro* model of antigen transfer. Before co-culture, LECs were pulsed with 647-OVA (1), followed by incubation with CD11c DCs for 60 minutes (2). Non-adherent and attached DCs were then retrieved for flow cytometry assessment of 647-OVA fluorescence (3).

Upon analysis by flow cytometry, sequential gating in GFP+CD11c+ populations allowed for OVA detection specifically in CD11c-positive dendritic cells (Figure 5.7). Fluorescently conjugated 647-OVA enabled quantification of the percentage of OVA-positive DCs and the geometric mean degree of OVA uptake within CD11c positive populations.

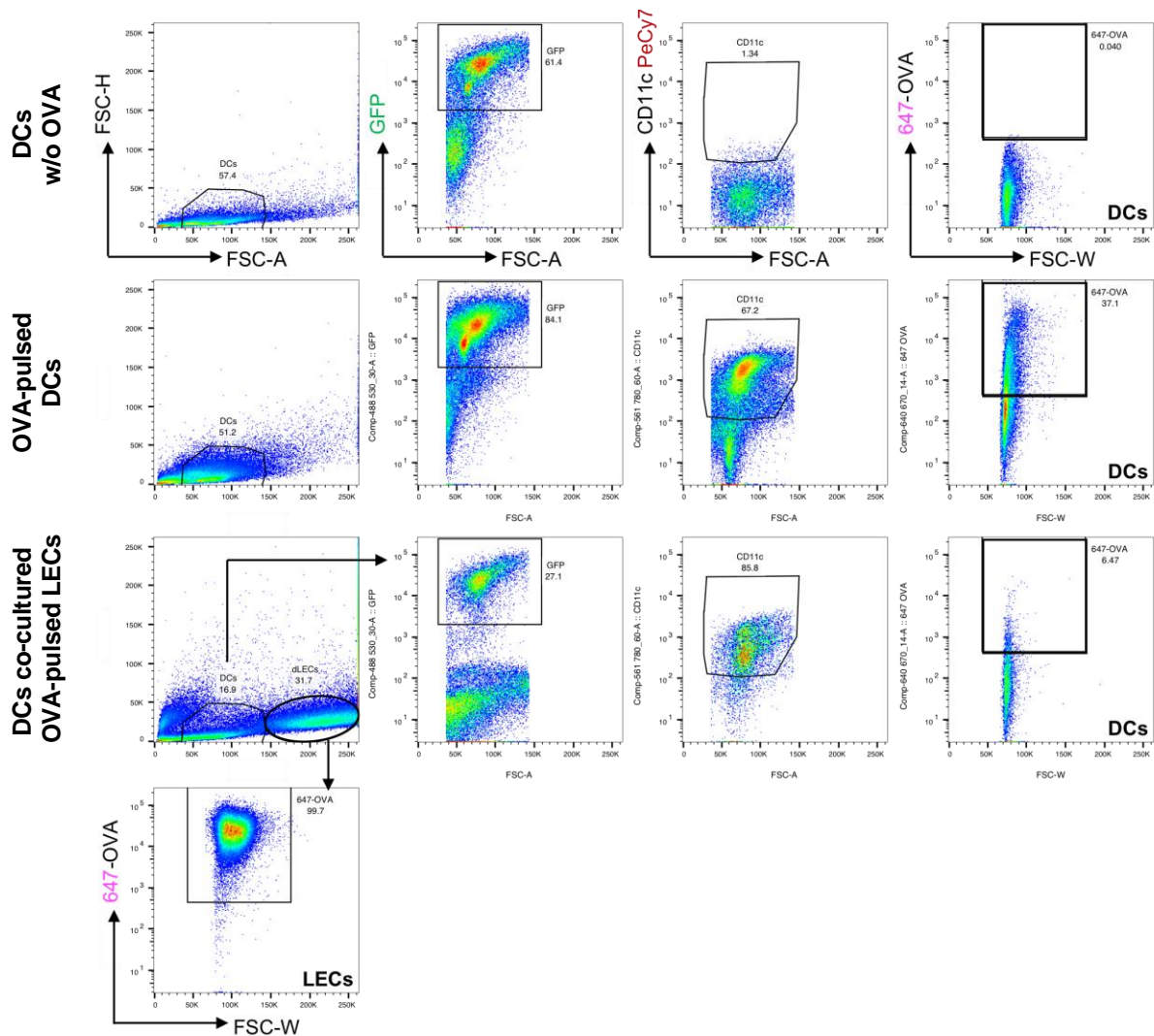


Figure 5.7. Gating strategy for flow cytometry analysis of OVA transfer. Flow cytometry was used to define 647-OVA uptake in GFP+CD11c+ DCs co-cultured with OVA-pulsed LECs. Representative gating for 647-OVA and CD11c was defined using unstained controls. Bulk GFP+CD11c isolated DCs pulsed with OVA was used as a positive control for intrinsic OVA uptake capacity. Adherent and non-adherent DCs were retrieved from LEC co-cultures, with adherent DCs retrieved alongside LECs. This allowed quantification of 647-OVA in both adherent GFP+ CD11c+ DCs and corresponding LECs. 647-OVA uptake was detected using the 640nm laser.

Preliminary experiments with 100µg/ml FITC-OVA pulsed LECs indicated that OVA uptake was significantly higher in adherent CD11c+ DCs as quantified by percentage of OVA+ DCs and the gMFI within CD11c+ DCs (Appendix 3). To more robustly examine this, ensuring only OVA uptake in added CD11c+ DCs was measured, we used GFP+ DCs purified for CD11c and 647-fluorescently conjugated OVA (647-OVA). A negative and positive threshold for OVA uptake was established using bulk DCs pulsed with OVA at the same concentration received by LECs (100µg/ml). OVA was detected in 35.3% ± 0.92 of total GFP+ CD11c+ dendritic cells and within this population, the average gMFI was 321 ± 22.5 (Figure 5.8a,b). Using these results as a guideline for uptake when DCs are directly saturated in soluble OVA, we determined the capacity and degree of OVA uptake, comparing non-adherent and adherent DCs from co-cultures with OVA-pulsed LECs. The percentage of OVA-positive DCs was significantly increased in adherent DCs compared with the non-adherent population, which were assumed *not* to have physically interacted with LECs. An average of 8.13% ± 0.87 adherent DCs were found to be OVA positive, whereas only 3.2% ± 0.46 of non-adherent were OVA positive. The gMFI in these cells was also significantly increased, with average gMFI calculated to be 32.3 ± 2.71 and 19.27 ± 1.01, in adherent and non-adherent DCs respectively. This indicates that not only were more DCs receiving OVA, but average uptake of LEC-derived antigen was greater in adherent DCs than in non-adherent DCs. Upon comparison with bulk DC positive controls, the percentage of OVA positive DCs and the gMFI were lower but this is likely due to the fact that bulk DCs were saturated with OVA, unlike the co-cultured DCs which relied on antigen transfer from LECs (Figure 5.8c,d).

This assay demonstrated that DCs which physically interact with LECs have more exposure to LEC-derived antigen and hence an increased likelihood of taking up said antigen. These results show for the first time, to our knowledge, that internal antigen can be physically transferred between LECs and attached DCs. When translated to lymph node dynamics *in vivo*, it is likely that rapid response antigen draining to the lymph node results in lymphatic uptake and subsequent presentation to incoming migratory dendritic cells.

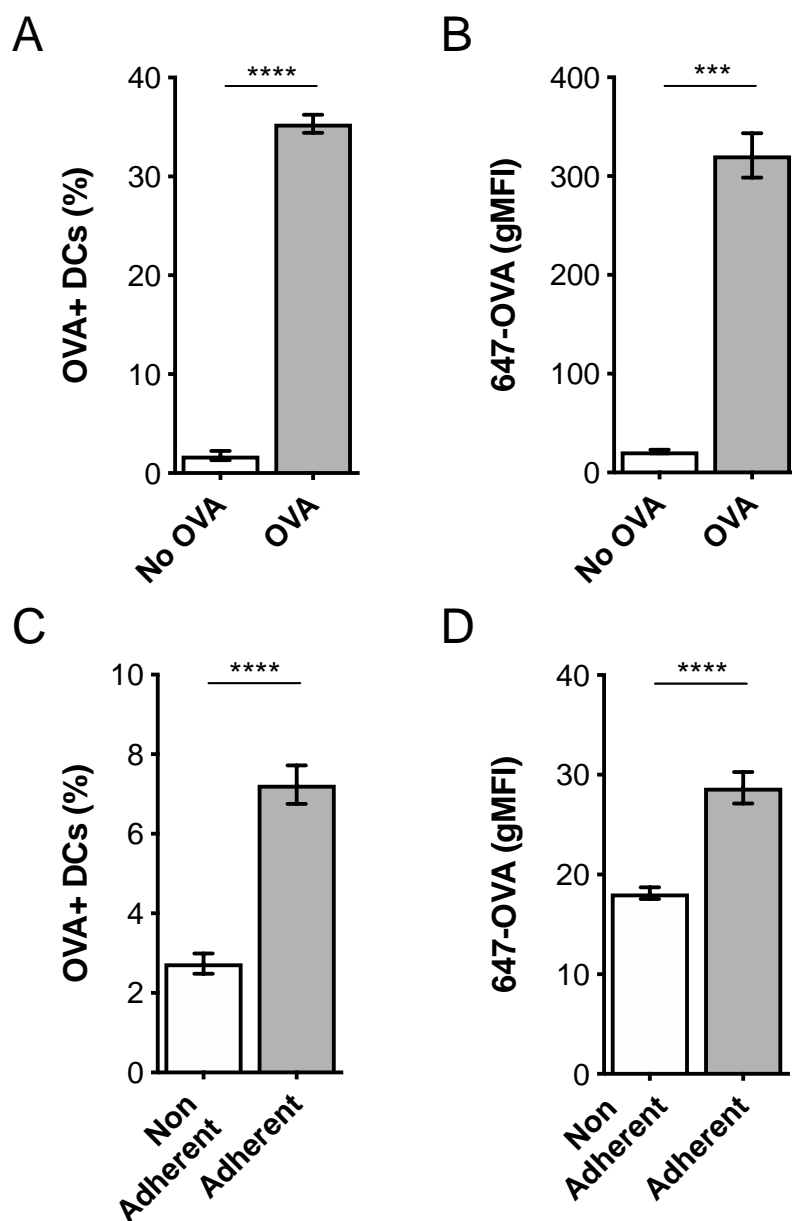


Figure 5.8. LEC-derived antigen is transferred to physically interacting DCs. Flow cytometry was used to define 647-OVA uptake in GFP+CD11c+ DCs co-cultured with OVA-pulsed LECs. 647-OVA was quantified as a percentage of total GFP+ CD11c+ cells (A) and as geometric mean fluorescent intensity within total GFP+CD11c+ cells (B) in bulk DCs pulsed with OVA, or non-adherent and adherent DCs from co-cultures with OVA-pulsed LECs (C, D). Data shown represents $n=2$ independent experiments, with $n=9$ non-adherent and $n=9$ adherent samples. Data presented as mean \pm SEM. Statistical significance calculated using the Mann-Whitney test, with $P \leq 0.05$.

To investigate whether lymphatic conditioning with TCM impacted the potential for antigen transfer, LECs were treated with CCM or TCM before and during OVA pulsing. GFP+CD11c+ DCs were then co-cultured using the same method as previously

described, with non-adherent and adherent DCs processed for flow cytometry. No difference in the percentage of OVA positive cells or the uptake of OVA, as defined by gMFI, could be seen between CCM and TCM conditions (Figure 5.9). This suggests that while conditioning of LECs with tumour-derived factors enhances DC-LEC interactions, it does not affect the process of antigen transfer over the time-frame examined.

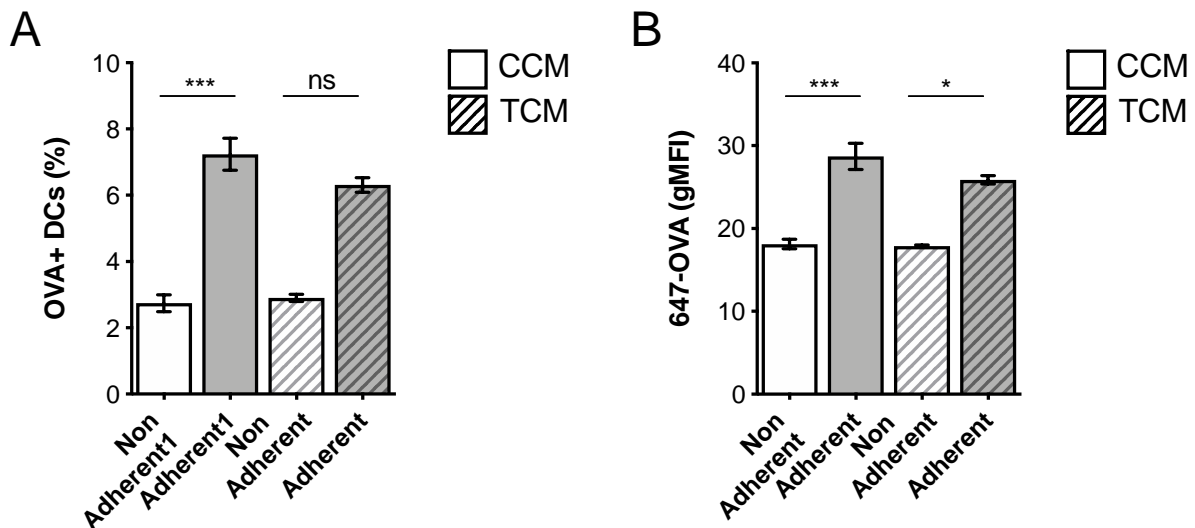


Figure 5.9. No change in antigen transfer between TCM-conditioned LECs and DCs. Flow cytometry was used to define 647-OVA uptake in GFP+CD11c+ DCs co-cultured with OVA-pulsed LECs pre-conditioned with either control-conditioned media (CCM) or tumour-conditioned media (TCM). 647-OVA was quantified as a percentage of total GFP+CD11c+ cells (A) and as geometric mean fluorescent intensity within total GFP+CD11c+ cells (B). Data shown represents n=2 independent experiments, with n=9 samples per group. Data presented as mean \pm SEM. Statistical significance calculated using the Mann-Whitney test, with $P \leq 0.05$.

5.3.4. LEC-primed DCs fail to induce T-cell proliferation *in vitro*

As introduced earlier, antigen primed DCs are key drivers of T-cell immunity in the lymph node, with the type of antigen presented, presence of co-stimulatory/co-inhibitory molecules, the cytokine and chemokine milieu, localisation of DCs and T-cells, and the duration of DC-T-cell interaction all contributing to immune outcome. Following the establishment of lymphatics as an additional layer on immune modulation, we assessed whether lymphatics could influence DC-mediated T-cell priming. Having demonstrated antigen transfer to DCs from LECs, we co-cultured these DCs with CFSE labelled OT-1 T-cells to determine if LEC-antigen bearing DCs could indeed induce antigen specific T-cell responses. Co-culture of DC's with CFSE-labelled T cells permits quantification of T-cell proliferation, as the fluorescent signal halves with every T cell division. OT-1 CD8a+ T-cells express T-cell receptors that specifically recognise SIINFEKL, the processed OVA peptide presented within MHC-I on antigen presenting cells, such as a DCs. Thus CFSE-labelled OT-1 CD8a+ T-cells were added to DCs acquired from OVA-primed LECs to measure antigen-specific T-cell proliferation in response to transferred antigen. Proliferation and viability were then quantified (Figure 5.10). CFSE-positive cells represent non-proliferative populations, with progressively negative CFSE populations representing each subsequent generation. Bulk DCs primed with OVA at the same concentration as LECs and cultured with T-cells at the same density as LEC-conditioned DCs, were used as the positive control. Throughout these co-cultures DCs were not pre-activated with any cytokine or bacterial-derived product, allowing us to assess the sole influence of pre-culturing with LECs on DC-mediated T-cell priming, with DCs cultured alone as the control.

Using the gating strategy outlined in Figure 5.10, bulk DCs and both adherent and non-adherent DCs derived from co-cultures with OVA-pulsed LECs, were processed for flow cytometry. Controls such as CFSE negative T-cells, bulk DCs co-cultured with CFSE T-cells in the absence of antigen, and unstained controls to delineate viable and CD8a+ T-cells were used to define gates. In the presence of bulk CD11c+ isolated DCs primed directly with OVA, an average of $52.5\% \pm 6.0$ of viable CD8a+ OT-1 T-cells proliferated, compared with $6.8\% \pm 1.12$ in the absence of OVA (Figure 5.11a).

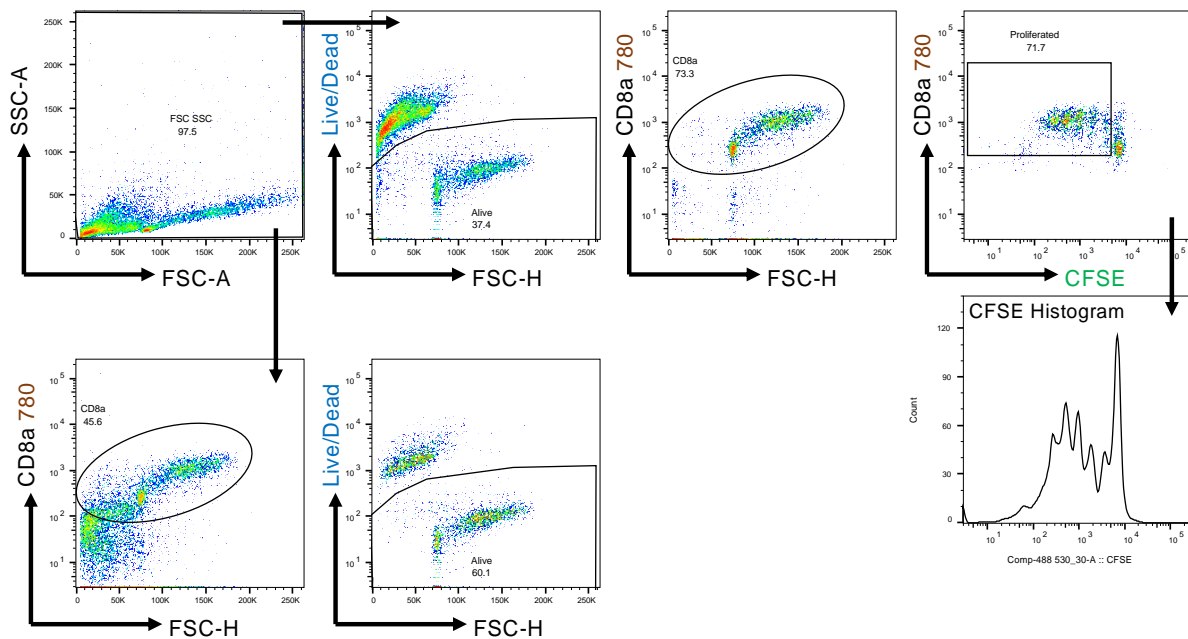


Figure 5.10. Gating strategy for quantification of OT-1 CD8a+ T-cell proliferation and viability. DCs primed directly with OVA or by OVA-bearing LECs were co-cultured with OT-1 CD8a+ T-cells for 72 hours. Cells stained with a viability dye and fluorescently conjugated anti-CD8a were processed for flow cytometry. For quantification of proliferation, CFSE negative cells were gated within CD8a+ viable cells, yielding a percentage of proliferated cells, as a total of all CD8a+ viable cells. For quantification of viable OT-1 CD8a+ T-cells, viable cells were gated within total CD8a+ cells, yielding a percentage of alive cells, as a total of all CD8a+ cells.

In the case of DCs collected from LEC co-cultures, neither adherent nor non-adherent DCs induced significant T-cell proliferative responses (Figure 5.11a). Compared with Bulk DC where 52.5% \pm 6.0 of OT-1 proliferated in response to stimulation, 12.6% \pm 3.0 of viable CD8a+ OT-1 T-cells proliferated when co-cultured with non-adherent DCs, and 5.49% \pm 2.7 proliferated in response to adherent DCs. T-cell viability does not appear to be a contributing factor to varying levels of proliferation seen across conditions, as percentage of viable CD8a+ OT-1 T-cells co-cultured with LEC-conditioned DCs was comparable with the viability of those co-cultured with bulk DCs (Bulk viability, 74.0% \pm 2.3; Adherent viability 69.2% \pm 2.8; Non-adherent viability 57.6 \pm 0.97) (Figure 5.11b).

As we detected lower levels of OVA uptake in DCs derived from LEC co-cultures in comparison to bulk DCs primed directly with OVA, we carried out an antigen titration experiment to observe levels of T-cell proliferation with lower levels of antigen. DC co-

culture densities with T-cells were maintained at 1:10, with OVA concentrations ranging from 1-100µg/ml (Figure 5.11c). The percentage of viable proliferating CD8a+ T-cells was >80% across OVA concentrations (Figure 5.11c), with no difference in viability seen across OVA concentrations either (Figure 5.11d). This suggested reduced viability with LEC-conditioned DCs, was not a consequence of lower levels of OVA available to present.

To ensure that DCs from OVA-pulsed LEC co-cultures did indeed uptake OVA, as per our original experiments, a sample from both non-adherent and adherent DCs from every independent experiment carried out, was processed for flow cytometry (Figure 5.11e). OVA uptake was almost undetectable in non-adherent DCs, which could explain the lack of proliferation in T-cells cultured with non-adherent DCs (Figure 5.11e). OVA could however be detected in adherent DCs (Figure 5.11e) with an average of 5.3% ± 1.45 found to be positive for OVA. This suggests that T-cells co-cultured with adherent DCs did not proliferate despite the presence of OVA-bearing DCs. As pre-conditioning with tumour-derived factors did not alter OVA uptake and processing by LECs, or the extent of antigen transfer to DCs, no changes in T-cell proliferation were expected. Indeed, preliminary data suggests no change in T-cell proliferation between DCs derived from CCM or TCM conditioned LECs.

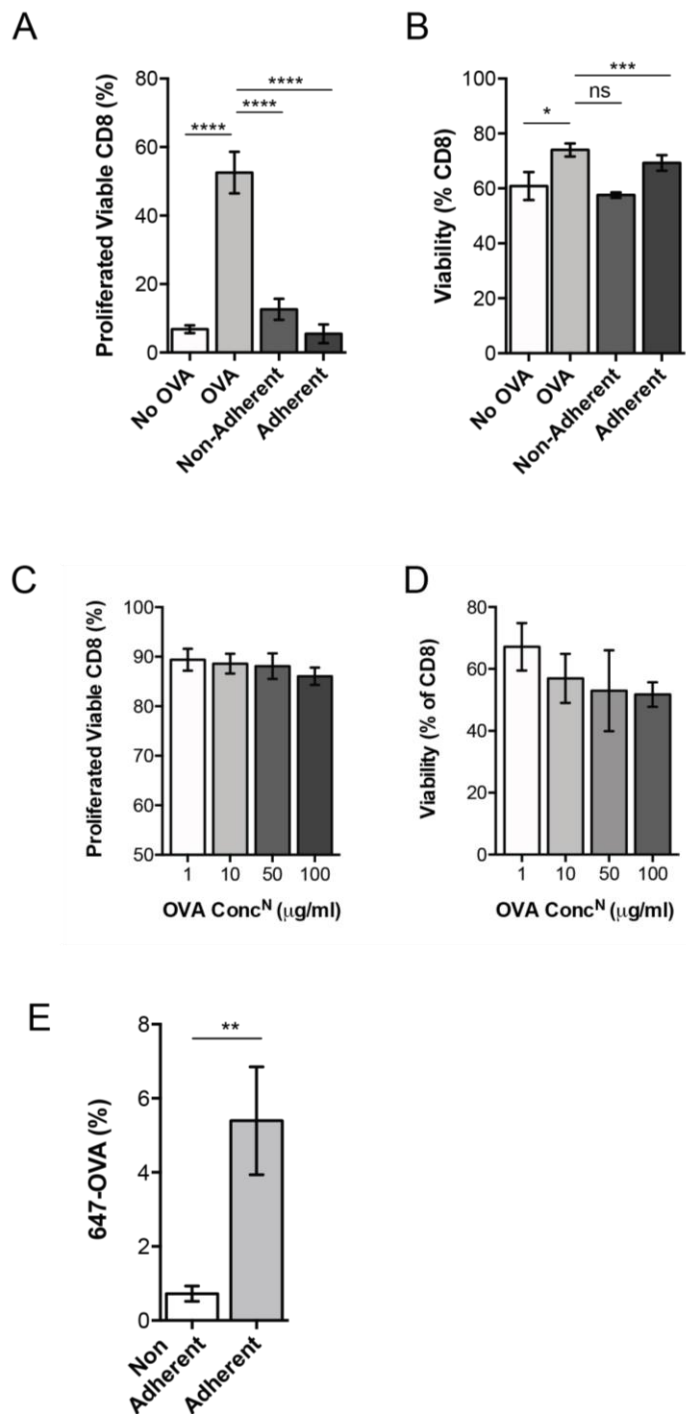


Figure 5.11. OT-1 T-cells do not proliferate in the presence of LEC-primed DCs. Flow cytometry was used to quantify proliferation and viability of OT-1 CD8a+ T-cells co-cultured with bulk DCs pulsed with OVA or non-adherent and adherent DCs derived from OVA-pulsed LECs (A,B). Flow cytometry was used to quantify proliferation and viability of OT-1 T-cells co-cultured with bulk DCs pulsed with a range of concentrations of OVA (C,D). Proliferation quantified as a percentage of viable CD8a+ T-cells and viability quantified as a percentage of total CD8a+ T-cells. Flow cytometry quantification of 647-OVA uptake in non-adherent and adherent DCs before being co-cultured. 647-OVA quantified as a percentage of total cells (E). Data shown is from $n > 3$ independent experiments with $n > 10$ samples per group. Data presented as mean \pm SEM. Statistical significance calculated using Student's t-test, with $P \leq 0.05$.

5.3.5. Draining antigen is predominantly taken up by resident LN-LECs

Having established that antigen is taken up and processed by LECs *in vitro* and can be transferred to physically interacting DCs *in vitro*, we sought to identify whether this phenomenon occurred *in vivo* and whether antigen dynamics was altered in TDLNs.

Firstly, to examine dynamics of drained antigen rather than antigen actively transported to the node by migratory APCs, we injected FITC-OVA subcutaneously to the front legs of tumour-bearing or control mice, to ensure rapid delivery of antigen directly to brachial lymph nodes with minimal exposure of antigen to the periphery. Analysis was performed using the gating strategy outlined in Figure 5.12, all non-immune stromal populations (FRCs, LECs and BECs) were gated using CD31 and Podoplanin expression in CD45 negative populations and dendritic cells were gated using CD11c expression in CD45 positive populations. FITC-OVA positive populations were gated within each stromal compartment and in dendritic cells with overall geometric mean fluorescent intensity of OVA in each subpopulation also calculated.

Upon analysis of the non-immune stromal compartments, LECs were the predominant FITC+ cell type having engulfed FITC-OVA within 15 minutes of delivery. Across resting NDNLs, an average of $66.1\% \pm 4.05$ of total LECs were FITC-OVA positive, compared only $17.3\% \pm 6.9$ of total FRCs and $8.5\% \pm 5.0$ of total BECs. Relative distribution was unchanged in early TDLNs, with an average of $57.6\% \pm 5.9$ of total LECs, $21.7\% \pm 9.2$ of FRCs and $14.0\% \pm 5.8$ of BECs calculated as FITC-OVA positive (Figure 5.13a). Immunofluorescent analysis of FITC-OVA distribution in nodes confirmed that FITC-OVA was predominantly detected in direct association with lymphatic marker, LYVE-1, in both resting NDNLs and Day 4 TDLNs (Figure 5.14).

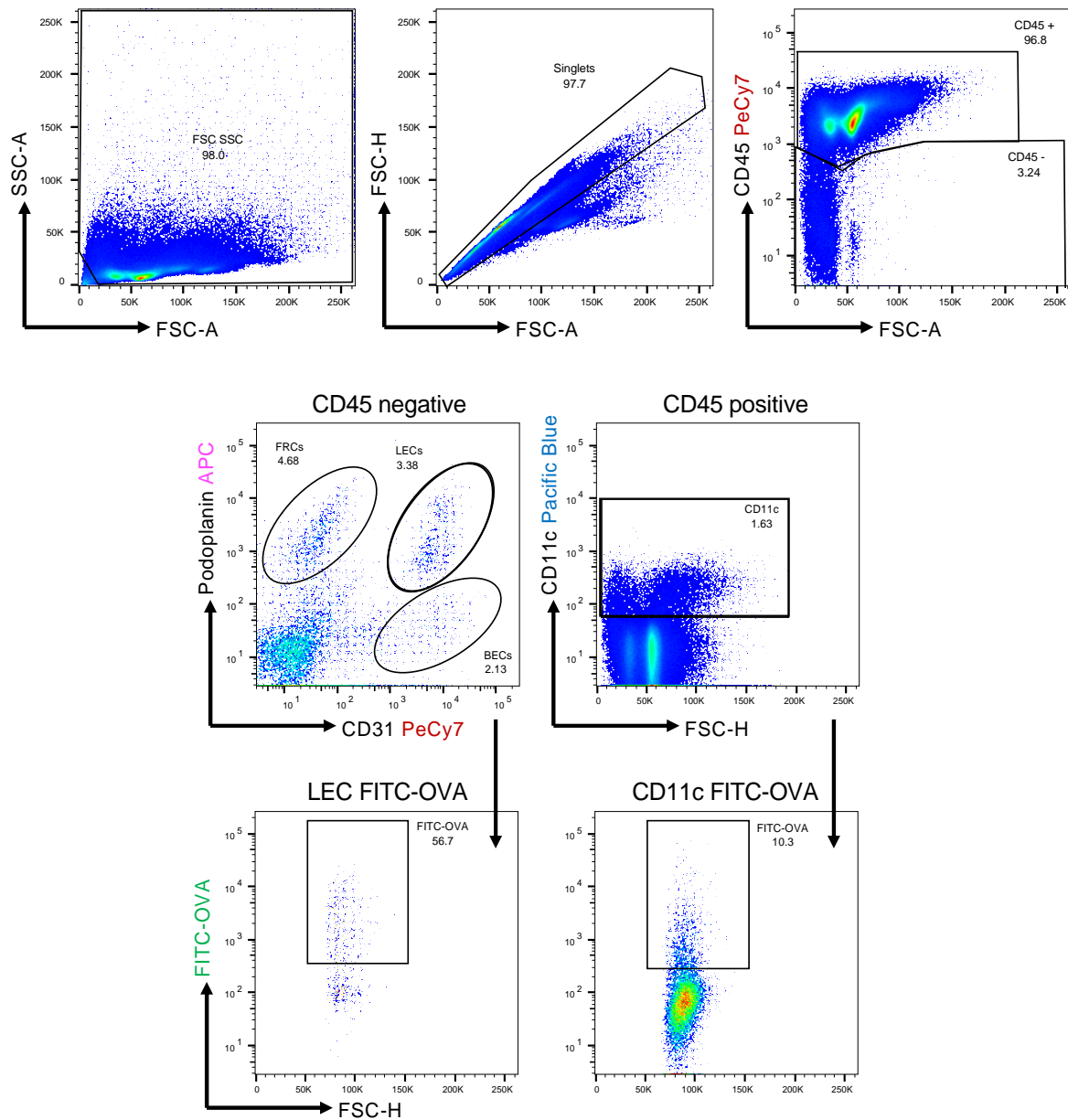


Figure 5.12. Flow cytometry gating strategy used to identify FITC-OVA localisation in TDLNs. Flow cytometry was used to determine FITC-OVA uptake in non-immune stromal and CD11c+ dendritic cell populations. Non-immune stromal cells were gated with CD45- singlets; Fibroblast reticular cells (FRCs) CD31- Podoplanin+; Lymphatic endothelial cells (LECs), CD31+ Podoplanin+; Blood endothelial cells (BECs), CD31+ Podoplanin-. Dendritic cells were gated upon CD11c+ populations within CD45+ singlets. Representative FITC-OVA gating within LECs (left) and CD11c (right) populations are shown.

Similar observations were made upon assessment of the degree of FITC-OVA uptake by each stromal compartment (Figure 5.13b), with gMFI of FITC-OVA in LECs averaging 8-fold higher than in BECs and FRCs in resting NDNLs (Average OVA gMFI: LECs – 554.5 ± 69.0 ; FRCs – 64.4 ± 28.8 ; BECs – 64.7 ± 31.1). In early TDLNs, the gMFI was marginally increased across CD45 negative stromal compartments, with a fold-change in OVA gMFI of 1.2 in LECs (Average OVA gMFI: NDNLs – 554.5 ± 69.0 ; D4 TDLNs – 676.6 ± 198.6) and fold-change of 1.5 in FRCs and BECs (Average OVA gMFI in FRCs: NDNLs – 64.4 ± 28.8 ; D4 TDLNs – 102.4 ± 54.4 and Average OVA gMFI in BECs; NDNLs – 64.7 ± 31.1 ; D4 TDLNs – 100.4 ± 31.8) (Figure 5.13b). These data clearly identified the lymphatics as the dominant compartment for uptake of draining antigen, however no significant change in the degree or distribution of uptake across non-immune stromal compartments, indicating that the capacity for LECs to sample exogenous lymph-borne antigen is a constitutive phenomenon.

Within the CD45 positive immune compartment, uptake of FITC-OVA by CD11c dendritic cells was substantially lower than observed for LECs, with an average of $10.1\% \pm 0.67$ OVA-positive DCs in resting NDNLs and $12.0\% \pm 1.8$ in early TDLNs (Figure 5.13c). The extent of uptake was also low, with the gMFI of OVA in CD11c DCs averaging 45.3 ± 7.33 in resting NDNLs and 55.8 ± 10.6 in early TDLNs (Figure 5.13d). Compared with the aforementioned values for OVA uptake in LECs, this data suggests that exposure of DCs to draining antigen is minimal within short time frames, and the slight increases may be attributed to altered permeability in early TDLN. Analysis of early TDLNs also showed identical distribution patterns, supporting flow cytometry data and suggesting that draining antigen is predominantly taken up by LECs in both resting and early TDLNs. Further kinetic analysis would identify if antigen is re-distributed with time and further still whether antigen is re-distributed differentially in early TDLNs.

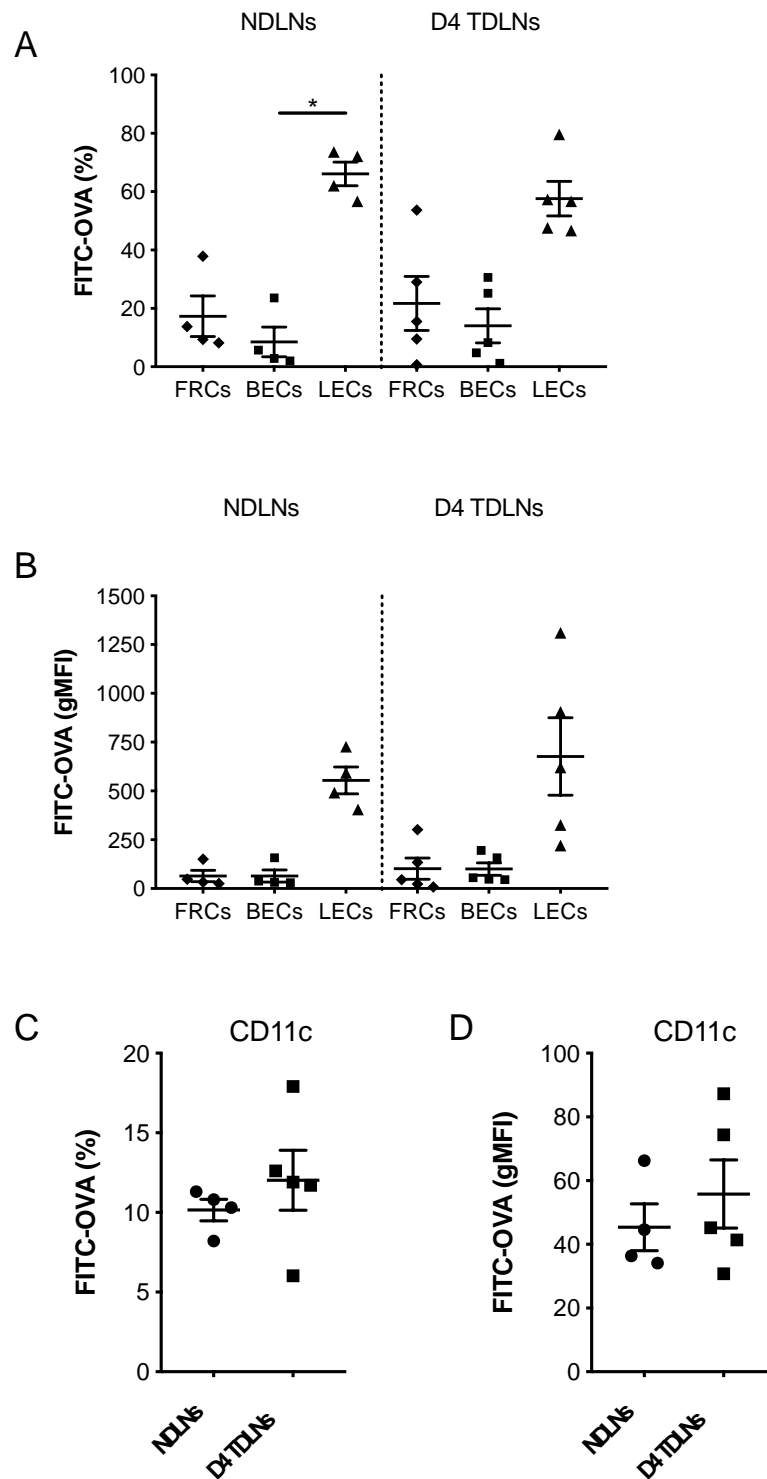


Figure 5.13. Antigen is taken-up primarily by LECs in NDNLs and TDLNs. Flow cytometry analysis of FITC-OVA uptake by non-immune stromal and CD11c dendritic cell compartments within resting NDNLs and early Day 4 TDLNs. FITC-OVA+ cells as a percentage of total cells (A, C) and the geometric mean fluorescent intensity of FITC-OVA within each population (B, D) is shown with each point representing a single lymph node. Data shown is from $n=2$ independent experiments with $n=5$ NDNLs and $n=5$ Day 4 TDLNs. Data presented as mean \pm SEM. Statistical significance calculated using the Kruskal-Wallis test with $P \leq 0.05$.

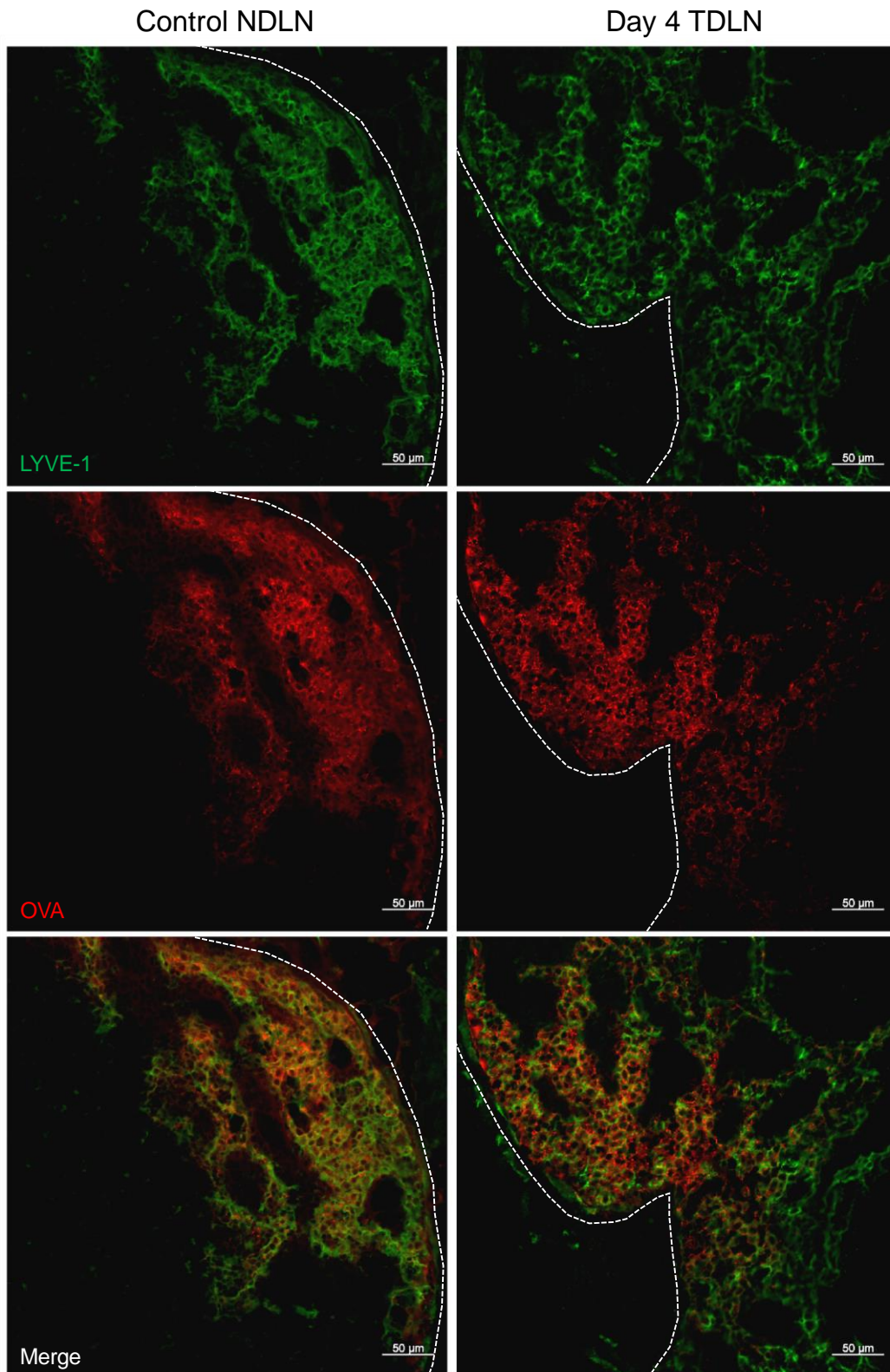


Figure 5.14. Antigen localises to LYVE-1 positive regions in Day 4 TDLNs. Representative confocal images of OVA (red) localisation relative to lymphatics, LYVE-1 (green). Control NDLNs and Day 4 TDLNs were imaged on a Zeiss 880, with tile scan images taken at 20x and 1024 resolution. Shown are representative ROIs of lymphatic rich subcapsular sinuses in control NDLNs (left panel) and Day 4 TDLNs (right panel). Dotted white lines outline the edge of the lymph node. Scale bars represent 50μm.

5.3.6. Draining antigen is predominantly processed by resident LN-LECs

In light of reports that infer a capacity of LECs to process antigen in nodes draining late, established tumours¹⁸⁸, we aimed to determine the changes in processing of engulfed antigen by LECs in early TDLNs. Similarly, to the *in vivo* FITC-OVA models used, we injected DQ-OVA which was detected using flow cytometry, enabling quantitation of the degree of processed OVA across lymph node compartments (Figure 5.15).

Since draining antigen is rapidly and preferentially taken up by lymphatics within both resting NDNLs and early TDLNs, we hypothesised that in the immediate 15 minutes post-administration, this would translate to preferential processing by lymphatics. Indeed, preliminary data shows that in the stromal compartment, an average of $86.7\% \pm 1.0$ of all LECs in resting NDNLs were positive for processed OVA, whereas for FRCs and BECs, only $12.6\% \pm 5.5$ and $23\% \pm 7.8$ respectively were positive for processed OVA (Figure 5.16a, left panel). No significant change in distribution of OVA processing capabilities was detected in early TDLNs. Similar dynamics were observed when quantifying extent of OVA processing, with the LEC compartment dominating (gMFI averaging 1645.5 ± 229.0 in resting NDNLs) compared with FRCs and BECs (gMFI averaging 84.6 ± 17.4 and 128.5 ± 27.5 , respectively) (Figure 5.16a, right panel). Interestingly, while the amount of antigen engulfed by LECs was elevated in LECs of TDLNs, the extent of processing by LECs was lower, albeit not significantly, with a fold change of 1.96 in gMFI (NDNLs – 1645.5 ± 229.5 ; Day 4 TDLNs – 839.3 ± 287.4) (Figure 5.16a, right panel). For FRCs and BECs, the small increases seen in uptake of FITC-OVA in early TDLNs continued to processing, likely due to increased availability, with average gMFI of FRCs 84.6 ± 17.4 vs. 105.1 ± 18.0 for NDNLs and Day 4 TDLNs respectively, and 128.5 ± 27.5 vs. 135.6 ± 7.7 for BECs of NDNLs and Day 4 TDLNs respectively (Figure 5.16a, right panel).

As antigen-containing lymph drains continually to lymph nodes, we also assessed processing longer term, beyond the acute processing response. Brachial LNs were retrieved 18 hours after DQ-OVA administration and the same gating strategy used to define extent of OVA processing across lymph node compartments.

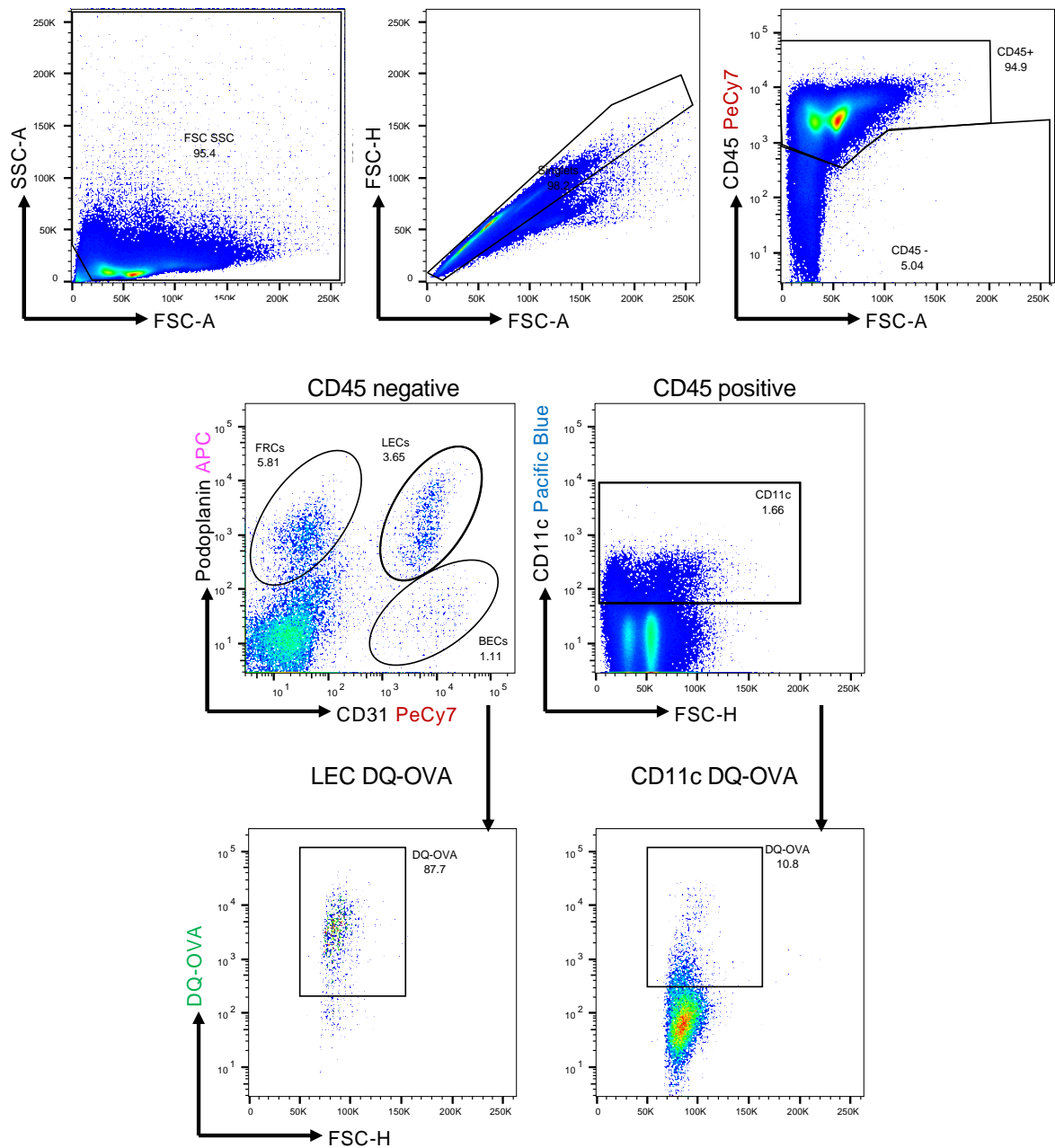


Figure 5.15. Flow cytometry gating strategy used to identify DQ-OVA processing in TDLNs. Flow cytometry was used to determine DQ-OVA processing in non-immune stromal and CD11c+ dendritic cell populations. Non-immune stromal cells were gated with CD45-singlets; Fibroblast reticular cells (FRCs) CD31- Podoplanin+; Lymphatic endothelial cells (LECs), CD31+ Podoplanin+; Blood endothelial cells (BECs), CD31+ Podoplanin-. Dendritic cells were gated upon CD11c+ populations within CD45+ singlets. Representative DQ-OVA gating within LECs (left) and CD11c (right) populations are shown.

Consistent with data from 15-minute time points, in NDNLs, LECs remained dominant OVA processors at 18 hours with an average of $69\% \pm 12.5$ of LECs positive for processed OVA. An average of $11.9\% \pm 1.0$ and $8.5\% \pm 0.4$ of FRCs and BECs in resting NDNLs, and $12.1\% \pm 2.1$ and $8.2\% \pm 1.4$ respectively in Day 4 TDLNs were found to have processed OVA (Figure 5.16b, left panel). At later time points, the proportion of LECs detected with fluorescent signal indicative of OVA processing was $43.5\% \pm 6.2$ compared with $86.7\% \pm 1.0$ immediately after inoculation (Figure 5.16b, right panel). A more drastic decrease in OVA gMFI could be seen in early TDLNs (Figure 5.16b, right panel), with the average gMFI of DQ-OVA down to 499.6 ± 135.7 , compared with NDNLs at 1441 ± 549.8 . However, this decrease was not significant due to variation in NDNLs. No changes were found in the gMFI of OVA in FRCs and BECs, with the gMFI in FRCs averaging 109.3 ± 4.6 and 102.5 ± 7.4 and in BECs averaging 99.5 ± 2.6 and 113.6 ± 9.7 , in resting NDNLs and Day 4 TDLNs respectively.

This data ultimately demonstrates that as in resting NDNLs, LECs are taking up and processing drained antigen in early TDLNs. It further demonstrates that despite no change in antigen uptake, there may be changes in the extent of antigen processing. Delayed kinetics could result in better presentation as antigen has more time to be processed efficiently; this could explain why the fluorescent signal is so decreased by 18 hours. As antigen presentation has not been explored in these experiments, the relative importance of these changes in processing, for antigen presentation remains undefined. Measuring SIINFEKL within MHC on the surface of APCs within the node would give a good indication of the extent of presentation relative to processing kinetics. Importantly however, it highlights that in terms of stromal involvement in antigen-associated processes, the lymphatics dominate over FRCs and BECs in both resting NDNLs and early TDLNs, identifying them as likely active contributors to antigen-mediated immunity in responding TDLNs in early stages of B16 tumour development.

Within CD11c-positive dendritic cells (gating in Figure 5.14), the percentage of DCs processing OVA at both 15 minutes and 18 hours post-administration remained unchanged (Figure 5.17a). The degree of processing mirrored this, with the gMFI of OVA not changing between DCs from resting NDNLs and Day 4 TDLNs (Figure 5.17a). When comparing the percentage of DCs that had processed DQ-OVA and the

extent of processing (Figure 5.17b), values were drastically lower than that shown for LECs, demonstrating again, that even after 18 hours (Figure 5.17b), drained antigen in both resting and early TDLNs is lymphatic dominated.

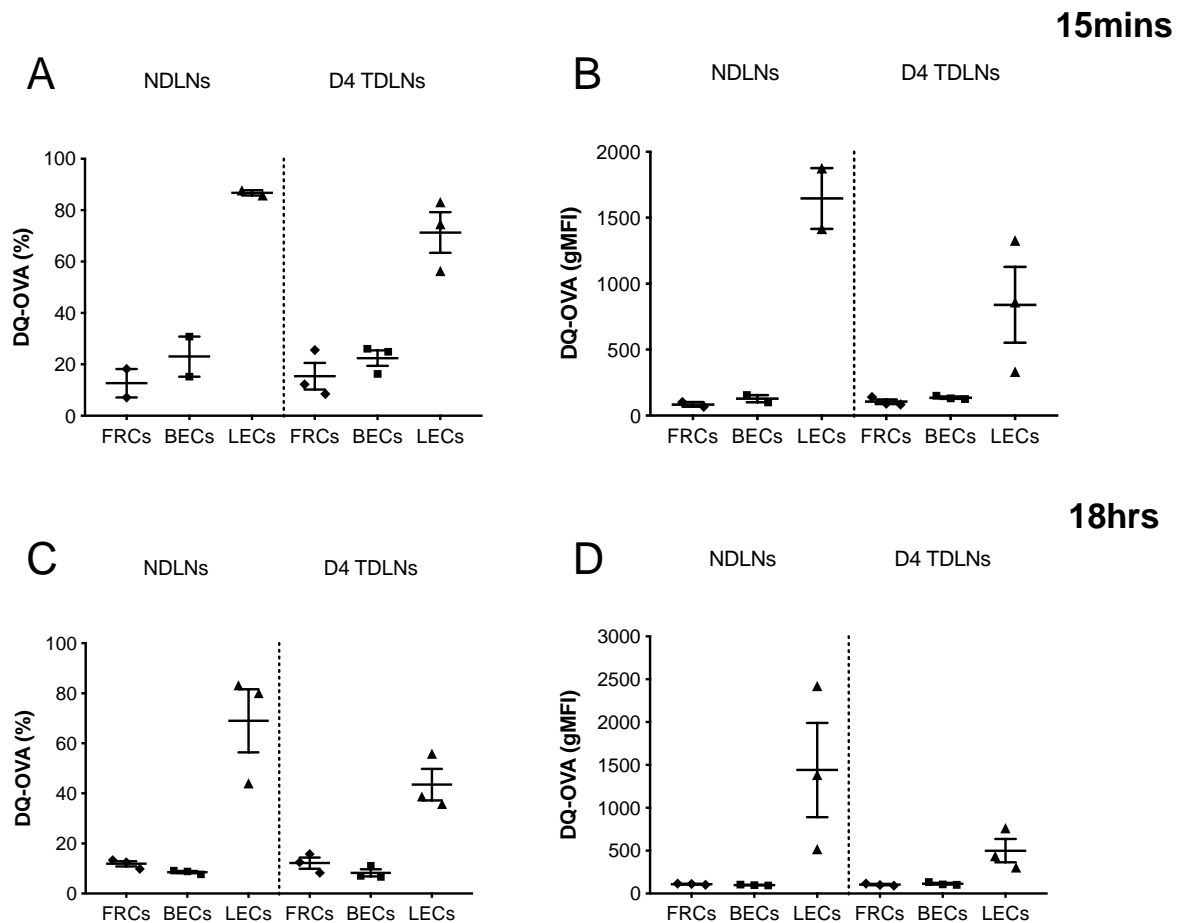


Figure 5.16. LECs efficiently process antigen in NDNLs and early TDLNs. Flow cytometry analysis of DQ-OVA uptake by non-immune stromal cells in resting NDNLs and early Day 4 TDLNs. DQ-OVA positive cells as a percentage of total cells (A, C) and the geometric mean fluorescent intensity (gMFI) of DQ-OVA within each population (B,D) is shown with each point representing a single lymph node. Brachial dLNs retrieved 15 minutes after (A,B) and 18 hours after (C,D) DQ-OVA administration. Data shown is from $n=1$ independent experiment, with $n=3$ NDNLs and $n=3$ Day 4 TDLNs. Data presented as mean \pm SEM. Statistical significance calculated using the Kruskal-Wallis test with $P \leq 0.05$.

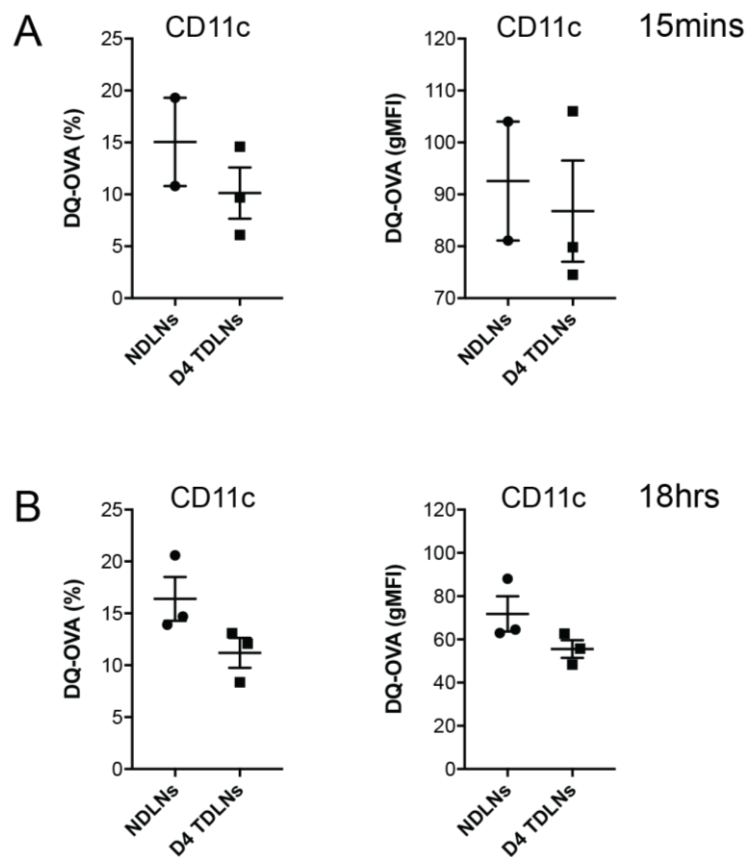


Figure 5.17. No difference in antigen processing by CD11c DCs between control NDNLNs and early TDLNs. Flow cytometry analysis of DQ-OVA processing by CD11c dendritic cells in resting NDNLNs and early Day 4 TDLNs. DQ-OVA positive cells as a percentage of total cells (A, B left panel) and the geometric mean fluorescent intensity (gMFI) of DQ-OVA within each population (A, B, right panel) is shown with each point representing a single lymph node. Brachial LNs retrieved 15 minutes after (A) and 18 hours after (B) DQ-OVA administration. Data shown is from n=1 independent experiment, with n=3 NDNLNs and n=3 Day 4 TDLNs. Data presented as mean \pm SEM. Statistical significance calculated using the Mann-Whitney test, with $P \leq 0.05$.

5.3.7. Migratory DCs process more DQ-OVA than resident DCs

Having demonstrated that draining antigen is predominantly taken-up by lymphatics early in tumour development, we next set out to ascertain whether DCs entering the node could access antigen from said lymphatics during the prolonged physical interactions described earlier. *In vitro* data certainly suggests that mature splenic DCs have the capacity to uptake antigen from lymphatics. To investigate this *in vivo*, we developed a simple assay to enable assessment of processing by different DC populations. Firstly, DQ-OVA was injected subcutaneously in the front leg allow rapid antigen drainage to the lymph node lymphatics independently of any tumour involvement. After 15 minutes the tumour-site was painted with TRITC. This ensured that tumour-derived DCs were TRITC positive, and that they originated from an OVA-free tissue site. Only once they reached the lymph node would they be able to interact with DQ-OVA that had rapidly drained after administration (Figure 5.18a). No OVA was present within the tumour-region, thus any TRITC cells positive for DQ-OVA in the lymph node, would hence have acquired that antigen AFTER they arrived, with OVA-bearing lymphatics as the likely dominant source.

Using the gating shown in Figure 5.18b, TRITC positive and negative cells DCs were identified, and then gated for DQ-OVA using the same strategy as previously used. In NDNLNs, a 1.6-fold increase in the percentage of DQ-OVA-positive, TRITC-positive migratory populations was detected when compared with TRITC negative resident populations ($15.3\% \pm 2.0$ in resident vs. $24.5\% \pm 5.1$ in migratory, Figure 5.18c). Detection in Day 4 TDLNs was reduced in both resident and migratory DCs, with $11.4\% \pm 1.2$ resident DCs found to have processed DQ-OVA and $8.25\% \pm 2.8$ migratory DCs having processed DQ-OVA. Upon assessing gMFI across both control NDNLNs and Day 4 TDLNs, gMFI was dramatically lower in migratory DCs than in resident DCs, with a difference between average gMFI of the populations, of 43.6 and 53.2, in control NDNLNs and Day 4 TDLNs respectively.

In terms of what this means of LN-antigen uptake and processing by DCs, we previously demonstrated that antigen could be taken up and processed by CD11c DCs within the lymph node, hence we expected to observe antigen processing by both resident DCs and any present migratory DCs. As we see an increasing trend in the

percentage of migratory DCs processing in control NDNLs, this preliminary data does suggest that migratory DCs may have better exposure to drained antigen than resident DCs, certainly in control NDNLs. However, due to other possible confounding factors influencing detection of DQ-OVA processing in the node, as discussed earlier; we may not be capturing the full extent of antigen processing using this method. This may explain why levels of detection are much lower in Day 4 TDLNs. Trends observed collectively do however indicate the possibility that migratory DCs are preferentially exposed to drained antigen through physical interactions with lymphatics, which are the primary compartment for antigen uptake in both resting and early TDLNs. Further analysis would be required to determine more precisely the kinetics of antigen processing in resident and migratory DCs in early TDLNs, with appropriate techniques needing to be optimised to do so.

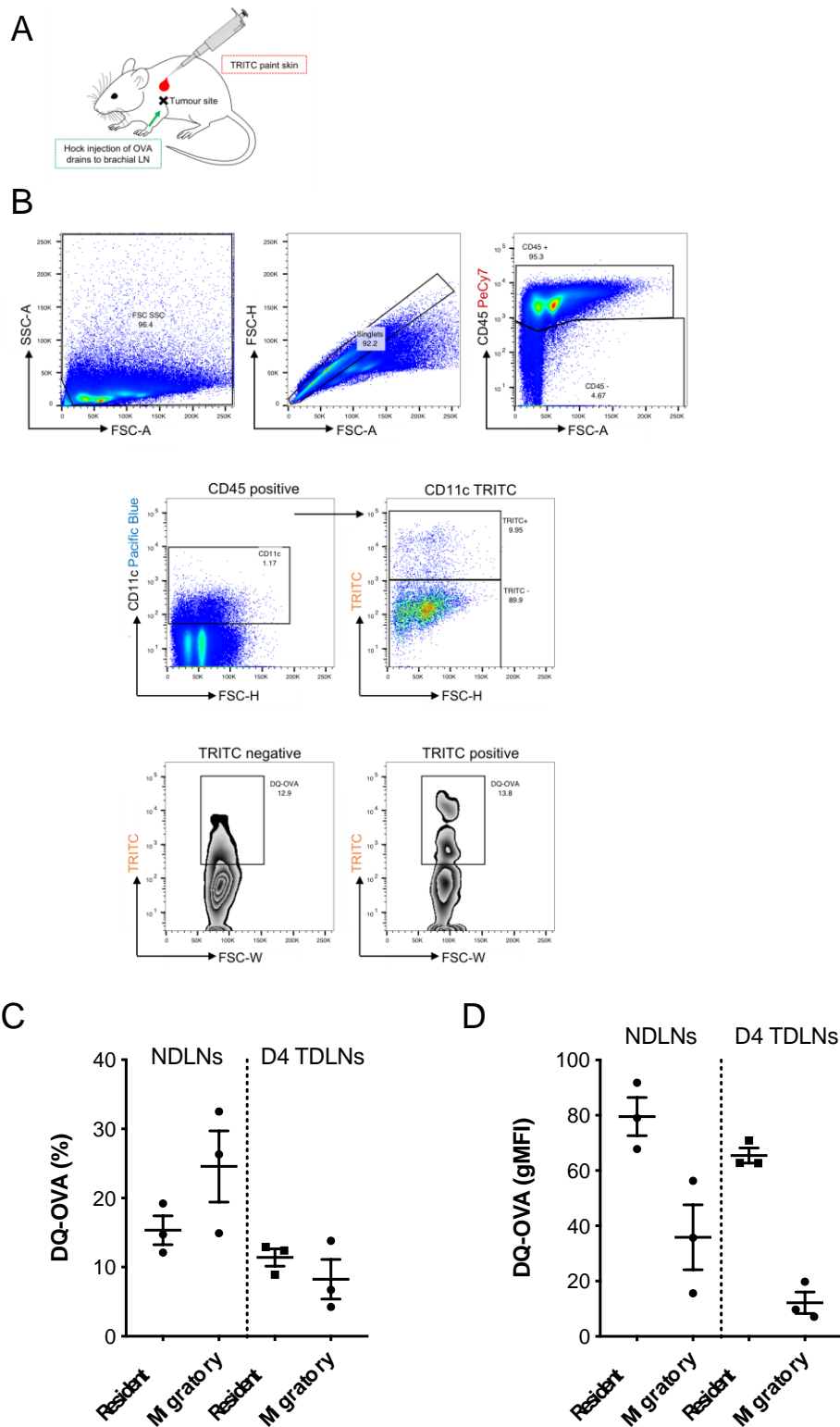


Figure 5.18. Migratory DCs process drained antigen in LNs. *In vivo* model to track processing of DQ-OVA by tumour-derived migratory DCs (A). Flow cytometry gating strategy for quantification of DQ-OVA processing by TRITC DCs (B). DQ-OVA positive cells as a percentage of total cells (C) and geometric mean (D) in control NDNLs and Day 4 TDNLs is shown. Each point represents a single brachial lymph node retrieved 18 hours after DQ-OVA administration and TRITC painting. Data shown is from $n=1$ independent experiment with $n=3$ NDNLs and $n=3$ Day 4 TDNLs. Data presented as mean \pm SEM. Statistical significance calculated using the Kruskal-Wallis test, with $P \leq 0.05$.

5.3.8. Migratory DCs are activated and mature in early TDLNs

Having shown that in early TDLNs, tumour-derived migratory DCs have prolonged interactions with lymphatics at the subcapsular sinus, and that physical interactions permit antigen transfer from antigen-pulsed LECs to DCs, we hypothesised that interactions between migratory DCs and lymphatics at the subcapsular sinus could result in functionally altered DCs. In support of this, *in vitro* data implied that DCs co-cultured with antigen-pulsed LECs were less capable of priming T-cells, despite sampling antigen.

We hence conducted a Mouse Dendritic and Antigen Presenting Cell RT² Profiler PCR Array on freshly isolated TRITC-positive cells from non-draining controls, and both early and late TDLNs (Figure 5.19a). The gating strategy for isolated TRITC-positive immune cells is shown in Appendix 11. The particular array used was tailored to *Dendritic and Antigen Presenting Cells*, with gene targets ranging across key APC functions such as antigen uptake and presentation and chemotaxis and cytokine production (Figure 5.19b). Qiagen software, designed to accompany these arrays for post-experiment analysis was used to calculate gene expression fold change values for Day 4 TDLNs and Day 11 TDLNs relative to control NDNLs. This data was used to create heatmaps using MeV software and as the Qiagen software does not calculate fold change values of individual control samples used, data for NDNLs is not displayed in heatmaps produced, as shown in Figure 5.19c.

Visualisation of gene expression profiles of migrated TRITC DCs from early Day 4 and late Day 11 TDLNs was done using heatmaps (Figure 5.19c). Early TDLNs revealed little change in gene expression fold change of DC maturation markers CD40, CD80 and CD86 relative to resting NDNLs. This is contrary to literature alluding to altered maturation and activation in APCs within the tumour microenvironment as the maturation of TRITC migratory DCs that reached the tumour-draining lymph nodes appeared unchanged at early stages of disease progression. Interestingly, expression of these markers was decreased in late TDLNs, suggesting an immature phenotype of DCs is associated more with later stages of tumour development. In contrast, many chemokine signalling molecules were altered, with CXCR4, CCL19 and CCL8 up regulated in TRITC-positive cells of Day 4 TDLNs. CXCR4 is expressed on the surface

of APCs, playing a critical role maturation, survival and CXCL12- mediated chemotaxis^{238,239}. Further assisting in APC migration is CCL19, which is not only a stromal-derived chemokine essential for facilitating migration of DCs into lymph nodes but is also an autologous chemokine which assists in naïve T-cell scanning behaviour²⁴⁰. In early TDLNs CCL19 expression is up regulated, whereas the opposite trend can be seen in late TDLNs. This suggests incoming migratory DCs are driving naïve T-cell responses specifically in early TDLNs, which may lead to altered T-cell dynamics in later TDLNs. Genes associated with antigen processing were also perturbed, with *Tapbp* and *Tap2* all up regulated and *H2-DMA* down-regulated. *Tapbp* and *Tap2* are critical in antigen processing, with both assisting in MHC Class I loading. Up regulation would suggest that TRITC migratory cells are capable of MHC Class-I loading and hence may retain capacity to cross present tumour antigen to CD8 effector T-cells. Conversely, MHC Class II associated *H2-DMA* is down regulated in early TDLNs, with a similar trend seen in late TDLNs. As MHC Class II is predominantly associated with antigen priming of CD4 T-cells, decreased expression of *H2-DMA* in TRITC migratory DCs implies possible dysfunction in this pathway. Furthermore, *ICAM-2*, which facilitates transendothelial migration of DCs²⁷⁷ and the immune synapse between mature DCs and naïve CD4 T-cells in lymph nodes²⁷⁸, was down-regulated in TRITC+ DCs derived from Day 4 TDLNs and up-regulated in those from Day 11 TDLNs.

Expression of a number of cytokines were also altered, with IL-6 and IL-2 increased and IL-10 and IL-12 decreased. IL-6 is a pleiotropic cytokine, associated mostly with pro-inflammatory effector function and anti-apoptotic features in specific relation to CD4 T-cells²⁴¹. IL-2 and IL-12 are also associated specifically with T-cell function, with IL-2 governing differentiation into effector and memory T-cells and IL-12 shown to promote IFN-gamma / Th1 responses²⁴² and synergise with IFN-alpha to prolong division of activated CD8 T-cells²⁴³. With IL-10 expression down regulated in early TDLNs, this cytokine signature collectively suggests early TDLNs, from the perspective of migratory DCs, are in a state of activation, skewed perhaps towards a more “pro-inflammatory” status.

Together, these data imply that migrated DCs are activated and mature in early TDLNs, with a distinct inflammatory signature, differential antigen processing and

cytokine profiles to DCs that trafficked to NDNLs. This suggests that despite prolonged interactions with lymphatics at the sinus of early TDLNs, these interactions may not alter maturation and activation *in vivo*, *instead serving to alter antigen repertoire and access/localisation cues*. As little is understood of lymphatic-mediated modulation of DC function especially in TDLNs, many of these signatures would have to be independently verified in the context of lymphatic conditioning to identify whether DC function is much more widely under the influence of stromal cells.

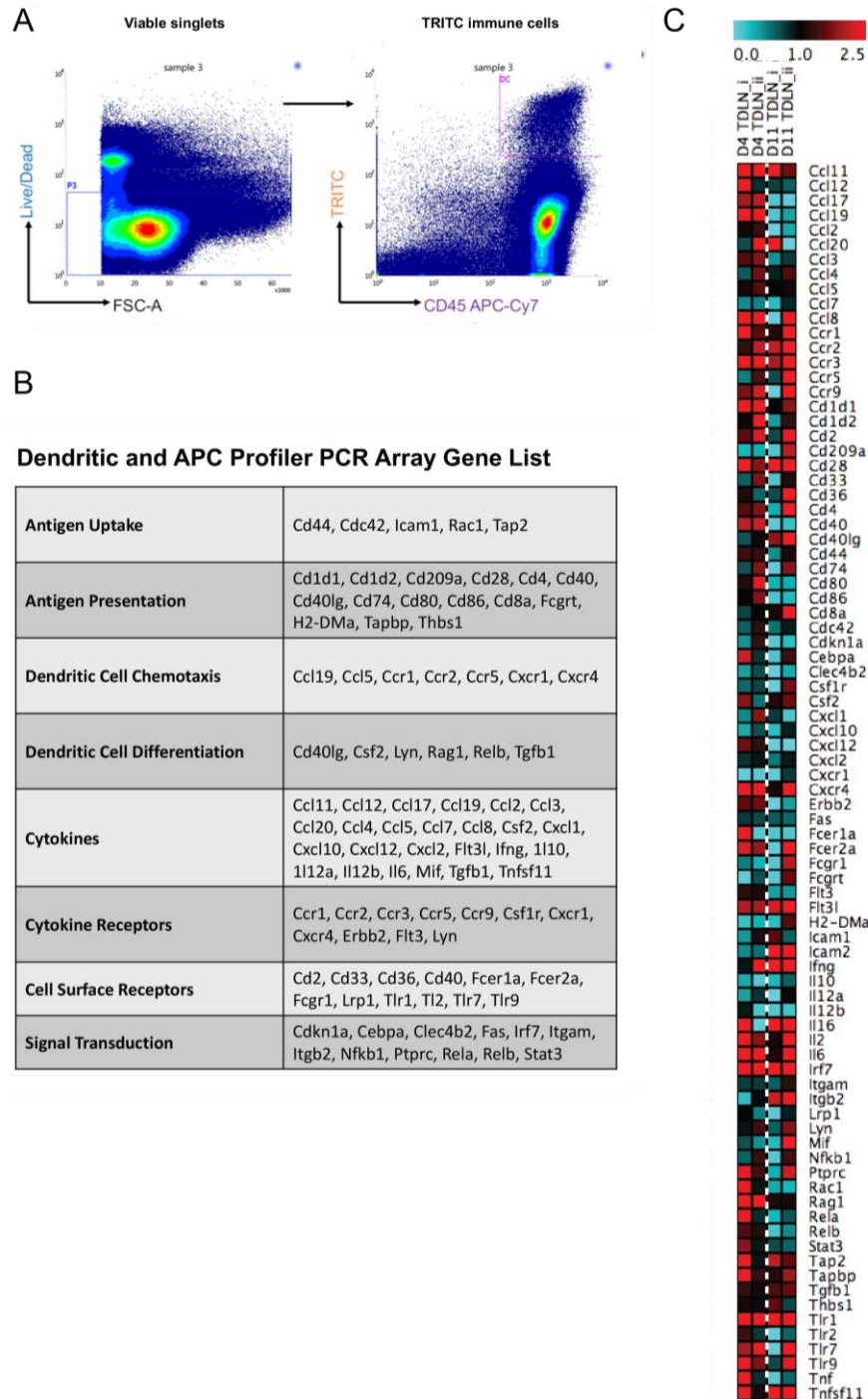


Figure 5.19. Migratory DCs are activated and mature in early TDLNs. Migratory immune cells, sorted based on double positive expression of TRITC and CD45 within singlets, was sorted for RNA (A). The Dendritic and Antigen Presenting Cell PCR Profiler Array includes 84 gene targets associated with antigen uptake and presentation, chemotaxis, DC differentiation and cytokine signalling, as well as cell surface markers and signal transduction molecules (B). Heatmap visualising fold change values for gene targets in early Day 4 and late Day 11 TDLNs. Fold changes calculated relative to SHAM control NDNLs. Values below 1 indicate down-regulation and coloured in turquoise with values above 2 indicating up-regulation, coloured in red (C). Data shown is from pooled nodes across n=3 independent experiments across conditions. Full gating strategy is detailed in Appendix 11.

5.3.9. No change to the PD1-PDL1 axis in early TDLNs

Despite providing an insight into expression profiles of key activation and maturation markers, as well as cytokines and chemokines, a number of important death ligand/receptor axes were not represented in the PCR Profiler Array. As shown across a number of studies and clinical trials, the PD1-PDL1 axis is critical in T-cell suppression across a number of cancer models^{244,245}. Furthermore, recent *in vivo* work in lymphangiogenic melanoma, has shown TDLN-resident LECs delete effector T-cells in a tumour-antigen specific manner via PD-L1. We hence chose to explore this axis across stromal compartments to determine whether PD-L1 expression was altered in early TDLNs, using flow cytometry as shown in Appendix 12. Across non-immune stromal compartments, PD-L1 could be detected mostly on endothelial cells in both control NDNLs and Day 4 TDLNs, with no change in expression seen in both BEC and LEC populations (Figure 5.20a,c). In Control NDNLs, the average gMFI of PD-L1 in LECs was 3555.2 ± 191.3 and in Day 4 TDLNs was 3670.4 ± 124.5 . This was in comparison to levels of expression in FRCs, with 95.7 ± 1.6 in Control NDNLs and 101.6 ± 3.6 in Day 4 TDLNs. Levels of PD-L1 expression in CD11c DCs appeared higher than in FRCs, with average gMFI in Control NDNLs of 411.0 ± 43.5 and in Day 4 TDLNs 554.9 ± 77.3 (Figure 5.20a,c). This was calculated as an average fold-change of 1.3, which may be a functionally relevant alteration, however does not represent a significant change in expression.

Looking at reciprocal receptor expression on T-cells within the LN, PD-1 expression could not be detected well in either CD4 or CD8 T-cells, with a population expressing a small shift in gMFI relative to the unstained control (Figure 5.20b). Little difference could hence be detected between Control NDNLs and TDLNs, with CD8 T-cells appearing to express lower levels of PD-1 than CD4 T-cells across LNs (Figure 5.20d). The same was observed for CD25 across both Control NDNLs and TDLNs and CD4 and CD8 T-cells (Figure 5.20b,d), however poor detection in this instance may be due to poor antibody efficiency.

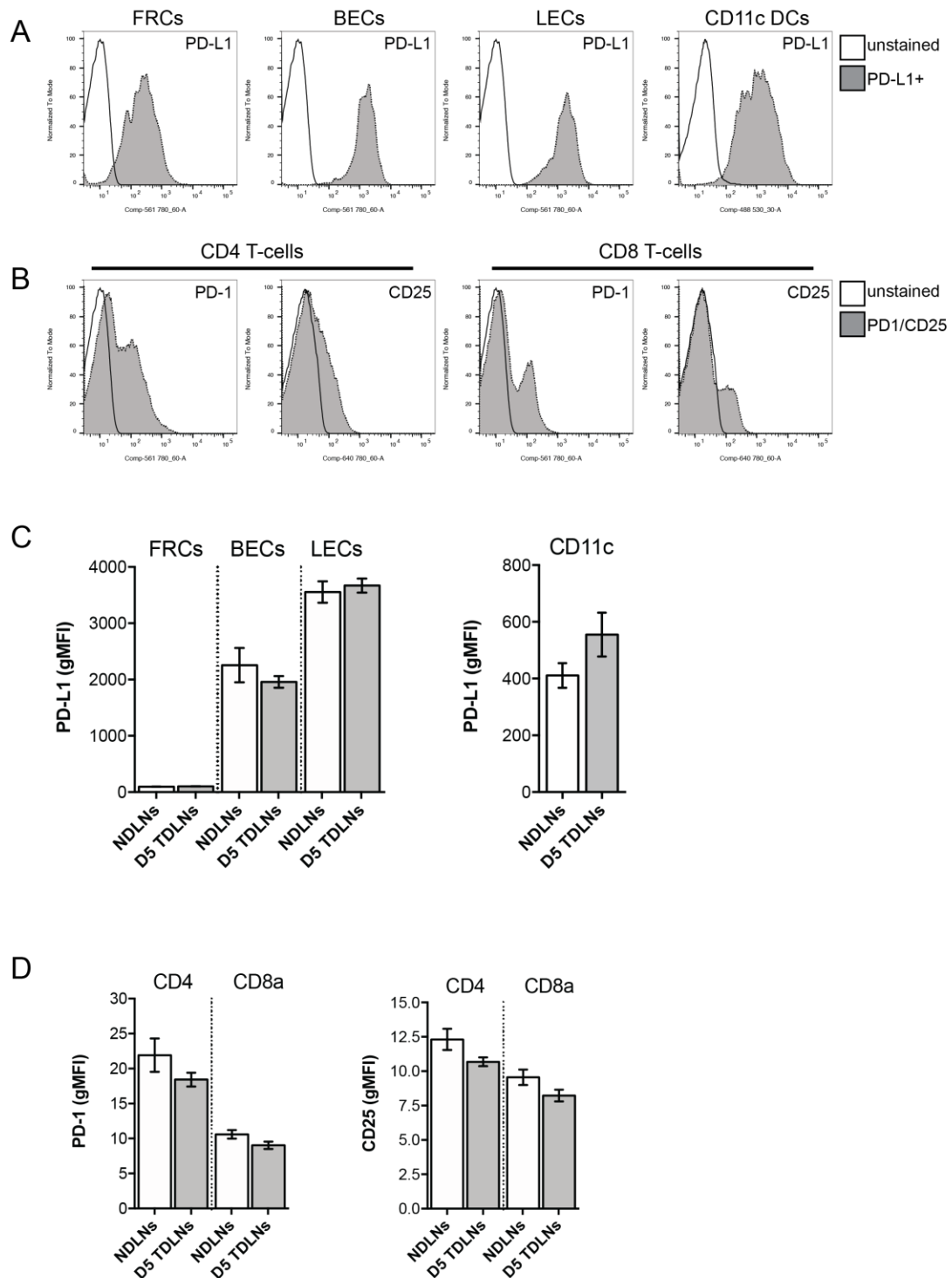


Figure 5.20. No change in PD-L1 and PD1 expression in immune compartments between control NDNLNs and early TDLNs. Flow cytometry gating strategy for quantification of PD-L1, PD-1 and CD25 expression in non-immune stromal populations (BECs, FRCs and LECs (A), and immune populations (CD11c DCs and CD4/CD8 T-cells (B). Quantification of gMFI of PD-L1 (C) and PD-1 and CD25 (D) in Control NDNLNs and Day 4 TDLNs in non-immune stromal populations (C, left panel) and CD11c DCs (C, right panel) and CD4 and CD8 T-cells (D). Data shown is from $n=2$ independent experiment with $n=6$ NDNLNs and $n=6$ Day 4 TDLNs. Data presented as mean \pm SEM. Statistical significance calculated using the Kruskal-Wallis test, with $P \leq 0.05$. Full gating strategy is detailed in Appendix 12.

5.3.10. Increased FoxP3 T-cells found in early TDLNs

To assess whether the changes observed in localisation and function of migrated DCs affect T-cell dynamics in TDLNs, we retrieved TDLNs from Day 5, 7 and 11. As changes in migratory DCs may not have immediate effect, these time points provided insight into how changes in early TDLNs influenced the responding lymph node.

TDLNs were taken from control and tumour-bearing mice and processed for flow cytometry where CD4 and CD8 T cells, and FoxP3 Tregs were quantified (Figure 5.21a) to determine T-cell subset dynamics across time. A significant increase in the number of T-cells per lymph node was found across time-points, with an average count of total CD3e T-cells in Control NDLNs, 0.9×10^5 ; Day 7, $2.5 \times 10^5 \pm 0.21$ and Day 11, $1.9 \times 10^5 \pm 0.2$. (Figure 5.21b). To determine whether this significant increase at Day 7 was attributable to expansion of both the CD8 and CD4 compartment, specific CD4 and CD8 T-cell counts were quantified (Figure 5.21c). Significant increases in CD8 T-cell count could be seen both at Day 7 and Day 11 (Control NDLNs, $0.41 \times 10^5 \pm 0.08$; Day 7 TDLNs, $1.15 \times 10^5 \pm 0.09$; Day 11 TDLNs, $0.88 \times 10^5 \pm 0.13$), whereas CD4 T-cell counts were seen to be significantly increased only at Day 7 (Control NDLNs, $0.45 \times 10^5 \pm 0.09$, Day 7 TDLNs, $1.23 \times 10^5 \pm 0.11$; Day 11 TDLNs, $0.91 \times 10^5 \pm 0.13$). Further analysis into CD4 T-cell expansion demonstrated a significant increase in the number of FoxP3 Tregs at Day 7 only (Control NDLNs, $0.38 \times 10^5 \pm 0.04$; Day 7 TDLNs, $1.03 \times 10^5 \pm 0.12$; Day 11 TDLNs, $0.83 \times 10^5 \pm 0.18$), suggesting the increasing trends in total CD4 T-cell at Day 7 to be attributable to expanded Foxp3 T-cells (Figure 5.21c). Our data hence agrees with published data, suggesting early tumour events encourage Treg accumulation in TDLNs. In terms of applying these findings to the phenotype observed in migratory DCs in early TDLNs, the lack of significant change in numbers of T-cells, across subpopulations, in Day 5 TDLNs, suggests that any change occurring in early TDLNs could be influencing T-cell dynamics over 48 hours later at Day 7. The specific contribution of altered DC migration in early TDLNs on T-cell dynamics in the ever-developing TDLN is unknown, and hence this work sheds some light on the temporal kinetics of T-cell/DC interactions and consequent T-cell immune responses. These timelines are critical for therapy, and hence must be considered for any immunotherapies that rely on T-cell/DC interactions in TDLNs.

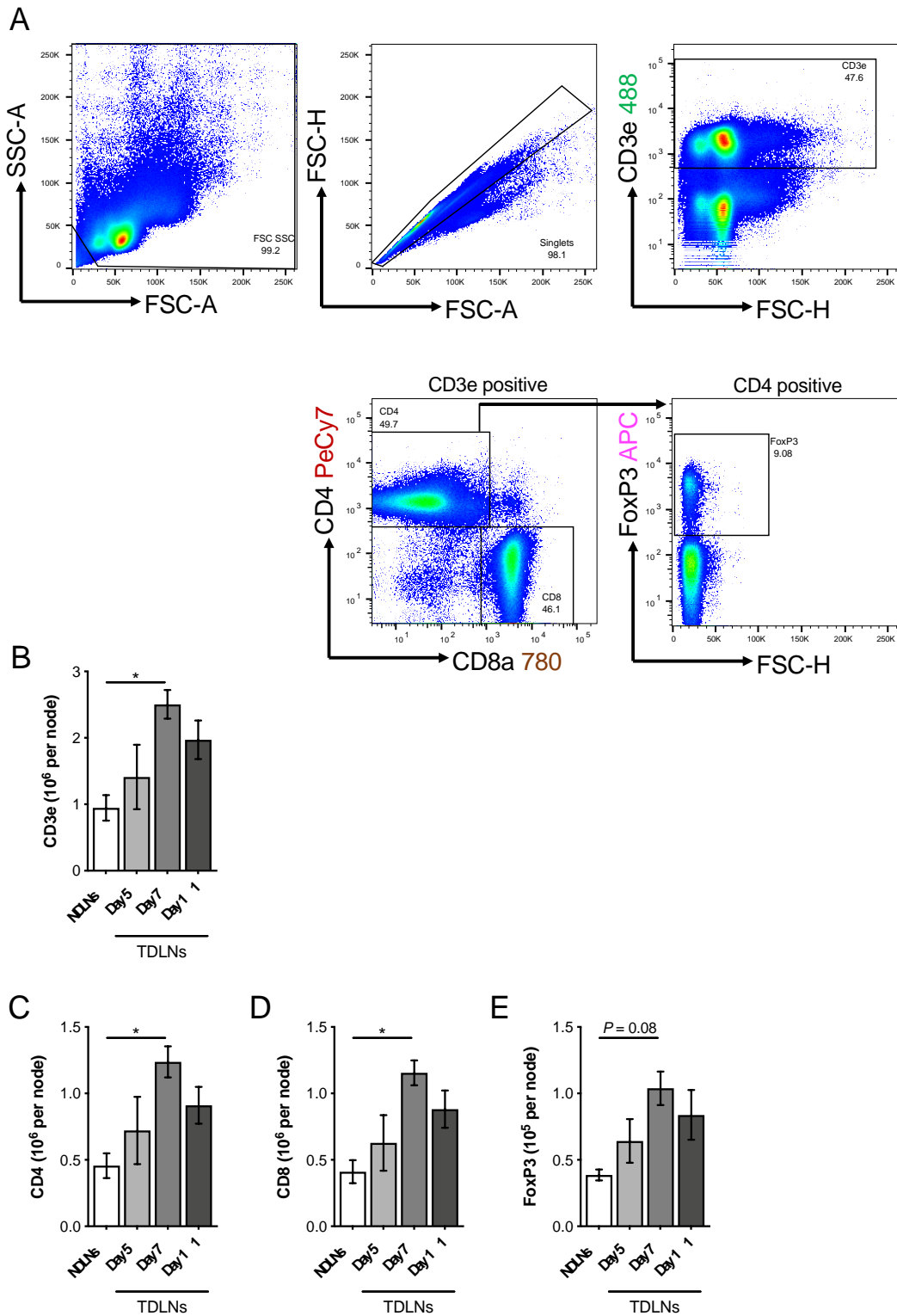


Figure 5.21. Altered T-cell profiles in TDLNs across time. LNs derived from control NDLNs and TDLNs were processed for flow cytometry, with T-cells defined by CD4 and CD8 expression within T-cell singlets, with regulatory T-cells (Tregs) defined within CD4 T-cell populations (A). Data shown is the quantification of total CD3e T-cells (B), CD4 T-cells (C), CD8 T-cells (D) and FoxP3 CD4 Tregs (E) per node. Data shown is from $n=2$ independent experiments with $n=9$ NDLNs, $n=2$ Day 5 TDLNs, $n=2$ Day 7 TDLNs and $n=5$ Day 11 TDLNs. Data presented as mean \pm SEM. Statistical significance calculated using the Kruskal-Wallis test, with $P \leq 0.05$ compared to control NDLNs.

5.4. Discussion

Having established transformed lymphatics in early and late TDLNs of B16-F10 melanoma tumours, with a number of immune signatures altered; we wished to explore the specific role of lymphatics in dendritic cell mediated immunity. Dendritic cells are in close contact with lymphatics for the duration of their journey from the periphery to the lymph node and we show that upon arrival at the node, migratory dendritic cells undergo prolonged physical interactions with the lymphatics at the subcapsular sinus. In addition to altered migratory and localisation patterns in early TDLNs, we wondered whether these interactions could have other functional consequences for migratory dendritic cells. With much research in basal settings demonstrating capacity for antigen to be transferred between lymphatic endothelial cells and migratory DCs, we wished to investigate relevance in the tumour microenvironment.

Firstly, we demonstrate that dendritic cells that physically interact with antigen-bearing lymphatic endothelial cells *in vitro* can uptake lymphatic-derived antigen. In these experiments, we bathed the LECs with FITC-OVA, however did not conduct analysis on the location of the antigen. Considering the time-frames of these assays and the saturation of LECs with FITC-OVA, we would predict antigen would be localised both in intracellular vesicles as well as on the cell surface. Antigen transfer could be occurring via exosomes or microparticles or through acquisition from the extracellular surface, and both mechanisms could indeed contribute to the acquisition of antigen by interacting DCs. However, the literature suggests this process is dependent on the physical-interaction of DCs with LECs¹²⁴ and does not occur via exosomes²⁸², so we would predict antigen is predominantly being transferred through physical interactions in this *in vitro* model. Future work must build on the mechanism driving this phenomenon and explore whether antigen transfer occurs in healthy and/or disease states and whether it is site-specific and only occurs in lymph nodes.

Secondly, lymphatics were shown to be the dominant compartment for antigen uptake and processing *in vivo*, over both short and medium-term periods. These findings suggest our *in vitro* observations of antigen transfer from LECs to DCs is highly plausible *in vivo*. Indeed, preliminary TRITC *in vivo* experiments found that migratory

DCs do process node-derived antigen more than resident DCs. As the lymph node drains antigen from the developing tumour, this mechanism may indeed allow for early tumour antigen which has drained to the TDLN, to be transferred between tumour-conditioned lymphatics and tumour-derived DCs. This is in line with recent published work which describes migratory DC antigen uptake from lymphatics and subsequent T-cell priming¹²⁴. This study was not however conducted in a tumour model, and hence our work extends upon their initial findings. As this work does not however account for possible changes in drainage of peripheral lymphatics or lymph node afferent lymphatic vessels, the differences in detected OVA and DQ-OVA is only explained in the context of LEC/DC capacity to uptake and process. However, these are critical factors in antigen drainage and delivery, in addition to other biophysical factors, which must be investigated in future work. Reviewing these findings in light of the described role for Podoplanin in mediating physical interactions between LECs and DCs (Chapter 4), future work should also assess the capacity for antigen transfer between LECs and DCs in over-expressed and knockout Podoplanin models. If Podoplanin knockout did indeed demonstrate perturbed transfer of antigen, this would be a highly novel observation and would identify Podoplanin as a unique regulator of antigen-mediated immunity.

In terms of implications for anti-tumour immunity, we show migratory DCs which have acquired tumour antigen from lymphatics, reach the T-cell zone. Albeit delocalised DCs and perturbed entry in early TDLNs, this indicated that tumour-derived migratory DCs are equipped with antigen for T-cell priming. We do however see that *in vitro*, DCs that have acquired lymphatic antigen are incapable of priming T-cell proliferation to their full capacity when compared with control DCs primed directly with antigen. Further investigation with a range of antigen concentrations suggested that this lack of T-cell proliferation was independent of the level of antigen taken up by DCs, as control DCs with low concentrations of antigen were still able to prime T-cell proliferation. Hence, despite lacking a more mechanistic investigation into why DCs do not induce T-cell proliferation *in vitro*, we do demonstrate differential T-cell responses *in vitro* between DCs that have or have not been conditioned by lymphatics. This contradicts findings by Kedl et al., whom described maintained T-cell priming functionality in DCs that acquired antigen from lymphatics¹²⁴. However, as their investigations in to T-cell proliferation used *in vivo* models, results cannot be directly

compared with those obtained with the *in vitro* OVA model used in this thesis. Further investigation into T-cell proliferation and viability *in vivo* would be needed to elucidate more precisely the role of lymphatic-dendritic cell crosstalk in early TDLNs.

Having established antigen transfer and potential loss of T-cell priming functionality *in vitro*, we looked to determine the phenotype of migratory DCs that had reached the T-cell zones *in vivo*. From PCR array profiling and flow cytometry data, we could conclude that migratory TRITC DCs appeared to retain their maturation and activation status, with expression of CD40, CD80 and CD86 confirmed in early TDLNs. Furthermore, their antigen processing capacity appeared retained which supports our preliminary findings that migratory DCs can uptake and process antigen from lymphatics at the sinus before traversing into the T-cell zone. A key difference observed in early TDLNs was perhaps the precise localisation of migratory DCs within the cortex (Figure 5.2, 5.3) and their chemotactic profiles (Figure 5.19). Interestingly, we saw DCs near the B-cell edge and around HEVs, which often are populated with naïve T-cells. Often naïve T-cells enter LNs from the circulation and seek out antigen-bearing DCs. If migratory, tumour-antigen bearing DCs are localised at the main entrance point to the LN, then the likelihood of exposure to antigen and subsequent priming is high. Marrying this with the array data, the stark increase in CC19 expression in migratory DCs from early TDLNs, does indeed indicate that migratory DCs are preferentially attracting naïve T-cells. Upon analysis of T-cell populations, increases in CD4, CD8 and more specifically FoxP3 T-cells were seen in Day 7 TDLNs (+2 days from our observations). This suggests that there is either an intrinsic switch towards a regulatory phenotype or that more regulatory T-cells are entering early TDLNs from the periphery. Further investigations into precise T-cell kinetics in TDLNs across tumour development and reciprocal mechanistic work to examine the precise role of lymphatic-conditioned DCs in T-cell kinetics is needed to shed light on whether these preliminary findings are merely correlative or are indeed causal.

In an attempt to dig further into the possibly mechanistic drivers of tolerance in TDLNs, we found expression of both PD1 and ligand, PDL1, to be equally expressed in control and early TDLNs. As this axis is often over-represented in the tumour microenvironment, driving effector T-cell deletion and maintenance of Treg phenotypes, we expected this axis to be altered in favour of suppression in TDLNs.

We hypothesised over-expression of one or both components of this axis, however found no change in expression across stromal and immune compartments. This suggests that either a permissive environment, that ordinarily maintains homeostatic immune balance is maintained and hence causing unwanted tolerance in early TDLNs, or alternatively may not be playing an important role in the establishment of a tolerogenic environment. Other molecules such as CTLA-4 have been identified as the preferential mechanism of induced tolerance in the node, with the PD1-PDL1 axis proposed to be more important for T-cell deletion at the primary tumour. We would hence need to do a more thorough examination of migratory DC phenotype in TDLNs to better understand their immunogenic capacity. Furthermore, as early TDLN immune kinetics are poorly understood, this data simply outlines a characterisation of migratory DCs in early TDLNs from B16-F10 melanomas. A finer analysis of their phenotype and how it changes with time and in line with changes at the primary tumour is imperative to concluding the role of migratory DCs in early immune response development. A clear *in vivo* phenotype would then allow for accompanying *in vitro* and *in vivo* models that utilise lymphangiogenic tumours, to determine the relative contribution of lymphatics to this early migratory DC phenotype.

CHAPTER 6

DISCUSSION

6. General Discussion

6.1. Project rationale and overview

Tumour progression is a complex process requiring not only proliferation of and evolution of tumour cell populations, but also contribution from “normal” stromal cells. The stromal compartment within the tumour microenvironment comprises of both immune and non-immune cells, namely fibroblasts, blood endothelial cells and lymphatic endothelial cells. The involvement of the stromal compartment in health and disease has been the focus of much research in recent years. Within the tumour microenvironment, the immune compartment is accepted to be dysfunctional, with suppression of anti-tumour immune responses described in a number of cancers. Despite establishing an understanding of some of the mechanisms contributing to immune suppression, the changes occurring early on in tumour development that define the immune landscape and set the scene for tumour progression are poorly understood. In addition to the temporal aspect of immune suppression, the spatial element must also be understood, with significant gaps on the role of TDLNs in anti-tumoural immunity remaining. Considering that lymph nodes function as immune hubs, but are also major sites of metastasis, there exists an unmet need to determine how tumour-associated tissues contribute to immune dysfunction from early phases of tumour development, ultimately allowing disease progression.

The extent of dysfunction of the non-immune stromal compartment in comparison remains unclear. The identification of LEC-specific markers has facilitated a growing field of research on the role of lymphatic vasculature in the tumour microenvironment. The lymphatics are now accepted to be active facilitators of tumour metastasis, with the VEGF pathway and several chemokine pathways identified as critical for tumour-lymphatic communication. In addition, the expansion of the lymphatic network is a characteristic of many cancers, in particular melanoma, which is considered to be both a highly lymphangiogenic and highly immunogenic cancer. Following the newly established role for lymphatics in immune modulation, we broadly aimed to determine the role of lymphatics in modulation of the anti-tumour response. However, as the lymphatics are the primary source of communication between primary tumours and

TDLNs, we focused on events occurring at TDLNs, hypothesising that LECs would contribute to conditioning of TDLNs and immune dysfunction from early disease. Together this thesis aimed to address the combined need for better spatial and temporal understanding of mechanisms underpinning immunity in the tumour microenvironment.

To do this we sought to determine the functional changes occurring in lymphatics in TDLNs and whether these changes had implications for immunity. With an interest in temporal restraints, we also wished to conduct analysis in TDLNs from **early** and **late** stages of disease, to understand when precisely these changes were occurring. Finally, due to the evidence highlighting lymphatic involvement in melanoma and the immunogenic nature of melanoma tumours, these investigations were conducted in the context of melanoma.

6.2. Lymphangiogenesis in the tumour microenvironment

To assess changes in TDLN-derived lymphatics in melanoma, we used a well-established injectable murine model of melanoma. Alongside colleagues, gross changes to TDLNs were reported with significant expansion of all non-immune stromal compartments in TDLNs from late, well-developed tumours. However, lymphangiogenic responses in particular appeared to be initiated earlier in tumour development, with increasing trends in LYVE-1 coverage observed from Day 4 prior to the established networks of Day 11 TDLNs. This was mirrored at the primary tumour where peritumoural lymphatics were often seen expanded in later tumours, in line with previous work demonstrating lymphangiogenesis in melanoma^{130, 126}, breast^{127,131} and non-small lung cancer¹³². These findings were also consistent with studies reporting incidence of lymphangiogenesis in TDLNs¹³⁸, however our initial findings took these observations beyond “pre-metastatic” to define the temporal contributions of LN lymphangiogenesis which was seen very early on in pre-metastatic TDLNs. Our findings also clearly demonstrate capacity for all stromal compartments of the TDLN to respond to factors draining from the tumour, highlighting a susceptibility to adapt. Furthermore, as TDLNs were robustly altered across time, with no evidence of this being a transient change and recovery to former homeostatic states, we demonstrate

that TDLNs retain an “altered phenotype” for as long as they can communicate with and drain from tumours. To this end, it would be exciting to determine how tumour resection impacts downstream lymph nodes and whether stromal cells within either exhibit a sense of plasticity returning to former states (as for infection²⁴⁶) or retain functional alterations upon removal of tumour derived stimuli.

These findings provide further insight as to when during tumour development a prominent lymphangiogenic signature develops. This has obvious implications for stratifying therapeutic intervention, as critical windows for therapy may in fact be much earlier on in disease progression. Considering further the consequences of blocking lymphangiogenesis in melanoma; as well as blocking the metastatic pathway^{94,145,247,248} recent published findings suggest lymphangiogenesis as a novel determinant for immunotherapy susceptibility^{249,189}. As we demonstrate here that lymphatics are indeed key modulators of immunity in the tumour microenvironment, potential anti-lymphangiogenic therapies must also consider side-effects on the immune response and thus combinatorial immunotherapies approaches may also be required for effective treatment strategies. Finally, as we have identified lymphatic changes in TDLNs from early disease stages, it may be the case that lymph node biopsies, routinely collected in the clinic, could be used to determine immune status, and extent of lymphatic involvement used to predict risk of metastasis.

In addition to characterizing gross lymphatic changes, transcriptional analysis of LECs from early and late TDLNs revealed many altered canonical pathways, mostly categorized into endothelial biology and immune associated pathways. As our hypothesis outlined a role for lymphatics in anti-tumour immunity, we focused on the immune changes occurring in both Day 4 and Day 11 TDLNs, with the expression of *Gp38*, *Ccl21* and endothelial junctional molecules *Jam3*, *Cdh5* and *Cldn11* all significantly altered. These genes all play critical role in successful immune cell trafficking. Lymphatics are well understood to facilitate migration of dendritic cells^{45,25,63} and reviewed in²⁵⁰ and novel findings have extended this to T-cell and neutrophil trafficking^{49,50,51}. As dendritic cells are essential for mounting an immune response once they've arrived at LNs, we concluded that altered expression of these gene targets in TDLN-derived LECs is likely to affect DC migration and hence DC-mediated immunity. We hence hypothesised that functional lymphatic changes would impact DC

migration in early TDLNs. Indeed, a number of studies report altered DC migration and behaviour in the context of perturbed lymphangiogenesis^{190,189,251,249,252}, and a wealth of evidence indicates the importance of CCL21 and endothelial junctions in regulating directional migration and transmigration^{57,63,253}.

Upon verification of these changes, we confirmed increased Podoplanin expression in LECs derived from Day 4 TDLNs at the protein level, however CCL21 appeared to be unchanged. As immunofluorescent analysis was used to visualise CCL21 this analysis did not tell us whether the relative lymphatic contribution was changed. Instead, our data highlighted trends in total CCL21 as both FRCs and LECs derived CCL21, and additional CCL21 drained from the periphery would be detected. In future, we could employ methods such as RNA Scope to quantify both localisation and levels of RNA production in TDLNs. However, to more specifically measure the relative importance of lymphatic-derived CCL21 in dendritic cell migration *in vivo*, we would require genetically modified mouse models with lymphatic-specific promoters, such as *Prox1* or *LYVE-1*. This would give us clearer insight into the functional significance at a protein level of down-regulated expression in TDLN-derived LECs and would highlight significance relative to other stromal populations, which also produce CCL21. This approach would also be needed to translate verified changes in junctional molecule expression, as qRT-PCR served to confirm trends observed in the microarray. This would particularly give insight into whether junctional changes in lymphatics affected overall permeability of LNs, antigen exposure across LN compartments and immune cell trafficking. Using these systems on a tumour background give us critical information regarding the functional contributions of lymphatic changes in tumour progression.

Further to this, we utilized TCGA data as a first line correlation with clinical samples. This approach identified *Gp38* as one of the only gene targets to positively correlate with dendritic cell infiltrate in TDLNs from melanoma patients, as *Ccl21* and *Jam3*, as well as many of the top up- and down-regulated gene targets did not significantly correlate. We acknowledge that as these TCGA samples have been acquired through biopsy and have a unified approach to RNA profiling, there is likely to be inaccuracies and poor detection of expression in some cases. However, despite this, the TCGA data does support the notion of Podoplanin as a mediator of DC infiltrate and

encourages further investigation into the role of lymphatic Podoplanin in DC migration in early TDLNs.

Collectively, these gross observations highlight a functional change in lymphatics in both **early** and **late** TDLNs, with temporal changes indicating distinct alterations at different phases throughout tumour development. Although transcriptional profiling of LECs has been conducted on peripheral lymphatics from fibrosarcoma ¹, this is the first study to transcriptionally characterise LECs in TDLNs and more specifically the first to characterise these changes over time. It is interesting to note that our dataset from lymph nodes, and that from the tumour exhibited some similarities, such as differential junctional molecule expression alluding to degrees of commonality between tumour models and across tissue sites. Investigation into site-specific and tumour-specific differences in lymphatic alterations would be a highly useful tool that would provide further context to our findings and provide critical insight into the role of lymphatics across tumour types and across the tumour microenvironment.

6.3. Modulation of DC migration in TDLNs mediated by Podoplanin positive lymphatics

Having identified alterations in TDLN-derived LECs that had implications for DC trafficking, we sought to explore the potential cross-talk between DCs and tumour-conditioned LECs. From the microarray data, Podoplanin emerged as a potential candidate for regulation of DC trafficking in LECs. This was supported by recent publications demonstrating that Podoplanin on LN-FRCs interacted with CLEC-2-expressing DCs ⁷⁷, and secondly demonstrating the importance of Podoplanin in lymph node infiltrate through lymphatic-specific knockout models ²³⁷. CLEC-2 knockout models further showed decreased lymphatic vessel entry in the peripheral tissues, indicating both a peripheral and lymph node role for Podoplanin⁷⁷. Both studies indicated engagement of the Podoplanin-CLEC2 axis in migration of DCs from the periphery to the lymph node, with the former highlighting the role of FRC-expressed Podoplanin⁷⁷ and the latter highlighting the role of LEC-expressed Podoplanin²³⁷. This indicated a function for Podoplanin across stromal compartments, across sites (periphery vs. lymph node) and in DC transmigration and trafficking. Thus,

the observation that expression of Podoplanin on LN-LECs was increased in early TDLNs at both RNA and protein level, we hypothesised that up-regulated Podoplanin expression was essential in mediating physical interactions between LECs and DCs in the extended tumour microenvironment.

Firstly, assessment of tumour-derived DC migration in early TDLNs *in vivo*, showed that migratory DCs clustered at the subcapsular sinus of Day 4 TDLNs. As migratory DCs were detected in the T-cell zones, we concluded that this phenotype was suggestive of enhanced interactions between incoming tumour-derived DCs and lymphatics at the subcapsular sinus. Modelling these interactions *in vitro* with splenic DCs expressing CLEC-2 and with TCM conditioned LECs we recorded an anchorage phenotype with DCs exhibiting enhanced adhesion, decreased transmigrating and mobility, and altered morphology. As this was a defined window of observation we could conclude that during the duration of the assay, DCs were physically interacting with LECs *in vitro* for prolonged durations of time, even though junctional integrity was likely compromised. This recapitulated our *in vivo* observations and suggested that tumour-derived factors condition lymphatic endothelium in favour of promoting prolonged physical interactions with DCs. Neutralization of LEC Podoplanin *in vitro*, resulted in decreased DC adhesion indicating that Podoplanin could indeed mediate these physical interactions. It is not known whether the Podoplanin antibody used for these assays binds the active binding site of CLEC-2, the glycosylated T34 amino acid in the PLAG domain, or if facilitates Fc-mediated anchoring. Podoplanin blockade may therefore reduce the number of migrating DCs through diminishing the number of CLEC-2 binding sites or by anchoring DCs to the endothelium layer. How the 8.1.1 clone antibody binds Podoplanin and the consequent effect on CLEC-2 ligation and DC migration, must therefore be investigated further. Experiments using different Podoplanin clones, non-specific antibodies and CLEC-2 blocking antibodies would assist in answering this question by ensuring the blockade is specifically perturbing interactions through the Podoplanin-CLEC2 axis.

Collectively, these results indicated that tumour-derived factors drive up-regulation of Podoplanin expression on lymphatics and this up-regulation likely promotes prolonged interactions between lymphatics and DCs. At the lymph node where observations were based, this has implications for DC entry into the node and potentially other

aspects of DC-mediated immunity. At the periphery, which was not addressed in this thesis, it may be the case that Podoplanin is acting as a facilitator of lymphatic vessel entry²³⁷. This notion is supported by *in vivo* observations in basal settings⁷⁷ and extends upon findings that other lymphatic markers, namely LYVE-1, also mediate lymphatic entry of DCs in the periphery⁵².

While we have shown that CLEC-2 is expressed on a population of splenic DCs, and to a lesser extent LN-derived DCs, an extensive characterisation of CLEC-2 expression on the subpopulations of migratory DCs is required. As CLEC-2 was less detectable in LN-derived DCs, CLEC-2 may be a feature of migratory, mature DCs. This would explain why in resting LNs, little CLEC-2 was detected. In the context of *in vivo* settings, whether CLEC-2 is restricted to skin-derived DC populations acting as a feature which enables DCs to migrate away from the periphery, must be elucidated. A study exploring CLEC-2 expression and detection of CLEC-2, using the same antibody clone as used in this thesis found CLEC-2 to be mostly expressed by mature, migratory DCs, further enforcing the role of CLEC-2 to be routed in migratory phenotypes^{77,254}. Beyond DCs, neutrophils also express CLEC-2 in the form of a phagocytic receptor²⁵⁵, however following identification that neutrophils use lymphatics to traffic to lymph nodes⁵¹, it may also be the case that the Podoplanin-CLEC2 axis is critical for lymphatic migration of other immune populations in health and disease. Use of single-cell RNA sequencing and proteomic analysis of *in vivo* derived tissue samples from a range of anatomical sites in healthy conditions, would help identify the basal expression of CLEC-2 across immune populations and hence their relative capacity to interact with Podoplanin and the influence that has on trafficking. Conducted in inflammatory or disease states, this would provide a much clearer understanding of the role of the Podoplanin-CLEC2 axis in immune trafficking in response to certain stimuli. In particular, investigation into the Podoplanin-CLEC2 axis in the tumour microenvironment is needed, as factors from the developing tumour may influence levels of CLEC-2 on immune cell subsets in the tumour microenvironment. As we have shown, lymphatics in the tumour microenvironment are transcriptionally altered in response to factors in the milieu, with Podoplanin up-regulated in response to B16-F10 factors. Hence, factors from the tumour microenvironment may reciprocally alter the expression of CLEC-2. *In vivo* profiling of myeloid subsets in skin versus early and late tumours, with matched draining lymph

nodes, would determine whether CLEC-2 expression is altered in healthy versus disease states in primary and draining tissue sites. If accompanied by *in vitro* assays, the driving factor for CLEC-2 expression changes at RNA and protein level, could be determined using single factor administration e.g. culture with a cytokine, or by using conditioned-media from cultured cells e.g. B16-F10 tumour conditioned media or CAF conditioned media. Furthermore, as CLEC-2 expression has been recently reported to be regulated by tetraspanins²⁷⁶, upstream signalling events and potential co-operative interactions add further levels of complexity to Podoplanin-CLEC2 mediated lymphatic migration. In addition to the unknown impact of tumour microenvironment factors on CLEC-2 expression, little is known of the impact on lymphatic derived chemokines and the expression of chemokine scavengers, for which both govern DC migration. *In vitro* experiments determining the role of the Podoplanin-CLEC2 axis must hence be conducted in the presence or absence of a chemotactic gradient to better capitulate *in vivo* settings and determine the independence or cooperativity of the Podoplanin-CLEC2 axis and lymphatic chemokines in DC migration. *In vivo* disruption to chemokine signalling in conjunction with perturbed Podoplanin signalling, on a tumour background, would support this line of investigation. Finally, as Podoplanin is known to bind CCL21²⁵⁶, the Podoplanin-CLEC2 axis and related DC migration patterns may be interlinked with CCL21 signalling and must be explored.

Having established a role for Podoplanin in DC interactions with lymphatics and identified tumour-derived factors as regulators of Podoplanin expression, we explored whether targeting Podoplanin expression influenced DC migration in the tumour microenvironment. Using antibodies previously described in Podoplanin targeting *in vivo*⁷⁷, we trialled an *in vivo* blocking regime in B16-tumour bearing mice. Results were variable across independent experiments with no significant changes seen in DC migration from tumours to early TDLNs. As blocking antibody was administered subcutaneously and could hence bind Podoplanin on a number of Podoplanin expressing stromal cells, it may be the case that these results are being confounded by targeting other cells. It may also be the case that the blocking regime itself requires further optimization; within the window of 18hr migration, the rate at which DC bind LEC Podoplanin, the duration of these interactions and the kinetics of Podoplanin turnover are not known. Finally, *in vitro* settings where this antibody successfully perturbed DC interactions and initial observations of TCM-induced Podoplanin up-

regulation were controlled and restricted to dermal LECs being exposed to blockade antibody or B16-F10 tumour conditioned-media which drove up-regulation of Podoplanin protein expression. However *in vivo*, there are many factors which could influence expression of Podoplanin on primary and lymph node lymphatics, as well as possible effects on reciprocal CLEC-2 expression, as discussed above. Hence the kinetics of Podoplanin expression, blockade and consequent DC physical interactions are likely to be different and mechanistically more complex. We hence utilised an *in vivo* knockout model, with the rationale that ablating RNA expression would more robustly affect Podoplanin expression and subsequent interactions at the protein level. Although a hypomorph, the PDPN-FL model, used in a number of published studies^{257, 258}, enabled *in vivo* titration of Podoplanin levels (heterozygous vs, homozygous) in tumour-bearing mice. We hypothesised that in the absence of Podoplanin, DC trafficking to TDLNs would be perturbed. Indeed, in homozygous mice, this was seen to be the case with markedly reduced migration of tumour-derived DCs. However, this was not observed in heterozygous mice, where both immunofluorescent and flow cytometry analysis yielded no differential patterns between wild type and heterozygous mice in terms of migratory DC infiltrate and localisation in early TDLNs. We believe that as heterozygous mice still have one Podoplanin allele, this is sufficient to translate protein and hence results in a lack of functional inhibition of DC trafficking. This is an important observation to make, as it informs future genetic targeting studies, with knockdown not being sufficient to have a prominent influence on immune trafficking. However, as this is not a lymphatic-specific Podoplanin knockout model, there are limitations to these observations. With global knockout of Podoplanin, come reduced litter viability, mixed blood and lymphatic vasculature and defected lymph node architecture, thus for any further studies we would want a lymphatic-specific knockdown model, such as the PROX-1 promoter knockdown model used by Watson and colleagues²³⁷. It would also be interesting to develop a conditional knockout model, whereby lymphatic Podoplanin could be targeted at different stages of tumour development, to truly highlight the temporal relevance of Podoplanin in the developing immune response. Furthermore, a recent study characterizing subpopulations of lymphatics in the lymph node¹²³, could be utilised to develop more complex knockout models that, for example, specifically target Podoplanin expression in lymphatics of the subcapsular sinus. The same could be applied to the periphery if better subpopulation characterisation was conducted.

Overall, these approaches would inform us not only of the temporal contributions of lymphatic Podoplanin in DC migration, but also of location specific roles. As mounting an immune response involves a series of complex processes and there are therapies that rely on effective DC migration to TDLNs, such as DC vaccines²⁵⁹, it is critical to understand the path that DCs and other immune cells take in their attempt to prime the immune system. Defining the molecular mechanisms involved, such as interactions with Podoplanin, would hence provide a crucial part of the puzzle.

6.4. Lymphatics as modulators of antigen-mediated immune priming

Further to the implications of lymphatics in modulating DC trafficking, lymphatics have also been shown to engage in antigen processing and presentation. In fact, very recent publications have shown LN lymphatics can transfer antigen to DCs, and more specifically to incoming migratory DCs^{120,124}. We show in this thesis that LECs exposed to antigen *in vitro*, can indeed transfer antigen to DCs in a manner that is dependent on physical contact. Despite microarray data implying altered antigen processing and presentation functionality in LECs, TCM-conditioning did not alter capacity to transfer, hence DCs that interacted with TCM-conditioned lymphatics took up as much antigen as those that interacted with control treated lymphatics. However, since more DCs interacted following TCM treatment, more LEC-derived antigen was ultimately transferred to immune cells. This extends upon the current literature, as it not only demonstrates antigen transfer in resting states, but also shows this mechanism occurs in tumour conditioned settings. To recapitulate this *in vivo*, we used fluorescent-conjugated antigens to track antigen uptake and processing in the lymph node. By injecting mice with antigen prior to TRITC painting this ensured that tumour-derived DCs had not come into contact with fluorescent antigen prior to arriving at the lymph node. This approach highlighted lymphatics as the dominant compartment to uptake and process antigen, implying that a major source of antigen in the node is indeed the lymphatics. We were able to detect antigen transfer to migratory DCs *in vivo*, however due to the properties of DQ-OVA, we were limited in what we could detect by flow cytometry; in this case, we have a window of optimal proteolytic processing where antigen can be detected between lymphatic and immune compartments, but neither full-length of fully digested antigenic peptide is fluorescent.

This is however, the first attempt to track antigen transfer in early TDLNs, and hence this preliminary data acts as a foundation to build upon in future experiments.

Bringing these observations back to the concept of prolonged interactions, we also do not know if kinetics of DC transit or the source of antigen can impact antigen processing and presentation. Our localisation analysis implies that through prolonged interactions at the subcapsular sinus, there is less T-cell zone coverage of migratory DCs, and hence perhaps fewer antigen-loaded DCs to interact with. However, whether the antigen taken up by DCs through these prolonged interactions has a differential impact on T-cell priming *in vivo* was not elucidated in this thesis. We did however demonstrate that DCs that underwent prolonged interactions with lymphatics *in vitro* were less able to stimulate T-cell proliferation. This implies that after prolonged interactions with lymphatics in early TDLNs, DCs subsequently migrate into more peripheral areas of T-cell zones and with a diminished capacity to prime T-cells. Interestingly, upon profiling of a panel of maturation, activation markers and death ligands at both RNA and protein levels, migratory DCs in early TDLNs are mature and activated and hence should be capable of mounting an immune response. This is opposite to the reported data pertaining to DC maturation and activation in primary tumours, which describe DCs as being immature and poor immune stimulators^{260,185}. Hence, in light of canonical maturation markers being expressed and the apparent distinction between lymph node and tumour DC profiles, it may be the case that the immune response can be inhibited independently of maturation. Indeed, our data suggests that migratory DC localisation and lymphatic exposure could be distinguishing features of a mounting immune response in TDLNs. A number of studies have demonstrated that localisation in the node is defined by DC subtype, with dermal CD11b+ DCs found to localise at the B-cell follicle/T-cell zone interface, with epidermal DCs migrating later and localising further into the T-cell zone²¹⁸. Due to varying capacities to antigen uptake present and cross present across DC subtypes, DC localisation is hence important in defining the type of immune response mounted. Further investigation into the subset of migratory DC that interacts for prolonged periods with lymphatics, and the subset specific localisation of migratory DCs in early TDLNs is needed to understand better the functional implications of these localisation phenotypes observed.

6.5. Driving factors involved in altered lymphatic and DC behaviour in the tumour microenvironment

As the changes to lymphatics and subsequent DC behaviour was restricted to TDLNs, it would next be key to elucidate the factors derived from the tumour microenvironment driving the observed changes. As the primary tumour microenvironment has a complex cellular composite and with dynamic biophysical and biochemical signals, we can assume that the changing biophysical and biochemical cues are also important at the TDLNs. From the literature and signatures in our microarray data, a few specific factors can be identified as likely players in lymphatic transformation.

Firstly, B16-F10 tumour cells produce a number of cytokines and other soluble factors. Proteomic analysis across tumour development of B16-F10 tumour cells growing in C57BL/6 mice, observed expression changes in proteins involved in inflammation, wound healing and chemotaxis²⁶¹. In addition, B16-F10 derived VEGF and TGF- β was found to contribute to immune tolerance with silencing found to revert tolerance and inhibit tumour growth and Treg accumulation in TDLNs, and alter immune infiltrate phenotypes²⁶². Interestingly, silencing of VEGF and TGF- β brought about separate transcriptional signatures in both early and late B16-F10 tumours, suggesting they have independent targets within the tumour microenvironment, with stage dependent implications also²⁶². Braf^{V600E} cells cultured *in vitro* were also found to express higher levels of IL-6, IL-8 and MMP-1, which promoted stromal transformation in the tumour microenvironment²⁶³. Indeed, our group has performed preliminary analysis of B16-F10 TCM and B16F-10 *in vivo* tumour secretomes revealing high levels of TGF- β ; an acknowledged driver of lymphangiogenesis¹⁰⁹, identifying this as a potential driver of lymphatic expansion in TDLNs. In addition, both TGF- β and IL-3 have been shown to regulate Podoplanin expression^{264,265}, identifying further factors that could be driving these changes in TDLNs. In light of this, future work should explore the role of tumour-derived TGF- β in Podoplanin expression. This could be achieved in the first instance by exposing *in vitro* LECs to recombinant TGF- β to determine the direct impact on Podoplanin expression at gene and protein level. In order to determine the relative contribution of B16-derived TGF- β , repeated quantification is required and could be mirrored using Braf-tumours to determine the exclusivity of TGF- β production in melanoma tumours. Determining the role of *in vivo* TGF- β in Podoplanin expression

in the tumour microenvironment, both on CAFs and FRCs/LECs in TDLNs, would require *in vivo* blockade or injection of TGF- β knockout B16-tumour cells.

Additional inflammatory signatures were observed in the TDLN-LEC microarray data, revealing altered expression of a number of IFN receptors and TLRs. This suggests potential functional responsiveness to IFN cytokines as well as tissue-damage products and danger-associated molecular patterns (DAMPs). As wound-healing signatures arise in both our microarray and B16-F10 tumours²⁶¹, it may be the case that wound-healing responses are the drivers of lymphatic and broader lymph node changes across early and late TDLNs. Further investigation into the precise drivers of particular aspects of lymphatic alterations is needed, as the drivers of different lymphatic changes are likely to be different. Future work must not simply investigate tumour cell-derived factors as drivers of lymphatic changes, but also immune cell-derived factors, as tumours are composites of immune cells as well as tumour cells, in particular melanoma tumours which are very rich in myeloid cells¹⁵². This could be conducted by assessing lymphatic changes in TDLNs of tumour-bearing transgenic mice, such as lysM-Cre/DTR mice which lack skin tissue and wound macrophages.

Lymphatics are also capable of mechanosensing, thus are susceptible to biophysical factors such as increased fluid flow²⁶⁶. It is well documented that changes in biophysical environment of tumours brings about changes in lymphatic drainage and lymphangiogenesis in the primary tumour site and associated lymph nodes. However, the biophysical impact on other functional transformations is unknown and must be explored further.

In addition to factors derived from the tumour microenvironment that influence lymphatic behaviour, much research is needed to assess the lymphatic secretome; how that changes upon tumour conditioning and its consequent influence on the tumour microenvironment. Literature suggests that factors such as anti-inflammatory factor, prostaglandin-E2, secreted in the tissue microenvironment by lymphatics can lead to decreased dendritic cell maturity²⁵¹. Aside from this study and the well-documented role of lymphatic derived chemokines in immune cell trafficking^{25,62,63,65,66,230,231}, little is known of the influence of lymphatic secretome on

immune cells. This is hence an area to pursue, with lymphatic secretome profiling in healthy and tumour states needed.

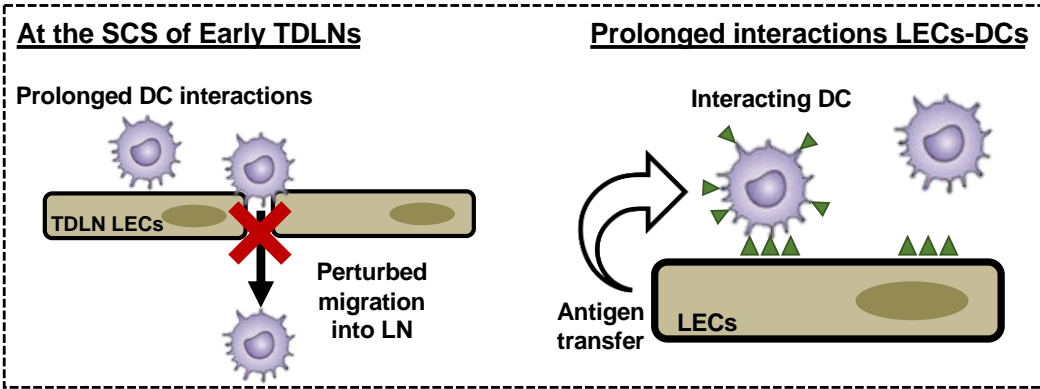
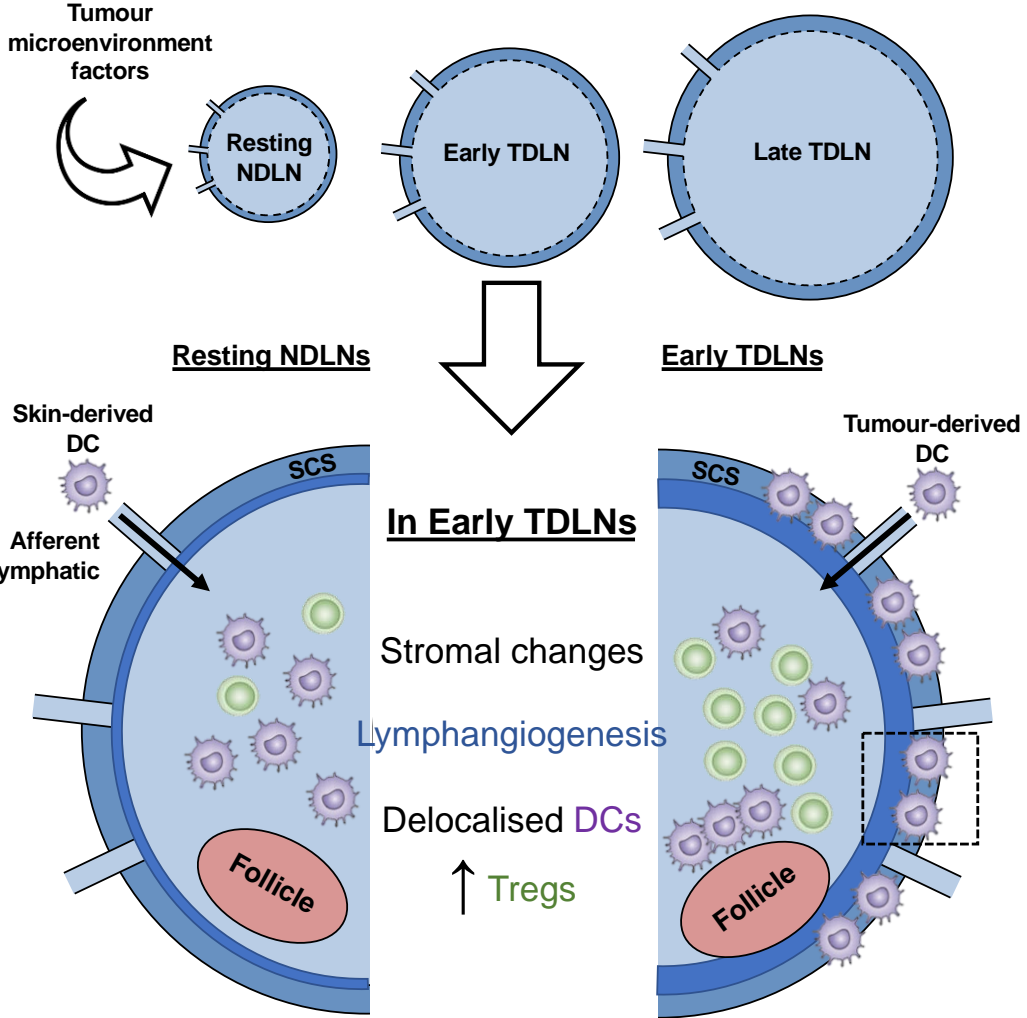
6.6. Summary and Future Perspectives

I have identified in this thesis an important role for tumour-associated lymphatics in modulating the anti-tumour immune response in TDLNs. I first demonstrate that early changes in TDLNs, downstream of B16-F10 tumours, result not only in gross architecture changes to the lymphatic network but functional changes also at a transcriptional level. Upon verification of key transcriptional changes, I next demonstrated TDLN-LECs to exhibit altered expression of critical gene targets involved in immune trafficking. Using the TRITC *in vivo* model with B16-F10 syngeneic tumours, I further show that these transcriptional changes manifest in altered localisation of migratory tumour-derived DCs in early TDLNs. Further functional analysis *in vitro* and *in vivo* identified a process by which B16-F10 tumour-derived factors drive an altered migratory phenotype in DCs interacting with lymphatics. Mechanistic analysis and microarray verification showed this mechanism to be driven by up-regulated expression of Podoplanin on tumour-conditioned lymphatic endothelium. As DCs were shown to express CLEC-2 and literature has shown migratory DCs to traffic to LNs through CLEC-2 expression, I show for the first time that the Podoplanin-CLEC2 axis is critical in trafficking of tumour-derived DCs in early stages of tumour development. Further elucidating other functional implications of prolonged interactions between DCs and LECs in the tumour microenvironment, I demonstrated drained antigen to be predominantly taken up by the lymphatic compartment in both resting NDNLs and TDLNs. Next, I demonstrated that this lymphatic antigen could be passed to interacting DCs; a process found to be dependent on physical interaction only. Preliminary *in vivo* studies using subcutaneously administered fluorescent-conjugated antigen in tumour-bearing mice supported these observations, with tumour-derived migratory DCs taking up lymph node-derived antigen upon arrival. Assessing the relevance of these interactions for the anti-tumour immune response, *in vitro* data demonstrated a lack of capacity to prime T-cells, in lymphatic-conditioned DCs despite DCs having taken-up antigen from antigen-pulsed lymphatics. *In vivo* observations further suggested that after prolonged interactions with lymphatics, tumour-derived DCs exhibit altered delocalisation relative

to T-cell zones and HEVs. T-cell dynamics in light of this were seen to favour expansion of FoxP3+ Tregs, which indicated altered DC priming post-lymphatic interactions.

Future work should focus on better modelling the Podoplanin-CLEC2 axis *in vivo* to highlight the functional relevance to specific subsets of DCs. These approaches should use lymphatic specific and conditional knockout to explore the specific lymphatic contributions within the tumour microenvironment, with temporal and spatial elements accounted for. In addition, due to the preliminary nature of these findings relating to antigen transfer and T-cell priming in the early developing tumour microenvironment, further *in vivo* is required to establish the kinetics of DC-mediated T-cell priming in early TDLNs, with corresponding *in vitro* experiments needed to shed light on how lymphatic-conditioning can further modulate this process. Overall, as this data demonstrates critical changes in lymphatics that have implications for immune modulation in early stages of tumour development, it is imperative to understand further how lymphatics can modulate the precise processes involved in mounting an anti-tumour immune response, with implications for both anti-lymphangiogenesis therapy and immunotherapy.

LN expansion during tumour development



-  Dendritic cell
-  Regulatory T-cell
-  Lymphatic endothelial cell
-  Subcapsular lymphatics
-  B-cell follicle
-  Lymphatic-derived antigen

Figure 6.1. Lymph node expansion and transformation during tumour development.

Using the injectable subcutaneous B16-F10 tumour model, we demonstrate that during tumour development (11 days) the brachial tumour-draining lymph node expands in size. In addition to size expansion, we observe stromal changes, both to the fibroblast reticular network¹⁹¹ and the lymphatic vasculature. Expansion of the lymphatic network, known as lymphangiogenesis, is seen in both early and late TDLNs, demonstrating this as an early arising and continue change which occurs throughout tumour development. This expansion is particularly prevalent at the subcapsular sinus (SCS) and in the medullary regions, accompanied with transcriptional changes, including many relating to immune function. Alongside expansion and immune function transcriptional changes, tumour-derived DCs cluster at the subcapsular sinus in early TDLNs and fail to permeate far into the T-cell cortex, unlike migratory patterns observed in control NDNLNs. Tumour-derived DCs which did reach the T-cell cortex were differentially localised and seen to cluster around the base of B-cell follicles, contrary to DC localisation in Control NDNLNs. At the subcapsular sinus, DC clustering appears indicative of prolonged physical interactions with the lymphatic endothelium, with supporting evidence from *in vitro* experiments, with the Podoplanin-CLEC2 axis identified as a likely candidate for promoting physical interactions. This appears to lead to perturbed or delayed migration into the lymph node, affecting coverage of DCs in T-cell zones. Prolonged interactions also resulted in enhanced antigen transfer and exchange between LECs and DCs, with LEC-conditioned DCs acting as poor T-cell primers. Regarding the T-cell compartment, analysis of T-cell populations across TDLNs, demonstrated a peak in expansion of FoxP3+ regulatory T-cells in early TDLNs (Day 7), indicative of a suppressive immune environment. Antigen presentation in lymph nodes is critical to development of a suppressive or active immune response and LEC-conditioning of tumour-derived DCs demonstrated a skew towards a suppressive phenotype *in vitro*. Expansion of FoxP3+ T-cells may therefore be resultant of LEC-DC interactions in early tumour-conditioned draining lymph nodes.

Bibliography

- 1 Clasper, S. *et al.* A novel gene expression profile in lymphatics associated with tumor growth and nodal metastasis. *Cancer Res* **68**, 7293-7303, doi:10.1158/0008-5472.CAN-07-6506 (2008).
- 2 Karnezis, T. *et al.* VEGF-D promotes tumor metastasis by regulating prostaglandins produced by the collecting lymphatic endothelium. *Cancer Cell* **21**, 181-195, doi:10.1016/j.ccr.2011.12.026 (2012).
- 3 Baluk, P. *et al.* Functionally specialized junctions between endothelial cells of lymphatic vessels. *J Exp Med* **204**, 2349-2362, doi:10.1084/jem.20062596 (2007).
- 4 Gerli, R., Solito, R., Weber, E. & Agliano, M. Specific adhesion molecules bind anchoring filaments and endothelial cells in human skin initial lymphatics. *Lymphology* **33**, 148-157 (2000).
- 5 Stacker, S. A. *et al.* Lymphangiogenesis and lymphatic vessel remodelling in cancer. *Nat Rev Cancer* **14**, 159-172, doi:10.1038/nrc3677 (2014).
- 6 Trzewik, J., Mallipattu, S. K., Artmann, G. M., Delano, F. A. & Schmid-Schonbein, G. W. Evidence for a second valve system in lymphatics: endothelial microvalves. *FASEB J* **15**, 1711-1717 (2001).
- 7 Mendoza, E. A Model for Mechanics of Primary Lymphatic Valves. *Journal of Biomechanical Engineering* **125**, doi:10.1115/1.1568128 (2003).
- 8 von der Weid, P. Y. & Zawieja, D. C. Lymphatic smooth muscle: the motor unit of lymph drainage. *Int J Biochem Cell Biol* **36**, 1147-1153, doi:10.1016/j.biocel.2003.12.008 (2004).
- 9 Quick, C. M., Venugopal, A. M., Gashev, A. A., Zawieja, D. C. & Stewart, R. H. Intrinsic pump-conduit behavior of lymphangions. *Am J Physiol Regul Integr Comp Physiol* **292**, R1510-1518, doi:10.1152/ajpregu.00258.2006 (2007).
- 10 Eisenhoffer, J., Kagal, A., Klein, T. & Johnston, M. G. Importance of valves and lymphangion contractions in determining pressure gradients in isolated lymphatics exposed to elevations in outflow pressure. *Microvasc Res* **49**, 97-110, doi:10.1006/mvre.1995.1008 (1995).
- 11 Sabin, F. On the origin of the lymphatic system from the veins, and the development of the lymph hearts and thoracic duct in the pig. *Am J Anat* **1**, 367-389 (1902).
- 12 Sabin, F. On the development of superficial lymphatics in the skin of the pig. *Am J Anat* **3**, 183-195, doi: 10.1002/aja.1000030205 (1904).
- 13 Banerji, S. *et al.* LYVE-1, a new homologue of the CD44 glycoprotein, is a lymph-specific receptor for hyaluronan. *J Cell Biol* **144**, 789-801 (1999).

- 14 Breiteneder-Geleff, S. *et al.* Angiosarcomas express mixed endothelial phenotypes of blood and lymphatic capillaries: podoplanin as a specific marker for lymphatic endothelium. *Am J Pathol* **154**, 385-394, doi:10.1016/S0002-9440(10)65285-6 (1999).
- 15 Wigle, J. T. *et al.* An essential role for Prox1 in the induction of the lymphatic endothelial cell phenotype. *EMBO J* **21**, 1505-1513, doi:10.1093/emboj/21.7.1505 (2002).
- 16 Podgrabska, S. *et al.* Molecular characterization of lymphatic endothelial cells. *Proc Natl Acad Sci U S A* **99**, 16069-16074, doi:10.1073/pnas.242401399 (2002).
- 17 Weninger, W. *et al.* Expression of vascular endothelial growth factor receptor-3 and podoplanin suggests a lymphatic endothelial cell origin of Kaposi's sarcoma tumor cells. *Lab Invest* **79**, 243-251 (1999).
- 18 Wilting, J. *et al.* The transcription factor Prox1 is a marker for lymphatic endothelial cells in normal and diseased human tissues. *FASEB J* **16**, 1271-1273, doi:10.1096/fj.01-1010fje (2002).
- 19 Petrova, T. V. *et al.* Lymphatic endothelial reprogramming of vascular endothelial cells by the Prox-1 homeobox transcription factor. *EMBO J* **21**, 4593-4599 (2002).
- 20 Hirakawa, S. *et al.* VEGF-A induces tumor and sentinel lymph node lymphangiogenesis and promotes lymphatic metastasis. *J Exp Med* **201**, 1089-1099, doi:10.1084/jem.20041896 (2005).
- 21 Wigle, J. T. & Oliver, G. Prox1 function is required for the development of the murine lymphatic system. *Cell* **98**, 769-778 (1999).
- 22 Johnson, N. C. *et al.* Lymphatic endothelial cell identity is reversible and its maintenance requires Prox1 activity. *Genes Dev* **22**, 3282-3291, doi:10.1101/gad.1727208 (2008).
- 23 Keuschnigg, J. *et al.* Plasticity of blood- and lymphatic endothelial cells and marker identification. *PLoS One* **8**, e74293, doi:10.1371/journal.pone.0074293 (2013).
- 24 Murfee, W. L., Rappleye, J. W., Ceballos, M. & Schmid-Schonbein, G. W. Discontinuous expression of endothelial cell adhesion molecules along initial lymphatic vessels in mesentery: the primary valve structure. *Lymphat Res Biol* **5**, 81-89, doi:10.1089/lrb.2007.1005 (2007).
- 25 Miteva, D. O. *et al.* Transmural flow modulates cell and fluid transport functions of lymphatic endothelium. *Circ Res* **106**, 920-931, doi:10.1161/CIRCRESAHA.109.207274 (2010).
- 26 Conway, D. E. *et al.* Fluid shear stress on endothelial cells modulates mechanical tension across VE-cadherin and PECAM-1. *Curr Biol* **23**, 1024-1030, doi:10.1016/j.cub.2013.04.049 (2013).

- 27 Coon, B. G. *et al.* Intramembrane binding of VE-cadherin to VEGFR2 and VEGFR3 assembles the endothelial mechanosensory complex. *J Cell Biol* **208**, 975-986, doi:10.1083/jcb.201408103 (2015).
- 28 Weis, S., Cui, J., Barnes, L. & Cheresh, D. Endothelial barrier disruption by VEGF-mediated Src activity potentiates tumor cell extravasation and metastasis. *J Cell Biol* **167**, 223-229, doi:10.1083/jcb.200408130 (2004).
- 29 Gavard, J. & Gutkind, J. S. VEGF controls endothelial-cell permeability by promoting the beta-arrestin-dependent endocytosis of VE-cadherin. *Nat Cell Biol* **8**, 1223-1234, doi:10.1038/ncb1486 (2006).
- 30 Eliceiri, B. P. *et al.* Selective requirement for Src kinases during VEGF-induced angiogenesis and vascular permeability. *Mol Cell* **4**, 915-924 (1999).
- 31 Behzadian, M. A., Wang, X. L., Windsor, L. J., Ghaly, N. & Caldwell, R. B. TGF-beta increases retinal endothelial cell permeability by increasing MMP-9: possible role of glial cells in endothelial barrier function. *Invest Ophthalmol Vis Sci* **42**, 853-859 (2001).
- 32 Rudini, N. *et al.* VE-cadherin is a critical endothelial regulator of TGF-beta signalling. *EMBO J* **27**, 993-1004, doi:10.1038/emboj.2008.46 (2008).
- 33 van Nieuw Amerongen, G. P., van Delft, S., Vermeer, M. A., Collard, J. G. & van Hinsbergh, V. W. Activation of RhoA by thrombin in endothelial hyperpermeability: role of Rho kinase and protein tyrosine kinases. *Circ Res* **87**, 335-340 (2000).
- 34 Wojciak-Stothard, B., Potempa, S., Eichholtz, T. & Ridley, A. J. Rho and Rac but not Cdc42 regulate endothelial cell permeability. *J Cell Sci* **114**, 1343-1355 (2001).
- 35 Clements, R. T., Minnear, F. L., Singer, H. A., Keller, R. S. & Vincent, P. A. RhoA and Rho-kinase dependent and independent signals mediate TGF-beta-induced pulmonary endothelial cytoskeletal reorganization and permeability. *Am J Physiol Lung Cell Mol Physiol* **288**, L294-306, doi:10.1152/ajplung.00213.2004 (2005).
- 36 Holinstat, M. *et al.* Suppression of RhoA activity by focal adhesion kinase-induced activation of p190RhoGAP: role in regulation of endothelial permeability. *J Biol Chem* **281**, 2296-2305, doi:10.1074/jbc.M511248200 (2006).
- 37 Shapiro, L. & Weis, W. I. Structure and biochemistry of cadherins and catenins. *Cold Spring Harb Perspect Biol* **1**, a003053, doi:10.1101/cshperspect.a003053 (2009).
- 38 Oas, R. G. *et al.* p120-catenin and beta-catenin differentially regulate cadherin adhesive function. *Mol Biol Cell* **24**, 704-714, doi:10.1091/mbc.E12-06-0471 (2013).
- 39 Clement, C. C. *et al.* An expanded self-antigen peptidome is carried by the human lymph as compared to the plasma. *PLoS One* **5**, e9863, doi:10.1371/journal.pone.0009863 (2010).
- 40 Fang, J. F. *et al.* Proteomic analysis of post-hemorrhagic shock mesenteric lymph. *Shock* **34**, 291-298, doi:10.1097/SHK.0b013e3181ceef5e (2010).

- 41 Clement, C. C. *et al.* Protein expression profiles of human lymph and plasma mapped by 2D-DIGE and 1D SDS-PAGE coupled with nanoLC-ESI-MS/MS bottom-up proteomics. *J Proteomics* **78**, 172-187, doi:10.1016/j.jprot.2012.11.013 (2013).
- 42 Hansen, K. C., D'Alessandro, A., Clement, C. C. & Santambrogio, L. Lymph formation, composition and circulation: a proteomics perspective. *Int Immunol* **27**, 219-227, doi:10.1093/intimm/dxv012 (2015).
- 43 D'Alessandro, A. *et al.* Dynamic changes in rat mesenteric lymph proteins following trauma using label-free mass spectrometry. *Shock* **42**, 509-517, doi:10.1097/SHK.0000000000000259 (2014).
- 44 Smith, J. B., McIntosh, G. H. & Morris, B. The traffic of cells through tissues: a study of peripheral lymph in sheep. *J Anat* **107**, 87-100 (1970).
- 45 Johnson, L. A. *et al.* An inflammation-induced mechanism for leukocyte transmigration across lymphatic vessel endothelium. *J Exp Med* **203**, 2763-2777, doi:10.1084/jem.20051759 (2006).
- 46 Sawa, Y. *et al.* Effects of TNF-alpha on leukocyte adhesion molecule expressions in cultured human lymphatic endothelium. *J Histochem Cytochem* **55**, 721-733, doi:10.1369/jhc.6A7171.2007 (2007).
- 47 Iwasawa, K., Kameyama, T., Ishikawa, H. & Sawa, Y. Induction of ICAM-1 and VCAM-1 on the mouse lingual lymphatic endothelium with TNF-alpha. *Acta Histochem Cytochem* **41**, 115-120, doi:10.1267/ahc.08017 (2008).
- 48 Chaitanya, G. V. *et al.* Differential cytokine responses in human and mouse lymphatic endothelial cells to cytokines in vitro. *Lymphat Res Biol* **8**, 155-164, doi:10.1089/lrb.2010.0004 (2010).
- 49 Teijeira, A. *et al.* T Cell Migration from Inflamed Skin to Draining Lymph Nodes Requires Intralymphatic Crawling Supported by ICAM-1/LFA-1 Interactions. *Cell Rep* **18**, 857-865, doi:10.1016/j.celrep.2016.12.078 (2017).
- 50 Rigby, D. A., Ferguson, D. J., Johnson, L. A. & Jackson, D. G. Neutrophils rapidly transit inflamed lymphatic vessel endothelium via integrin-dependent proteolysis and lipoxin-induced junctional retraction. *J Leukoc Biol* **98**, 897-912, doi:10.1189/jlb.1HI0415-149R (2015).
- 51 Arokiasamy, S. *et al.* Endogenous TNFalpha orchestrates the trafficking of neutrophils into and within lymphatic vessels during acute inflammation. *Sci Rep* **7**, 44189, doi:10.1038/srep44189 (2017).
- 52 Johnson, L. A. *et al.* Dendritic cells enter lymph vessels by hyaluronan-mediated docking to the endothelial receptor LYVE-1. *Nat Immunol* **18**, 762-770, doi:10.1038/ni.3750 (2017).

- 53 Braun, A. *et al.* Afferent lymph-derived T cells and DCs use different chemokine receptor CCR7-dependent routes for entry into the lymph node and intranodal migration. *Nat Immunol* **12**, 879-887, doi:10.1038/ni.2085 (2011).
- 54 Stoitzner, P. *et al.* Visualization and characterization of migratory Langerhans cells in murine skin and lymph nodes by antibodies against Langerin/CD207. *J Invest Dermatol* **120**, 266-274, doi:10.1046/j.1523-1747.2003.12042.x (2003).
- 55 Russo, E., Nitschke, M. & Halin, C. Dendritic cell interactions with lymphatic endothelium. *Lymphat Res Biol* **11**, 172-182, doi:10.1089/lrb.2013.0008 (2013).
- 56 Rantakari, P. *et al.* The endothelial protein PLVAP in lymphatics controls the entry of lymphocytes and antigens into lymph nodes. *Nat Immunol* **16**, 386-396, doi:10.1038/ni.3101 (2015).
- 57 Vaahtomeri, K. *et al.* Locally Triggered Release of the Chemokine CCL21 Promotes Dendritic Cell Transmigration across Lymphatic Endothelia. *Cell Rep* **19**, 902-909, doi:10.1016/j.celrep.2017.04.027 (2017).
- 58 Stoitzner, P., Pfaller, K., Stossel, H. & Romani, N. A close-up view of migrating Langerhans cells in the skin. *J Invest Dermatol* **118**, 117-125, doi:10.1046/j.0022-202x.2001.01631.x (2002).
- 59 Torzicky, M. *et al.* Platelet endothelial cell adhesion molecule-1 (PECAM-1/CD31) and CD99 are critical in lymphatic transmigration of human dendritic cells. *J Invest Dermatol* **132**, 1149-1157, doi:10.1038/jid.2011.420 (2012).
- 60 Bradfield, P. F. *et al.* JAM-C regulates unidirectional monocyte transendothelial migration in inflammation. *Blood* **110**, 2545-2555, doi:10.1182/blood-2007-03-078733 (2007).
- 61 Ballet, R. *et al.* Blocking junctional adhesion molecule C enhances dendritic cell migration and boosts the immune responses against *Leishmania major*. *PLoS Pathog* **10**, e1004550, doi:10.1371/journal.ppat.1004550 (2014).
- 62 Tal, O. *et al.* DC mobilization from the skin requires docking to immobilized CCL21 on lymphatic endothelium and intralymphatic crawling. *J Exp Med* **208**, 2141-2153, doi:10.1084/jem.20102392 (2011).
- 63 Russo, E. *et al.* Intralymphatic CCL21 Promotes Tissue Egress of Dendritic Cells through Afferent Lymphatic Vessels. *Cell Rep* **14**, 1723-1734, doi:10.1016/j.celrep.2016.01.048 (2016).
- 64 Ivanov, S. *et al.* CCR7 and IRF4-dependent dendritic cells regulate lymphatic collecting vessel permeability. *J Clin Invest* **126**, 1581-1591, doi:10.1172/JCI84518 (2016).

- 65 Bryce, S. A. *et al.* ACKR4 on Stromal Cells Scavenges CCL19 To Enable CCR7-Dependent Trafficking of APCs from Inflamed Skin to Lymph Nodes. *J Immunol* **196**, 3341-3353, doi:10.4049/jimmunol.1501542 (2016).
- 66 Ulvmar, M. H. *et al.* The atypical chemokine receptor CCRL1 shapes functional CCL21 gradients in lymph nodes. *Nat Immunol* **15**, 623-630, doi:10.1038/ni.2889 (2014).
- 67 Roozendaal, R. *et al.* Conduits mediate transport of low-molecular-weight antigen to lymph node follicles. *Immunity* **30**, 264-276, doi:10.1016/j.immuni.2008.12.014 (2009).
- 68 Saunderson, S. C., Dunn, A. C., Crocker, P. R. & McLellan, A. D. CD169 mediates the capture of exosomes in spleen and lymph node. *Blood* **123**, 208-216, doi:10.1182/blood-2013-03-489732 (2014).
- 69 Asano, K. *et al.* CD169-positive macrophages dominate antitumor immunity by crosspresenting dead cell-associated antigens. *Immunity* **34**, 85-95, doi:10.1016/j.immuni.2010.12.011 (2011).
- 70 Junt, T. *et al.* Subcapsular sinus macrophages in lymph nodes clear lymph-borne viruses and present them to antiviral B cells. *Nature* **450**, 110-114, doi:10.1038/nature06287 (2007).
- 71 Phan, T. G., Green, J. A., Gray, E. E., Xu, Y. & Cyster, J. G. Immune complex relay by subcapsular sinus macrophages and noncognate B cells drives antibody affinity maturation. *Nat Immunol* **10**, 786-793, doi:10.1038/ni.1745 (2009).
- 72 Girard, J. P., Moussion, C. & Forster, R. HEVs, lymphatics and homeostatic immune cell trafficking in lymph nodes. *Nat Rev Immunol* **12**, 762-773, doi:10.1038/nri3298 (2012).
- 73 Takeda, A., Sasaki, N. & Miyasaka, M. The molecular cues regulating immune cell trafficking. *Proc Jpn Acad Ser B Phys Biol Sci* **93**, 183-195, doi:10.2183/pjab.93.012 (2017).
- 74 Forster, R., Braun, A. & Worbs, T. Lymph node homing of T cells and dendritic cells via afferent lymphatics. *Trends Immunol* **33**, 271-280, doi:10.1016/j.it.2012.02.007 (2012).
- 75 Sixt, M. *et al.* The conduit system transports soluble antigens from the afferent lymph to resident dendritic cells in the T cell area of the lymph node. *Immunity* **22**, 19-29, doi:10.1016/j.immuni.2004.11.013 (2005).
- 76 Bajenoff, M. *et al.* Stromal cell networks regulate lymphocyte entry, migration, and territoriality in lymph nodes. *Immunity* **25**, 989-1001, doi:10.1016/j.immuni.2006.10.011 (2006).
- 77 Acton, S. E. *et al.* Podoplanin-rich stromal networks induce dendritic cell motility via activation of the C-type lectin receptor CLEC-2. *Immunity* **37**, 276-289, doi:10.1016/j.immuni.2012.05.022 (2012).

- 78 Stein, J. V. *et al.* The CC chemokine thymus-derived chemotactic agent 4 (TCA-4, secondary lymphoid tissue chemokine, 6Ckine, exodus-2) triggers lymphocyte function-associated antigen 1-mediated arrest of rolling T lymphocytes in peripheral lymph node high endothelial venules. *J Exp Med* **191**, 61-76 (2000).
- 79 Baekkevold, E. S. *et al.* The CCR7 ligand e1c (CCL19) is transcytosed in high endothelial venules and mediates T cell recruitment. *J Exp Med* **193**, 1105-1112 (2001).
- 80 Okada, T. *et al.* Chemokine Requirements for B Cell Entry to Lymph Nodes and Peyer's Patches. *The Journal of Experimental Medicine* **196**, 65-75, doi:10.1084/jem.20020201 (2002).
- 81 Lian, J. & Luster, A. D. Chemokine-guided cell positioning in the lymph node orchestrates the generation of adaptive immune responses. *Curr Opin Cell Biol* **36**, 1-6, doi:10.1016/j.ceb.2015.05.003 (2015).
- 82 Krummel, M. F., Bartumeus, F. & Gerard, A. T cell migration, search strategies and mechanisms. *Nat Rev Immunol* **16**, 193-201, doi:10.1038/nri.2015.16 (2016).
- 83 Bousso, P. & Robey, E. Dynamics of CD8+ T cell priming by dendritic cells in intact lymph nodes. *Nat Immunol* **4**, 579-585, doi:10.1038/ni928 (2003).
- 84 Underhill, D. M., Bassetti, M., Rudensky, A. & Aderem, A. Dynamic interactions of macrophages with T cells during antigen presentation. *J Exp Med* **190**, 1909-1914 (1999).
- 85 Ley, K. The second touch hypothesis: T cell activation, homing and polarization. *F1000Res* **3**, 37, doi:10.12688/f1000research.3-37.v2 (2014).
- 86 Baeyens, A., Fang, V., Chen, C. & Schwab, S. R. Exit Strategies: S1P Signaling and T Cell Migration. *Trends Immunol* **36**, 778-787, doi:10.1016/j.it.2015.10.005 (2015).
- 87 Halin, C., Tobler, N. E., Vigl, B., Brown, L. F. & Detmar, M. VEGF-A produced by chronically inflamed tissue induces lymphangiogenesis in draining lymph nodes. *Blood* **110**, 3158-3167, doi:10.1182/blood-2007-01-066811 (2007).
- 88 Huggenberger, R. *et al.* An important role of lymphatic vessel activation in limiting acute inflammation. *Blood* **117**, 4667-4678, doi:10.1182/blood-2010-10-316356 (2011).
- 89 Lachance, P. A., Hazen, A. & Sevick-Muraca, E. M. Lymphatic vascular response to acute inflammation. *PLoS One* **8**, e76078, doi:10.1371/journal.pone.0076078 (2013).
- 90 Goldman, J. *et al.* Cooperative and redundant roles of VEGFR-2 and VEGFR-3 signaling in adult lymphangiogenesis. *FASEB J* **21**, 1003-1012, doi:10.1096/fj.06-6656com (2007).

- 91 Cursiefen, C. *et al.* VEGF-A stimulates lymphangiogenesis and hemangiogenesis in inflammatory neovascularization via macrophage recruitment. *J Clin Invest* **113**, 1040-1050, doi:10.1172/JCI20465 (2004).
- 92 Kerjaschki, D. The crucial role of macrophages in lymphangiogenesis. *J Clin Invest* **115**, 2316-2319, doi:10.1172/JCI26354 (2005).
- 93 Maruyama, K. *et al.* Inflammation-induced lymphangiogenesis in the cornea arises from CD11b-positive macrophages. *J Clin Invest* **115**, 2363-2372, doi:10.1172/JCI23874 (2005).
- 94 Lee, A. S. *et al.* Vascular endothelial growth factor-C and -D are involved in lymphangiogenesis in mouse unilateral ureteral obstruction. *Kidney Int* **83**, 50-62, doi:10.1038/ki.2012.312 (2013).
- 95 Kataru, R. P. *et al.* Critical role of CD11b+ macrophages and VEGF in inflammatory lymphangiogenesis, antigen clearance, and inflammation resolution. *Blood* **113**, 5650-5659, doi:10.1182/blood-2008-09-176776 (2009).
- 96 Tan, K. W. *et al.* Neutrophils contribute to inflammatory lymphangiogenesis by increasing VEGF-A bioavailability and secreting VEGF-D. *Blood* **122**, 3666-3677, doi:10.1182/blood-2012-11-466532 (2013).
- 97 Angeli, V. *et al.* B cell-driven lymphangiogenesis in inflamed lymph nodes enhances dendritic cell mobilization. *Immunity* **24**, 203-215, doi:10.1016/j.immuni.2006.01.003 (2006).
- 98 Dubey, L. K., Karempudi, P., Luther, S. A., Ludewig, B. & Harris, N. L. Interactions between fibroblastic reticular cells and B cells promote mesenteric lymph node lymphangiogenesis. *Nat Commun* **8**, 367, doi:10.1038/s41467-017-00504-9 (2017).
- 99 Flister, M. J. *et al.* Inflammation induces lymphangiogenesis through up-regulation of VEGFR-3 mediated by NF-kappaB and Prox1. *Blood* **115**, 418-429, doi:10.1182/blood-2008-12-196840 (2010).
- 100 Norder, M. *et al.* Lymph node-derived lymphatic endothelial cells express functional costimulatory molecules and impair dendritic cell-induced allogenic T-cell proliferation. *FASEB J* **26**, 2835-2846, doi:10.1096/fj.12-205278 (2012).
- 101 Shin, K. *et al.* TH2 cells and their cytokines regulate formation and function of lymphatic vessels. *Nat Commun* **6**, 6196, doi:10.1038/ncomms7196 (2015).
- 102 Makinen, T. *et al.* Inhibition of lymphangiogenesis with resulting lymphedema in transgenic mice expressing soluble VEGF receptor-3. *Nat Med* **7**, 199-205, doi:10.1038/84651 (2001).
- 103 Sugaya, M. *et al.* Lymphatic dysfunction impairs antigen-specific immunization, but augments tissue swelling following contact with allergens. *J Invest Dermatol* **132**, 667-676, doi:10.1038/jid.2011.349 (2012).

- 104 Lukacs-Kornek, V. *et al.* Regulated release of nitric oxide by nonhematopoietic stroma controls expansion of the activated T cell pool in lymph nodes. *Nat Immunol* **12**, 1096-1104, doi:10.1038/ni.2112 (2011).
- 105 Card, C. M., Yu, S. S. & Swartz, M. A. Emerging roles of lymphatic endothelium in regulating adaptive immunity. *J Clin Invest* **124**, 943-952, doi:10.1172/JCI73316 (2014).
- 106 Sawa, Y. *et al.* LPS-induced IL-6, IL-8, VCAM-1, and ICAM-1 expression in human lymphatic endothelium. *J Histochem Cytochem* **56**, 97-109, doi:10.1369/jhc.7A7299.2007 (2008).
- 107 Martinez, F. O. *et al.* IL-8 induces a specific transcriptional profile in human neutrophils: synergism with LPS for IL-1 production. *Eur J Immunol* **34**, 2286-2292, doi:10.1002/eji.200324481 (2004).
- 108 Malhotra, D. *et al.* Transcriptional profiling of stroma from inflamed and resting lymph nodes defines immunological hallmarks. *Nat Immunol* **13**, 499-510, doi:10.1038/ni.2262 (2012).
- 109 James, J. M., Nalbandian, A. & Mukoyama, Y. S. TGFbeta signaling is required for sprouting lymphangiogenesis during lymphatic network development in the skin. *Development* **140**, 3903-3914, doi:10.1242/dev.095026 (2013).
- 110 Irigoyen, M. *et al.* Hypoxia alters the adhesive properties of lymphatic endothelial cells. A transcriptional and functional study. *Biochim Biophys Acta* **1773**, 880-890, doi:10.1016/j.bbamcr.2007.03.001 (2007).
- 111 Onder, L. *et al.* IL-7-producing stromal cells are critical for lymph node remodeling. *Blood* **120**, 4675-4683, doi:10.1182/blood-2012-03-416859 (2012).
- 112 Iolyeva, M. *et al.* Interleukin-7 is produced by afferent lymphatic vessels and supports lymphatic drainage. *Blood* **122**, 2271-2281, doi:10.1182/blood-2013-01-478073 (2013).
- 113 Sharma, M. D. *et al.* Plasmacytoid dendritic cells from mouse tumor-draining lymph nodes directly activate mature Tregs via indoleamine 2,3-dioxygenase. *J Clin Invest* **117**, 2570-2582, doi:10.1172/JCI131911 (2007).
- 114 Lee, J. W. *et al.* Peripheral antigen display by lymph node stroma promotes T cell tolerance to intestinal self. *Nat Immunol* **8**, 181-190, doi:10.1038/ni1427 (2007).
- 115 Magnusson, F. C. *et al.* Direct presentation of antigen by lymph node stromal cells protects against CD8 T-cell-mediated intestinal autoimmunity. *Gastroenterology* **134**, 1028-1037, doi:10.1053/j.gastro.2008.01.070 (2008).
- 116 Nichols, L. A. *et al.* Deletional Self-Tolerance to a Melanocyte/Melanoma Antigen Derived from Tyrosinase Is Mediated by a Radio-Resistant Cell in Peripheral and

- Mesenteric Lymph Nodes. *The Journal of Immunology* **179**, 993-1003, doi:10.4049/jimmunol.179.2.993 (2007).
- 117 Schuler, P. *et al.* Direct presentation of a melanocyte-associated antigen in peripheral lymph nodes induces cytotoxic CD8+ T cells. *Cancer Res* **68**, 8410-8418, doi:10.1158/0008-5472.CAN-08-0809 (2008).
- 118 Cohen, J. N. *et al.* Lymph node-resident lymphatic endothelial cells mediate peripheral tolerance via Aire-independent direct antigen presentation. *J Exp Med* **207**, 681-688, doi:10.1084/jem.20092465 (2010).
- 119 Tewalt, E. F. *et al.* Lymphatic endothelial cells induce tolerance via PD-L1 and lack of costimulation leading to high-level PD-1 expression on CD8 T cells. *Blood* **120**, 4772-4782, doi:10.1182/blood-2012-04-427013 (2012).
- 120 Tamburini, B. A., Burchill, M. A. & Kedl, R. M. Antigen capture and archiving by lymphatic endothelial cells following vaccination or viral infection. *Nat Commun* **5**, 3989, doi:10.1038/ncomms4989 (2014).
- 121 Rouhani, S. J. *et al.* Roles of lymphatic endothelial cells expressing peripheral tissue antigens in CD4 T-cell tolerance induction. *Nat Commun* **6**, 6771, doi:10.1038/ncomms7771 (2015).
- 122 Hirose, S. *et al.* Steady-state antigen scavenging, cross-presentation, and CD8+ T cell priming: a new role for lymphatic endothelial cells. *J Immunol* **192**, 5002-5011, doi:10.4049/jimmunol.1302492 (2014).
- 123 Cohen, J. N. *et al.* Tolerogenic properties of lymphatic endothelial cells are controlled by the lymph node microenvironment. *PLoS One* **9**, e87740, doi:10.1371/journal.pone.0087740 (2014).
- 124 Kedl, R. M. *et al.* Migratory dendritic cells acquire and present lymphatic endothelial cell-archived antigens during lymph node contraction. *Nat Commun* **8**, 2034, doi:10.1038/s41467-017-02247-z (2017).
- 125 Padera, T. P. *et al.* Lymphatic metastasis in the absence of functional intratumor lymphatics. *Science* **296**, 1883-1886, doi:10.1126/science.1071420 (2002).
- 126 Shields, J. D. *et al.* Lymphatic density and metastatic spread in human malignant melanoma. *Br J Cancer* **90**, 693-700, doi:10.1038/sj.bjc.6601571 (2004).
- 127 Skobe, M. *et al.* Induction of tumor lymphangiogenesis by VEGF-C promotes breast cancer metastasis. *Nat Med* **7**, 192-198, doi:10.1038/84643 (2001).
- 128 Hagendoorn, J. *et al.* Onset of abnormal blood and lymphatic vessel function and interstitial hypertension in early stages of carcinogenesis. *Cancer Res* **66**, 3360-3364, doi:10.1158/0008-5472.CAN-05-2655 (2006).
- 129 Hoshida, T. *et al.* Imaging steps of lymphatic metastasis reveals that vascular endothelial growth factor-C increases metastasis by increasing delivery of cancer cells

- to lymph nodes: Therapeutic implications. *Cancer Research* **66**, 8065-8075, doi:10.1158/0008-5472.Can-06-1392 (2006).
- 130 Dadras, S. S. *et al.* Tumor lymphangiogenesis predicts melanoma metastasis to sentinel lymph nodes. *Mod Pathol* **18**, 1232-1242, doi:10.1038/modpathol.3800410 (2005).
- 131 Du, B. *et al.* Metastasis-associated protein 1 induces VEGF-C and facilitates lymphangiogenesis in colorectal cancer. *World J Gastroenterol* **17**, 1219-1226, doi:10.3748/wjg.v17.i9.1219 (2011).
- 132 Renyi-Vamos, F. *et al.* Lymphangiogenesis correlates with lymph node metastasis, prognosis, and angiogenic phenotype in human non-small cell lung cancer. *Clin Cancer Res* **11**, 7344-7353, doi:10.1158/1078-0432.2005.Ccr-05-1077 (2005).
- 133 Emmett, M. S. *et al.* Prediction of melanoma metastasis by the Shields index based on lymphatic vessel density. *BMC Cancer* **10**, 208, doi:10.1186/1471-2407-10-208 (2010).
- 134 Shields, J. D. *et al.* Chemokine-mediated migration of melanoma cells towards lymphatics--a mechanism contributing to metastasis. *Oncogene* **26**, 2997-3005, doi:10.1038/sj.onc.1210114 (2007).
- 135 Munson, J. M. & Shieh, A. C. Interstitial fluid flow in cancer: implications for disease progression and treatment. *Cancer Manag Res* **6**, 317-328, doi:10.2147/CMAR.S65444 (2014).
- 136 Polacheck, W. J., Charest, J. L. & Kamm, R. D. Interstitial flow influences direction of tumor cell migration through competing mechanisms. *Proc Natl Acad Sci U S A* **108**, 11115-11120, doi:10.1073/pnas.1103581108 (2011).
- 137 Harrell, M. I., Iritani, B. M. & Ruddell, A. Tumor-induced sentinel lymph node lymphangiogenesis and increased lymph flow precede melanoma metastasis. *Am J Pathol* **170**, 774-786, doi:10.2353/ajpath.2007.060761 (2007).
- 138 Ruddell, A., Kelly-Spratt, K. S., Furuya, M., Parghi, S. S. & Kemp, C. J. p19/Arf and p53 suppress sentinel lymph node lymphangiogenesis and carcinoma metastasis. *Oncogene* **27**, 3145-3155, doi:10.1038/sj.onc.1210973 (2008).
- 139 Hirakawa, S. *et al.* VEGF-C-induced lymphangiogenesis in sentinel lymph nodes promotes tumor metastasis to distant sites. *Blood* **109**, 1010-1017, doi:10.1182/blood-2006-05-021758 (2007).
- 140 Liu, B. *et al.* Lymphangiogenesis and its relationship with lymphatic metastasis and prognosis in malignant melanoma. *Anat Rec (Hoboken)* **291**, 1227-1235, doi:10.1002/ar.20736 (2008).
- 141 Schoppmann, S. F. *et al.* Tumor-Associated Macrophages Express Lymphatic Endothelial Growth Factors and Are Related to Peritumoral Lymphangiogenesis. *The*

- American Journal of Pathology* **161**, 947-956, doi:10.1016/s0002-9440(10)64255-1 (2002).
- 142 Zampell, J. C. *et al.* HIF-1alpha coordinates lymphangiogenesis during wound healing and in response to inflammation. *FASEB J* **26**, 1027-1039, doi:10.1096/fj.11-195321 (2012).
- 143 Semenza, G. L. Cancer-stromal cell interactions mediated by hypoxia-inducible factors promote angiogenesis, lymphangiogenesis, and metastasis. *Oncogene* **32**, 4057-4063, doi:10.1038/onc.2012.578 (2013).
- 144 Stacker, S. A., Baldwin, M. E. & Achen, M. G. The role of tumor lymphangiogenesis in metastatic spread. *Faseb Journal* **16**, 922-934, doi:DOI 10.1096/fj.01-0945rev (2002).
- 145 He, Y. L. *et al.* Suppression of tumor lymphangiogenesis and lymph node metastasis by blocking vascular endothelial growth factor receptor 3 signaling. *J Natl Cancer I* **94**, 819-825, doi:DOI 10.1093/jnci/94.11.819 (2002).
- 146 Rutkowski, J. M. *et al.* VEGFR-3 Neutralization Inhibits Ovarian Lymphangiogenesis, Follicle Maturation, and Murine Pregnancy. *American Journal of Pathology* **183**, 1596-1607, doi:10.1016/j.ajpath.2013.07.031 (2013).
- 147 Thompson, E. D., Enriquez, H. L., Fu, Y. X. & Engelhard, V. H. Tumor masses support naive T cell infiltration, activation, and differentiation into effectors. *Journal of Experimental Medicine* **207**, 1791-1804, doi:10.1084/jem.20092454 (2010).
- 148 Galon, J. *et al.* Type, density, and location of immune cells within human colorectal tumors predict clinical outcome. *Science* **313**, 1960-1964, doi:10.1126/science.1129139 (2006).
- 149 Gooden, M. J. M., de Bock, G. H., Leffers, N., Daemen, T. & Nijman, H. W. The prognostic influence of tumour-infiltrating lymphocytes in cancer: a systematic review with meta-analysis. *Brit J Cancer* **105**, 93-103, doi:10.1038/bjc.2011.189 (2011).
- 150 Sato, E. *et al.* Intraepithelial CD8(+) tumor-infiltrating lymphocytes and a high CD8(+)/regulatory T cell ratio are associated with favorable prognosis in ovarian cancer. *P Natl Acad Sci USA* **102**, 18538-18543, doi:10.1073/pnas.0509182102 (2005).
- 151 Feig, C. *et al.* Targeting CXCL12 from FAP-expressing carcinoma-associated fibroblasts synergizes with anti-PD-L1 immunotherapy in pancreatic cancer. *P Natl Acad Sci USA* **110**, 20212-20217, doi:10.1073/pnas.1320318110 (2013).
- 152 Salmon, H. *et al.* Matrix architecture defines the preferential localization and migration of T cells into the stroma of human lung tumors. *Journal of Clinical Investigation* **122**, 899-910, doi:10.1172/Jci45817 (2012).

- 153 Brichard, V. G. & Lejeune, D. GSK's antigen-specific cancer immunotherapy programme: Pilot results leading to Phase III clinical development. *Vaccine* **25**, B61-B71, doi:10.1016/j.vaccine.2007.06.038 (2007).
- 154 Mlecnik, B. *et al.* Histopathologic-based prognostic factors of colorectal cancers are associated with the state of the local immune reaction. *J Clin Oncol* **29**, 610-618, doi:10.1200/JCO.2010.30.5425 (2011).
- 155 Baitsch, L. *et al.* Exhaustion of tumor-specific CD8(+) T cells in metastases from melanoma patients. *J Clin Invest* **121**, 2350-2360, doi:10.1172/JCI46102 (2011).
- 156 Mognol, G. P. *et al.* Exhaustion-associated regulatory regions in CD8(+) tumor-infiltrating T cells. *Proc Natl Acad Sci U S A* **114**, E2776-E2785, doi:10.1073/pnas.1620498114 (2017).
- 157 Harlin, H. *et al.* Chemokine Expression in Melanoma Metastases Associated with CD8(+) T-Cell Recruitment. *Cancer Research* **69**, 3077-3085, doi:10.1158/0008-5472.Can-08-2281 (2009).
- 158 Spranger, S. *et al.* Up-regulation of PD-L1, IDO, and T(regs) in the melanoma tumor microenvironment is driven by CD8(+) T cells. *Sci Transl Med* **5**, 200ra116, doi:10.1126/scitranslmed.3006504 (2013).
- 159 Krahenbuhl, L. *et al.* A Longitudinal Analysis of IDO and PDL1 Expression during Immune- or Targeted Therapy in Advanced Melanoma. *Neoplasia* **20**, 218-225, doi:10.1016/j.neo.2017.12.002 (2018).
- 160 Kakavand, H. *et al.* PD-L1 Expression and Immune Escape in Melanoma Resistance to MAPK Inhibitors. *Clin Cancer Res* **23**, 6054-6061, doi:10.1158/1078-0432.Ccr-16-1688 (2017).
- 161 Chen, J. Y. *et al.* Cancer/stroma interplay via cyclooxygenase-2 and indoleamine 2,3-dioxygenase promotes breast cancer progression. *Breast Cancer Res* **16**, doi:10.1186/s13058-014-0410-1 (2014).
- 162 Chung, T. W. *et al.* Induction of Indoleamine 2,3-dioxygenase (IDO) Enzymatic Activity Contributes to Interferon-Gamma Induced Apoptosis and Death Receptor 5 Expression in Human Non-small Cell Lung Cancer Cells. *Asian Pac J Cancer P* **15**, 7995-8001, doi:10.7314/Apjcp.2014.15.18.7995 (2014).
- 163 Abiko, K. *et al.* IFN-gamma from lymphocytes induces PD-L1 expression and promotes progression of ovarian cancer. *Br J Cancer* **112**, 1501-1509, doi:10.1038/bjc.2015.101 (2015).
- 164 Garcia-Diaz, A. *et al.* Interferon Receptor Signaling Pathways Regulating PD-L1 and PD-L2 Expression. *Cell Rep* **19**, 1189-1201, doi:10.1016/j.celrep.2017.04.031 (2017).

- 165 Anderson, A. C., Joller, N. & Kuchroo, V. K. Lag-3, Tim-3, and TIGIT: Co-inhibitory Receptors with Specialized Functions in Immune Regulation. *Immunity* **44**, 989-1004, doi:10.1016/j.immuni.2016.05.001 (2016).
- 166 Gandhi, M. K. *et al.* Expression of LAG-3 by tumor-infiltrating lymphocytes is coincident with the suppression of latent membrane antigen-specific CD8+ T-cell function in Hodgkin lymphoma patients. *Blood* **108**, 2280-2289, doi:10.1182/blood-2006-04-015164 (2006).
- 167 Curran, M. A., Montalvo, W., Yagita, H. & Allison, J. P. PD-1 and CTLA-4 combination blockade expands infiltrating T cells and reduces regulatory T and myeloid cells within B16 melanoma tumors. *Proc Natl Acad Sci U S A* **107**, 4275-4280, doi:10.1073/pnas.0915174107 (2010).
- 168 Wolchok, J. D. & Saenger, Y. The mechanism of anti-CTLA-4 activity and the negative regulation of T-cell activation. *Oncologist* **13 Suppl 4**, 2-9, doi:10.1634/theoncologist.13-S4-2 (2008).
- 169 Linedale, R. *et al.* Elevated frequencies of CD8 T cells expressing PD-1, CTLA-4 and Tim-3 within tumour from perineural squamous cell carcinoma patients. *PLoS One* **12**, e0175755, doi:10.1371/journal.pone.0175755 (2017).
- 170 Lee, S. & Margolin, K. Cytokines in cancer immunotherapy. *Cancers (Basel)* **3**, 3856-3893, doi:10.3390/cancers3043856 (2011).
- 171 Thomas, D. A. & Massague, J. TGF-beta directly targets cytotoxic T cell functions during tumor evasion of immune surveillance. *Cancer Cell* **8**, 369-380, doi:10.1016/j.ccr.2005.10.012 (2005).
- 172 Moo-Young, T. A. *et al.* Tumor-derived TGF-beta mediates conversion of CD4+Foxp3+ regulatory T cells in a murine model of pancreas cancer. *J Immunother* **32**, 12-21, doi:10.1097/CJI.0b013e318189f13c (2009).
- 173 Lakins, M. A., Ghorani, E., Munir, H., Martins, C. P. & Shields, J. D. Cancer-associated fibroblasts induce antigen-specific deletion of CD8(+) T Cells to protect tumour cells. *Nat Commun* **9**, doi:10.1038/s41467-018-03347-0
10.1038/s41467-018-03347-0 (2018).
- 174 Tu, J. F. *et al.* Regulatory T cells, especially ICOS(+) FOXP3(+) regulatory T cells, are increased in the hepatocellular carcinoma microenvironment and predict reduced survival. *Sci Rep* **6**, 35056, doi:10.1038/srep35056 (2016).
- 175 Kumar, S., Wang, J., Thomson, A. W. & Gandhi, C. R. Hepatic stellate cells increase the immunosuppressive function of natural Foxp3(+) regulatory T cells via IDO-induced AhR activation. *J Leukocyte Biol* **101**, 429-438, doi:10.1189/jlb.2A0516-239R (2017).

- 176 Han, Y. M. *et al.* Human hepatocellular carcinoma-infiltrating CD4(+)CD69(+)Foxp3(-) regulatory T cell suppresses T cell response via membrane-bound TGF-beta 1. *J Mol Med* **92**, 539-550, doi:10.1007/s00109-014-1143-4 (2014).
- 177 Amedei, A. *et al.* Ex vivo analysis of pancreatic cancer infiltrating T cells reveals that ENO1-specific Tregs accumulate in tumor tissue and frustrate Th1/Th17 effector cell functions. *Int J Mol Med* **32**, S41-S41 (2013).
- 178 Scurr, M. *et al.* Highly prevalent colorectal cancer-infiltrating LAP(+) Foxp3(-) T cells exhibit more potent immunosuppressive activity than Foxp3(+) regulatory T cells. *Mucosal Immunol* **7**, 428-439, doi:10.1038/mi.2013.62 (2014).
- 179 Chaudhary, B. & Elkord, E. Regulatory T Cells in the Tumor Microenvironment and Cancer Progression: Role and Therapeutic Targeting. *Vaccines* **4**, doi: 10.3390/vaccines4030028. (2016).
- 180 Shurin, M. R., Yurkovetsky, Z. R., Tourkova, I. L., Balkir, L. & Shurin, G. V. Inhibition of CD40 expression and CD40-mediated dendritic cell function by tumor-derived IL-10. *International Journal of Cancer* **101**, 61-68, doi:10.1002/ijc.10576 (2002).
- 181 Murugaiyan, G., Martin, S. & Saha, B. Levels of CD40 expression on dendritic cells dictate tumour growth or regression. *Clin Exp Immunol* **149**, 194-202, doi:10.1111/j.1365-2249.2007.03407.x (2007).
- 182 Singh, M. *et al.* Intratumoral CD40 activation and checkpoint blockade induces T cell-mediated eradication of melanoma in the brain. *Nat Commun* **8**, 1447, doi:10.1038/s41467-017-01572-7 (2017).
- 183 Aalamian, M. *et al.* Human prostate cancer regulates generation and maturation of monocyte-derived dendritic cells. *Prostate* **46**, 68-75 (2001).
- 184 Chaux, P., Moutet, M., Faivre, J., Martin, F. & Martin, M. Inflammatory cells infiltrating human colorectal carcinomas express HLA class II but not B7-1 and B7-2 costimulatory molecules of the T-cell activation. *Laboratory Investigation* **74**, 975-983 (1996).
- 185 Michielsen, A. J. *et al.* Tumour tissue microenvironment can inhibit dendritic cell maturation in colorectal cancer. *PLoS One* **6**, e27944, doi:10.1371/journal.pone.0027944 (2011).
- 186 Lim, T. S. *et al.* CD80 and CD86 differentially regulate mechanical interactions of T-cells with antigen-presenting dendritic cells and B-cells. *PLoS One* **7**, e45185, doi:10.1371/journal.pone.0045185 (2012).
- 187 Zheng, Y. *et al.* CD86 and CD80 Differentially Modulate the Suppressive Function of Human Regulatory T Cells. *The Journal of Immunology* **172**, 2778-2784, doi:10.4049/jimmunol.172.5.2778 (2004).

- 188 Lund, A. W. *et al.* VEGF-C promotes immune tolerance in B16 melanomas and cross-presentation of tumor antigen by lymph node lymphatics. *Cell Rep* **1**, 191-199, doi:10.1016/j.celrep.2012.01.005 (2012).
- 189 Fankhauser, M. *et al.* Tumor lymphangiogenesis promotes T cell infiltration and potentiates immunotherapy in melanoma. *Sci Transl Med* **9**, doi:10.1126/scitranslmed.aal4712. (2017).
- 190 Lund, A. W. *et al.* Lymphatic vessels regulate immune microenvironments in human and murine melanoma. *Journal of Clinical Investigation* **126**, 3389-3402, doi:10.1172/Jci79434 (2016).
- 191 Riedel, A., Shorthouse, D., Haas, L., Hall, B. A. & Shields, J. Tumor-induced stromal reprogramming drives lymph node transformation. *Nature Immunology* **17**, 1118-+, doi:10.1038/ni.3492 (2016).
- 192 Overwijk, W. W. & Restifo, N. P. B16 as a mouse model for human melanoma. *Curr Protoc Immunol* **Chapter 20**, Unit 20 21, doi:10.1002/0471142735.im2001s39 (2001).
- 193 Wick, N. *et al.* Transcriptomal comparison of human dermal lymphatic endothelial cells ex vivo and in vitro. *Physiol Genomics* **28**, 179-192, doi:10.1152/physiolgenomics.00037.2006 (2007).
- 194 Kunnen, S. J., Malas, T. B., Semeins, C. M., Bakker, A. D. & Peters, D. J. M. Comprehensive transcriptome analysis of fluid shear stress altered gene expression in renal epithelial cells. *J Cell Physiol* **233**, 3615-3628, doi:10.1002/jcp.26222 (2018).
- 195 Evens, A. M. *et al.* Hypoxia-inducible factor-1 {alpha} expression predicts superior survival in patients with diffuse large B-cell lymphoma treated with R-CHOP. *J Clin Oncol* **28**, 1017-1024, doi:10.1200/JCO.2009.24.1893 (2010).
- 196 Lee, H., Goetzl, E. J. & An, S. Lysophospholipids LPA and S1P increase PECAM expression on endothelial cell. *Faseb Journal* **14**, A414-A414 (2000).
- 197 Han, J. K. *et al.* Interaction between platelets and endothelial progenitor cells via LPA-Edg-2 axis is augmented by PPAR-delta activation. *J Mol Cell Cardiol* **97**, 266-277, doi:10.1016/j.yjmcc.2016.06.002 (2016).
- 198 Panetti, T. S., Nowlen, J. & Mosher, D. F. Sphingosine-1-phosphate and lysophosphatidic acid stimulate endothelial cell migration. *Arterioscl Throm Vas* **20**, 1013-1019, doi:Doi 10.1161/01.Atv.20.4.1013 (2000).
- 199 Dvorak, H. F., Flier, J. & Frank, H. Tumors - Wounds That Do Not Heal - Similarities between Tumor Stroma Generation and Wound-Healing. *New Engl J Med* **315**, 1650-1659 (1986).
- 200 Hagele, H. *et al.* Double-stranded DNA activates glomerular endothelial cells and enhances albumin permeability via a toll-like receptor-independent cytosolic DNA

- recognition pathway. *Am J Pathol* **175**, 1896-1904, doi:10.2353/ajpath.2009.090182 (2009).
- 201 Jounai, N., Kobiyama, K., Takeshita, F. & Ishii, K. J. Recognition of damage-associated molecular patterns related to nucleic acids during inflammation and vaccination. *Front Cell Infect Microbiol* **2**, 168, doi:10.3389/fcimb.2012.00168 (2012).
- 202 Kaczmarek, A., Vandenabeele, P. & Krysko, D. V. Necroptosis: the release of damage-associated molecular patterns and its physiological relevance. *Immunity* **38**, 209-223, doi:10.1016/j.immuni.2013.02.003 (2013).
- 203 Samama, B. & Boehm, N. Reelin immunoreactivity in lymphatics and liver during development and adult life. *Anat Rec A Discov Mol Cell Evol Biol* **285**, 595-599, doi:10.1002/ar.a.20202 (2005).
- 204 Lutter, S., Xie, S., Tatin, F. & Makinen, T. Smooth muscle-endothelial cell communication activates Reelin signaling and regulates lymphatic vessel formation. *J Cell Biol* **197**, 837-849, doi:10.1083/jcb.201110132 (2012).
- 205 Folsie, D. S., Beathard, G. A. & Granholm, N. A. Smooth-Muscle in Lymph-Node Capsule and Trabeculae. *Anat Rec* **183**, 517-521, doi:DOI 10.1002/ar.1091830404 (1975).
- 206 Guangqi, E. *et al.* Endogenous Vascular Endothelial Growth Factor-A (VEGF-A) Maintains Endothelial Cell Homeostasis by Regulating VEGF Receptor-2 Transcription. *Journal of Biological Chemistry* **287**, 3029-3041, doi:10.1074/jbc.M111.293985 (2012).
- 207 Abe, J. & Berk, B. C. Hypoxia and HIF-1 alpha stability - Another stress-sensing mechanism for Shc. *Circulation Research* **91**, 4-6, doi:10.1161/01.Res.0000026654.65882.55 (2002).
- 208 Morandi, E. M. *et al.* ITGAV and ITGA5 diversely regulate proliferation and adipogenic differentiation of human adipose derived stem cells. *Sci Rep-Uk* **6**, doi:10.1038/srep28889. (2016).
- 209 Rao, S. *et al.* CXCL12 Mediates Trophic Interactions between Endothelial and Tumor Cells in Glioblastoma. *Plos One* **7**, doi: 10.1371/journal.pone.0033005 (2012).
- 210 Pitt, L. A. *et al.* CXCL12-Producing Vascular Endothelial Niches Control Acute T Cell Leukemia Maintenance. *Cancer Cell* **27**, 755-768, doi:10.1016/j.ccell.2015.05.002 (2015).
- 211 Pfeiffer, F. *et al.* Distinct molecular composition of blood and lymphatic vascular endothelial cell junctions establishes specific functional barriers within the peripheral lymph node. *Eur J Immunol* **38**, 2142-2155, doi:10.1002/eji.200838140 (2008).

- 212 Hao, S. N. *et al.* JAM-C promotes lymphangiogenesis and nodal metastasis in non-small cell lung cancer. *Tumor Biol* **35**, 5675-5687, doi:10.1007/s13277-014-1751-1 (2014).
- 213 Reglerol, N. *et al.* JAM-C deficiency primes endothelial cells for a pro-inflammatory state. *Faseb Journal* **30** (2016).
- 214 Morita, K. *et al.* Expression of claudin-5 in dermal vascular endothelia. *Exp Dermatol* **12**, 289-295, doi:DOI 10.1034/j.1600-0625.2003.120309.x (2003).
- 215 O'Rourke, M. G. E. *et al.* Durable complete clinical responses in a phase I/II trial using an autologous melanoma cell/dendritic cell vaccine. *Cancer Immunol Immun* **52**, 387-395, doi:10.1007/s00262-003-0375-x (2003).
- 216 Palucka, A. *et al.* Dendritic cells as therapeutic vaccines in cancer. *J Immunother* **29**, 654-654 (2006).
- 217 de Vries, I. J. M. *et al.* Effective migration of antigen-pulsed dendritic cells to lymph nodes in melanoma patients is determined by their maturation state. *Cancer Research* **63**, 12-17 (2003).
- 218 Eidsmo, L. *et al.* Differential Migration of Epidermal and Dermal Dendritic Cells during Skin Infection. *Journal of Immunology* **182**, 3165-3172, doi:10.4049/jimmunol.0802950 (2009).
- 219 Zimmerli, S. C. & Hauser, C. Langerhans cells and lymph node dendritic cells express the tight junction component claudin-1. *Journal of Investigative Dermatology* **127**, 2381-2390, doi:10.1038/sj.jid.5700882 (2007).
- 220 Kissenpfennig, A. *et al.* Dynamics and function of langerhans cells in vivo: Dermal dendritic cells colonize lymph node areas distinct from slower migrating langerhans cells. *Immunity* **22**, 643-654, doi:10.1016/j.immuni.2005.04.004 (2005).
- 221 Roberts, E. W. *et al.* Critical Role for CD103(+)/CD141(+) Dendritic Cells Bearing CCR7 for Tumor Antigen Trafficking and Priming of T Cell Immunity in Melanoma. *Cancer Cell* **30**, 324-336, doi:10.1016/j.ccell.2016.06.003 (2016).
- 222 Swetman, C. A. *et al.* Extension, retraction and contraction in the formation of a dendritic cell dendrite: distinct roles for Rho GTPases. *Eur J Immunol* **32**, 2074-2083, doi:Doi 10.1002/1521-4141(200207)32:7<2074::Aid-Immu2074>3.0.Co;2-S (2002).
- 223 Takamatsu, H. *et al.* Semaphorins guide the entry of dendritic cells into the lymphatics by activating myosin II. *Nature Immunology* **11**, 594-U560, doi:10.1038/ni.1885 (2010).
- 224 Morote-Garcia, J. C., Napiwotzky, D., Kohler, D. & Rosenberger, P. Endothelial Semaphorin 7A promotes neutrophil migration during hypoxia. *Proceedings of the National Academy of Sciences* **109**, 14146-14151, doi:10.1073/pnas.1202165109 (2012).

- 225 Nishide, M. *et al.* Semaphorin 4D inhibits neutrophil activation and is involved in the pathogenesis of neutrophil-mediated autoimmune vasculitis. *Annals of the Rheumatic Diseases* **76**, 1440-1448, doi:10.1136/annrheumdis-2016-210706 (2017).
- 226 Movassagh, H. *et al.* Chemorepellent Semaphorin 3E Negatively Regulates Neutrophil Migration In Vitro and In Vivo. *The Journal of Immunology* **198**, 1023-1033, doi:10.4049/jimmunol.1601093 (2017).
- 227 O'Connor, B. P. *et al.* Semaphorin 6D regulates the late phase of CD4(+) T cell primary immune responses. *P Natl Acad Sci USA* **105**, 13015-13020, doi:10.1073/pnas.0803386105 (2008).
- 228 Segarra, M. *et al.* Semaphorin 6A regulates angiogenesis by modulating VEGF signaling. *Blood* **120**, 4104-4115, doi:10.1182/blood-2012-02-410076 (2012).
- 229 Bielenberg, D. R. *et al.* Semaphorin 3F, a chemorepellent for endothelial cells, induces a poorly vascularized, encapsulated, nonmetastatic tumor phenotype. *Journal of Clinical Investigation* **114**, 1260-1271, doi:10.1172/Jci200421378 (2004).
- 230 Britschgi, M. R., Favre, S. & Luther, S. A. CCL21 is sufficient to mediate DC migration, maturation and function in the absence of CCL19. *Eur J Immunol* **40**, 1266-1271, doi:10.1002/eji.200939921 (2010).
- 231 Johnson, L. A. & Jackson, D. G. Inflammation-induced secretion of CCL21 in lymphatic endothelium is a key regulator of integrin-mediated dendritic cell transmigration. *Int Immunol* **22**, 839-849, doi:10.1093/intimm/dxq435 (2010).
- 232 Ko, Y. C. *et al.* Endothelial CD200 is heterogeneously distributed, regulated and involved in immune cell-endothelium interactions. *Journal of Anatomy* **214**, 183-195, doi:10.1111/j.1469-7580.2008.00986.x (2009).
- 233 Gonzalvo-Feo, S. *et al.* Endothelial Cell-Derived Chemerin Promotes Dendritic Cell Transmigration. *Journal of Immunology* **192**, 2366-2373, doi:10.4049/jimmunol.1302028 (2014).
- 234 Kaur, J., Adya, R., Tan, B. K., Chen, J. & Randevara, H. S. Identification of chemerin receptor (ChemR23) in human endothelial cells: Chemerin-induced endothelial angiogenesis. *Biochem Biophys Res Commun* **391**, 1762-1768, doi:10.1016/j.bbrc.2009.12.150 (2010).
- 235 Acton, S. E. *et al.* Dendritic cells control fibroblastic reticular network tension and lymph node expansion. *Nature* **514**, 498+, doi:10.1038/nature13814 (2014).
- 236 Astarita, J. L. *et al.* The CLEC-2-podoplanin axis controls the contractility of fibroblastic reticular cells and lymph node microarchitecture. *Nature Immunology* **16**, 75+, doi:10.1038/ni.3035 (2015).
- 237 Bianchi, R. *et al.* Postnatal Deletion of Podoplanin in Lymphatic Endothelium Results in Blood Filling of the Lymphatic System and Impairs Dendritic Cell Migration to Lymph

- NodesHighlights. *Arteriosclerosis, Thrombosis, and Vascular Biology* **37**, 108-117, doi:10.1161/atvbaha.116.308020 (2017).
- 238 Kabashima, K. *et al.* CXCL12-CXCR4 engagement is required for migration of cutaneous dendritic cells. *American Journal of Pathology* **171**, 1249-1257, doi:10.2353/ajpath.2007.070225 (2007).
- 239 Kabashima, K. *et al.* CXCR4 engagement promotes dendritic cell survival and maturation. *Biochem Bioph Res Co* **361**, 1012-1016, doi:10.1016/j.bbrc.2007.07.128 (2007).
- 240 Kaiser, A., Donnadieu, E., Abastado, J. P., Trautmann, A. & Nardin, A. CC chemokine ligand 19 secreted by mature dendritic cells increases naive T cell scanning behavior and their response to rare cognate antigen. *Journal of Immunology* **175**, 2349-2356, doi:DOI 10.4049/jimmunol.175.4.2349 (2005).
- 241 Dienz, O. & Rincon, M. The effects of IL-6 on CD4 T cell responses. *Clin Immunol* **130**, 27-33, doi:10.1016/j.clim.2008.08.018 (2009).
- 242 Yoshimoto, T. *et al.* IL-12 up-regulates IL-18 receptor expression on T cells, Th1 cells, and B cells: Synergism with IL-18 for IFN-gamma production. *Journal of Immunology* **161**, 3400-3407 (1998).
- 243 Starbeck-Miller, G. R., Xue, H. H. & Harty, J. T. IL-12 and type I interferon prolong the division of activated CD8 T cells by maintaining high-affinity IL-2 signaling in vivo. *Journal of Experimental Medicine* **211**, 105-120, doi:10.1084/jem.20130901 (2014).
- 244 Gong, J., Chehrazi-Raffle, A., Reddi, S. & Salgia, R. Development of PD-1 and PD-L1 inhibitors as a form of cancer immunotherapy: a comprehensive review of registration trials and future considerations. *J Immunother Cancer* **6**, doi: 10.1186/s40425-018-0316-z (2018).
- 245 Alsaab, H. O. *et al.* PD-1 and PD-L1 Checkpoint Signaling Inhibition for Cancer Immunotherapy: Mechanism, Combinations, and Clinical Outcome. *Front Pharmacol* **8**, doi: 10.3389/fphar.2017.00561 (2017).
- 246 Gregory, J. L. *et al.* Infection Programs Sustained Lymphoid Stromal Cell Responses and Shapes Lymph Node Remodeling upon Secondary Challenge. *Cell Reports* **18**, 406-418, doi:10.1016/j.celrep.2016.12.038 (2017).
- 247 Pytowski, B. *et al.* Complete and specific inhibition of adult lymphatic regeneration by a novel VEGFR-3 neutralizing antibody. *J Natl Cancer I* **97**, 14-21, doi:10.1093/jnci/dji003 (2005).
- 248 Roberts, N. *et al.* Inhibition of VEGFR-3 activation with the antagonistic antibody more potently suppresses lymph node and distant metastases than inactivation of VEGFR-2. (vol 66, pg 2650, 2006). *Cancer Research* **67**, 6528-6528, doi:10.1158/0008-5472.Can-67-13-Cor (2007).

- 249 Muchowicz, A. *et al.* Inhibition of lymphangiogenesis impairs antitumour effects of photodynamic therapy and checkpoint inhibitors in mice. *Eur J Cancer* **83**, 19-27, doi:10.1016/j.ejca.2017.06.004 (2017).
- 250 Teijeira, A., Russo, E. & Halin, C. Taking the lymphatic route: dendritic cell migration to draining lymph nodes. *Semin Immunopathol* **36**, 261-274, doi:10.1007/s00281-013-0410-8 (2014).
- 251 Christiansen, A. J. *et al.* Lymphatic endothelial cells attenuate inflammation via suppression of dendritic cell maturation. *Oncotarget* **7**, 39421-39435, doi:10.18632/oncotarget.9820 (2016).
- 252 Zhang, W., Shou, W. D., Xu, Y. J., Bai, W. K. & Hu, B. Low-frequency ultrasound-induced VEGF suppression and synergy with dendritic cell-mediated anti-tumor immunity in murine prostate cancer cells in vitro. *Sci Rep-Uk* **7**, doi: 10.1038/s41598-017-06242-8 (2017).
- 253 Schumann, K. *et al.* Immobilized Chemokine Fields and Soluble Chemokine Gradients Cooperatively Shape Migration Patterns of Dendritic Cells. *Immunity* **32**, 703-713, doi:10.1016/j.immuni.2010.04.017 (2010).
- 254 Lowe, K. L. *et al.* The expression of mouse CLEC-2 on leucocyte subsets varies according to their anatomical location and inflammatory state. *Eur J Immunol* **45**, 2484-2493, doi:10.1002/eji.201445314 (2015).
- 255 Kerrigan, A. M. *et al.* CLEC-2 Is a Phagocytic Activation Receptor Expressed on Murine Peripheral Blood Neutrophils. *Journal of Immunology* **182**, 4150-4157, doi:10.4049/jimmunol.0802808 (2009).
- 256 Tejchman, A. *et al.* Tumor hypoxia modulates podoplanin/CCL21 interactions in CCR7+NK cell recruitment and CCR7+tumor cell mobilization. *Oncotarget* **8**, 31876-31887 (2017).
- 257 Staines, K. A. *et al.* Hypomorphic conditional deletion of E11/Podoplanin reveals a role in osteocyte dendrite elongation. *J Cell Physiol* **232**, 3006-3019, doi:10.1002/jcp.25999 (2017).
- 258 Prideaux, M. *et al.* Parathyroid Hormone Induces Bone Cell Motility and Loss of Mature Osteocyte Phenotype through L-Calcium Channel Dependent and Independent Mechanisms. *Plos One* **10**, doi:10.1371/journal.pone.0125731 (2015).
- 259 Kitadani, J. *et al.* Cancer Vaccine Therapy Using Carcinoembryonic Antigen - expressing Dendritic Cells generated from Induced Pluripotent Stem Cells. *Sci Rep-Uk* **8**, doi:10.1038/s41598-018-23120-z (2018).
- 260 Hargadon, K. M. Tumor-Altered Dendritic Cell Function: Implications for Anti-Tumor Immunity. *Frontiers in Immunology* **4**, doi:10.3389/fimmu.2013.00192 (2013).

- 261 Culp, W. D. *et al.* Proteomic analysis of tumor establishment and growth in the B16-F10 mouse melanoma model. *J Proteome Res* **5**, 1332-1343, doi:10.1021/pr060059q (2006).
- 262 Courau, T. *et al.* TGF-beta and VEGF cooperatively control the immunotolerant tumor environment and the efficacy of cancer immunotherapies. *Jci Insight* **1**, 10.1172/jci.insight.85974 (2016).
- 263 Whipple, C. A. & Brinckerhoff, C. E. BRAF(V600E) melanoma cells secrete factors that activate stromal fibroblasts and enhance tumourigenicity. *Brit J Cancer* **111**, 1625-1633, doi:10.1038/bjc.2014.452 (2014).
- 264 Ekwall, A. K. H. *et al.* The tumour-associated glycoprotein podoplanin is expressed in fibroblast-like synoviocytes of the hyperplastic synovial lining layer in rheumatoid arthritis. *Arthritis Res Ther* **13**, doi: 10.1186/ar3274 (2011).
- 265 Groger, M. *et al.* IL-3 induces expression of lymphatic markers Prox-1 and podoplanin in human endothelial cells. *Journal of Immunology* **173**, 7161-7169, doi:DOI 10.4049/jimmunol.173.12.7161 (2004).
- 266 Boardman, K. C. & Swartz, M. A. Interstitial flow as a guide for lymphangiogenesis. *Circulation Research* **92**, 801-808, doi:10.1161/01.Res.0000065621.69843.49 (2003).
- 267 Dankort, D., *et al.* Braf(V600E) cooperates with Pten loss to induce metastatic melanoma. *Nat Genet* **41**, 544-552, doi: 10.1038/ng.356 (2009)
- 268 Han, L., *et al.* Interleukin-33 promotes inflammation-induced lymphangiogenesis via ST2/TRAF6-mediated Akt/eNos/NO signalling pathway. *Scientific Reports* **7**, 10602, doi:10.1038/s41598-017-10894-x (2017)
- 269 Baluk, P., *et al.* TNF-alpha drives remodeling of blood vessels and lymphatics in sustained airway inflammation in mice. *J Clin Invest*, **119**, 2954-2964, doi: 10.1172/JCI37626 (2009)
- 270 Pflücke, H., and Sixt, M. Preformed portals facilitate dendritic cell entry into afferent lymphatic vessels. *J Exp Med*, **206**, 2925-2935, doi: 10.1084/jem.20091739 (2009)
- 271 Allan, R., *et al.* Migratory dendritic cells transfer antigen to a lymph node-resident dendritic cell population for efficient CTL priming. *Immunity*, **25**, 153-162, doi: 10.1016/j.immuni.2006.04.017 (2006)
- 272 Weber, M., *et al.* Interstitial dendritic cell guidance by haptotactic chemokine gradients. *Science*, **339**, 328-332, doi:10.1126/science.1228456 (2013).
- 273 Weber, M. and Sixt, M. Live cell imaging of chemotactic dendritic cell migration in explanted mouse ear preparations. *Methods Mol Biol*, **1013**, 215-226, doi: 10.1007/978-1-62703-426-5_14 (2013).

- 274 Kilarski, W., et al. Intravital immunofluorescence for visualising the microcirculatory and immune microenvironments in mouse ear dermis. *PLoS One*, **8**, e57135, doi: 10.1371/journal.pone.0057135 (2013).
- 275 Schindelin, J., et al. Fiji: an open-source platform for biological image analysis. *Nat Methods*, **9**, 676-682, doi: 10.1038/nmeth.2019 (2012).
- 276 de Winde, C., et al. C-type lectin-like receptor 2 (CLEC-2)-dependent DC migration is controlled by tetraspanin CD37. *Journal of Cell Science*, doi: 10.1242/jcs.214551 (2018).
- 277 Wethmar, K., et al. Migration of immature mouse DC across resting endothelium is mediated by ICAM-2 but independent of beta2-integrins and murine DC-SIGN homologues. *Eur J Immunol*, **36**, 2781-2794, doi:10.1002/eji.200526311 (2006).
- 278 Feigelson, S., et al. ICAMs are not obligatory for functional immune synapses between naïve CD4 T-cells and lymph node DCs. *Cell Reports*, **22**, 849-859, doi:10.1016/j.celrep.2017.12.103 (2018).
- 279 Saeki, H., et al. Cutting edge: secondary lymphoid-tissue chemokine (SLC) and CC chemokine receptor 7 (CCR7) participate in the emigration pathway of mature dendritic cells from the skin to regional lymph nodes. *J Immunol*, **162**, 2472-2475 (1999).
- 280 Nakano, H and Gunn, M.D. Gene duplications at the chemokine locus on mouse chromosome 4: multiple strain-specific haplotypes and the deletion of secondary lymphoid-organ chemokine and EBI-1 ligand chemokine genes in the plt mutation. *J Immunol*, **166**, 361-369, (2001).
- 281 Vassileva, G., et al. The reduced gene expression of 6Ckine in the plt mouse results from the deletion of one of two 6Ckine genes. *J Exp Med*, **190**, 1183-1188, (1999).
- 282 Dubrot, J., et al. Lymph node stromal cells acquire peptide-MHCII complexes from dendritic cells and induce antigen-specific CD4+ T-cell tolerance. *JEM*, **211**, 1153-1166, doi: 10.1084/jem.20132000 (2014).
- 283 Goren, I., et al. A transgenic mouse model of inducible macrophage depletion. *Am J Pathol*, **175**, 132-147, doi:10.2353/ajpath.2009.081002 (2009).
- 284 Baumgartner, J., et al. Melanoma induces immunosuppression by upregulating FOXP3+ Regulatory T-cells. *J Surg Res*, **141**, 72-77, doi: 10.1016/j.jss.2007.03.053 (2007).

- 285 Chen, G., et al. Exosomal PD-L1 contributes to immunosuppression and is associated with anti-PD-1 response. *Nature*, **560**, 382-386, doi: 10.1038/s41586-018-0392-8 (2018).
- 286 Long, G., et al. Combination nivolumab and ipilimumab or nivolumab alone in melanoma brain metastases: a multicentre randomised phase 2 study. *The Lancet Oncology*, **19**, 672-681, doi: [https://doi.org/10.1016/S1470-2045\(18\)30139-6](https://doi.org/10.1016/S1470-2045(18)30139-6) (2018).
- 287 Wolchok, J., et al. Overall survival with combined Nivolumab and Ipilimumab in advanced melanoma. *N Engl J Med*, **377**, 1345-1356, doi: 10.1056/NEJMoa1709684 (2017).
- 288 Hodi, F., et al. Improved survival with Ipilimumab in patients with metastatic melanoma. *N Engl J Med*, **363**, 711-723, doi: 10.1056/NEJMoa1003466 (2010).

APPENDICES

Appendix 1 – Altered gene targets in TDLN-derived LECs

Top up- and down-regulated gene targets in Day 4 (D4) and Day11 (D11) TDLN-LECs, from B16-F10 tumour-bearing mice. Gene targets are listed in order, as shown in the heatmap in Figure 3.7c.

	Up-regulated		Down-regulated	
D11	<ol style="list-style-type: none"> 1. <i>Edg2</i> 2. <i>Gbp6</i> 3. <i>Edg2</i> 4. <i>Pfn1</i> 5. <i>Mras</i> 6. <i>Tgif1</i> 7. <i>Hist1h3e</i> 8. <i>Cdca8</i> 9. <i>Hist1h3d</i> 10. <i>Rab7</i> 11. <i>Ung</i> 12. <i>Loc100047628</i> 13. <i>Kcnj10</i> 14. <i>Ab124611</i> 15. <i>Slc45a4</i> 16. <i>Anp32a</i> 17. <i>2btb7a</i> 18. <i>Fyb</i> 19. <i>Ccl20</i> 20. <i>Scl0003542.1.1</i> 21. <i>D130004hd4rik</i> 22. <i>Mrps34</i> 23. <i>H2-dmb2</i> 24. <i>Znhit6</i> 25. <i>Ambra1</i> 	<ol style="list-style-type: none"> 26. <i>Loc381212</i> 27. <i>Xpnpep1</i> 28. <i>Tmem177</i> 29. <i>Ifnar2</i> 30. <i>Df4e3</i> 31. <i>Mki67</i> 32. <i>Pqbp1</i> 33. <i>2610301g19rik</i> 34. <i>Ptx3</i> 35. <i>Cxcl2</i> 36. <i>Eef2</i> 37. <i>Ptx3</i> 38. <i>Crygn</i> 39. <i>Man1a2</i> 40. <i>Ogfrl-1</i> 41. <i>Myst3</i> 42. <i>Eme2</i> 43. <i>Pdpk1</i> 44. <i>Zmym3</i> 45. <i>Mmp24</i> 46. <i>Ostf1</i> 47. <i>B4galnt1</i> 48. <i>Rlf</i> 49. <i>2310032m22rik</i> 50. <i>Dock7</i> 	<ol style="list-style-type: none"> 1. <i>Loc100045343</i> 2. <i>Bcd46404</i> 3. <i>C130057N11rik</i> 4. <i>Reln</i> 5. <i>9230103k20rik</i> 6. <i>2b10410a03rik</i> 7. <i>Muted</i> 8. <i>Mapk9</i> 9. <i>Egfl7</i> 10. <i>Ngfr</i> 11. <i>Sphk1</i> 12. <i>Unc13b</i> 13. <i>Phldb2</i> 14. <i>Gata2</i> 15. <i>Josd2</i> 16. <i>Noxo1</i> 17. <i>A830080h07rik</i> 18. <i>Tmem53</i> 19. <i>Phxr4</i> 20. <i>Acad8</i> 21. <i>Klhl13</i> 22. <i>Ttc3</i> 23. <i>Plekha4</i> 24. <i>2500004h21rik</i> 25. <i>Nfatc4</i> 	<ol style="list-style-type: none"> 26. <i>Rxrb</i> 27. <i>Ddx51</i> 28. <i>Ubxnb</i> 29. <i>Myd116</i> 30. <i>B230365cd1rik</i> 31. <i>Plekhm2</i> 32. <i>A830092p18rik</i> 33. <i>Polr3h</i> 34. <i>F2r</i> 35. <i>Socs3</i> 36. <i>Rag1ap1</i> 37. <i>2310016m24rik</i> 38. <i>Mrg1</i> 39. <i>Gpr180</i> 40. <i>Sct</i> 41. <i>Nfat5</i> 42. <i>U5hbp1</i> 43. <i>Txnip</i> 44. <i>C5nk1d</i> 45. <i>5n3a</i> 46. <i>D630014a15rik</i> 47. <i>Hoxd10</i> 48. <i>Scl0002357.164</i> 49. <i>Stab1</i> 50. <i>Fcgrt</i>
D4	<ol style="list-style-type: none"> 1. <i>Col5a1</i> 2. <i>Cenpl</i> 3. <i>Mcat</i> 4. <i>Kif23</i> 5. <i>9130404d08rik</i> 6. <i>Nrd1</i> 7. <i>Sntg2</i> 8. <i>D10jhu81e</i> 9. <i>Abhd2</i> 10. <i>Pyroxd1</i> 11. <i>Chmp7</i> 12. <i>Ppap2c</i> 13. <i>Hrb2</i> 14. <i>Osbpl2</i> 15. <i>Tgif1</i> 16. <i>Cmklr1</i> 17. <i>4632413c10rik</i> 18. <i>Tmem134</i> 19. <i>Nsmce2</i> 20. <i>2500002l14rik</i> 21. <i>Eya1</i> 22. <i>Tmem161a</i> 23. <i>A630072j24rik</i> 24. <i>Eif2b5</i> 25. <i>Xpnpep1</i> 	<ol style="list-style-type: none"> 26. <i>Gtf3c2</i> 27. <i>Lrrc8</i> 28. <i>Znhit6</i> 29. <i>C030032g21rik</i> 30. <i>Zfand3</i> 31. <i>Ube3b</i> 32. <i>4931417g12rik</i> 33. <i>D130027a21rik</i> 34. <i>Hist1h2be</i> 35. <i>Mcm5</i> 36. <i>Nkpd1</i> 37. <i>Mllt11</i> 38. <i>Setds</i> 39. <i>Snapin</i> 40. <i>Vrk3</i> 41. <i>Ai931714</i> 42. <i>Mki67</i> 43. <i>Klk1b26</i> 44. <i>Gp38</i> 45. <i>9430043d10rik</i> 46. <i>A930010m14rik</i> 47. <i>Lbac1</i> 48. <i>Dyn112</i> 		

Appendix 2 – Gene targets altered in Day 4 and Day 11 TDLN-derived LECs

Gene targets with altered expression in both Day 4 and Day11 TDLN-LECs, from B16-F10 tumour-bearing mice. This list details overlap analysis shown in Figure 3.7d.

Genes down-regulated in Day 4 and Day 11		Genes up-regulated in Day 4 and Day 11	
<i>Rag1ap1</i>	<i>A230046k03rik</i>	<i>D10jhu81e</i>	<i>Nid1</i>
<i>Mrps24</i>	<i>Adrbk2</i>	<i>Tgif1</i>	<i>Tbn-Pending</i>
<i>Sct</i>	<i>Mir16</i>	<i>Nsmce2</i>	<i>Loc100042405</i>
<i>Tmem53</i>	<i>Hyi</i>	<i>2500002114rik</i>	<i>Csnk1e</i>
<i>Loc630337</i>	<i>6330509m05rik</i>	<i>Xpnpep1</i>	<i>Rin2</i>
<i>Plekha4</i>	<i>Cep63</i>	<i>Znhit6</i>	<i>Rab8a</i>
<i>Gpr180</i>	<i>Igfbp3</i>	<i>Hist1h2be</i>	<i>Prmt5</i>
<i>Pdzd8</i>	<i>Mansc1</i>	<i>Snapin</i>	<i>Itgav</i>
<i>Acad8</i>	<i>Robo4</i>	<i>Mki67</i>	<i>Cep55</i>
<i>Ddx51</i>	<i>Lman2</i>	<i>Rrm2</i>	<i>Ndufs8</i>
<i>Sin31</i>	<i>2410004b18rik</i>	<i>Cdca8</i>	<i>2700060e02rik</i>
<i>Sema3f</i>	<i>Adh1</i>	<i>Hist1h2bk</i>	<i>Zfp292</i>
<i>Ly6a</i>	<i>1700027m01rik</i>	<i>Olfm1</i>	<i>Ccl5</i>
<i>Tada3l</i>	<i>Nol8</i>	<i>Hist1h2af</i>	<i>Loc100047827</i>
<i>Mdm4</i>	<i>C130080k17rik</i>	<i>Crygn</i>	<i>Rif1</i>
<i>Extl3</i>	<i>B430201c15rik</i>	<i>Myst3</i>	<i>Ung</i>
<i>Ubxn8</i>	<i>Ccl21a</i>	<i>Uhrf1</i>	<i>Klhdc2</i>
<i>Mterfd2</i>	<i>Prdm2</i>	<i>Zmym3</i>	<i>2610301g19rik</i>
<i>D930038m13rik</i>		<i>Ptx3</i>	<i>Ddc26</i>
<i>Plec1</i>		<i>Nudt19</i>	<i>Nap111</i>
<i>Flt1</i>		<i>Epm2a</i>	<i>Pxdn</i>
<i>Loc100048082</i>		<i>Hist1h2an</i>	<i>D130004h04rik</i>
<i>2810410a03rik</i>		<i>2310032m22rik</i>	<i>Hspbab1</i>
<i>Il2rg</i>		<i>Whsxc2</i>	<i>Golga2</i>
<i>Mrps12</i>		<i>D930011h02rik</i>	<i>Senp5</i>
			<i>Zfp664</i>
			<i>Egln1</i>
			<i>Sf3b4</i>

Appendix 3 – Gene ontology pathways for altered genes

Gene Ontology (GO) canonical pathways associated with gene targets with altered expression in TDLN-LECs, from B16-F10 tumour-bearing mice. GO canonical pathways are listed in descending order according to their $-\log_{10}(\text{FDR})$ value, as shown in the bar chart in Figure 3.8a.

1. Genes involved in immune system
2. Genes involved in cell cycle
3. Genes involved in hemostasis
4. Genes involved in cell cycle, mitotic
5. Genes involved in Mitotic M-M/G1 phases
6. Genes involved in immune system
7. Genes involved in DNA replication
8. Pathways in cancer
9. Genes involved in cell cycle checkpoints
10. Genes involved in assembly of pre-replicative complex
11. Focal adhesion
12. Genes involved in cytokine signalling in immune system
13. Genes involved in transcription
14. Genes involved in Class I MHC-mediated antigen P&P
15. Genes involved in mRNA processing
16. Genes involved in M/G1 transition
17. Genes involved in antigen processing: Ub and proteasomal
18. Genes involved in mitotic G1 G1/S phases
19. Genes involved in regulation of mitotic cell cycle
20. Genes involved in axon guidance
21. Genes involved in platelet activation signalling and aggregation
22. Genes involved in metabolism of RNA
23. Genes involved in apoptosis
24. Genes involved in G1/S transition
25. Ensemble of genes encoding ECM proteins
26. Ubiquitin-mediated proteolysis
27. Genes involved in mitotic prometaphase
28. Genes involved in S Phase
29. Cell cycle
30. Axon guidance
31. Genes involved in mRNA splicing
32. Genes involved in antigen processing-cross presentation
33. Proteasome
34. Genes involved in metabolism of lipids and lipoproteins
35. VEGFR1 specific signals
36. Genes involved in metabolism of mRNA
37. IL2-mediated signalling events
38. VEGF, Hypoxia and angiogenesis
39. T-cell receptor signalling pathway
40. Genes involved in signalling by ERBB4
41. Genes involved in G1 DNA damage response
42. Genes involved in regulation of apoptosis
43. Genes involved in GPV1-mediated activation cascade
44. VEGF signalling pathway
45. Genes involved in interferon signalling
46. Endocytosis
47. Genes involved in ER-Phagosome pathway
48. Validated targets of C-Myc transcriptional repression
49. Genes involved in cross-presentation of soluble exogenous antigens (endosomes)
50. Genes involved in CDK-mediated phosphorylation and removal of Cdc6
51. HIF-2-alpha transcription

Appendix 3 (continued)

Gene Ontology (GO) canonical pathways associated with gene targets with altered expression in TDLN-LECs, from B16-F10 tumour-bearing mice. GO canonical pathways are listed in descending order according to their $-\log_{10}(\text{FDR})$ value, as shown in the bar chart in Figure 3.8a.

52. CXCR4-mediated signalling events
53. Genes involved in regulation of ornithine decarboxylase (ODC)
54. Class I PI3K signalling events
55. FoxO family signalling
56. Genes involved in signalling by Wnt
57. Regulation of actin cytoskeleton
58. Cytokine cytokine receptor pathway
59. TCR signalling in CD4+ T-cells
60. Spliceosome
61. mTOR signalling pathway
62. p53 signalling pathway
63. Genes involved in regulation of hypoxia-inducible factor (HIF) by oxygen
64. TCR signalling in CD8+ T-cells
65. Aurora B signalling
66. TGF-beta receptor signalling
67. Genes involved in Meiosis

Appendix 4 – Altered canonical pathways and associated gene targets

Gene targets with altered expression in TDLN-LECs from B16-F10 tumour-bearing mice, grouped according to their Gene Ontology (GO) canonical pathways association. Gene targets are listed in order, as shown in the heatmap in Figure 3.8b.

Tight Junctions	VEGF Signalling	HIF Signalling	Semaphorins
<ol style="list-style-type: none"> 1. <i>Prkcz</i> 2. <i>Prkcz</i> 3. <i>Rhoa</i> 4. <i>Jam3</i> 5. <i>Cldn11</i> 6. <i>Nras</i> 7. <i>Ppp2r2a</i> 8. <i>Tjap1</i> 9. <i>Exoc4</i> 10. <i>Mras</i> 	<ol style="list-style-type: none"> 1. <i>Flt1</i> 2. <i>Nfatc1</i> 3. <i>Pik3cg</i> 4. <i>Sphk1</i> 5. <i>Cav1</i> 6. <i>Hspb1</i> 7. <i>Vegfa</i> 8. <i>Nfatc4</i> 9. <i>Nfat5</i> 10. <i>Shc1</i> 11. <i>Eif2b5</i> 12. <i>Hif1a</i> 13. <i>Nfatc1</i> 14. <i>Ptgs2</i> 15. <i>Pdpk1</i> 16. <i>Nras</i> 	<ol style="list-style-type: none"> 1. <i>Cd36</i> 2. <i>Ppard</i> 3. <i>Shc1</i> 4. <i>Kif23</i> 5. <i>Itgav</i> 6. <i>Ppard</i> 7. <i>Pdpk1</i> 8. <i>Ube2k</i> 9. <i>Vav1</i> 10. <i>Nras</i> 	<ol style="list-style-type: none"> 1. <i>Sema6a</i> 2. <i>Dpysl4</i> 3. <i>Rhoa</i> 4. <i>Sema7a</i> 5. <i>Cd72</i> 6. <i>Pak2</i> 7. <i>Sema6d</i> 8. <i>Ptprc</i>
Focal Adhesion	Platelet Activation		
<ol style="list-style-type: none"> 1. <i>Flt1</i> 2. <i>Pik3cg</i> 3. <i>Mylk</i> 4. <i>Cav1</i> 5. <i>Rhoa</i> 6. <i>Vegfa</i> 7. <i>Mapk9</i> 8. <i>Reln</i> 9. <i>Pdgfa</i> 10. <i>Shc1</i> 11. <i>Itgav</i> 12. <i>Lamc1</i> 13. <i>Pak2</i> 14. <i>Vav1</i> 15. <i>Pdpk1</i> 	<ol style="list-style-type: none"> 1. <i>Prkcz</i> 2. <i>Prkcz</i> 3. <i>Rhoa</i> 4. <i>Vegfa</i> 5. <i>F8</i> 6. <i>Pdgfa</i> 7. <i>Cd36</i> 8. <i>Shc1</i> 9. <i>F2r</i> 10. <i>Pik3cg</i> 11. <i>Pdpk1</i> 12. <i>Gnai1</i> 13. <i>Itga2b</i> 14. <i>Srgn</i> 15. <i>Calu</i> 16. <i>Tmsb4x</i> 17. <i>Vav1</i> 18. <i>Pfn1</i> 		

Appendix 4 (continued)

Gene targets with altered expression in TDLN-LECs from B16-F10 tumour-bearing mice, grouped according to their Gene Ontology (GO) canonical pathways association. Gene targets are listed in order, as shown in the heatmap in Figure 3.8b.

Cytokine and Chemokine Signalling		Antigen Processing and Presentation	
1. <i>Ngfr</i>	26. <i>Ifit3</i>	1. <i>Flt1</i>	26. <i>Psm�4</i>
2. <i>Pdgfa</i>	27. <i>Eif4e3</i>	2. <i>Hgs</i>	27. <i>Psm�7</i>
3. <i>Csf1</i>	28. <i>Gbp5</i>	3. <i>Rab11fip3</i>	28. <i>Cdc20</i>
4. <i>Socs3</i>	29. <i>Tnfrsf1b</i>	4. <i>Pkkcz</i>	29. <i>Cdc27</i>
5. <i>Nup210</i>	30. <i>Tnfrsf10b</i>	5. <i>Psd3</i>	30. <i>Rbx1</i>
6. <i>Acvr2b</i>	31. <i>Ccl7</i>	6. <i>Adrbk2</i>	31. <i>Wwp1</i>
7. <i>Adr8k2</i>	32. <i>Cxcr2</i>	7. <i>Pkkcz</i>	32. <i>Smurf1</i>
8. <i>Pik3cg</i>	33. <i>Ccl5</i>	8. <i>Il2rg</i>	33. <i>Ube2k</i>
9. <i>Rbx1</i>	34. <i>Ifnar2</i>	9. <i>Sh3glb2</i>	34. <i>Keap1</i>
10. <i>Cxcl12</i>	35. <i>Pdpk1</i>	10. <i>Traf6</i>	35. <i>Mkrn1</i>
11. <i>Ccl21a</i>	36. <i>Irf9</i>	11. <i>Tceb2</i>	36. <i>Carn</i>
12. <i>Prkcz</i>	37. <i>Eif4e3</i>	12. <i>Socs3</i>	
13. <i>Ifnb1</i>	38. <i>Ccl5</i>	13. <i>Klhl13</i>	
14. <i>Traf6</i>	39. <i>Tnfrsf1b</i>	14. <i>Cd36</i>	
15. <i>Nup11</i>	40. <i>Sp100</i>	15. <i>5kp2</i>	
16. <i>Vegfa</i>	41. <i>Cd44</i>	16. <i>Zfyve20</i>	
17. <i>Rhoa</i>	42. <i>Socs2</i>	17. <i>Psm�11</i>	
18. <i>Peli1</i>	43. <i>Nras</i>	18. <i>Ube2q2</i>	
19. <i>Cxcl16</i>	44. <i>Pdpk1</i>	19. <i>Tap2</i>	
20. <i>Shc1</i>	45. <i>Adam17</i>	20. <i>Sec61a2</i>	
21. <i>Pik3r3</i>	46. <i>Nup93</i>	21. <i>Rab22a</i>	
22. <i>Stat5a</i>	47. <i>Vav1</i>	22. <i>Itgav2</i>	
23. <i>Flt1</i>	48. <i>Cxcl12</i>	23. <i>Psma4</i>	
24. <i>Inpp5d</i>	49. <i>Ifit2</i>	24. <i>Psma5</i>	
25. <i>Il2rg</i>	50. <i>Ccl20</i>	25. <i>Psm�2</i>	
	51. <i>Gbp6</i>		

Appendix 5 – Manual categorisation of canonical pathways

Manual categorisation of Gene Ontology (GO) canonical pathways with altered gene profiles as shown in Figure 3.9. Categorised altered pathways in Day 4 TDLN-LECs from B16-F10 tumour-bearing mice detailed below.

<p>Immunity</p> <p>Reactome_Immune System Reactome_Cytokine signalling in immune system Reactome_IL7 signalling Reactome_Adaptive immune system Reactome_Interferon signalling PID_IL2 1pathway PID_Integrin3 pathway Reactome_Interferon alpha beta signalling PID_IL4 2pathway PID_Integrin1 pathway</p>	<p>Signalling Pathways</p> <p>KEGG_P53 signalling pathway PID_Myc repress pathway PID_Delta NP63 pathway KEGG_Pathways in cancer Reactome_Signalling by SCF KIT BIOCARTEA_MCM pathway PID_SMAD2 3nuclear pathway PID_P53 downstream pathway PID_TAP63 pathway PID_Aurora A pathway KEGG_JAK STAT signalling pathway</p>
<p>Endothelial</p> <p>KEGG_Focal adhesion NABA_Core matrisome Reactome_Signalling by PDGF NABA_Matrisome BIOCARTEA_VEGF pathway</p>	<p>Metabolism</p> <p>KEGG_Oxidative phosphorylation Reactome_TCA cycle and respiratory electron transport Reactome_Transcription Reactome_Metabolism of lipids and lipoproteins</p>
<p>DNA Replication</p> <p>Reactome_DNA replication Reactome_Assembly of the pre-replicative complex Reactome_Synthesis of DNA PID_ERA Genomic pathway</p>	<p>Other</p> <p>Reactome_ORC1 removal from chromatin Reactome_HIV infection Reactome_Host interactions of HIV factors Reactome_Hemostasis KEGG_Cytosolic DNA sensing pathway Reactome_Late phase of HIV life cycle KEGG_Aldosterone regulated sodium reabsorption Reactome_HIV life cycle Reactome_Metal ion SLC transporters Reactome_Developmental biology KEGG_Glioma</p>

Appendix 5 (continued)

Manual categorisation of Gene Ontology (GO) canonical pathways with altered gene profiles as shown in Figure 3.9. Categorised altered pathways in Day 11 TDLN-LECs from B16-F10 tumour-bearing mice detailed below.

<p>Immunity</p> <p>Reactome_Immune system Reactome_Adaptive immune system Reactome_Class I MHC mediated antigen processing presentation Reactome_Antigen processing ubiquitination proteasome degradation PID_TGFBR pathway Reactome_Antigen processing cross presentation KEGG_Endocytosis KEGG_Chemokine signalling pathway KEGG_T cell receptor signalling pathway Reactome_Semaphorin interactions Reactome_Signalling by the B cell receptor BCR PID_S1P S1P1 pathway PID_CXCR4 pathway ST Integrin Signalling pathway Reactome_Cytokine signalling in immune system</p>	<p>Endothelial</p> <p>KEGG_Focal adhesion Reactome_Factors involved in Megakaryocyte development and platelet production PID_VEGFR1 pathway NABA_Matrisome Reactome_Platelet activation signalling and aggregation KEGG_VEGF signalling pathway NABA_ECM glycoproteins BIOCARTA_ECM pathway NABA_Core matrisome Reactome_Autodegradation of CDH1 by CDH1 APC Reactome_Cell surface interactions at the vascular wall BIOCARTA_EDG1 pathway PID_VEGFR1 2 pathway BIOCARTA_VEGF pathway Reactome_GPVI mediated activation cascade</p>
<p>Cell Cycle</p> <p>Reactome_Cell cycle Reactome_Cell cycle mitotic Reactome_Mitotic M M G1 phases Reactome_APC C CDH1 mediated degradation of CDC20 and other APC C CDH1 targeting proteins in late mitosis early G1 Reactome_Cell cycle checkpoints Reactome_M G1 transition Reactome_Regulation of mitotic cell cycle Reactome_Meiosis Reactome_SCF Beta TRCP mediated degradation of EMI1 Reactome_APC C CDC20 mediated degradation of mitotic proteins Reactome_G1 S transition Reactome_Meiotic recombination Reactome_CDK mediated phosphorylation and removal of CDC6</p>	<p>DNA Replication</p> <p>Reactome_DNA replication Reactome_Assembly of the pre-replicative complex Reactome_Synthesis of DNA</p> <p>Transcription</p> <p>Reactome_Transcription Reactome_Processing of capped intro containing pre-mRNA Reactome_MRNA processing Reactome_MRNA splicing Reactome_Destabilisation of MRNA by AUF1 HNRNP D0 KEGG_Spliceosome Reactome_RNA POL I Promoter opening Reactome_Regulation of MRNA Stability by proteins that bind AU rich elements Reactome_RNA POL I transcription</p>

Appendix 5 (continued)

Manual categorisation of Gene Ontology (GO) canonical pathways with altered gene profiles as shown in Figure 3.9. Categorised altered pathways in Day 11 TDLN-LECs from B16-F10 tumour-bearing mice detailed below.

<p>Signalling Pathways</p> <p>KEGG_Pathways in cancer PID_P75 NTR pathway KEGG_Renal Cell Carcinoma KEGG_Regulation of actin cytoskeleton KEGG_Small Cell Lung cancer PID_FOXO pathway PID_PI3CI pathway PID_MET pathway PID_P53 regulation pathway Reactome_ER phagosome pathway Reactome_Signalling by ERBB4 PID_Insulin pathway KEGG_Adipocytokine signalling pathway</p>	<p>Metabolism</p> <p>Reactome_Metabolism of RNA Reacome_RNA POL I RNA POL III and Mitochondrial transcription Reactome_Metabolism of proteins Reactome_Regulation of Ornithine decarboxylase ODC</p>
<p>Other</p> <p>Reactome_Hemostasis KEGG_Axon guidance Reactome_HIV infection Reactome_Host interactions of HIV factors KEGG_Systemic lupus erythematosus Reactome_VIF mediated degradation of APOBEC3G Reactome_Axon guidance KEGG_Ubiquitin mediated proteolysis Reactome_ORC1 removal from chromatin Reactome_Regulated proteolysis of P75NTR Reactome_Amyloids Reactome_Developmental biology Reactome_Activation of chaperone genes by XBP1S PID_Ceramide pathway</p>	<p>Hypoxia</p> <p>Reactome_Regulation of hypoxia inducible factor HIF by oxygen PID_HIF2 pathway Reactome_Oxygen dependent proline hydroxylation of hypoxia inducible factor alpha PID_HIF1 TF pathway</p> <p>Apoptosis</p> <p>Reactome_Apoptosis Reactome_Regulation of apoptosis</p>

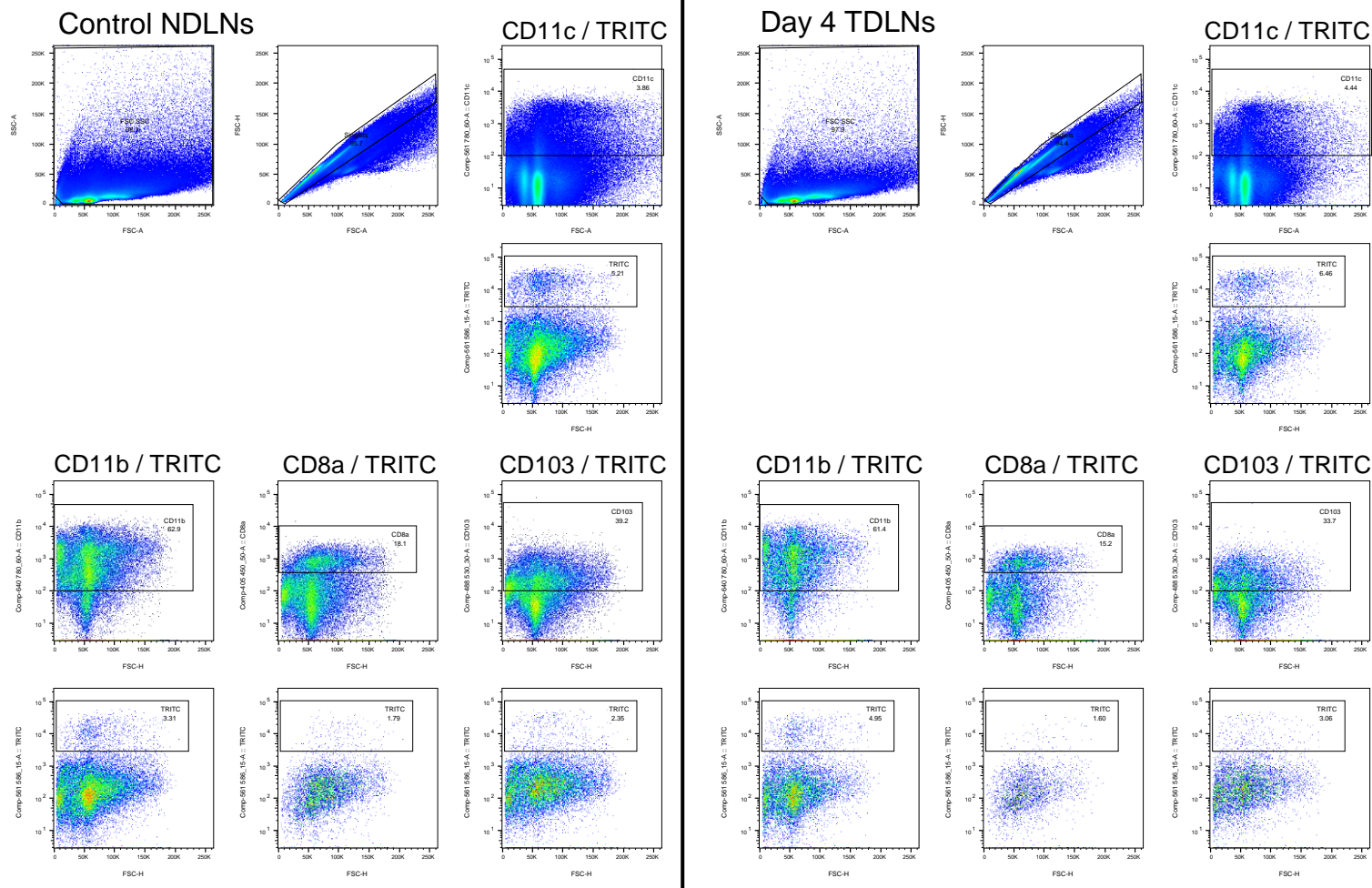
Appendix 6 – Altered *Immunity* associated gene targets

Altered *Immunity* associated gene targets in Day 4 (D4) and Day11 (D11) TDLN-LECs, from B16-F10 tumour-bearing mice. Gene targets are listed in order, as shown in the heatmaps in Figure 3.11.

Day 4		Day 11		
<i>Col1a2</i>	<i>Dync2h1</i>	<i>Mapk9</i>	<i>Cxcl16</i>	<i>Ppp2r2a</i>
<i>Col5a1</i>	<i>Cyn112</i>	<i>Ngfr</i>	<i>Cav1</i>	<i>Dusp3</i>
<i>Pik3r</i>	<i>Egln1</i>	<i>Sphk1</i>	<i>Inpp5d</i>	<i>Cdc20</i>
<i>Rnf125</i>	<i>Gbp5</i>	<i>Klhl13</i>	<i>Dpy5l4</i>	<i>Adam17</i>
<i>Ppp2r5d</i>	<i>Ifit2</i>	<i>Nfatc4</i>	<i>Pik3cg</i>	<i>Gstp1</i>
<i>Psmc2</i>	<i>Ifnb1</i>	<i>Rxb</i>	<i>Cd36</i>	<i>Cycc</i>
<i>Ccl21a</i>	<i>Igf1</i>	<i>F2r</i>	<i>Sh3glb2</i>	<i>Capza2</i>
<i>Cd8b</i>	<i>Il2rg</i>	<i>Socs3</i>	<i>Lamc1</i>	<i>Ctsa</i>
<i>Ifit3</i>	<i>Irf9</i>	<i>Nfat5</i>	<i>Hif1a</i>	<i>Psmb2</i>
<i>Kif23</i>	<i>Itga2b</i>	<i>Txnip</i>	<i>Psma4</i>	<i>Wwp1</i>
<i>Mdm2</i>	<i>Itgav</i>	<i>Vegfa</i>	<i>E2f2</i>	<i>Mkrn1</i>
<i>Peij1</i>	<i>Msh6</i>	<i>Cxcl12</i>	<i>Rbx1</i>	<i>Vav1</i>
<i>Ube3b</i>	<i>Nid1</i>	<i>Rab11fip3</i>	<i>Egln1</i>	<i>Smurf1</i>
<i>Nupl1</i>	<i>Nup210</i>	<i>Sema6a</i>	<i>Dctn1</i>	<i>Psma5</i>
<i>Aim2</i>	<i>Gp38</i>	<i>Pdgfa</i>	<i>Nras</i>	<i>Psmd2</i>
<i>Ap1g1</i>	<i>Polr3k</i>	<i>Il2rg</i>	<i>Itgav</i>	<i>Tnfrsf1b</i>
<i>Bcl6</i>	<i>Prkca</i>	<i>Prkcz</i>	<i>Psmd4</i>	<i>Cd44</i>
<i>Birc5</i>	<i>Psmb1</i>	<i>Flt1</i>	<i>Ncoa4</i>	<i>Psmd7</i>
<i>Ccl5</i>	<i>Socs2</i>	<i>Mylk</i>	<i>Keap1</i>	<i>Tlr4</i>
<i>Cd55</i>	<i>Stat5a</i>	<i>Angpt2</i>	<i>Calr</i>	<i>Rab22a</i>
<i>Cdc16</i>	<i>Them4</i>	<i>Arhgap20</i>	<i>Tek</i>	<i>Sema6d</i>
<i>Cyr61</i>	<i>Zbp1</i>	<i>Csf1</i>	<i>Acsl5</i>	<i>Cd22</i>
<i>Dvl1</i>		<i>Ccl21a</i>	<i>Pak2</i>	<i>Tpm3</i>
		<i>Arhgef7</i>	<i>Sp100</i>	<i>Slc7a7</i>
		<i>Unc93b1</i>	<i>Cdc27</i>	<i>Pdpk1</i>
		<i>Rhoa</i>	<i>Gbp6</i>	<i>Cxcl2</i>
		<i>Traf6</i>	<i>Ptprc</i>	<i>Eif4e3</i>
		<i>Acvr2b</i>	<i>Ptg52</i>	<i>Ifnar2</i>
		<i>Shc1</i>	<i>Nup93</i>	<i>Ccl20</i>
		<i>Adrbk2</i>	<i>Ccl5</i>	<i>Fyb</i>
		<i>Acacb</i>	<i>Capza1</i>	<i>Rab7a</i>
		<i>Jam3</i>	<i>Ube2k</i>	<i>Mras</i>

Appendix 7 – Flow cytometry gating for profiling dendritic cells

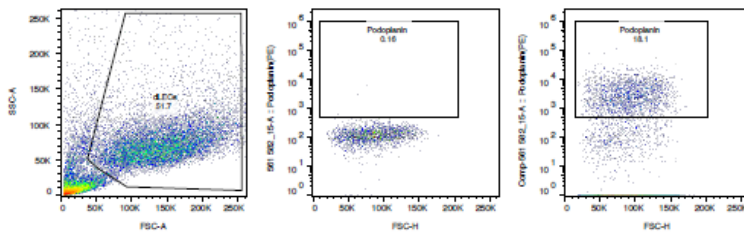
Flow cytometry gating strategy for profiling dendritic cells in Control NDNLs (left panel) and Day4 TDLNs (right panel), from B16-F10 tumour-bearing mice painted with TRITC. Data shown are representative Control NDNL and Day 4 TDLN samples.



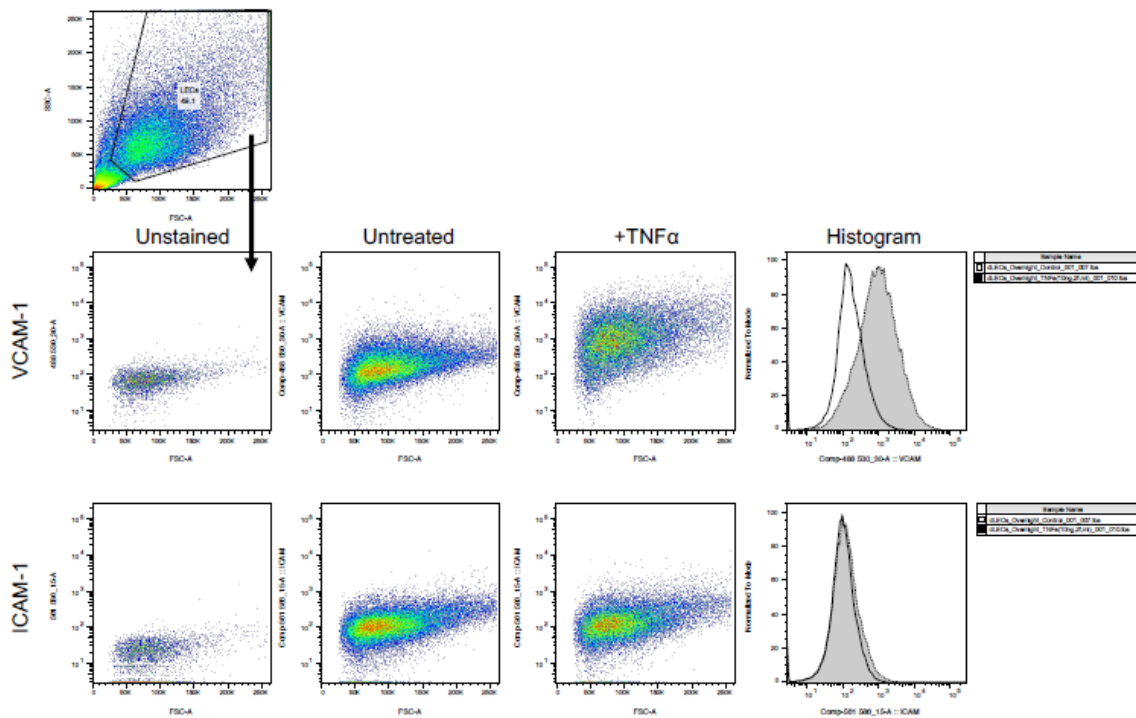
Appendix 8 – Flow cytometry gating for profiling LECs *in vitro*

Flow cytometry gating strategy for profiling lymphatic endothelial cells cultured *in vitro* on collagen-coated plates. Surface expression of Podoplanin (A) and VCAM and ICAM (B). Data obtained using this gating strategy is shown in Figure 4.16.

A *In vitro*: Podoplanin gMFI measured within “dLECs” gate (SSC-A vs FSC-A)



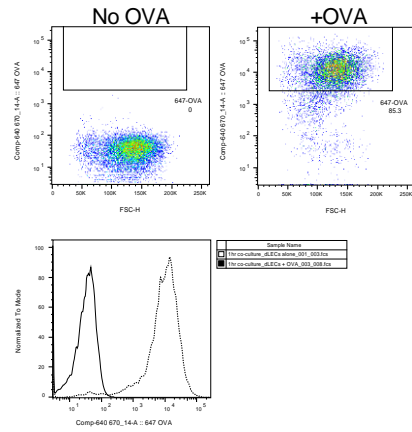
B *In vitro*: ICAM-1 and VCAM-1 gMFI measured within “LECs” gate (SSC-A vs FSC-A) +/- TNF α



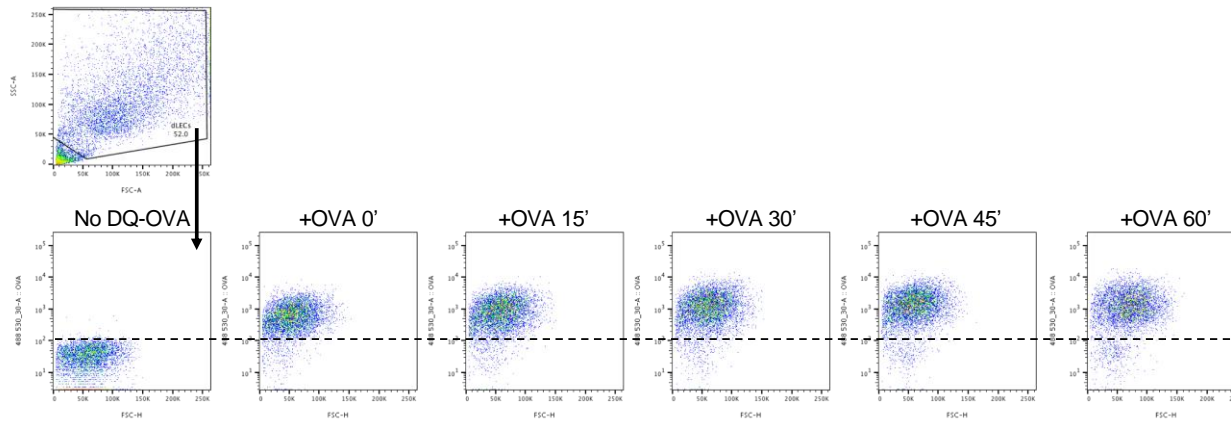
Appendix 9 – Flow cytometry gating for *in vitro* OVA assays

Flow cytometry gating strategy for quantifying FITC-OVA uptake and DQ-OVA processing in lymphatic endothelial cells cultured *in vitro* on collagen-coated plates. Data obtained using this gating strategy is shown in Figure 5.5.

A *In vitro*: 647-OVA uptake by LECs

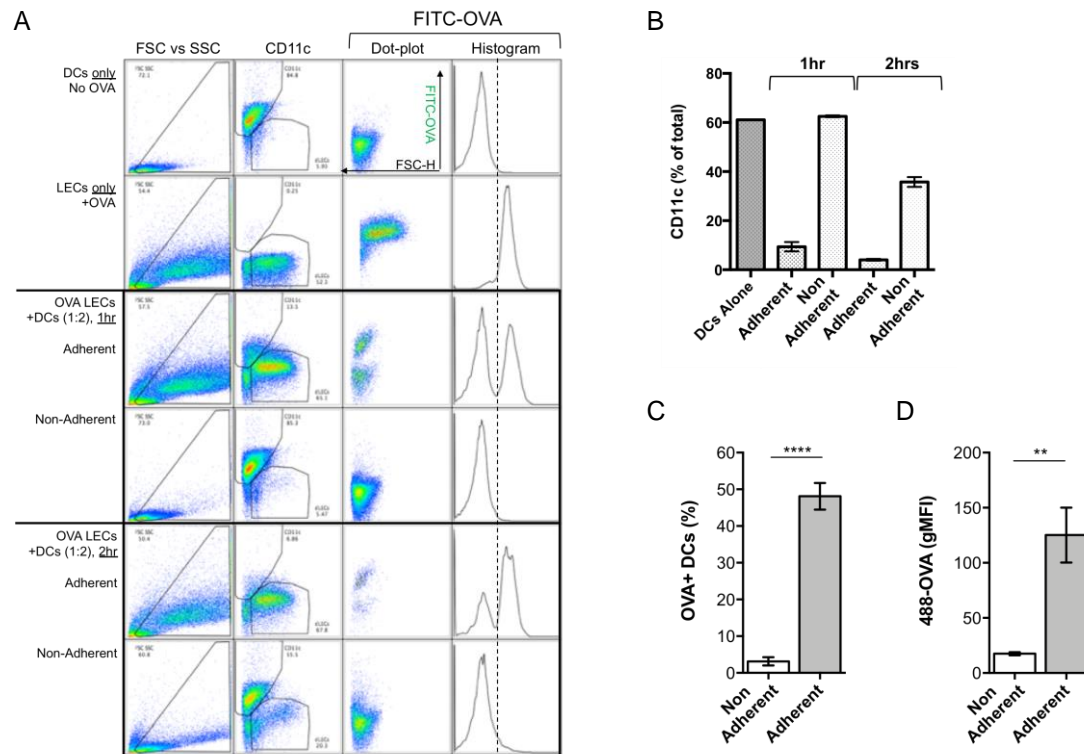


B *In vitro*: DQ-OVA processing by LECs



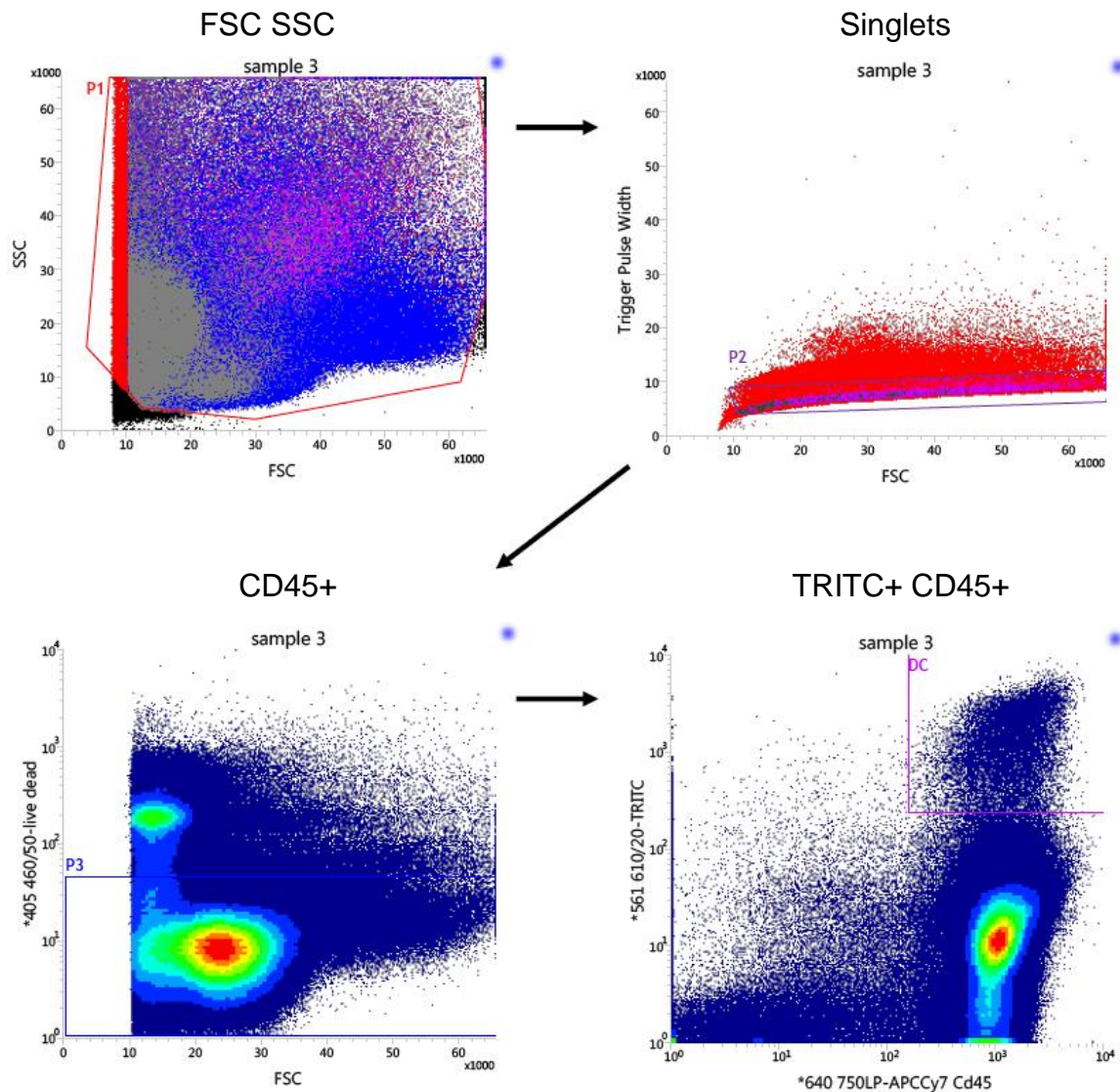
Appendix 10 – Optimisation of the *in vitro* antigen transfer assay

Optimisation of the *in vitro* antigen transfer assay using co-cultured primary lymphatic endothelial cells and splenic CD11c+ isolated dendritic cells. Gating strategy used to quantify amount of FITC-OVA in adherent and non-adherent dendritic cells when cultured at 1:2 ratio (DCs:LECs) for 1hr or 2hrs (A). Quantification of the percentage of FITC-OVA+ CD11c+ dendritic cells, in single cultures + OVA (DCs alone) or co-cultured with LECs (adherent and non-adherent). Data is a representative experiment and presented as mean \pm SEM (B). Dendritic cells co-cultured with LECs at 1:2 ration (DCs:LECs) for 1hr. Shown is quantification of the percentage of FITC-OVA+ CD11c+ dendritic cells (C) and the geometric mean of fluorescence (gMFI) of FITC-OVA in CD11c+ populations (C). Data is representative of n=3 experiments and presented as mean \pm SEM. Statistical significance calculated using the Mann-Whitney test with $P \leq 0.05$.



Appendix 11 – FACS gating for isolating TRITC immune cells

FACS gating for isolating TRITC+ immune cells from Control NDLN and Day4 TDLNs, from B16-F10 tumour-bearing mice painted with TRITC. Data shown is a representative sample. TRITC+ CD45+ cells were gated within viable singlets. Isolated cells were used for the Qiagen PCR array and data obtained shown in Figure 5.19.



Appendix 12 – Flow cytometry gating strategy for profiling lymph node cells

Flow cytometry gating strategy for profiling non-immune stromal cells and immune cells in Control NDLYNs and Day4 TDLNs, from B16-F10 tumour-bearing mice. Surface expression of PD-L1 on CD45- non-immune stromal cells (FRCs: Fibroblast reticular cells; BECs: Blood endothelial cells; LECs: Lymphatic endothelial cells) and CD45+ CD11c+ dendritic cells (A). Surface expression of PD-1 and CD25 in CD45+ CD4+ and CD45+ CD8+ T-cells (B). Shown is a representative sample. Data obtained using this gating strategy is shown in Figure 5.20.

